Macroscopic Freeway Modelling and Control.

Denis Jacquet

Institut National Polytechnique de Grenoble

No. attribué par la bibliothèque

THESE

pour obtenir le grade de

DOCTEUR DE L'INPG

Spécialité : **AUTOMATIQUE-PRODUCTIQUE**

préparée au Laboratoire d'Automatique de Grenoble

dans le cadre de l'École Doctorale :

Électronique, Électrotechnique, Automatique, Traitement du Signal

présentée et soutenue publiquement par

Denis JACQUET

le 14 novembre 2006

Titre :

Modélisation Macroscopique du Trafic et Contrôle des Lois de Conservation Non Linéaires Associées

Directeurs de thèse :

M. Carlos CANUDAS-DE-WIT (INP Grenoble)

M. Damien KOENIG (INP Grenoble)

JURY :

M. Didier GEORGES (INP Grenoble)	Président
M. Georges BASTIN (Université Catholique de Louvain)	Rapporteur
M. Pierre ROUCHON (École des Mines de Paris)	Rapporteur
M. Roberto HOROWITZ (Université de Californie Berkeley)	Examinateur
M. Jean-Patrick LEBACQUE (École Nationale des Ponts-et-Chaussées)	Examinateur
M. Carlos CANUDAS-DE-WIT (INP Grenoble)	Directeur de thèse
M. Damien KOENIG (INP Grenoble)	Co-encadrant

à mes parents.

Ainsi on peut dire que, de quelque manière que Dieu aurait créé le monde, il aurait toujours été régulier et dans un certain ordre général. Mais Dieu a choisi celui qui est le plus parfait, c'est-à-dire celui qui est en même temps ***le plus simple en hypothèses et le plus riche en phénomènes****, comme pourrait être une ligne de géométrie dont la construction serait aisée et les propriétés et effets seraient fort admirables et d'une grande étendue.*

Gottfried Wilhelm Leibniz (1646-1716),
Discours de métaphysique, VI, 1686.

Table des matières

Introduction

Les problématiques de gestion du trafic

On observe dans les pays développés, mais aussi de plus en plus dans les pays en voie de développement, une augmentation des situations de congestion qui ont un impact important, tant au niveau économique que sociétal. Par exemple, le Urban Mobility Report [Schrank & Lomax, 2004] mentionne pour les Etats-Unis un coût monétaire équivalent de 63,2 milliards de dollars en 2002, correspondant à un total de 3,5 milliards d'heures perdues dans les bouchons et à 5,7 milliards de gallons d'essence gaspillés. De manière similaire, le Bureau of Transportation Statistics du département des transports aux Etats-Unis a calculé un coût monétaire équivalent de 12,8 millions de dollars pour la seule ville de Los Angeles en 2001.

En réponse à ces enjeux individuels et collectifs et dans l'objectif d'optimiser l'utilisation des infrastructures existantes, la notion de Systèmes Intelligents de Transport, connue dans sa traduction anglaise sous le nom de Intelligent Transportation Systems (ITS), a émergé dans les années 70-80. Ces systèmes proposent d'équiper les infrastructures et les véhicules de systèmes électroniques et de traitement de l'information afin d'améliorer la performance des infrastructures ainsi que la sécurité, l'information et le confort des usagers. Parmi les systèmes ITS utilisés aujourd'hui, on peut citer la prédiction des temps de parcours, le guidage dynamique par panneaux à messages variables, le séquencement dynamique de la signalisation à certaines intersections, le contrôle par feux tricolores de l'accès aux autoroutes ainsi que la variation dynamique des limites de vitesse. Ces outils ayant démontré leur efficacité [*Twin Cities Ramp Meter Evaluation Report*, 2001], de nombreux systèmes ITS sont aujourd'hui à l'étude, soit pour améliorer des procédés existants soit pour en proposer de nouveaux. Dans le cas des autoroutes et voies rapides urbaines, il est communément accepté que l'usage des infrastructures peut encore être optimisé par des méthodes non invasives telles que le contrôle d'accès dynamique et la régulation des limites de vitesse. Ces deux domaines nécessitent cependant encore des efforts en recherche et développement. En ce qui concerne le contrôle d'accès, si des méthodes locales comme ALINEA [Papageorgiou, Haj-Salem & Middelham, 1997] ont été développées et expérimentées en Californie, dans le Minnesota, aux Pays-Bas et en Grande Bretagne, peu de résultats sont disponibles dans le cas coordonné, potentiellement plus performant.

Le contrôle d'accès est un exemple de système rentrant dans le formalisme capteur-système-actionneur de l'automatique, comme représenté sur les Figures 1 et 2. Les modèles macroscopiques de trafic peuvent être soit continus soit discrets et l'objectif de commande peut être défini comme un critère à optimiser, tel que la distance totale voyagée, ou la poursuite d'une trajectoire de référence. En ce qui concerne la partie capteur, de nombreux réseaux routiers sont équipés de boucles magnétiques de comptage comme représenté en Figure 2. Il permettent de mesurer le flux de véhicules [veh/h], sa vitesse moyenne [km/h] et le taux d'occupation locale [%] qui est une image de la densité [veh/km] à la longueur moyenne des véhicules près. Cependant, il est reconnu que leur fiabilité est souvent discutable en raison de la vétusté des installations et de nouvelles méthodes de mesure sont à l'étude. De plus, leur nombre et leur positionnement ne sont pas toujours adaptés à des opérations de contrôle d'accès.

Définition du périmètre des travaux

Les travaux présentés dans ce document sont le résultat d'une thèse de doctorat effectuée au Laboratoire d'Automatique de Grenoble d'octobre 2003 à septembre 2006 sous la direction de Carlos Canudas de Wit, Directeur de Recherche au CNRS et Damien Koenig, Maître de Conférence à l'INPG. Au cours de cette période, une collaboration étroite a été établie avec les Universités de Californie de Berkeley et de San Diego où l'auteur a effectué plusieurs séjours, en partie grâce au soutien du Fonds France Berkeley.

Nous nous intéressons dans cette thèse aux problèmes de modélisation et de commande du trafic routier dans le cadre des autoroutes et voies rapides urbaines, l'objectif étant de développer de nouvelles stratégies pour la gestion des congestions en utilisant les méthodologies et les outils du contrôle. Cette approche, basée sur l'utilisation d'un modèle dynamique, a fait ses preuves dans de nombreux domaines d'ingénierie où elle a permis de mettre au point des algorithmes de commande performants et robustes. Pour ces raisons, elle fut introduite dans les années 90 dans le domaine des transports et a conduit à une activité importante de recherche dans les communautés du transport, des mathématiques appliquées et du contrôle. Les problèmes de gestion du trafic autoroutier auxquels nous nous intéressons dans cette thèse concernent :

1. le contrôle d'accès dynamique et coordonné où les flux d'entrée d'une autoroute sont modulés pour améliorer la performance de l'infrastructure et diminuer les temps de parcours,
2. l'estimation de données manquantes sur l'état du trafic, ce dernier étant classiquement mesuré par des boucles magnétiques de comptage placées sous le bitume,
3. la mise à jour d'informations d'origine-destination à l'aide des mesures de flux aux entrées et sorties d'un réseau ainsi qu'à certains points intermédiaires.

Notre approche dans le traitement de ces problèmes de contrôle est plutôt théorique et repose sur de nombreux travaux antérieurs en modélisation du trafic autoroutier, aussi

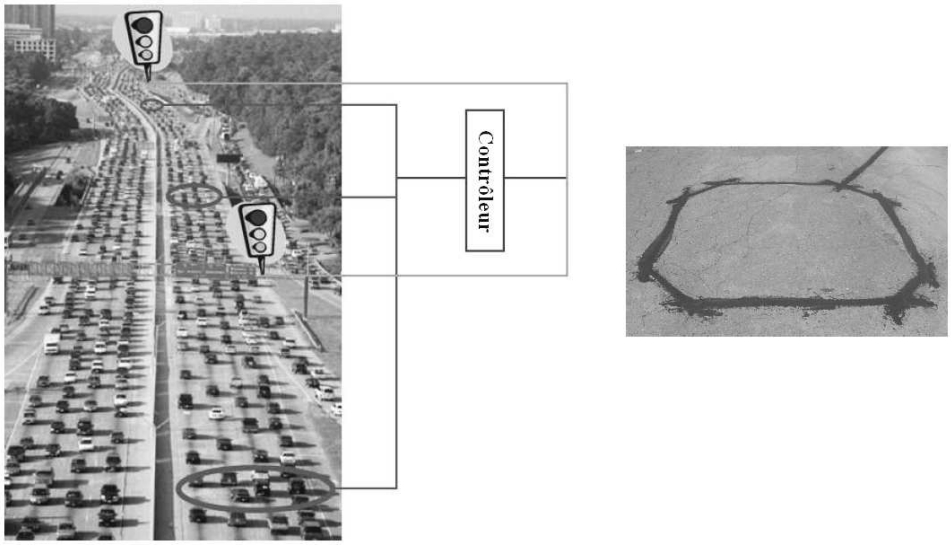

Figure 1: Gauche : Principe du contrôle d'accès coordonné. Droite : boucle de comptage.

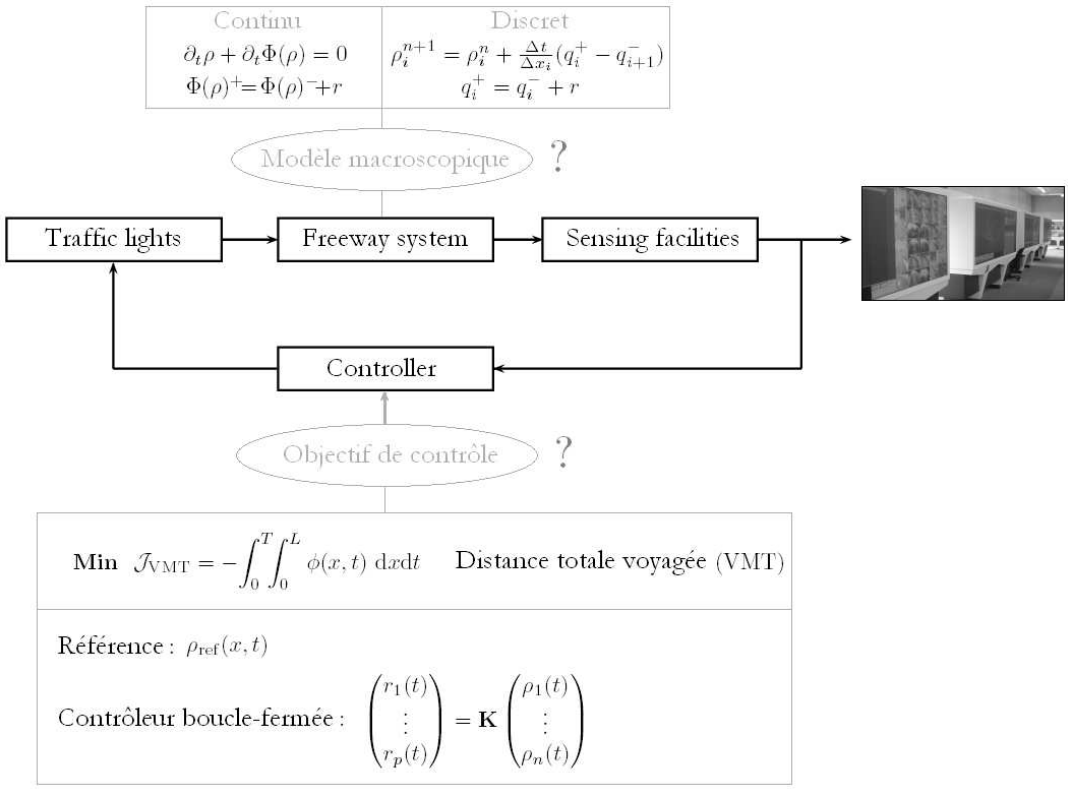

Figure 2: Formalisme capteur-système-actionneur de la commande.

bien dans le domaine du transport que des mathématiques appliquées. Etant donné la taille importante du système, qui est en général constitué de milliers de véhicules, l'utilisation de modèles macroscopiques où le trafic est vu comme un continuum est privilégié pour le développement des algorithmes de commande et d'estimation. A titre d'exemple, la Figure 3 représente une abstraction de l'état du trafic le long d'une autoroute à l'aide d'une distribution spatiale de la densité des véhicules. Suivant les phénomènes devant être reproduits, la précision souhaitée et le niveau de complexité acceptable, il est possible de considérer les distributions d'autres grandeurs agrégées telles que la vitesse moyenne et le flux des véhicules. De nombreux modèles de trafic

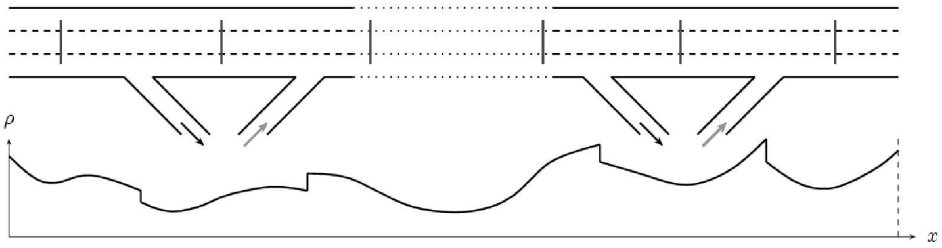

Figure 3: Abstraction macroscopique de l'état de congestion d'une autoroute.

ont été suggérés dans la littérature et ce secteur est toujours un sujet important de recherche. Les algorithmes proposés dans cette thèse reposent sur trois des modèles les plus acceptés aujourd'hui dans la littérature pour représenter la dynamique du trafic : le modèle d'équilibre LWR [Lighthill & Whitham, 1955; Richards, 1956], le modèle de non équilibre ARZ [Aw & Rascle, 2000; Zhang, 2002] et le modèle multi-classes d'origine-destination MOD [Lebacque, 1996; Zhang & Jin, 2002]. Dans ces modèles, l'évolution temporelle des grandeurs macroscopiques de densité, vitesse et flux est régie par des systèmes d'équations aux dérivées partielles non-linéaires appelées lois de conservation [Lax, 1957; Bressan, 2000]. Une des spécificités de cette classe d'équation est qu'elle génère des flots irréguliers dont l'analyse mathématique est récente. Par exemple, la caractérisation des solutions pour les lois de conservation scalaires date des années 70 [Kružkov, 1970; Bardos, LeRoux & Nedelec, 1979] alors que le cas des systèmes n'est pas encore totalement résolu, les avancées les plus récentes datant des années 2000 [Bressan, 2000]. Les trois caractéristiques importantes qui rendent la manipulation de ces équations délicate sont décrites ci-après :

1. des discontinuités appelées ondes de choc [Hopf, 1950; Dafermos, 2000] peuvent se développer et se propager le long des solutions, ce qui complique l'analyse [LeFloch, 2002; Bressan, 2000] et la simulation [LeVeque, 1992; Godlewski & Raviart, 1999] de tels systèmes,

2. les conditions aux limites ne peuvent pas être appliquées pour tout temps en général et sont uniquement proposées [Bardos et al., 1979; Dubois & LeFloch, 1988],

3. l'information se propage à vitesse finie [LeVeque, 1992] au travers d'ondes, ce qui donne lieu à une région d'influence limitée et non déterminée a priori.

Les deux approches retenues dans cette thèse pour contrôler les lois de conservation décrivant l'évolution du trafic sont la commande optimale et une méthode de dissipation. La difficulté principale lors de l'application de la commande optimale aux modèles macroscopiques de trafic est que le flot qu'ils génèrent est en général irrégulier, les ondes de choc représentant la propagation des fronts de congestion. Il n'est donc pas évident, a priori, que ces équations peuvent être linéarisées et permettent d'effectuer les calculs de sensibilité nécessaires dans la méthode adjointe proposée dans [Lions, 1971]. Ce problème est résolu en montrant que cette méthode peut être généralisée moyennant quelques aménagements au cas irrégulier des lois de conservation, et cela avec une transparence remarquable. La solution proposée est basée sur un théorème d'intégration par parties généralisé pour les flots irréguliers dans $\mathbb{R}^2$ et utilise la théorie de la mesure. Concernant l'approche dissipative, la méthodologie proposée consiste à utiliser un schéma de discrétisation approprié permettant de réduire la dimension du système et ainsi être en mesure d'utiliser la théorie existante. En raison du caractère irrégulier des lois de conservation, les méthodes classiques telles que les différences finies ou les éléments finis ne peuvent pas être utilisées car elles sont susceptibles de générer des instabilités ou de donner des vitesses de propagation des chocs erronées [LeVeque, 1992]. Nous montrons qu'un schéma hybride utilisant les méthodes de Godunov [Godunov, 1959] et de "Front Tracking" [Holden, Holden & Hoegh-Krohn, 1988] permet de mettre une loi de conservation scalaire sous la forme d'un système affine par morceaux, aussi appelé PWA pour "PieceWise Affine" dans la littérature. Basé sur les méthodes proposées dans [Johansson & Rantzer, 1998] et [Ferrari-Trecate, Cuzzola, Mignone & Morari, 2002], nous développons ensuite des algorithmes de contrôle en se fixant des objectifs de stabilisation, de rejet de perturbation de type $\mathcal{H}_\infty$ ou de régulation LQ (Linear Quadratic). La théorie de la dissipativité appliquée aux systèmes PWA donne lieu à des Inégalités Matricielles Linéaires ou LMI (Linear Matrix Inequalities) qui peuvent être résolues efficacement à l'aide d'outils logiciels largement disponibles, dont la Matlab© LMI Toolbox. Les méthodes de contrôle proposées dans cette thèse sont à l'état d'algorithmes expérimentaux. Ils ont été implémentés dans l'environnement Matlab© et testés en simulation sur des données réelles de trafic obtenues des Directions Départementales de l'Equipement (DDE) de l'Isère et du Rhône.

Un des défis dans la présentation des travaux de cette thèse est d'introduire le lecteur à la modélisation du trafic, aux systèmes de lois de conservation, à la commande optimale des équations aux dérivées partielles et à la théorie de la dissipativité. Les problématiques de gestion des autoroutes et voies rapies constituent ainsi un cas exemplaire de la convergence de l'ingénierie du trafic, des mathématiques appliquées et de la théorie du contrôle.

Etat de l'art en modélisation et commande du trafic

En ce qui concerne les modèles de trafic, Lighthill, Whitham [Lighthill & Whitham, 1955] et Richards [Richards, 1956] sont les premiers à avoir proposé d'utiliser une équation

aux dérivées partielles, notée LWR, pour modéliser l'évolution de la densité du trafic le long des autoroutes. Le seul paramètre de ce modèle est le diagramme fondamental [Pipes, 1967] qui donne une relation empirique (en général concave) entre la densité ρ [veh/km] et le flux ϕ [veh/h] en tout point. Ce modèle est bien maîtrisé depuis les travaux de [Whitham, 1974; Lax, 1973], même en présence de conditions aux limites [Bardos et al., 1979] et d'inhomogénéités dans les paramètres [Lebacque, 1996]. De plus, plusieurs schémas numériques sont disponibles pour de telles équations, comme le schéma de Godunov [Godunov, 1959]. Il faut souligner la large antériorité des travaux concernant l'analyse du modèle LWR et de ces extensions dans la communauté du transport, en particulier aux Etats-Unis [Michalopoulos, Stephanopoulos & Stephanopoulos, 1981; Michalopoulos, Beskos & Lin, 1984; Bui, Nelson & Narasimhan, 1992] et en France [Lebacque, 1984; Lebacque, 1996].

Plusieurs développements ont été proposés depuis. Dans [Payne, 1971], l'auteur propose un modèle avec une équation dynamique de vitesse mais il est fortement critiquée dans [Daganzo, 1995*b*] en raison de la présence d'ondes se propageant à des vitesses plus importantes que celles des véhicules, ce qui contredit l'anisotropie du trafic. Un schéma numérique est donné dans [Leo & Pretty, 1992] pour ce modèle. Aw, Rascle [Aw & Rascle, 2000] et Zhang [Zhang, 2002] ont ensuite proposé un modèle anisotrope, noté ARZ, ne présentant pas ce type de problème. Certaines extensions de ce modèle sont données dans [Greenberg, 2001; Aw, Klar, Materne & Rascle, 2002] et un schéma numérique de type Godunov est proposé dans [Mammar, Lebacque & Haj-Salem, 2005].

Une extension naturelle de ces modèles est de considérer des interconnections de liens modélisés par les équations LWR, ARZ ou MOD. Les travaux pionniers dans cette voie pour le modèle LWR sont [Holden & Risebro, 1995] et [Lebacque, 1996] qui sont poursuivis dans [M.Herty & Klar, 2003; Coclite, Garavello & Piccoli, 2005] du côté mathématiques appliquées et [Buisson, Lebacque & Lesort, 1996; Lebacque, 2003*b*; Lebacque & Khoshyaran, 2005] du côté transport. D'autres modèles empiriques d'interconnections sont fournis dans [Daganzo, 1995*a*; Jin & Zhang, 2003]. Le traitement des intersections pour le modèle ARZ est étudié dans [Lebacque, Haj-Salem & Mammar, 2005], [Herty & Rascle, 2006] et [Garavello & Piccoli, 2006*b*]. Enfin, des modèles d'interconnection ont été proposés dans [Lebacque & Khoshyaran, 2002], [Garavello & Piccoli, 2005] et [Herty, Kirchner & Moutari, 2006] pour le modèle MOD.

Une autre extension intéressante du modèle LWR consiste à désagréger la densité totale en classes de véhicules comme proposé dans [Lebacque, 1996; Zhang & Jin, 2002; Wong & Wong, 2002; Lebacque & Khoshyaran, 2002; Gavage & Colombo, 2003; Lebacque & Khoshyaran, 2005]. Si ces classes sont les origines-destinations des véhicules présents dans le réseau, ce modèle est appelé MOD pour "Multiclass Origin-Destination". Ce type de modèle est approprié pour l'estimation des données d'origine-destination.

Enfin, Lebacque propose dans [Lebacque, 1997] une modification du modèle LWR où les véhicules ont une accélération bornée, ce qui rend le modèle plus réaliste et fournit une alternative au traitement des discontinuités.

En ce qui concerne la commande du trafic, M. Papageorgiou a joué un rôle prépondérant dans l'avènement des méthodologies du contrôle dans le secteur du transport [Papageorgiou, 1983; Papageorgiou, 1984; Papageorgiou, 1990; Papageorgiou, Blosseville & Haj-Salem, 1990]. Il est aussi l'un des auteurs de la méthode ALINEA de contrôle d'accès local [Papageorgiou, Blosseville & Haj-Salem, 1991] qui a été expérimentée dans plusieurs pays [Papageorgiou et al., 1997]. Plusieurs autres méthodes de contrôle d'accès ont été proposées depuis, parmi lesquelles [Zhang & Levinson, 2004; Zhang, Ritchie & Jayakrishnan, 2001; Kotsialos & Papageorgiou, 2004; Gomes & Horowitz, 2004; Sun & Horowitz, 2005]. Elles sont parfois associées à des stratégies de limitation variable de vitesse comme dans [Alessandri, Febbaro, Ferrara & Punta, 1998; Hegyi, Schutter, Hellendoorn & van den Boom, 2002].

Contributions

La première partie de cette thèse traite de la modélisation macroscopique du trafic dans l'objectif de développer des lois de commande applicables aux problèmes de la gestion des autoroutes et des périphériques. Nous montrons, en nous appuyant sur la vaste littérature à notre disposition, que les modèles LWR, ARZ et MOD peuvent être traités de manière unifiée, en particulier en ce qui concerne les conditions aux limites et les conditions d'interface pour les rampes d'accès et de sortie. Sur la base de cette analyse, nous proposons une modélisation des conditions d'interface aux abords des singularités sous la forme d'automates hybrides, ce qui permet de travailler avec des grandeurs de la même dimension, en l'occurrence les variables de densité. Cette approche est adaptée pour le traitement des problèmes de contrôle et d'optimisation, par exemple dans le cas des calculs de sensibilité.

La deuxième partie concerne la commande de ces systèmes. Nous proposons dans un premier temps une théorie générale pour les problèmes d'optimisation faisant intervenir des lois de conservation puis appliquons les résultats obtenus aux problèmes de gestion du trafic. Une des contributions de cette partie est la généralisation de la méthode du calcul adjoint lorsque l'état du système est une fonction à variation bornée (BV), comme c'est le cas pour les modèles de trafic. Nous proposons également une méthodologie de synthèse basée sur la dissipativité pour la commande et l'observation des versions discrétisées des lois de conservation scalaires. Cette méthode est appliquée au contrôle d'accès et permet d'obtenir des algorithmes en boucle-fermée, contrairement à l'approche par commande optimale.

Les contributions scientifiques de cette thèse peuvent être résumées ainsi:

1. une formulation hybride des entrées/sorties pour les modèles LWR, ARZ et MOD,
2. une condition d'entropie pour les entrées/sorties avec le modèle LWR,
3. un schéma de discrétisation simplifié de type "CTM" pour le modèle ARZ,

4. une méthode adjointe d'évaluation de gradients pour les lois de conservation,

5. un algorithme pratique d'optimisation pour le contrôle et l'observation des modèles macroscopiques de trafic,

6. un algorithme boucle-fermée à base de dissipativité et de LMI pour les lois de conservation scalaires avec une application au contrôle d'accès,

7. des simulations numériques des algorithmes de commande utilisant des données réelles des périphériques de Grenoble et Lyon.

Cette thèse a donné lieu à la présentation des papiers de conférences suivants :

[1] D. Jacquet, J. Jaglin, D. Koenig and C. Canudas de Wit, *Non-Local Feedback Ramp Metering Controller Design*, Proceedings of the 11th IFAC Symposium on Control in Transportation Systems (CTS), Delft, The Netherlands, 2006.

[2] D. Jacquet and Roberto Horowitz, *Input Estimation in Interconnected Systems of Conservation Laws, Application to OD Volume Update*, Proceedings of the 17th International Symposium on Mathematical Theory of Networks and Systems (MTNS), Kyoto, Japan, 2006.

[3] D. Jacquet, M. Krstic and C. Canudas de Wit, *Optimal Control of Scalar One-Dimensional Conservation Laws*, Proceedings of the 2005 American Control Conference, Minneapolis, U.S.A., 2006.

[4] D. Koenig, D. Jacquet and S. Mammar, *Delay-dependent H-infinity Observer of Linear Delay Descriptor Systems*, Proceedings of the 2005 American Control Conference, Minneapolis, U.S.A., 2006.

[5] Jacquet, C. Canudas de Wit, and D. Koenig, *Optimal Control of Systems of Conservation Laws and Application to Non-Equilibrium Traffic Control*, Proceedings of the 13th IFAC Workshop on Control Applications of Optimisation, Cachan, France, 2006.

[6] Jacquet, C. Canudas de Wit, and D. Koenig, *Traffic Control and Monitoring with a Macroscopic Model in the Presence of Strong Congestion Waves*, Proceedings of the 44th Conference on Decision and Control & European Control Conference, Sevilla, Spain, 2005.

[7] Jacquet, C. Canudas de Wit, and D. Koenig, *Optimal Ramp Metering Strategy with an Extended LWR Model: Analysis and Computational Methods*, Proceedings of the 16th IFAC World Congress, Praha, Czech Republic, 2005.

Résumé détaillé

Analyse phénoménologique du trafic

Les modèles de trafic étant jugés pour leur faculté à reproduire des phénomènes observés sur les infrastructures routières en exploitation, une analyse préliminaire des données fournies par les boucles de comptage s'impose. A cet effet, la Figure 4 donne un exemple de la disposition des boucles de comptage sur la partie sud-est du périphérique de Lyon ainsi qu'un exemple de la série temporelle de la vitesse moyenne pour l'un de ces capteurs le 18 octobre 2005 entre 12h00 and 23h00. La baisse de vitesse observée autour de 18h00 est prévisible et correspond à la présence d'une congestion. La Figure 5 donne l'ensemble des séries temporelles de vitesse pour les 8 boucles de comptage présentes sur les voies principales de la section représentée en Figure 4. En dehors de quelques fluctuations autour des limites de vitesse, le phénomène principal apparaissant sur la Figure 5 est une baisse importante de vitesse dans une région correspondant à la présence d'une congestion en fin d'après midi. Sur la base de cette observation, les caractéristiques suivantes doivent retenir notre attention:

1. la baisse de vitesse apparaît d'abord de façon abrupte sur la station numéro 4,
2. elle se propage ensuite en arrière suivant un front de congestion brusque,
3. l'état fluide réapparaît à partir de la frontière amont et se propage en avant,
4. la partie aval à la station 4 est peu affectée durant la période de congestion.

Cette succession d'événements s'explique par la présence d'un goulot d'étranglement entre les stations 4 et 5, du à une demande des rampes d'accès supérieure à la capacité de l'infrastructure à cet endroit. De plus, la présence de plusieurs rampes d'accès et de sortie dans cette région peut produire un effet de confusion sur les conducteurs qui aggrave la situation. Si l'impact de ce type de congestion peut être minimisé en utilisant une méthode de contrôle d'accès, il est primordial que les modèles servant à la mettre en oeuvre prennent en compte ce type de phénomènes.

Les modèles macroscopiques de trafic

Le modèle LWR

Le modèle LWR proposé par Lighthill, Whitham [Lighthill & Whitham, 1955] et Richards [Richards, 1956] est basé sur le principe de conservation des véhicules et l'hypothèse que l'état du trafic suit une relation empirique $\phi = \Phi(\rho) = \rho V(\rho)$ entre la densité ρ et le flux ϕ. Une telle fonction $\Phi(\cdot)$, appelée diagramme fondamental dans la communauté du transport, est représentée en Figure 6 pour le capteur identifié en Figure 4. Des expres-

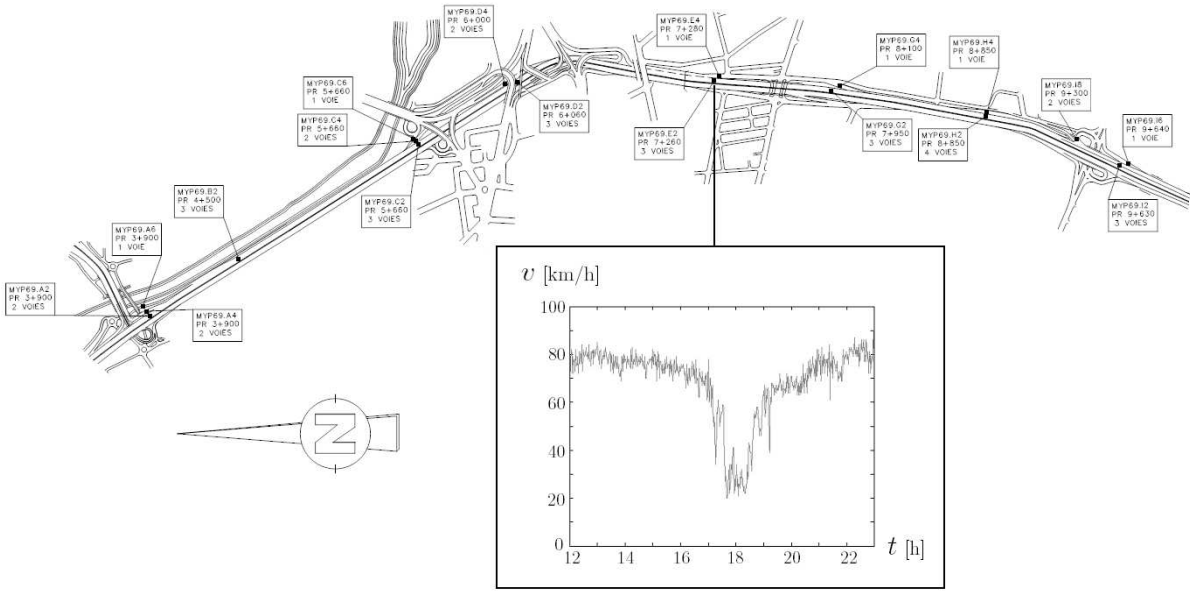

Figure 4: Configuration des boucles magnétiques de comptage (points noirs) le long du périphérique sud-est de Lyon et série temporelle de la vitesse moyenne fournie par l'un des capteurs (période d'échantillonnage de 1 minute).

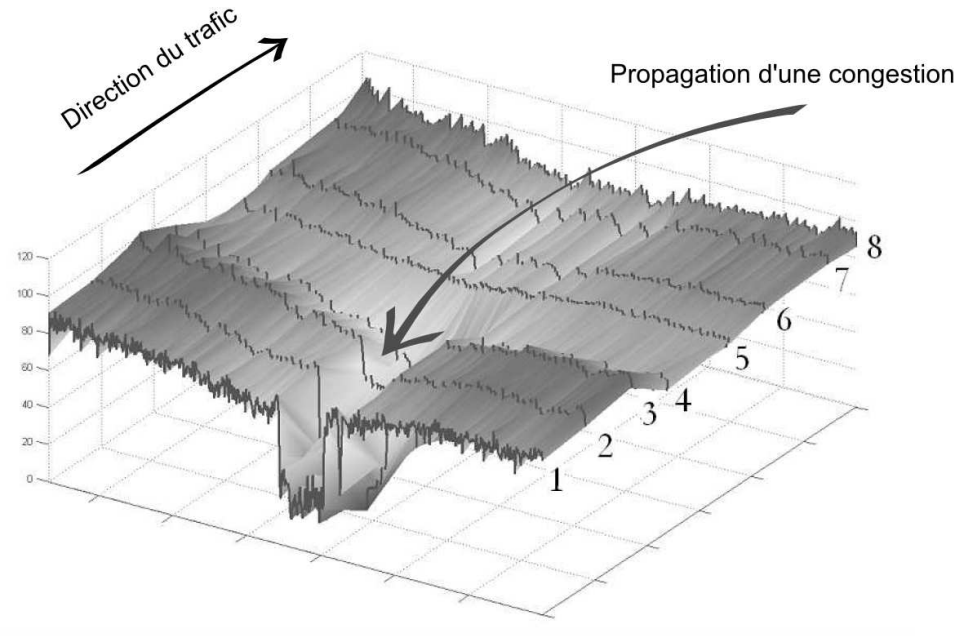

Figure 5: Diagramme des séries temporelles de vitesse pour les 8 boucles présentes sur les voies principales.

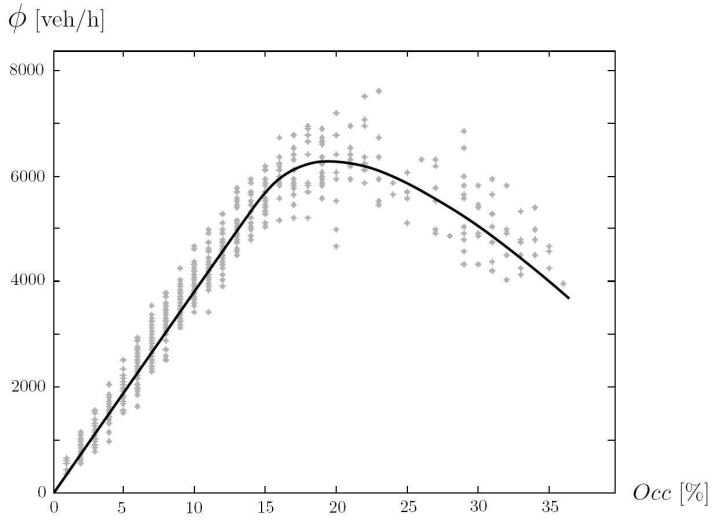

Figure 6: Exemple de diagramme fondamental.

sions analytiques possibles de ce type de diagramme sont par exemple celles données par les flux de Greenshield (GS) et Greenberg (GB) [Pipes, 1967]

$$\Phi_{\mathrm{GS}}(\rho) = \rho.v_{\mathrm{f}} - \frac{\rho^2.v_{\mathrm{f}}}{\rho_{\mathrm{m}}} \qquad \Phi_{\mathrm{GB}}(\rho) = \rho.v_{\mathrm{f}} \ln\left(\frac{\rho_{\mathrm{m}}}{\rho}\right)$$

où v_{f} est la vitesse libre observée lorsqu'il n'y a pas de congestion et ρ_{m} est la densité maximale, définissant la capacité de stockage d'une section d'autoroute. En notant x la variable spatiale, le principe de conservation des véhicules s'écrit pour tout intervalle (x_L, x_R)

$$\begin{gathered}\text{Evolution du nombre de voitures dans } (x_L, x_R) \\ = \\ \textstyle\sum \text{Flux entrant en } x_L - \sum \text{Flux sortant en } x_R\end{gathered}$$

Quelques manipulations élémentaires donnent le modèle LWR décrit par

$$\partial_t \rho + \partial_x \Phi(\rho) = 0 \tag{LWR}$$

Cette équation appartient à la classe des équations aux dérivées partielles appelée *lois de conservation*. Elles ont été abondamment étudiées dans la littérature mathématique [Hopf, 1950; Lax, 1957; Kružkov, 1970; Bardos et al., 1979; LeFloch, 2002] et leurs solutions sont connues pour développer des irrégularités appelées ondes de choc. De plus, les résultats d'existence et d'unicité pour (LWR) donnés dans [Kružkov, 1970] sont obtenus dans l'espace BV des fonctions à variations bornées [Evans, 1998], qui est une variation de l'espace des fonctions C^1 par morceaux. Les discontinuités, aussi appelées ondes de choc et notées $x = s(t)$, se propagent à une vitesse vérifiant la condition de Rankine-Hugoniot [LeVeque, 1992]

$$\dot{s}_i(t)[\rho(s_i(t), t)] = [\Phi\rho(s_i(t), t))] \tag{RH}$$

avec $[\rho(s_i(t),t)] = \rho^+{}_{|_{x=s_i(t)}} - \rho^-{}_{|_{x=s_i(t)}} = \lim_{x\downarrow s_i(t)} \rho(x,t) - \lim_{x\uparrow s_i(t)} \rho(x,t)$ le saut de densité à $x = s_i(t)$. Par ailleurs, seules les discontinuités vérifiant la condition d'entropie de Lax [Lax, 1973]

$$\Phi'\left(\rho^-{}_{|_{x=s_i(t)}}\right) \;>\; \dot{s}_i(t) \;>\; \Phi'\left(\rho^+{}_{|_{x=s_i(t)}}\right) \tag{L}$$

sont admissibles. Les équations (RH) et (L) fournissent donc des informations pertinentes qui caractérisent les solutions de (LWR).

Lorsque l'on considère un problème avec des conditions aux limites de la forme

$$\begin{cases} \partial_t \rho + \partial_x \Phi(\rho) = g(x,\rho,u) \\ \rho(x,0) = \rho_I(x) \\ \rho(0,t) = \rho_0(t) \text{ and } \rho(L,t) = \rho_L(t) \end{cases}$$

le seul résultat d'existence et d'unicité de la solution, donné dans [Bardos et al., 1979], stipule que les traces $\rho(0,t)$ et $\rho(L,t)$ de la solution aux frontières vérifient

$$\begin{array}{ll} \sup_{k\in I(\rho(0,t),\rho_0(t))} & \operatorname{sign}\big(\rho(0,t)-\rho_0(t)\big)\big(\Phi(\rho(0,t))-\Phi(k)\big) = 0 \\ \inf_{k\in I(\rho(L,t),\rho_L(t))} & \operatorname{sign}(\rho(L,t)-\rho_L(t))\big(\Phi(\rho(L,t))-\Phi(k)\big) = 0 \end{array} \tag{BLN}$$

avec $I(a,b) = (\min(a,b), \max(a,b))$. Dans l'hypothèse où $\Phi(\rho)$ est concave, ce qui est en général le cas [Pipes, 1967], il est possible d'expliciter ces conditions (BLN) de diverses manières. Pour la condition amont (la condition aval se comportant de façon similaire), les formulations suivantes ont été proposées :

1. La formulation de LeFloch [LeFloch, 1988]

$$\begin{cases} \rho(0,t) = \rho_0(t) \text{ et } \Phi'(\rho_0(t)) \geq 0 \quad \text{ou} \\ \Phi'(\rho(0,t)) \leq 0 \text{ et } \Phi'(\rho_0(t)) \leq 0 \quad \text{ou} \\ \Phi'(\rho(0,t)) \leq 0, \Phi'(\rho_0(t)) \geq 0 \text{ et } \Phi(\rho_0(t)) \geq \Phi(\rho(0,t)) \end{cases}$$

2. La formulation d'Osher [Osher, 1984]

$$\phi_0(t) = \begin{cases} \inf_{k\in[\rho_0(t),\rho_I(0,t)]} & \Phi(k) & \text{si } \rho_0(t) \leq \rho_I(0,t) \\ \sup_{k\in[\rho_I(0,t),\rho_0(t)]} & \Phi(k) & \text{si } \rho_I(0,t) < \rho_0(t) \end{cases}$$

   avec $\phi_0(t)$ le flux au niveau de la frontière amont.

3. La formulation de Lebacque [Lebacque, 1996]

$$\phi_0(t) = \min\Big\{D(\rho_0(t)), S(\rho_I(0,t))\Big\}$$

   avec les fonctions d'offre et de demande données respectivement par

$$D(\rho) = \begin{cases} \Phi(\rho) & \text{si } \Phi'(\rho) > 0 \\ \Phi_m & \text{si } \Phi'(\rho) \leq 0 \end{cases} \qquad S(\rho) = \begin{cases} \Phi(\rho) & \text{if } \Phi'(\rho) < 0 \\ \Phi_m & \text{if } \Phi'(\rho) \geq 0 \end{cases}$$

   où $\Phi_m = \max \Phi(\cdot)$.

Le traitement des inhomogénéités (Figure 7) comme les rampes d'accès, les rampes de sortie et les variations brutales de paramètres (changement du nombre de voies ou de la limitation de vitesse) est plus compliqué. Ces éléments ponctuels donnent lieu à des

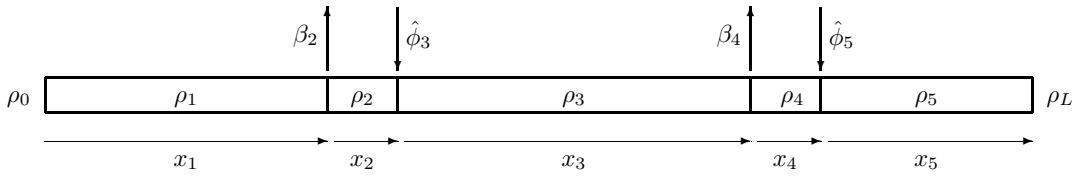

Figure 7: Section d'autoroute avec entrées et sorties.

conditions d'interface qui peuvent être vues comme la combinaison de deux conditions aux limites, avec un couplage dont la causalité reste à définir. Les deux hypothèses naturelles s'appliquant aux interfaces sont :

1. Les conditions (BLN) s'appliquent à gauche et à droite des inhomogénéités.
2. La conservation du flux doit être assurée.

Il est connu que ces conditions ne sont cependant pas suffisantes pour rendre le problème bien posé car elles ne permettent pas d'obtenir une solution unique. Nous proposons dans cette thèse une condition d'entropie pour les interfaces qui s'écrit

$$\Phi'_L(\rho_L) > 0 \qquad \text{ou} \qquad \Phi'_R(\rho_R) \leq 0 \qquad \text{ou les deux}$$

les indices L et R se rapportant respectivement aux grandeurs définies à gauche et à droite. Cette condition permet en particulier de déterminer la solution analytique du problème prototype de Riemann, i.e. avec une condition initiale constante par morceau. Elle est identique à l'hypothèse de maximisation du flux d'interface qui est en général utilisée dans cette situation, et qui peut sembler plus ou moins arbitraire au premier abord.

Nous proposons également une interprétation hybride du comportement des rampes d'accès et de sortie, cette interprétation étant issue de la résolution méthodique du problème de Riemann correspondant. Par exemple, dans le cas d'une rampe d'accès avec un flux $\hat{\phi}(t)$ vérifiant $\hat{\phi}(t) < S(\rho_R(t))$, les 3 états discrets relatifs à son statut sont :

1. **Libre (F)**: $\rho_R(t) = \Phi^{-l}\big(\Phi(\rho_L(t)) + \hat{\phi}(t)\big)$ avec $\Phi^{-l}(\cdot)$ l'inverse à gauche de $\Phi(\cdot)$.
2. **Congestionné (C)**: $\rho_L(t) = \Phi^{-r}\big(\Phi(\rho_R(t)) - \hat{\phi}(t)\big)$ avec $\Phi^{-r}(\cdot)$ l'inverse à droite.
3. **Découplé (D)**: $\rho_R(t) = \rho_c$ et $\rho_L(t) = \Phi^{-r}\big(\Phi_m - \hat{\phi}(t)\big)$.

On peut prouver que l'interface suit la machine d'état donnée en Figure 8. L'un des intérêts de cette formulation est d'expliciter la causalité dans le transfert des conditions aux limites. La transition $\mathbf{F} \rightarrow \mathbf{D}$ s'opère lorsque

$$\Phi(\rho_L(t)) + \hat{\phi}_i > \Phi_m$$

et correspond à l'apparition d'un bouchon dû à un goulot d'étranglement.

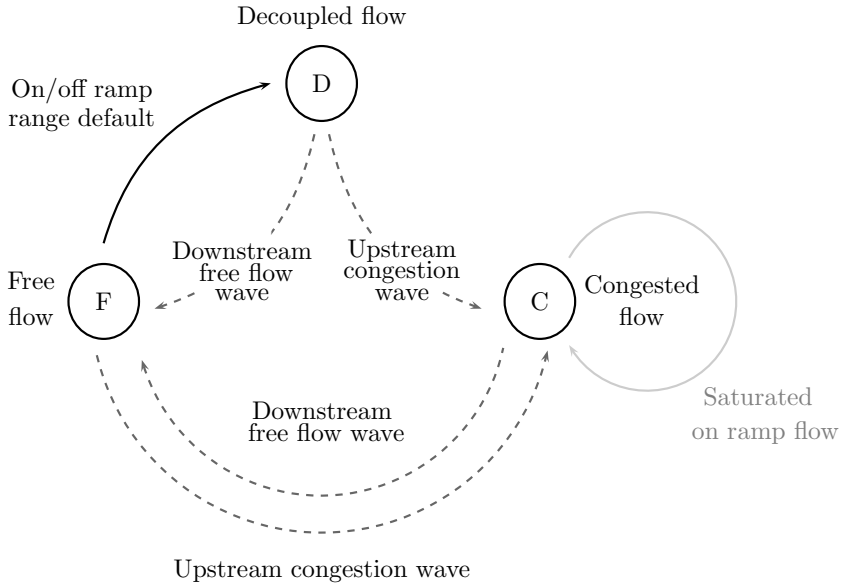

Figure 8: Machine d'état suivie par une interface avec rampe d'accès.

Le modèle ARZ

Le modèle ARZ proposé dans [Aw & Rascle, 2000; Zhang, 2002] s'écrit

$$\partial_t \begin{pmatrix} \rho \\ y \end{pmatrix} + \partial_x \underbrace{\begin{pmatrix} y + \Phi(\rho) \\ (y + \Phi(\rho))\frac{y}{\rho} \end{pmatrix}}_{F(\rho,y)} = \begin{pmatrix} 0 \\ -\frac{y}{\tau} \end{pmatrix} \tag{ARZ}$$

avec $y = \phi - \Phi(\rho)$ le flux relatif comme introduit dans [Mammar et al., 2005] et τ un paramètre de relaxation. L'intérêt de ce modèle est qu'il autorise des états du trafic qui ne sont pas nécessairement sur le diagramme fondamental, comme c'est le cas pour les données mesurées (Figure 6). De plus, les champs caractéristiques de (ARZ) ont pour vitesse d'onde $\lambda_1 = v + \rho V(\rho)$ et $\lambda_2 = v$, montrant bien l'anisotropie du modèle, toute perturbation se déplacant à une vitesse λ_1 ou λ_2 inférieure à celle du trafic. Un autre intérêt du modèle ARZ est qu'il est possible de calculer une solution analytique de son problème de Riemann, comme cela a été montré dans [Aw & Rascle, 2000; Lebacque et al., 2005].

Selon [Dubois & LeFloch, 1988; Joseph & LeFloch, 1999], la condition aux limites en $x = 0$ du modèle ARZ doit vérifier

$$\mathbf{u}(0,t) \in \mathcal{V}_{\text{up}}(\mathbf{u}_{\text{up}}(t)) = \left\{ w(0+, \mathbf{u}_{\text{up}}(t), \mathbf{u}) : \mathbf{u} \in \mathbb{R}^2_+ \right\}$$

avec $w(x/t, \mathbf{u}_{\text{up}}(t), \mathbf{u})$ la solution du problème de Riemann avec les états $\mathbf{u}_{\text{up}}(t)$ et $\mathbf{u}$ respectivement à gauche et à droite. Pour calculer les ensembles $\mathcal{V}_{\text{up}}(\mathbf{u}_{\text{up}}(t))$, il faut considérer les cinq configurations possibles de la solution du problème de Riemann, identifiées par l'onde présente dans le champ "vraiment non linéaire" [Serre, 1996]: choc se déplaçant en avant, onde de raréfaction se déplaçant en avant, choc se déplaçant

en arrière, onde de raréfaction se déplaçant en arrière et raréfaction sonique. Nous déterminons dans cette thèse les ensembles $\mathcal{V}_{\text{up}}(\mathbf{u}_{\text{up}}(t))$ en fonction de $\mathbf{u}_{\text{up}}(t)$.

Dans le cas inhomogène, [Lebacque et al., 2005] propose une formulation offre/demande ingénieuse sous la forme d'un diagramme fondamental translaté lorsque des inhomogénéités apparaissent dans les paramètres du modèle ARZ. Cette approche peut être étendue au cas des rampes d'entrée et de sortie. Comme pour le modèle LWR, nous proposons une formulation hybride des conditions d'interface correspondantes.

Le modèle MOD

Le modèle MOD [Zhang & Jin, 2002; Lebacque & Khoshyaran, 2002; Jin & Zhang, 2004] pour "Multiclass Origin-Destination" s'écrit

$$\partial_t \boldsymbol{\rho} + \partial_x \Big(\boldsymbol{\rho}\, V\left(|\boldsymbol{\rho}|\right) \Big) = 0 \tag{MOD}$$

avec $\boldsymbol{\rho} = (\rho_1, ..., \rho_{N_R})^T$ le vecteur des densités désagrégées par route et $V(\rho)$ le même diagramme de vitesse que pour le modèle LWR. Les vitesses caractéristiques de (MOD) sont données par [Zhang & Jin, 2002]

$$\begin{cases} \lambda_1(\boldsymbol{\rho}) & = & V(|\boldsymbol{\rho}|) \\ \quad \vdots & & \quad \vdots \\ \lambda_{N_R-1}(\boldsymbol{\rho}) & = & V(|\boldsymbol{\rho}|) \\ \lambda_{N_R}(\boldsymbol{\rho}) & = & V(|\boldsymbol{\rho}|) + |\boldsymbol{\rho}| V'(|\boldsymbol{\rho}|) \end{cases}$$

montrant que le modèle est anisotrope et que seul le N_R-champ qui est "vraiment non linéaire" [Serre, 1996] peut générer des ondes se propageant à des vitesses négatives.

Les conditions aux limites sont traitées de façon similaire au cas du modèle ARZ et les ensembles $\mathcal{V}_{\text{up}}(\mathbf{u}_{\text{up}}(t))$ sont déterminés dans cette thèse.

Le traitement des rampes d'accès et de sortie est un peu plus compliqué pour le modèle MOD en raison des différences de taille entre les systèmes interconnectés. En considérant une rampe d'accès du même type que celle représentée en Figure 9, les principes de conservation du flux s'écrivent

$$\begin{cases} \phi_{R_1}^{L_1} = \phi_{R_1}^{L_2} \\ \phi_{R_2}^{L_2} = \hat{\phi} \end{cases}$$

De plus, en considérant que le diagramme de flux s'applique à l'interface, on obtient

$$\begin{cases} \phi_{R_1}^{L_1} = \Phi(\rho_{R_1}^{L_1}) = \rho_{R_1}^{L_1} V(\rho_{R_1}^{L_1}) \\ \phi_{R_1}^{L_2} = \rho_{R_1}^{L_2} V(\rho_{R_1}^{L_2} + \rho_{R_2}^{L_2}) \\ \phi_{R_2}^{L_2} = \rho_{R_2}^{L_2} V(\rho_{R_1}^{L_2} + \rho_{R_2}^{L_2}) \end{cases}$$

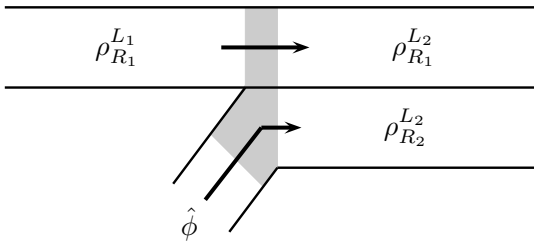

Figure 9: Exemple de rampe d'accès pour le modèle MOD.

Une série de manipulation analytique de ces équations fournit des contraintes pour les variables $\phi_{R_1}^{L_2}$, $\phi_{R_1}^{L_2}$, $\phi_{R_1}^{L_1}$ et $|\rho^{L_2}|$. Il est alors possible de montrer que les interfaces ayant des rampes d'accès ou de sortie suivent une machine d'état similaire aux modèles LWR et ARZ.

Méthodes numériques

De nombreux schémas numériques sont proposés dans la littérature pour simuler les modèles LWR, ARZ et MOD. Nous utilisons dans cette thèse les schémas de type Godunov [Godunov, 1959; LeVeque, 1992] qui sont réputés performants. Parmi les schémas proposés dans la littérature, citons [Daganzo, 1994; Lebacque, 1996] et [Lebacque et al., 2005] qui permettent respectivement de simuler les modèles LWR et ARZ, et ce même en présence d'inhomogénéités dans les paramètres. Ces schémas ont été validés en simulation sur des données réelles provenant du périphérique sud-est de Lyon en utilisant la méthode offre/demande et la formulation sous forme d'automate hybride.

Sur la commande optimale des lois de conservation

Nous proposons dans cette thèse d'étendre la méthode adjointe développée dans [Lions, 1971] pour la commande optimale des équations aux dérivées partielles aux flots irréguliers générés par des lois de conservation. Cette méthode reposant sur une formule d'intégration par parties, nous prouvons le théorème suivant qui s'applique aux champs C^1 par morceaux et BV.

Théorème 1 *Soit $\Omega \subset \mathbb{R}^2$ avec les composantes (x,t) un domaine ouvert et borné de frontière $\partial\Omega$ Lipschitzienne et ayant ν pour normale unitaire, et soit $u = (u_1, u_2)$ une fonction $BV(\Omega, \mathbb{R}^2)$ ou C^1 par morceaux avec N_s singularités Lipschitziennes notées $\Gamma_i \subset \Omega$ et paramétrées par $\Gamma_i = \{(x,t) : x = s_i(t),\ t \in [t_i^I, t_i^F]\}$. Alors , pour toute fonction $\phi \in C^1(\mathbb{R}^2)$, la formule suivante d'intégration par parties est vérifiée*

$$\int_\Omega u \cdot \nabla\phi \ \mathrm{d}\mathcal{L}^2 = -\int_{\Omega\setminus\cup_i\Gamma_i} \phi \ \mathrm{div} u \ \mathrm{d}\mathcal{L}^2 + \int_{\partial\Omega} u\cdot\nu \ \phi \ \mathrm{d}\mathcal{H}^1 + \sum_{i=1}^{N_s} \int_{t_i^I}^{t_i^F} \dot{s}_i(t)[u_2\phi]_{|_{x=s_i(t)}} - [u_1\phi]_{|_{x=s_i(t)}} dt$$

où $\mathcal{L}^2$ représente la mesure de Lebesgue de dimension 2 et $\mathcal{H}^1$ la mesure de Hausdorff de dimension 1.

Le problème de commande optimale que nous traitons est de la forme

$$\begin{aligned}
\underset{y_I,u}{\textbf{Min}} \quad \mathcal{J}(y,s,u) &= \mathcal{J}_{\text{obs}}(y) + \mathcal{J}_{\text{s}}(s) + \mathcal{J}_{\text{bar}}(u) \\
&= \textstyle\int_\Omega \mathcal{P}(y(x,t))\,\mathrm{d}x\mathrm{d}t + \sum_{i=1}^{N_s} \int_{t_i}^{T} \mathcal{Q}_i(s_i(t))\,\mathrm{d}t + \int_0^T \mathcal{R}(u(t))\,\mathrm{d}t
\end{aligned}$$

$$\textbf{Avec} \quad \begin{cases}
\partial_t y + \partial_x f(y) = g(x,y,u) \\
y(x,t=0) = y_I(x) \\
y(0,t) \sim y_0(t) \text{ et } y(L,t) \sim y_L(t) \\
y_I \in BV(\mathbb{R}) \text{ et } u \in \mathcal{U}_{\text{ad}}
\end{cases}$$

où $\mathcal{J}_{\text{obs}}(y)$ sert à influencer l'état distribué y, $\mathcal{J}_{\text{s}}(s)$ sert à influencer la position des ondes de choc s et $\mathcal{J}_{\text{bar}}(u)$ sert à contrôler la valeur de commande $u = (u_1, ..., u_{N_u})$ et à la restreindre par des méthodes de barrière [Boyd & Vandenberghe, 2004] à l'ensemble convexe admissible $\mathcal{U}_{\text{ad}}$. Les conditions aux limites s'appliquent au sens faible et ne sont pas toujours actives, d'où l'utilisation du symbole $\sim$.

Nous prouvons alors le théorème suivant:

Théorème 2 *L'équation linéarisée autour de la trajectoire de référence $(\bar{y}, \bar{u})$ donnée par*

$$\begin{cases}
\partial_t \tilde{y} + \partial_x\big(f'(\bar{y})\tilde{y}\big) = \partial_y g(x,\bar{y},\bar{u})\tilde{y} + \partial_u g(x,\bar{y},\bar{u})\tilde{u} \\
\tilde{y}(0,x) = \tilde{y}_I \\
\tilde{y}(t,0) = 0 \text{ et } \tilde{y}(t,L) = 0
\end{cases}$$

dans $\Omega = (0;L) \times (0,T)$ a une solution faible unique dans l'espace des mesures qui est donnée par la formule

$$\tilde{y} = \tilde{y}_s + \sum_{i=1}^{N_s} \kappa_i \delta_{\Gamma_i}$$

avec $\Gamma_i = \{(\bar{s}_i(t), t) : t \in [t_i^I, T]\}$ les N_s ondes de choc présentent dans $\bar{y}$, $\tilde{y}_s$ la solution forte définie dans $\Omega \backslash \cup_i \Gamma_i$ de l'équation aux dérivées partielles

$$\begin{cases}
\partial_t \tilde{y}_s + \partial_x\big(f'(\bar{y})\tilde{y}_s\big) = \partial_y g(x,\bar{y},\bar{u})\tilde{y}_s + \partial_u g(x,\bar{y},\bar{u})\tilde{u} \\
\tilde{y}_s|_{t=0} = \tilde{y}_I \\
\tilde{y}_s|_{x=0} = 0 \quad \text{et} \quad \tilde{y}_s|_{x=L} = 0
\end{cases}$$

et κ_i, pour $i = \{1, \ldots, N_s\}$ la solution de l'équation différentielle ordinaire

$$\begin{cases}
\frac{d\kappa_i}{dt} = \kappa_i \partial_y g(x,\bar{y},\bar{u})_{|_{x=\bar{s}_i(t)}} - [f'(\bar{y})\tilde{y}_s]_{|_{x=\bar{s}_i(t)}} + \dot{\bar{s}}_i [\tilde{y}_s]_{|_{x=\bar{s}_i(t)}} \\
\kappa_i(t_i^I) = 0
\end{cases}$$

où κ_i est lié au déplacement infinitésimal $\tilde{s}_i$ du choc i par $\kappa_i = -\tilde{s}_i [\bar{y}]_{|_{x=\bar{s}_i(t)}}$.

En adoptant les notations

$$\begin{cases} \partial_t \tilde{y}_s + \partial_x \alpha(x,t)\tilde{y}_s = \beta(x,t)\tilde{y}_s + \gamma(x,t)\tilde{u} \\ \tilde{y}_s(x,0) = \tilde{y}_I,\ \tilde{y}_s(0,t) = 0 \text{ et } \tilde{y}_s(L,t) = 0 \\ \dot{\kappa}_i = \beta(\bar{s}_i(t),t)\kappa_i - [\alpha(\bar{s}_i(t),t)\tilde{y}_s(\bar{s}_i(t),t)] + \dot{\bar{s}}_i(t)[\tilde{y}_s(\bar{s}_i(t),t)] \\ \kappa_i(0) = 0 \end{cases}$$

pour la solution du problème linéarisé, nous en déduisons le théorème suivant:

Théorème 3 *Les gradients de $\mathcal{J}(y,s,u)$ par rapport aux variables de décision u et y_I autour de la trajectoire de référence $(\bar{y},\bar{u})$ sont donnés par*

$$\nabla_u \mathcal{J} = \mathcal{R}'(\bar{u}) + \int_0^L \gamma(x,t)\lambda(x,t)\mathrm{d}x$$
$$\nabla_{y_I} \mathcal{J} = \lambda(x,0)$$

avec λ la solution de

$$\begin{cases} \dot{\mu}_i = -\beta_{|_{x=\bar{s}_i(t)}}\mu_i + \frac{\mathcal{Q}_i'(\bar{s}_i)}{[\bar{y}]_{|_{x=\bar{s}_i(t)}}} \\ \mu(T) = 0 \\ \lambda^-{}_{|_{x=\bar{s}_i(t)}} = \lambda^+{}_{|_{x=\bar{s}_i(t)}} = \mu_i \\ -\partial_t\lambda - \alpha(x,t)\partial_x\lambda = \beta(x,t)\lambda + \mathcal{P}'(\bar{y}) \\ \lambda(x,T) = 0 \\ \lambda(0,t) = 0 \text{ et } \lambda(L,t) = 0 \end{cases}$$

Un résultat similaire est obtenu pour le cas des systèmes de lois de conservation. Cependant, il ne permet pas de prendre en compte la sensibilité par rapport aux discontinuités éventuellement présentes dans l'état.

Considérons à titre exemple le problème du contrôle d'accès pour un périphérique où les variables de décision sont les taux de modulation des feux tricolores sur les rampes d'accès, notés $u_i \in (0,1)$, $i = 1,...,N_u$. La distance totale voyagée étant un indicateur de la performance de l'infrastructure, nous considérons le problème de sa maximisation, noté

$$\textbf{Min}\ \ \mathcal{J}_{\mathrm{VMT}}(\phi) = -\int_0^T\int_0^L \phi(x,t)\ \mathrm{d}x\mathrm{d}t$$

auquel il faut ajouter le terme de barrière

$$\mathcal{J}_{\mathrm{bar}}(u) = -\frac{1}{M}\sum_{i=1}^{N_u}\int_0^T \ln\big(u_i(1-u_i)\big)\ \mathrm{d}t$$

pour chaque u_i afin de s'assurer que $u_i \in (0,1)$. Par ailleurs, le modèle LWR peut se mettre sous la forme compacte

$$\partial_t\rho + \partial_x\Phi(\rho) = \underbrace{\sum_{i=1}^{N_u}\delta_{\hat{x}_i}(x)\ u_i(t)\ \Psi_i(\rho(x,t)) - \sum_{j=1}^{N_\beta}\delta_{\check{x}_j}(x)\ \beta_j\ \Phi(\rho(x,t))}_{g(x,\rho,u)}$$

où $\Psi_i(\cdot)$ est une fonction de saturation qui vérifie

- $\Psi_i(\xi) = \bar{\phi}_i$ pour $\xi \in (0, \gamma)$, où $\bar{\phi}_i$ est le flux maximal à la rampe i,
- $\Psi_i'(\cdot) \leq 0$ pour $\xi \in (\gamma, \rho_m)$ étant donné que le flux d'entrée diminue avec la densité,
- $\Psi_i(\rho_m) = 0$ car aucun véhicule ne peut entrer à la densité maximale.

et limite le flux des rampes pour des valeurs élevées de la densité sur les voies principales. En utilisant les résultats que nous avons établis pour la commande optimale des lois de conservation, on peut montrer que

$$\nabla_u \mathcal{J} = \begin{pmatrix} -\Psi_1(\bar{\rho}(\cdot, \hat{x}_1))\ \lambda(\cdot, \hat{x}_1) - \frac{1}{M}\left(\frac{1}{\bar{u}_1} - \frac{1}{1-\bar{u}_1}\right) \\ \vdots \\ -\Psi_{N_u}(\bar{\rho}(\cdot, \hat{x}_{N_u}))\ \lambda(\cdot, \hat{x}_{N_u}) - \frac{1}{M}\left(\frac{1}{\bar{u}_{N_u}} - \frac{1}{1-\bar{u}_{N_u}}\right) \end{pmatrix}$$

où la variable adjointe λ est la solution de

$$\begin{cases} -\partial_t \lambda - \Phi'(\bar{\rho})\partial_x \lambda = \Phi'(\bar{\rho}) + \sum_{i=1}^{N_u} \delta_{\hat{x}_i} \bar{u}_i \Psi_i'(\bar{\rho})\lambda - \sum_{i=1}^{N_w} \delta_{\check{x}_i} \beta_i \Phi'(\bar{\rho})\lambda \\ \lambda(x, T) = 0 \\ \lambda(0, t) = 0 \text{ quand } \Phi'(\bar{\rho}(0, t)) < 0 \\ \lambda(L, t) = 0 \text{ quand } \Phi'(\bar{\rho}(L, t)) > 0 \\ \lambda_{|\Gamma_i} = 0 \text{ avec } \Gamma_i = \{(x, t) : [\bar{\rho}(x, t)] \neq 0\} \end{cases}$$

En utilisant un algorithme récursif tel que l'Algorithme 1 pour un problème avec trois rampes d'accès pouvant être contrôlées, nous obtenons les résultats présentés sur les Figures 3.1 et 3.2 qui montrent l'efficacité de la méthode. D'autres objectifs de commande ainsi que des objectifs d'estimation peuvent être traités en modifiant l'expression du critère $\mathcal{J}$. De même, cette méthode a été utilisée de manière similaire pour le modèle ARZ et pour le modèle MOD dans le cadre de l'estimation des données origines-destinations.

Sur la commande boucle fermée du modèle LWR

En utilisant les schémas de Godunov [Godunov, 1959] et de "Front Tracking" [Holden et al., 1988], il est possible de mettre le modèle LWR sous la forme

$$\begin{cases} \rho_{k+1} = A_{\alpha_k}\rho_k + B_{\alpha_k}u_k + W_{\alpha_k}w_k + a_{\alpha_k} \\ \alpha_k = g(\rho_k, u_k, w_k) \\ \rho_{k=0} = \rho_0 \quad \text{et} \quad \alpha_{k=0} = \alpha_0 \end{cases}$$

où k est le temps, $\alpha_k \in \mathcal{I} = \{1, ..., h\}$ est un signal discret, $\rho_k \in \mathbb{R}^n$ l'état du système, $u_k \in \mathbb{R}^m$ la variable de contrôle (taux de modulation feux tricolores), $w_k \in \mathbb{R}^p$ un signal exogène connu de façon incertaine, et $g(\rho_k, u_k, w_k)$ une loi de commutation. Un

Algorithm 1 Algorithme de descente du gradient avec fonction barrière.

Require: $\bar{u} := u^{\text{init}} \in (0,1)$, $\bar{y}_I = y_I^{\text{init}}$, $\epsilon > 0$

  while $|\nabla_u \mathcal{J} + \nabla_{y_I} \mathcal{J}| > \epsilon$ **do**

    Résoudre le problème LWR avec $\bar{y}$ with $\bar{u}$ and $\bar{y}_I$

    Calculer μ_i et λ solutions de l'équation adjointe

    Calculer $\tilde{u} = -\nabla_u \mathcal{J}$ à l'aide de la formule de gradient

    Mettre à jour la commande avec $\bar{u} := \bar{u} + t_1 \tilde{u}$ tel que $u \in (0,1)$

  end while

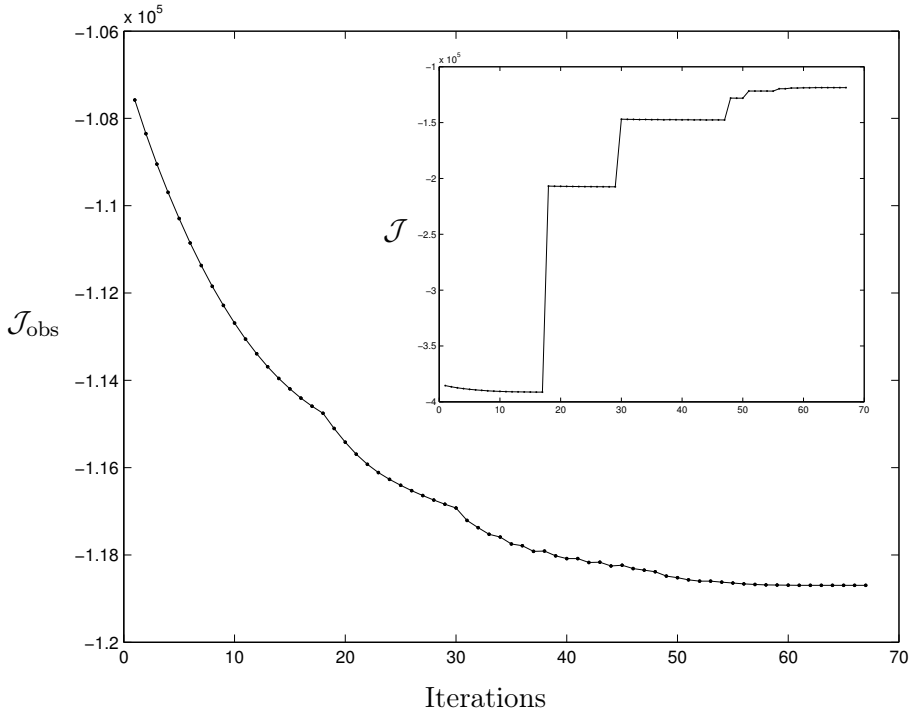

Figure 3.1: Décroissance des coûts $\mathcal{J}_{\text{obs}}$ et $\mathcal{J}$.

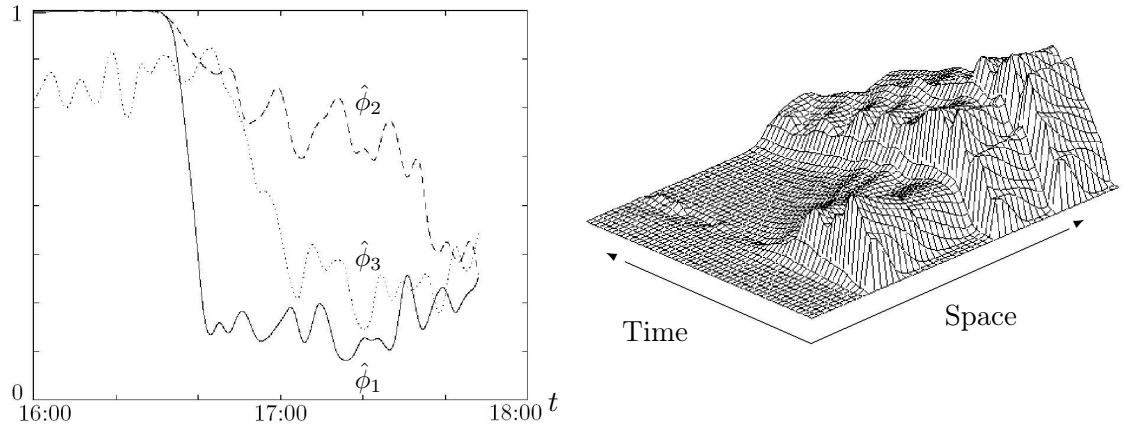

Figure 3.2: Contrôle d'accès optimal et distribution de l'amélioration du flux.

tel modèle, qui appartient à la famille des systèmes dits affines par morceaux ou PWA (pour PieceWise Affine), a déjà été étudiée dans la communauté du contrôle [Johansson & Rantzer, 1998; Ferrari-Trecate et al., 2002]. Nous montrons qu'il est possible, pour ces systèmes, d'associer une Inégalité Matricielle Linéaire (LMI) aux objectifs de contrôle suivants :

- la stabilisation,
- la stabilisation avec terme intégral,
- le rejet de perturbation $\mathcal{H}_\infty$,
- la commande à coût quadratique garantie,

Nous appliquons cette méthode au problème de contrôle d'accès et interprétons les résultats obtenus par rapport à l'état de l'art de ce type de pratique.

Perspective

Les travaux présentés dans cette thèse permettent de mieux comprendre la dynamique du trafic et proposent des méthodes génériques de commande et d'observation pour les problèmes de gestion du trafic. Cependant, les outils développés se présentent sous une forme académique et nécessitent encore un travail assez conséquent pour les rendre opérationnels dans les années à venir.

Part I

Macroscopic Freeway Traffic Models

A poem is never finished, only abandoned.

Paul Valéry (1871-1945),
French author and Symbolist poet.

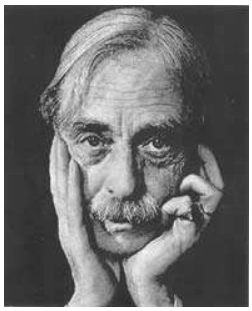

Chapter 1

A Primer to Freeway Modelling and Control

Intelligent transportation systems for freeways

In developed countries, increased travel time in congested sections a have dramatic economic impact. For instance, the 2004 Urban Mobility Report [Schrank & Lomax, 2004] reports an equivalent monetary cost of $63.2 billion in 2002 due to congestions in USA with a calculated 3.5 billion hours of delay and 5.7 billion gallons of wasted fuel. Similarly, the Bureau of Transportation Statistics (BTS), U.S. Department of Transportation, claims that the single city of Los Angeles, which is one of the most congested area in the world, suffered in 2001 of $12,837 millions of equivalent highway congestion cost with 52 hours of delay per person and 996 millions wasted fuel gallons.

As a partial response to the spread of congestion, Intelligent Transportation Systems (ITS) have emerged in the $80's$ and use recent advances in modelling, decision science and information technologies to enhance the infrastructure efficiency while preserving safety and to inform the users. ITS applications such as dynamic route guidance with variable message panel, adaptive intersection traffic light sequencing and travel time prediction, are now common in developed countries and have shown their efficiency.

This book is focused on freeway management application and do not treat the urban case. After several failed attempts to equip vehicles with additional devices to develop new traffic management strategies, it is commonly accepted that the infrastructure usage should be optimized first through non-invasive methods. Freeway systems are usually centrally monitored by a so-called Traffic Control Centers that informs authorities about possible accidents and take decisions about possible deviations using variable message panel. These Traffic Control Centers gets more and more sophisticated as shown on Figure 1.1 where monitoring panels can managed hundreds of real-time videos and thousands of traffic measurements along freeways.

Interesting freeway control applications such as ramp metering still requires some development and it is a remarkable fact that control theory just begins to be used in

Figure 1.1: Panels of the traffic control centre of Rhoon, Netherlands.

this strategic field. Ramp metering consists in controlling the flow of vehicles allowed to enter the freeway at on-ramps by using traffic lights. This tool is already functioning in some states in USA as in California and Minnesota as well as in Netherlands and UK. Though local and static, existing installations have proven to improve freeway operation by influencing the traffic both in time and space. Considering the well-known spatial dependencies acting in freeways, it is reasonable to assume that the maximum benefits can only be attained by traffic responsive and coordinated strategy that uses all of the available data to compute the metering rates. For an immediate implementation, this information can be obtained from inductive loops detectors embedded under the pavement as shown on Figure 1.2.

Figure 1.3, which is an abstraction of the ramp metering setting introduced in Figure 1.2, clearly shows the system-sensor-actuator paradigm familiar in control theory. As shown in Figure 1.3, the freeway system can be modelled by macroscopic traffic models that may be either continuous or discrete. Based on such a model, the ramp metering design problem consists in computing a controller that fulfils some specified control objectives such that the trajectory optimality or the robust tracking of a predefined reference.

Available measurements in traffic engineering

One of the main goals of traffic engineers is to observe the flow of vehicles along freeways and to determine some patterns that appear to be repeated. Based on these experimental evidences, they then look for a rational explanation and try to develop mathematical models the reproduce the observed phenomena with reasonable accuracy.

Since the 70', this methodology is facilitated by the wide spread of magnetic loop detectors that measure at given locations the traffic flow [veh/h], the local average velocity [km/h] and the local vehicle occupancy [%], which is related to the vehicle density [veh/km] through the average vehicle length. A picture of such a magnetic loop sensor is given in Figure 1.4. Nevertheless, the reliability of these loop detectors is discutable. Most of installed detectors around the world are single loops that cannot measure the velocity (contrary to newer double loops) and the occupancy measurement requires an accurate calibration which often lead to some biases. Moreover, the oldness of many

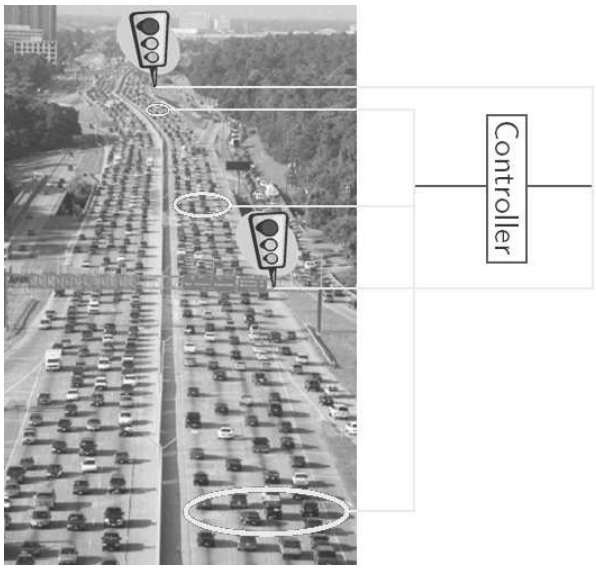

Figure 1.2: Principle of traffic responsive and coordinated ramp metering.

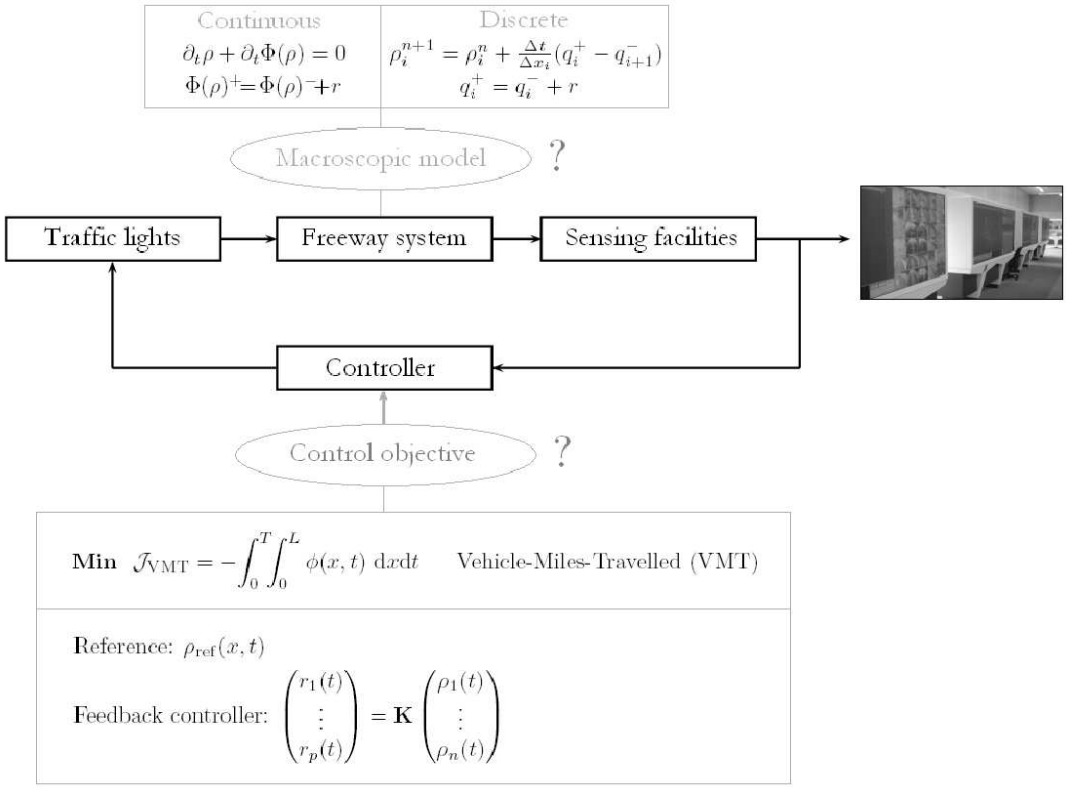

Figure 1.3: System-sensor-actuator control paradigm for freeway systems.

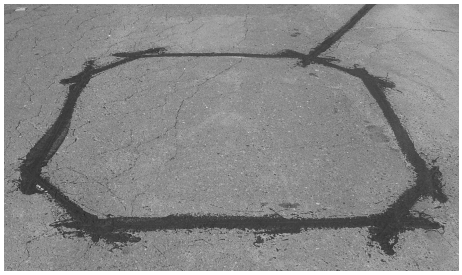

Figure 1.4: Loop detector buried under the roadway.

installations and repetitive work activities on the pavement lead to a high proportion of malfunctioning detectors, and thus to erroneous measurements. For instance, the Performance Measurement System (website at http://pems.eecs.berkeley.edu), which records all the loop detector data in the entire state of California, reports an average 20 % of malfunctioning sensors. This constatation highlights the need of robust methods when designing traffic control algorithms that relies on the loop measurements.

Figure 1.5 gives an example of the configuration of these loop detectors on the South-Est beltway of Lyon, France along with a velocity time series for one of them.

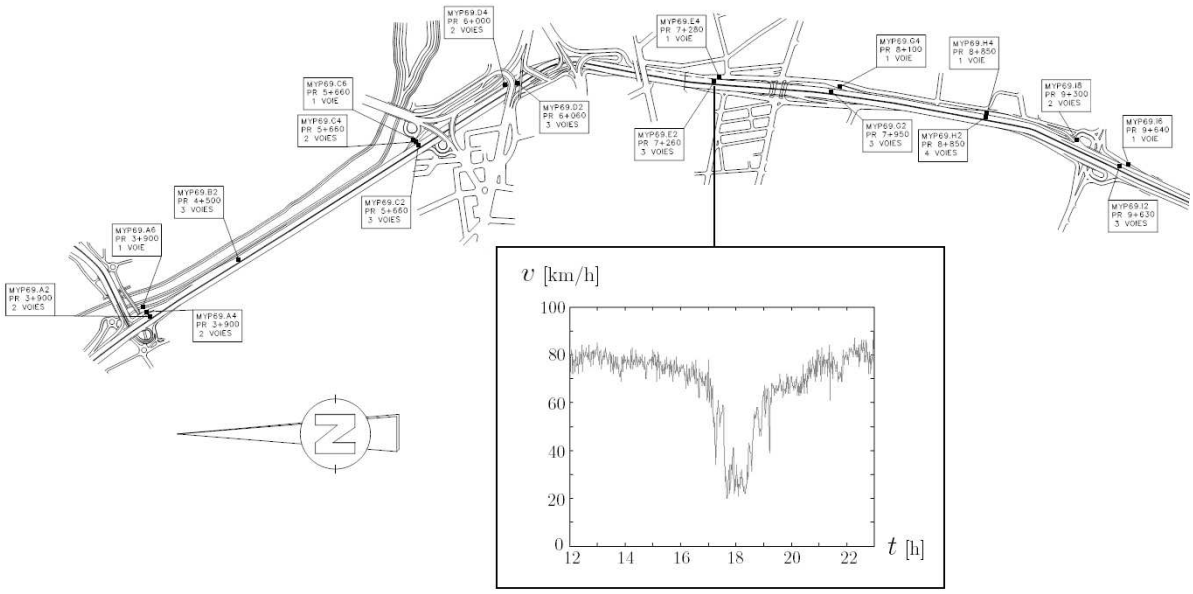

Figure 1.5: Configuration of the loop detectors on the South-Est beltway of Lyon, France. The black labelled boxes are the sensor locations and the plot shows the velocity time series of a senor on October 18th, 2005 between 12:00 and 23:00. The velocity drop around 18:00 comes form a congestion in the afternoon rush hours.

Concerning these experimental data, a phenomenological finding of historical importance is the existence of a relationship between the density ρ [veh/km] and the flow ϕ [veh/h] at a given location. An example of this relation, called the fundamental diagram [Pipes, 1967] in traffic engineering, is given in Figure 1.6 with the same sensor data as

the one used in Figure 1.5. This fundamental diagram is an important feature of freeway

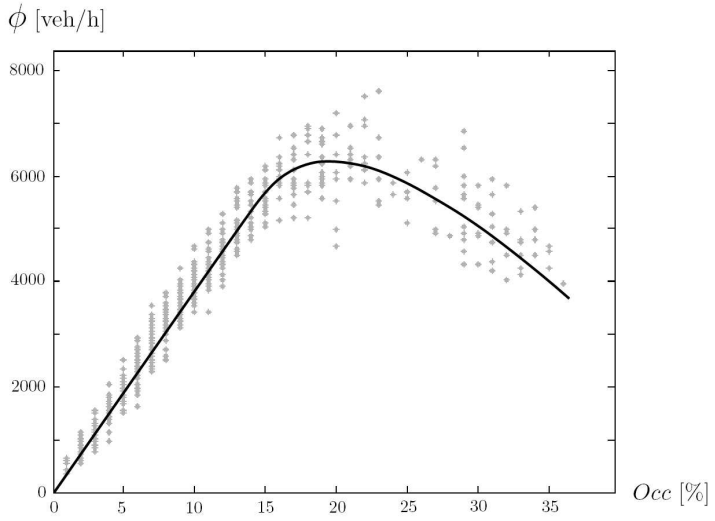

Figure 1.6: Example of a fundamental diagram with field data.

traffic theory as it was at the origin of the first traffic flow model proposed by Lighthill, Whitham [Lighthill & Whitham, 1955] and Richards [Richards, 1956]. Freeway traffic modelling has been a very active research field since then and there has been several contributions in microscopic, macroscopic and mesoscopic modelling.

Modelling issues in traffic engineering

This thesis only deals with macroscopic models, which are more adapted for the design of freeway management algorithms given the size of the system. Beside modelling traffic propagation and congestion waves, one of the most important feature that should be reproduced by these models is the capacity, which is the maximal admissible flow at a given location. For instance, based on the field data of Figure 1.6, the capacity at this sensor location is given by the maximum value of the fundamental diagram. This capacity, which is around 6500 veh/h for 3 lanes in Figure 1.6, is reached at an important traffic state called the critical density, which is around 18% occupancy in Figure 1.6. An other important modelling issue concerns on and off ramps where complicated dynamical behaviors have been observed such as the onset of congestions and their backward propagation, the capacity drop due to vehicle acceleration, the instantaneous breakdown phenomena and the off-ramp queue spillback.

Macroscopic freeway models in the form of conservation laws have the property to generate and propagate discontinuities. This feature, which is not classical in partial differential equations, has been empirically observed as reported on Figure 1.7 with the data from the South-Est beltway of Lyon, France. Note the backward propagation of the congestion after its birth (black dot and connected line) and the forward propagation of the free flow wave that removes the congestion (line without dot).

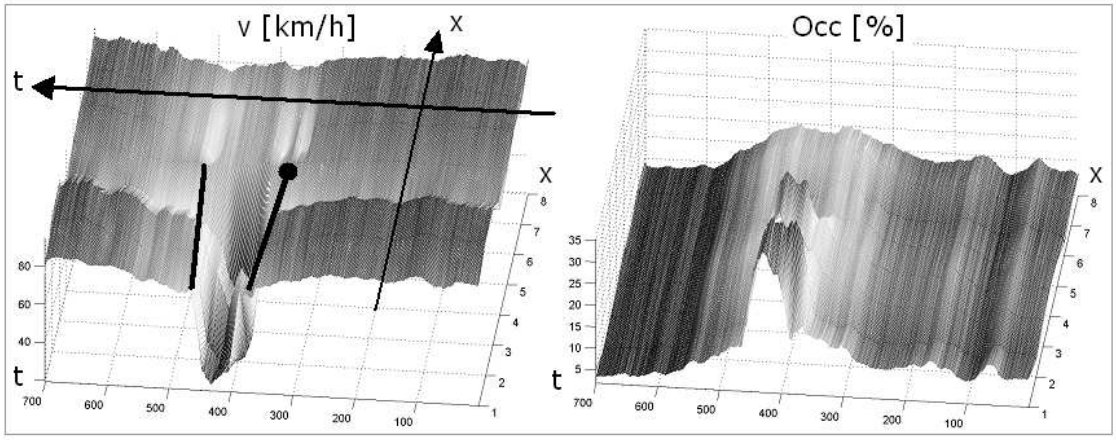

Figure 1.7: Experimental evidence of shock waves and backward propagation.

State of the art in freeway modelling

Concerning freeway models, Lighthill, Whitham [Lighthill & Whitham, 1955] and Richards [Richards, 1956] were the firsts to propose in the 50's a scalar partial differential equation to model crowed roads using an equilibrium flux function known as the fundamental diagram [Pipes, 1967]. This model being a scalar conservation law, the behavior of its solution is well understood [Whitham, 1974; Lax, 1973], even in the presence of boundary conditions [Bardos et al., 1979] and inhomogeneities in its parameters [Lebacque, 1996]. Moreover, several numerical schemes may be used as the Godunov scheme [LeVeque, 1992; Lebacque, 1996].

Many developments have been proposed since then. Payne proposed in [Payne, 1971] a non-equilibrium model that allows the traffic to deviate from the fundamental diagram as observed on field measurements. Based on the criticism of Daganzo in [Daganzo, 1995*b*] due to the presence of wave moving faster than the traffic in this model, Aw-Rascle [Aw & Rascle, 2000] and Zhang [Zhang, 2002] proposed independently a 2-equation model that corrects these deficiencies. The addition of a relaxation term in this model can be found in [Greenberg, 2001] and its connection with a microscopic model in [Aw et al., 2002].

A possible extension to the LWR model is to split the vehicle flow in partial flows, each of them being related to a specific vehicle class as proposed in [Lebacque, 1996], [Zhang & Jin, 2002] and [Gavage & Colombo, 2003] and [Wong & Wong, 2002]. An interesting example is to consider the vehicle classes to be the origin-destination information of the vehicles, making such model suitable for the origin-destination estimation problem.

A natural extension of these models is to consider an interconnection of homogeneous links. When considering interconnection of conservation laws, A recent major step in this direction is the wellposedness results obtained respectively in [Holden & Risebro, 1995; M.Herty & Klar, 2003; Coclite et al., 2005] for the LWR model, in [Herty & Rascle, 2006; Garavello & Piccoli, 2006*b*] for the ARZ model and in [Garavello & Piccoli, 2005; Herty, Kirchner & Moutari, 2006] for the multiclass origin-destination model. In the above

references, the treatment of the interface conditions requires a routing matrix and the behavioral assumption that the flow should be maximized at the node. Other behavioral approaches have been proposed in [Daganzo, 1995*a*; Jin & Zhang, 2003].

Finally, an interesting modification of the LWR model proposed in [Lebacque, 1997; Lebacque, 2003*b*] is to bound the maximal vehicle acceleration to make 1^{th} order models more realistic.

State of the art in freeway control

Freeway traffic control is a recent field which started in the 70's-80's. M. Papageorgiou plays a prominent role in the advent of the control methodology in traffic engineering as can be seen in [Papageorgiou, 1983; Papageorgiou, 1984; Papageorgiou, 1990; Papageorgiou et al., 1990]. He is also one of the author of the local ramp metering algorithm ALINEA [Papageorgiou et al., 1991; Papageorgiou et al., 1997] which have been tested in several countries. Several other methods have been proposed for ramp metering since then as in [Zhang & Levinson, 2004], [Zhang et al., 2001], [Kotsialos & Papageorgiou, 2004] and [Sun & Horowitz, 2005]. Variable speed limit have been proposed as well to control freeway, sometimes in coordination with ramp metering as proposed in [Alessandri et al., 1998] and [Hegyi et al., 2002].

Active research groups in freeway modelling and control

Several communities worked or are currently working on the problems of traffic modelling and control. We give below a non-exhaustive list of some laboratories and researchers active in these fields, most of which we had relation with during this PhD.

In the traffic engineering community:

- INRETS, Arceuil, France:
  Jean-Patrick Lebacque, Habib Haj-Salem.
- INRETS, Bron, France:
  Jean-Baptiste Lesort, Christine Buisson, Ludovic Leclercq.
- Department of Civil Engineering, University of Minnesota, USA:
  Panos Michalopoulos, Henry Liu.
- Department of Civil Engineering, University of California Berkeley, USA:
  Carlos F. Daganzo, Michael Cassidy, Alexandre Bayen.
- Department of Civil Engineering, University of California Davis, USA:
  Michael Zhang.

In the applied mathematics community:

- Laboratoire Jean-Alexandre Dieudonné, Université de Nice, France:
  Michel Rascle.

- Istituto per le Applicazioni del Calcolo (I.A.C.), Roma, Italy:
  Benedetto Piccoli

- Fachbereich Mathematik, Technische Universität Kaiserslautern, Germany:
  Michael Herty.

- Dipartimento di Matematica, Università degli Studi di Brescia, Italy:
  Rinaldo Colombo.

- Dipartimento di Matematica e Applicazioni, Università degli Studi di Milano, Italy:
  Mauro Garavello.

- Institut Camille Jordan, Université Claude Bernard, Lyon, France:
  Sylvie Benzoni-Gavage.

In the control community:

- CESAME, Université Catholique de Louvain, Louvain-la-Neuve, Belgium:
  Georges Bastin, Nicolas Haut.

- Department of Mechanical Engineering, University of California Berkeley, USA:
  Roberto Horowitz, J.K. Hedrick, Gabriel Gomes, Xiaotan Sun.

- Department of Electrical Engineering, University of California Berkeley, USA:
  Pravin Varaiya.

- Dynamic Systems and Simulation Laboratory, Technical University of Crete, Greece:
  Markos Papageorgiou.

- Laboratoire d'Automatique de Grenoble, France:
  Denis Jacquet, Carlos Canudas de Wit, Damien Koenig.

Beside these institution, there are few transversal programs such as PATH in California, USA. PATH was established in 1986 and is administered by the Institute of Transportation Studies (ITS) University of California, Berkeley, in collaboration with Caltrans. PATH is a multi-disciplinary program with staff, faculty and students from universities statewide, and cooperative projects with private industry, state and local agencies, and non-profit institutions. Since its creation, PATH conducted researches in automated highways, platooning, macroscopic and hybrid freeway modelling and ramp metering to name a few. Check `www.path.berkeley.edu` for more information on this program.

The differential equations of the propagation of heat express the most general conditions, and reduce the physical questions to problems of pure analysis, and this is the proper object of theory.

Jean Baptiste Joseph Fourier (1768-1830),
French mathematician and physicist.

Chapter 2

The Lighthill-Whitham-Richards equilibrium model

2.1 Theoretical fondations

The simplest continuous macroscopic freeway model, involving the density ρ only, is the LWR model proposed initially by Lighthill, Whitham [Lighthill & Whitham, 1955] and Richards [Richards, 1956]. It is based on the car conservation principle and the constitutive assumption motivated by experimental data that vehicles tend to travel at an equilibrium speed $v = V(\rho)$ for all locations and all times. This relationship leads to an equilibrium flow function $\Phi(\rho) = \rho V(\rho)$ called the fundamental diagram in traffic engineering and is classically assumed to be concave (i.e. $\Phi'' = 2V' + \rho V'' < 0$). The materials presented here may nevertheless be extended to non-concave cases under slight modifications. Moreover, space-varying flow functions, i.e. $\phi(x,t) = \Phi(x, \rho(x,t))$ may be used to model varying travel conditions along the freeway. Simple concave flow functions proposed in the traffic literature are the Greenshield (GS) and Greenberg (GB) models [Greenshields, 1935; Greenberg, 1959]

$$\Phi_{\mathrm{GS}}(\rho) = \rho.v_f - \frac{\rho^2.v_f}{\rho_m} \qquad \Phi_{\mathrm{GB}}(\rho) = \rho.v_f \ln\left(\frac{\rho_m}{\rho}\right) \tag{2.1.1}$$

where v_{f} is the free flow speed and ρ_{m} the maximal density. Newell (NW) proposed in [Newell, 1961] the concave flow function

$$\Phi_{\mathrm{NW}}(\rho) = \rho.v_f \left[1 - \exp\left\{-\frac{\lambda}{v_f}\left\{\frac{1}{\rho} - \frac{1}{\rho_m}\right\}\right\}\right] \tag{2.1.2}$$

with the additional parameter λ. These three functions share the property that they can be derived from some car-following models under steady-state conditions. Daganzo proposed in [Daganzo, 1994] a so-called cell transmission model using sending and receiving cells to model traffic propagation and shows its equivalence with the piecewise affine flow function

$$\Phi_{\mathrm{D}}(\rho) = \min\{v_f.\rho, w.(\rho_m - \rho), \Phi_m\} \tag{2.1.3}$$

where Φ_m is the maximal capacity also called capacity in transportation engineering. Though concave, this flow diagram is not strictly concave and not smooth but fits well traffic data in free flow. Other flow models have been proposed in the literature such as

$$\Phi_{\mathrm{DCB}}(\rho) = \rho.v_f \left[1 - \exp\left(1 - \exp\left[\tfrac{c}{v_f}\left(\tfrac{\rho_m}{\rho} - 1\right)\right]\right)\right] \quad \text{[Castillo \& Benitez, 1995]}$$

$$\Phi_{\mathrm{P}}(\rho) = \rho.v_f \exp\left(-\tfrac{1}{a}\left(\tfrac{\rho}{\rho_c}\right)^a\right) \quad \text{[Papageorgiou, 1990]}$$

$$\Phi_{\mathrm{UW}}(\rho) = \rho.v_f \exp\left(-\tfrac{\rho}{\rho_c}\right) \quad \text{[Underwood, 1961]}$$

$$\Phi_{\mathrm{PS}}(\rho) = \rho.v_f \left(1 - \tfrac{\rho}{\rho_m}\right)^a \quad \text{[Pipes, 1967]}$$

where c is the kinematic wave speed at ρ_m, ρ_c is the critical density at maximal flow and a is a dimensionless shaping parameter.

Though there is some interest in seeking theoretical justifications for the different flow diagrams, their main requirement is to fit the experimental data freeway models are supposed to reproduce. For instance, Figure 2.1 shows some parameter fitting for the Greenshield, Greenberg and Newell models with real field data. Two phenomena can be noticed from these three flow diagrams. First, the parameters may loose their physical meanings to fit the data, e.g. the low maximal density in the Greenshield case and the high one in the Greenberg case. Second, some degrees of freedom seem to be lacking to fit the data for the whole density range. As predictable and illustrated in Figure 2.2, more sophisticated diagrams such as the one proposed by Del Castillo and Papageorgiou fit the data a little better. An other option is to define a flow diagram that is not parameterized to enhance the appearance of the fitting. In any case, an obvious limitation of the flow diagrams is the spreading of data points in the congested region, i.e. at large density.

The derivation of the LWR model is as following. Let $x \subset \mathbb{R}$ denotes the spacial variable along an infinitely long homogeneous freeway. For any arbitrary section $(x_L, x_R) \subset \mathbb{R}$, the car conservation principle states that

$$\begin{gathered} \text{Evolution of the number of vehicles in } (x_L, x_R) \\ = \\ \textstyle\sum \text{Inflows at } x_L - \sum \text{Outflows at } x_R \end{gathered} \tag{2.1.4}$$

which writes mathematically as

$$\frac{\mathrm{d}}{\mathrm{d}t}\int_{x_L}^{x_R} \rho(x,t)\ \mathrm{d}x = \Phi(\rho(x_L,t)) - \Phi(\rho(x_R,t)) \qquad \forall\ (x_L, x_R) \subset \mathbb{R} \tag{2.1.5}$$

Assuming ρ and $\Phi(\rho)$ have derivatives in a sense to be defined later then

$$\frac{\mathrm{d}}{\mathrm{d}t}\int_{x_L}^{x_R} \rho(x,t)\ \mathrm{d}x = \int_{x_L}^{x_R} \partial_t\rho(x,t)\ \mathrm{d}x$$

and

$$\Phi(\rho(x_L,t)) - \Phi(\rho(x_R,t)) = -\int_{x_L}^{x_R} \partial_x\rho(x,t)\ \mathrm{d}x$$

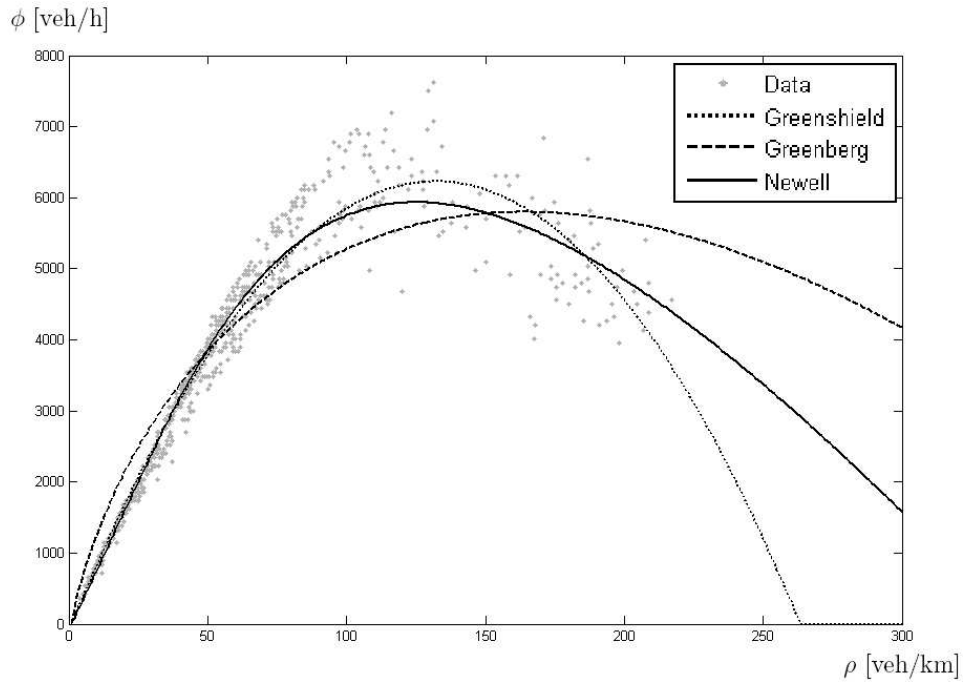

Figure 2.1: Least square curve fitting of traffic measurements from the Lyon beltway (France) with the Greenshield, Greenberg and Newell flow functions.

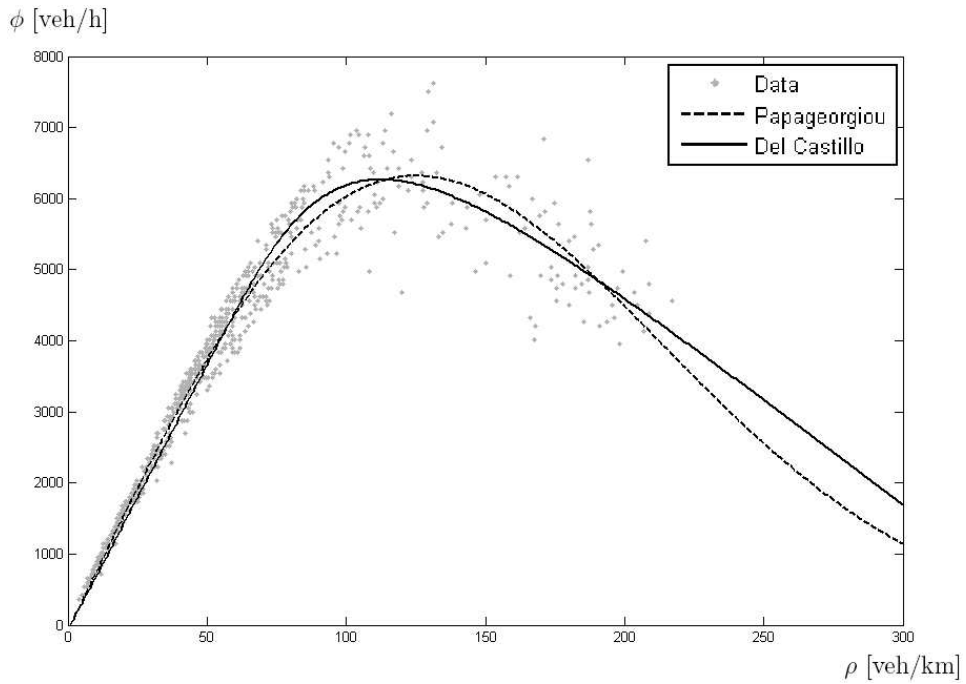

Figure 2.2: Least square curve fitting of traffic measurements from the Lyon beltway (France) with the Papageorgiou and Del Castillo flow functions.

As $(x_L, x_R) \subset (x_0, x_L)$ is arbitrary, the infinite family of balance equations (6.1.1) can be transformed to the unique scalar LWR divergence equation

$$\partial_t \rho + \partial_x \Phi(\rho) = 0 \tag{2.1.6}$$

Nonlinear hyperbolic equations of the form (2.1.6), also known as conservation laws, are known to be difficult to solve, both theoretically and numerically. The main properties of the solutions to this class of equations is their ability to develop discontinuities, called shock waves, in finite time [LeVeque, 1992] and the ubiquity of their boundary conditions [Bardos et al., 1979]. Two approaches may be followed to analyse the solution of conservation laws: either ρ is assumed to be piecewise-C^1 or a function of bounded variations [Evans & Gariepy, 1991]. Though more sophisticated, this last framework should be used [Kružkov, 1970; Bardos et al., 1979] to ensure rigorously the wellposedness of initial boundary value problems involving scalar conservation laws.

2.2 Solution of the LWR Cauchy problem

The LWR Cauchy problem is the initial value problem

$$\begin{cases} \partial_t \rho + \partial_x \Phi(\rho) = 0 \\ \rho(x, 0) = \rho_I(x) \end{cases} \tag{2.2.1}$$

with $\rho_I(x)$ the initial condition at time $t = 0$. In a Cauchy problem, the space domain is considered infinite, which is obviously unphysical for freeways. Nevertheless, (2.2.1) can be rewritten $\partial_t \rho + \Phi'(\rho)\partial_x \Phi'(\rho) = 0$ which is a nonlinear advection equation with wave speed $\Phi'(\rho)$. As this quantity is bounded, the finite propagation speed of the waves involved in (2.2.1) justifies this simplification at the beginning to get some insight about the solution locally. Two approaches are adopted to study (2.2.1), the first one using the space of piecewise-C^1 functions and the second using the space of functions with bounded variations.

2.2.1 The piecewise-C^1 approach

Let denote C^1_P the space of piecewise-C^1 functions and assume, without loss of generality, that ρ has a single discontinuity along the curve parameterized by $x = s(t)$ with $s(t)$ a

Lipschitz function. If $\rho \in C_P^1$ in the balance law (6.1.1), we have on one hand

$$\begin{aligned}
&\frac{\mathrm{d}}{\mathrm{d}t}\int_{x_L}^{x_R}\rho(x,t)\ \mathrm{d}x = \\
&\quad\frac{\mathrm{d}}{\mathrm{d}t}\left[\int_{x_L}^{s(t)}\rho(x,t)\ \mathrm{d}x + \int_{s(t)}^{x_R}\rho(x,t)\ \mathrm{d}x\right] = \\
&\quad\dot{s}(t)\rho(s(t)^-,t) + \int_{x_L}^{s(t)}\partial_t\rho(x,t)\ \mathrm{d}x - \dot{s}(t)\rho(s(t)^+,t) + \int_{s(t)}^{x_R}\partial_t\rho(x,t)\ \mathrm{d}x = \\
&\quad\int_{x_L}^{x_R}\partial_t\rho(x,t)\ \mathrm{d}x - \dot{s}(t)[\rho(\cdot,t)]_{s(t)}
\end{aligned}$$

with $\rho(s(t)^-,t)$ and $\rho(s(t)^+,t)$ respectively the left and right limits in space of the solution ρ along the discontinuity and $[\rho(\cdot,t)]_{s(t)} = \rho(s(t)^+,t) - \rho(s(t)^-,t)$ the corresponding jump value. On the other hand, with $\Phi(\rho)$ a C^1 function, $\Phi(\rho(x,t))$ is piecewise-C^1 and $\partial_x\Phi(\rho(x,t))$ is the distribution

$$\partial_x\Phi(\rho(x,t)) = \big\{\partial_x\Phi(\rho(x,t))\big\} - [\Phi(\rho(\cdot,t))]_{s(t)}\delta(x-s(t))$$

where $\big\{\partial_x\Phi(\rho(x,t))\big\}$ is the usual piecewise-continuous derivative defined almost everywhere and $\delta(x-s(t))$ the singular Dirac distribution defined along the discontinuity. Consequently, we have

$$\begin{aligned}
\Phi(\rho(x_L,t)) - \Phi(\rho(x_R,t)) &= \int_{x_L}^{x_R} -\partial_x\Phi(\rho(x,t))\ \mathrm{d}x \\
&= \int_{x_L}^{x_R} -\big\{\partial_x\Phi(\rho(x,t))\big\}\ \mathrm{d}x + [\Phi(\rho(\cdot,t))]_{s(t)}
\end{aligned}$$

The conservation principle of Equation (6.1.1) then leads to

$$\begin{cases} \partial_t\rho + \partial_x\Phi(\rho) = 0 \ \text{ a.e.} \\ \dot{s}_i(t)[\rho(s_i(t),t)] = [\Phi(\rho(s_i(t),t))] \end{cases} \tag{2.2.2}$$

The second equation in (2.2.2) is known as the Rankine Hugoniot condition [LeVeque, 1992; Ansorge, 1990] and tells how discontinuities propagate when the left and right densities differ. Equation (2.2.2) provides a way to construct a piecewise-C^1 solution to (6.1.1) using the method of characteristics [Evans, 1998] until some characteristics intersect and then tracking the discontinuities using the Rankine-Hugoniot condition given in Equation (2.2.2). Though the development above proves the existence of a piecewise-C^1 solution, its does not provide unicity. For a further analysis of the piecewise-C^1 setting, we refer to the works of Dafermos on generalized characteristics in [Dafermos, 1977*a*] and [Dafermos, 1977*b*].

2.2.2 The BV approach

Conservation laws being balance equations in the form of an infinite family of integral equations, the functional space L^1 of measurable functions seems natural to prove their

wellposedness. Unfortunately, L^1 does not have the required compactness property and the space BV of functions with Bounded Variations has been proven to be more appropriate since the seminar paper of Kružkov [Kružkov, 1970]. Few literature is available on BV functions and we recommend [Federer, 1969], [Ziemer, 1989] and more specifically [Evans & Gariepy, 1991] to the interested reader. Two equivalent definitions of a BV function on an open set Ω are the followings.

Definition 2.2.1 *$u(x) \in BV(\Omega) \subset L^1(\Omega)$ if its first order partial derivatives $\partial_{x_i} u(x)$ are Radon measures, i.e. if there exists Borel measures μ_i with $|\mu_i(K)| < \infty$ for each compact subset $K \subset \Omega$, such that*

$$-\int_\Omega u(x) \frac{\partial \phi(x)}{\partial x_i} \, \mathrm{d}x = \int_\Omega \phi(x) \, \mathrm{d}\mu_i \qquad \forall \phi \in C_0^1(\Omega)$$

Definition 2.2.2 *$u(x) \in BV(\Omega) \subset L^1(\Omega)$ if its total variation is bounded, i.e.*

$$TV(u) = \sup \left\{ \int_\Omega u(x) \ \mathrm{div}\phi(x) \ \mathrm{d}x \ : \ \phi \in C_0^1(\Omega, \mathbb{R}^n), \ |\phi| \leq 1 \right\} < \infty$$

The first definition shows that the first order (distributional) partial derivatives of a BV function, as they appear in conservation laws, are Radon measures. The second definition relies on the seminorm TV and it can be proven that the space BV is a Banach space with the norm $||u||_{BV} = TV(u) + ||u||_{L^\infty}$. The interest of using the space BV instead of L^1 is that $BV \cap L^\infty$ is compact, meaning that for an infinite sequence of functions u_ϵ with $||u_\epsilon||_{BV} < \infty$, we can extract a subsequence such that $u_\epsilon \to u$ in L^1 with $||u||_{BV} < \infty$. This result, known as Helly's theorem, is the most important ingredient used in the wellposedness analysis of conservation laws with u_ϵ a sequence of smooth approximations of u.

Wellposedness of scalar conservation laws have been studied in the mathematics community in two frameworks: first using BV functions [Kružkov, 1970; Bardos et al., 1979] and then using Young measures [Diperna, 1985; Szepessy, 1989], but we only restrict to the BV setting here. The theory of generalized solutions as introduced by Kružkov in [Kružkov, 1970] states that there exists a unique solution $\rho \in BV(\mathbb{R}\times\mathbb{R}^+) \bigcap L^\infty(\mathbb{R}\times\mathbb{R}^+)$ to the Cauchy problem (2.2.1) characterized by:

$\forall \ k \in \mathbb{R}, \ \forall \ \phi \in C_0^2, \ \phi \geq 0$, we have

$$\int_{\mathbb{R}^+}\int_{\mathbb{R}} |\rho - k| \, \partial_t \phi + \mathrm{sg}(\rho - k)(\Phi(\rho) - \Phi(k)) \, \partial_x \phi \ \mathrm{d}x\mathrm{d}t + \int_{\mathbb{R}} |\rho_I - k| \, \phi_{|_{t=0}} \geq 0 \tag{2.2.3}$$

with $\mathrm{sg}(\cdot)$ the classical sign function defined by

$$\mathrm{sg}(\xi) = \begin{cases} -1 & , \quad x < 0 \\ 0 & , \quad x = 0 \\ 1 & , \quad x > 0 \end{cases}$$

Thought the infinite set of inequalities (2.2.3) seems unpractical, it provides (as demonstrated in the appendix) all the information needed to characterize the unique generalized solution.

Indeed, we have

1. By choosing successively $k > \sup \rho$ and $k < \inf \rho$ in (2.2.3), performing an integration by parts and using the fact that $\phi(-\infty, t) = \phi(\infty, t) = \phi(x, \infty) = 0$, we obtain the so-called weak formulation

$$\int_{\mathbb{R}^+}\int_{\mathbb{R}} \rho\partial_t\phi + \Phi(\rho)\partial_x\phi \, \mathrm{d}x\mathrm{d}t + \int_{\mathbb{R}} \rho_I\phi_{|_{t=0}} = 0 \qquad \forall\phi \in C_0^2 \tag{2.2.4}$$

   Assuming the presence of a discontinuity and the existence of strong traces of ρ on both sides of it, some integrations by parts in Equation (2.2.4) give the Rankine-Hugoniot condition

$$\dot{s} = \frac{\Phi(\rho^+) - \Phi(\rho^-)}{\rho^+ - \rho^-} \tag{2.2.5}$$

   as provided by the piecewise-C^1 formulation. Note that the Rankine-Hugoniot condition (2.2.5) can be rewritten

$$\dot{s} = \frac{1}{\rho^+ - \rho^-}\int_{\rho^-}^{\rho^+} \Phi'(\xi) \, \mathrm{d}\xi$$

   meaning that the shock speed can be interpreted as the average of the characteristics entering in the shock. An other interpretation is that there is a kind of *competition* of the entering characteristics to decide of the shock speed.

2. Choosing $\rho^- \leq k \leq \rho^+$ along discontinuities gives the Oleinik entropy condition [Oleĭnik, 1964] that states that a shock wave is admissible if

$$\frac{\Phi(v) - \Phi(\rho^-)}{v - \rho^-} \geq \frac{\Phi(\rho^+) - \Phi(v)}{\rho^+ - v} \qquad \forall\ v \in \mathrm{Conv}(\rho^-, \rho^+) \tag{2.2.6}$$

   with $\mathrm{Conv}(\rho^-, \rho^+)$ the convex set with extremities ρ^- and ρ^+. Equation (2.2.6) gives immediately the more practical Lax condition [Lax, 1973]

$$\Phi'(\rho^-) \geq \dot{s} \geq \Phi'(\rho^+) \tag{2.2.7}$$

   meaning that the characteristics should go towards the shock to be admissible, a rarefaction wave occurring otherwise. Note that for a concave flux function $\Phi(\rho)$ as in traffic models, the Lax entropy condition writes simply $\rho^- \leq \rho^+$. It means that discontinuities are allowed to occur only when the vehicles experience an increase in the density when crossing the shock. This is exactly what happens when reaching a congestion on a freeway, implying immediate braking.

The entropy conditions (2.2.6) or (2.2.7) provided by the Kruzkov formulation discriminate the possible discontinuities that are allowed to occur and enable to select the

unique physically meaningful solution to (2.1.6). This extra information with respect to the piecewise-C^1 formulation is of paramount importance as it is possible to construct several piecewise-C^1 weak solutions to the same Cauchy problem. We will see in chapter 6 that all the information given by the Kruzkov formulation, i.e. the weak formulation (2.2.4), the Rankine-Hugoniot condition (2.2.5) and the Lax entropy condition (2.2.7), is needed to solve optimal control problems involving conservation laws.

2.2.3 Solution representations

The method of characteristics

The method of characteristics [Evans, 1998] states that the solution of the LWR equation (2.1.6) can be written $\rho(\xi(t,x_0),t) = \sigma(t,x_0)$ where (ξ,σ) solves the ordinary differential equation

$$\begin{cases} \dot{\xi}(t,x_0) = \Phi'\big(\sigma(t,x_0)\big) \\ \dot{\sigma}(t,x_0) = 0 \\ \xi(0,x_0) = x_0 \\ \sigma(0,x_0) = \rho_I(x_0) \end{cases} \quad \Rightarrow \quad \begin{cases} \dot{\xi}(t,x_0) = \Phi'\big(\rho_I(x_0)\big) \\ \xi(0,x_0) = x_0 \\ \sigma(t,x_0) = \rho_I(x_0) \end{cases} \tag{2.2.8}$$

In this setting, the straight lines $\xi(t,x_0)$ are called the projected characteristics with roots x_0 and the density value ρ is constant along them. This method thus enables to compute in time a candidate solution from the initial condition. Figure 2.3 illustrates this method for the LWR model with a Greenshield flow function and highlights its limits by showing overlapping projected characteristics that lead to a multivalued solution.

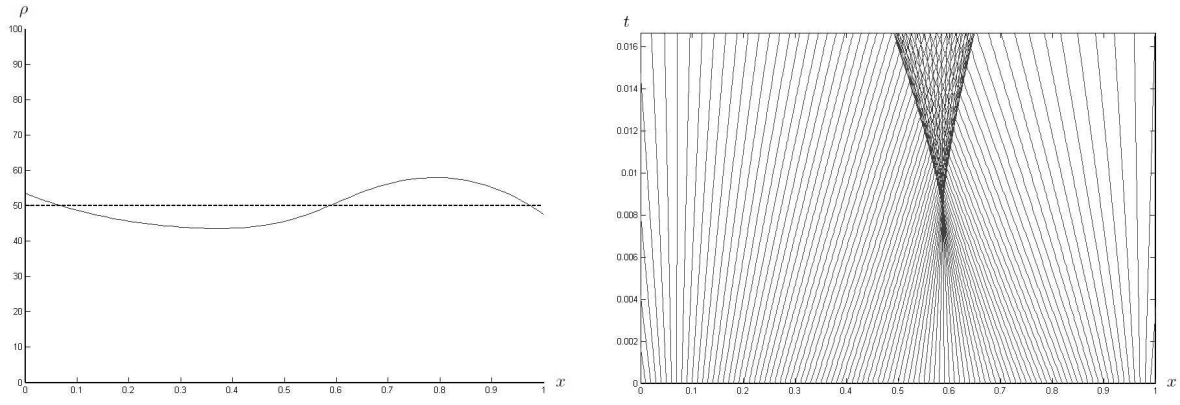

Figure 2.3: Left: initial density condition. Right: projected characteristics in space-time.

In contrast, Figure 2.4 illustrates how shock waves remove this ambiguity by correcting the solution folding. Moreover, it shows why shocks are only allowed when projected characteristics are crossing as expressed by the Lax entropy condition (2.2.7). Accompanied with the Rankine-Hugoniot condition (2.2.5) and the Lax entropy condition (2.2.7), the method of characteristics is thus still a valuable tool to get an idea of the solution.

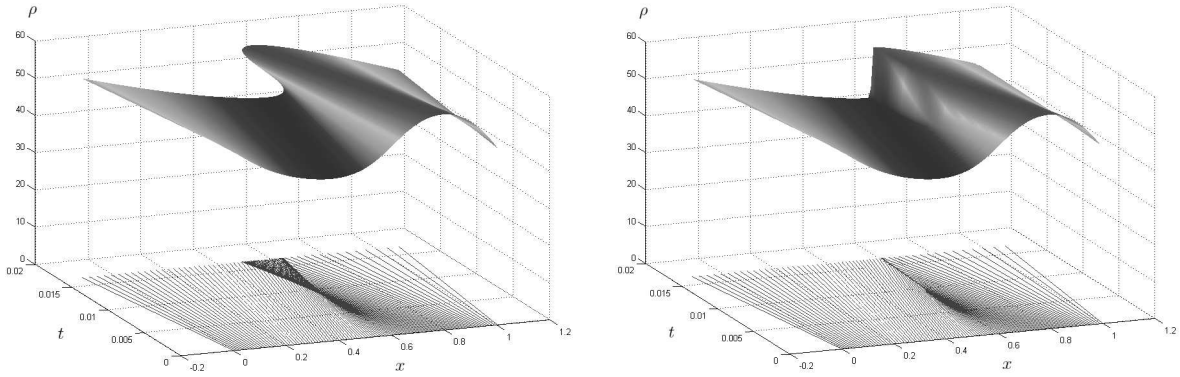

Figure 2.4: Left: folding of the solution surface. Right: effect of a shock wave.

Using differential calculus operators

In this section, the LWR model is rewritten using some differential calculus operators such as the gradient, the divergence and the curl. All of them use the classical nabla operator given by

$$\nabla = \begin{pmatrix} \partial_x \\ \partial_t \end{pmatrix}$$

and provide new interpretations of the freeway dynamics.

First, assuming that the density ρ is differentiable, the LWR model can be written

$$\partial_t \rho + \partial_x \Phi(\rho) = 0 \qquad \Leftrightarrow \qquad \begin{pmatrix} \Phi'(\rho) \\ 1 \end{pmatrix} \cdot \nabla \rho = 0$$

which highlights the nonlinearity of the partial differential equation. It means that the directional derivative of ρ is null along $(\Phi'(\rho), 1)$ so that ρ is constant along this direction. However, this vector is unknown a priori as it requires the knowledge of ρ. We recognize here the method of characteristics and note that this formulation is not valid across shocks where the directional variation of ρ undergoes a step.

Let now consider the following compact writing for the LWR model

$$\partial_t \rho + \partial_x \Phi(\rho) = 0 \qquad \Leftrightarrow \qquad \nabla \cdot \vec{G} = 0$$

where the vector field $\vec{G}$ is given by

$$\vec{G} = \begin{pmatrix} \phi \\ \rho \end{pmatrix} = \begin{pmatrix} \Phi(\rho) \\ \rho \end{pmatrix} = \rho \begin{pmatrix} V(\rho) \\ 1 \end{pmatrix} = \rho \, \vec{V}(\rho)$$

We recognize a space-time incompressibility property meaning that the number of vehicles is conserved. As a remark, it should be pointed out that freeways are not conservative when considered lane by lane due to the lane changing done by some drivers. Nevertheless, freeways are conservative on the average when lanes are aggregated. In the same

spirit, the velocity field should not be associated to the vehicle trajectories but to the average velocity of the multilane traffic.

An other interesting formulation of the LWR model is

$$\partial_t \rho + \partial_x \Phi(\rho) = 0 \qquad \Leftrightarrow \qquad \nabla \times \vec{F} = 0$$

where

$$\vec{F} = \begin{pmatrix} \rho \\ -\phi \end{pmatrix} = \begin{pmatrix} \rho \\ -\Phi(\rho) \end{pmatrix} = \rho \begin{pmatrix} 1 \\ -V(\rho) \end{pmatrix} = \rho \, \vec{V}^{\perp}(\rho)$$

meaning that the vector field $\vec{F}$ is conservative, also called irrotational. This property implies the followings

1. $\oint \vec{F} \cdot d\vec{s} = 0$ along closed space-time paths,
2. $\int \vec{F} \cdot d\vec{V} = 0$, i.e. $\vec{F}$ and $\vec{V}$ are orthogonal,
3. There exists a scalar potential ψ such that $\vec{F} = \nabla\psi$ and the identity $\nabla \times \nabla\psi = 0$ is its compatibility condition.
4. The vehicle flow is laminar, i.e. all the vehicles in a given layer of constant potential will move to another layer a constant potential. An other interpretation of this fact is that LWR traffic flows are First-In-First-Out (FIFO).

One interesting feature of the potential ψ is that

$$\int_A^B \vec{F} \, \mathrm{d}l = \psi(B) - \psi(A)$$

so that the integral of $\vec{F}$ along a path with extremities $A = (x_A, t_A)$ and $B = (x_B, t_B)$ in the space-time domain can be expressed directly as the difference of the potential between these 2 points. In particular, if $\hat{t} = t_A = t_B$ and $x_B > x_A$, then the quantity $\psi(B) - \psi(A) = \int_{x_A}^{x_B} \rho(x, \hat{t}) \, \mathrm{d}x$ is the number of vehicles at time $\hat{t}$ between $x = x_A$ and $x = x_B$. Similarly, if $\hat{x} = x_A = x_B$ and $t_B > t_A$, then $\psi(B) - \psi(A) = -\int_{t_A}^{t_B} \phi(\hat{x}, t) \, \mathrm{d}t$ is the inverse of the flow of vehicles at $x = \hat{x}$ between times t_A and t_B. Finally, for paths AB with $t_A < t_B$ and $x_A < x_B$ that are not aligned to the time or space coordinates, a negative (respectively positive) difference $\psi(B) - \psi(A)$ means that the average traffic speed in the triangle $(x_A, t_A) - (x_B, t_A) - (x_B, t_B)$ is larger (respectively smaller) than the slope of the line linking A to B.

2.2.4 Cumulative variables and Hamilton-Jacobi equations

Let now show that the scalar potential ψ of the conservative vector field $\vec{F} = (\rho, -\phi)$ introduced in the previous section is linked to the cumulated vehicle variable given by

$$N(x,t) = \int_0^x \rho(\zeta, t) \, \mathrm{d}\zeta \qquad \Leftrightarrow \qquad \rho(x,t) = \partial_x N(x,t)$$

As the time evolution of $N(x,t)$ for a given x follows the flow conservation principle

$$\partial_t N(x,t) = \phi_0(t) - \phi(x,t)$$

with $\phi_0(t)$ the upstream flow and $\phi(x,t) = \Phi(\rho(x,t))$ in the LWR model, $N(x,t)$ is solution of the inhomogeneous Hamilton-Jacobi [Evans, 1998] equation

$$\begin{cases} \partial_t N + \Phi(\partial_x N) = \phi_0(t) \\ N(x,0) = \int_0^x \rho_I(\zeta)\ \mathrm{d}\zeta \end{cases}$$

Setting for the scalar potential

$$\psi(x,t) = N(x,t) - \int_0^t \phi_0(\tau)\ \mathrm{d}\tau \tag{2.2.9}$$

we easily check that

$$\nabla\psi = \begin{pmatrix} \partial_x \\ \partial_t \end{pmatrix} \left[N(x,t) - \int_0^t \phi_0(\tau)\ \mathrm{d}\tau \right] = \begin{pmatrix} \partial_x N(x,t) \\ \partial_t N(x,t) - \phi_0(t) \end{pmatrix} = \begin{pmatrix} \partial_x N \\ -\Phi(\partial_x N) \end{pmatrix} = \begin{pmatrix} \rho \\ -\Phi(\rho) \end{pmatrix}$$

thus proving that $\nabla\psi = \vec{F}$. Equation (2.2.9) tells that the potential $\psi(x,t)$ is the number of vehicles at time t in the stretch $(0,x)$ minus the total number of vehicles that entered at the upstream boundary $x = 0$ since $t = 0$. It easily follows from (2.2.9) that the scalar potential ψ solves the homogeneous Hamilton-Jacobi equation

$$\begin{cases} \partial_t \psi + \Phi(\partial_x \psi) = 0 \\ \psi(x,0) = \int_0^x \rho_I(\zeta)\ \mathrm{d}\zeta \end{cases} \tag{2.2.10}$$

The method of characteristic can be used for any Hamilton-Jacobi equation [Evans, 1998] though it may lead to an ill-defined (multivalued) solution as in the case of conservation laws. For (2.2.10), the method of characteristic tells that $\psi(\xi(t,x_0),t) = \sigma(t,x_0)$ and $\partial_x\psi(\xi(t,x_0),t) = \eta(t,x_0)$ with ξ, σ and η the solutions of

$$\begin{cases} \dot{\eta}(t,x_0) = 0 \\ \dot{\xi}(t,x_0) = \Phi'\big(\eta(t,x_0)\big) \\ \dot{\sigma}(t,x_0) = \Phi'\big(\eta(t,x_0)\big)\eta(t,x_0) - \Phi\big(\eta(t,x_0)\big) \\ \eta(0,x_0) = \rho_I(x_0) \\ \xi(0,x_0) = x_0 \\ \sigma(0,x_0) = \int_0^{x_0} \rho_I(\zeta)\ \mathrm{d}\zeta \end{cases} \tag{2.2.11}$$

This system can be solved explicitly and gives

$$\begin{cases} \eta(t,x_0) = \rho_I(x_0) \\ \xi(t,x_0) = x_0 + \Phi'\big(\rho_I(x_0)\big).t \\ \sigma(t,x_0) = \int_0^{x_0} \rho_I(\zeta)\ \mathrm{d}\zeta + \Big(\Phi'\big(\rho_I(x_0)\big)\rho_I(x_0) - \Phi\big(\rho_I(x_0)\big)\Big).t \end{cases}$$

We observe that the projected characteristics $\xi(t, x_0)$ are the same than for the associated conservation law (2.2.8) but that the value of the solution $\sigma(t, x_0)$ evolves linearly in time along them. The characteristic system (2.2.11) generates straight lines that may intersect at the shock location as illustrated on Figure 2.5 (bottom-left), thus leading to a multivalued solution. A selection principle is thus necessary to recover the physical solution.

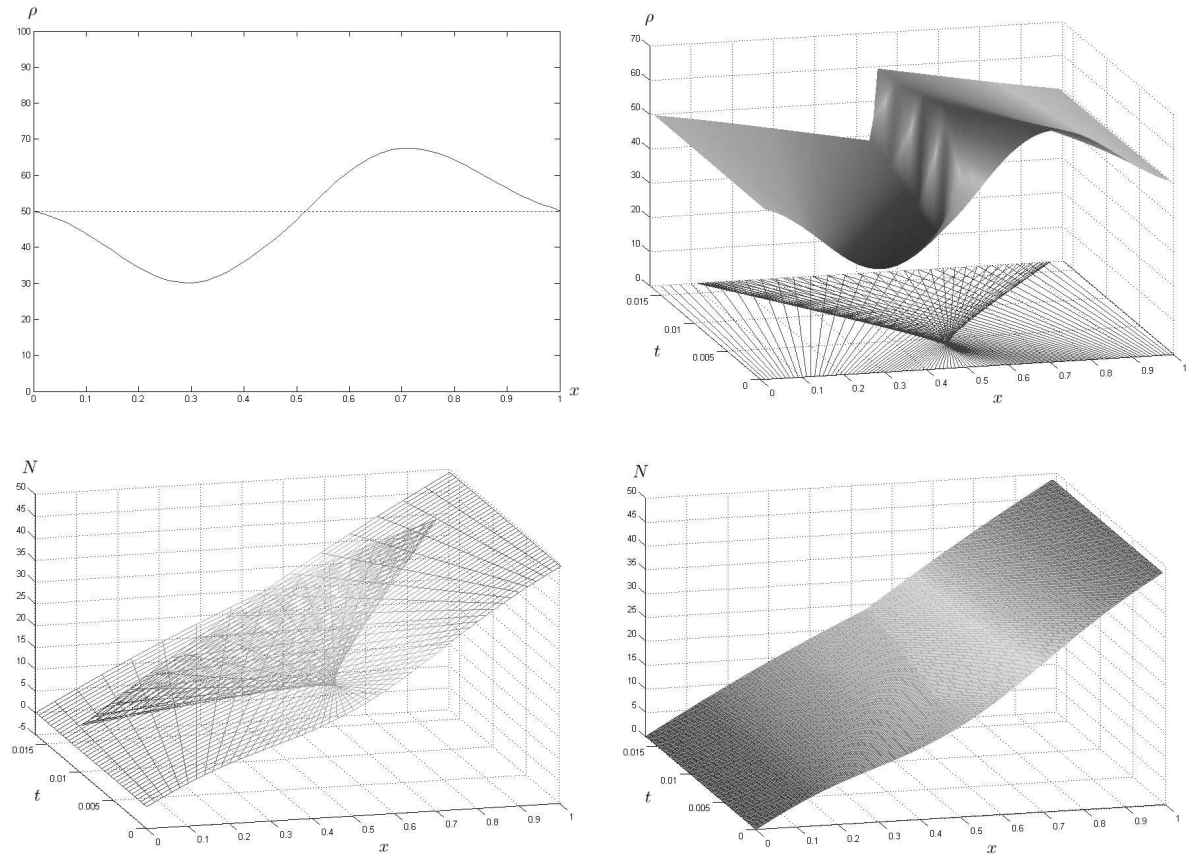

Figure 2.5: Top left: initial condition. Top right: solution with a shock. Bottom left: solution of the Hamilton-Jacobi characteristic system. Bottom right: the upper envelop as the physical solution to the Hamilton-Jacobi equation.

Hamilton-Jacobi equations such as (2.2.10) have a long history in the study of variational and optimal control problems. Their solutions were first studied in the convex (or concave) case using the explicit Hopf-Lax formula that dates back to the 50's [Hopf, 1950; Lax, 1957]. As $\Phi(\cdot)$ can be taken to be concave in the LWR model, we can use the *concave* Hopf-Lax formula [Evans, 1998] given by

$$\psi(x,t) = \max_y \left\{ t\ \Phi^*\left(\frac{x-y}{t}\right) + \int_0^y \rho_I(\zeta)\ \mathrm{d}\zeta \right\} \tag{2.2.12}$$

with $\Phi^*(\cdot)$ the *concave* Legendre transform of $\Phi(\cdot)$ defined by

$$\Phi^*(q) = \inf_{p\in\mathbb{R}} \Big\{ q \cdot p - \Phi(p) \Big\}$$

However, the domain of $\Phi(\cdot)$ is restricted to $(0, \rho_m)$ in the LWR model, which poses to problem of defining the value of the flux function outside its domain. Figure 2.6 shows 3 possible extensions of the Greenshield flux function with their respective Legendre transforms. However, there is no physical motivation for choosing one of them. Let show that such a selection is actually not necessary.

The Legendre transform is a classical tool of convex (respectively concave) optimization where is it used [Hiriart-Urruty & Lemaréchal, 1993] to analyze subdifferentials (respectively superdifferentials). In the case of scalar concave functions, the superdifferential of f at x is the set $\partial f(x) = \{s \in \mathbb{R} \ : \ f(x') \leq f(x) + s \cdot (x' - x), \ \forall \ x' \in \mathbb{R}\}$ and we have $0 \in \partial f(x)$ when f attains a (possibly local) maximum at x. This property along with the inversion property $q \in \partial\Phi(p) \ \Leftrightarrow \ p \in \partial\Phi^*(q)$ enables to restrict the interval of the maximization in (2.2.12) and to remove the need for an extension of $\Phi(\cdot)$ over $\mathbb{R}$. Indeed, the Hopf-Lax formula (2.2.12) can be rewritten $\psi(x,t) = T(y^\star)$ where the function $T(y)$ is defined by

$$T(y) = t \ \Phi^* \left(\frac{x-y}{t} \right) + \int_0^y \rho_I(\zeta) \ \mathrm{d}\zeta \tag{2.2.13}$$

and $y^\star$ verifies $T(y^\star) \geq T(y)$ for all $y \in \mathbb{R}$. Before showing that this last property gives a condition on the domain of $y^\star$, note that $y^\star$ is not unique when (x,t) belong to a "shock". Nevertheless, all the possible values lead to the same end value for $T(\cdot)$. The second term in (2.2.13) is differentiable almost everywhere, i.e. outside the discontinuities of $\rho_I(\cdot)$, and its derivative is equal to $\rho_I(y^\star)$ at $y^\star$. We thus have

$$-\rho_I(y^\star) \in \partial \left\{ t\Phi^* \left(\frac{x-y}{t} \right) \right\}_{y=y^\star} = -\partial\Phi^* \left(\frac{x-y^\star}{t} \right)$$

We deduce that $\rho_I(y^\star) \in \partial\Phi^* \left(\frac{x-y^\star}{t} \right)$, which translates with the inversion property to $\frac{x-y^\star}{t} \in \partial\Phi(\rho_I(y^\star))$ and finally to $\frac{x-y^\star}{t} = \Phi'(\rho_I(y^\star))$ as $\Phi(\cdot)$ is differentiable. As we have $\rho_I(x) \in (0, \rho_m)$ and $\Phi'(\cdot)$ is monotonically decreasing, we deduce the finite propagation speed property $y^\star \in (x - \Phi'(0)t, x - \Phi'(\rho_m)t)$. We conclude that the Hopf-Lax formula (2.2.12) can be written more accurately

$$\psi(x,t) = \max_{y \in (x-\Phi'(0)t, x-\Phi'(\rho_m)t)} \left\{ t \ \Phi^* \left(\frac{x-y}{t} \right) + \int_0^y \rho_I(\zeta) \ \mathrm{d}\zeta \right\} \tag{2.2.14}$$

This gives some degrees of freedom for $\Phi^*(\cdot)$ outside the bounds given above for y. Any extension of $\Phi(\cdot)$ is thus allowed as soon as it fulfills the concavity assumption. $\Phi^*(\cdot)$ becomes an equivalent class of functions for which a specific representative is obtained from a specific representative of $\Phi(\cdot)$.

For instance, the *concave* Legendre transform of the Greenshield function $\Phi_{\mathrm{GS}}(\cdot)$ as defined in (2.1.1) is

$$\Phi^*_{\mathrm{GS}}(q) = \inf_{p \in \mathbb{R}} \left\{ q \cdot p - p.v_f \left(1 - \frac{p}{\rho_m} \right) \right\} = -\frac{\rho_m}{4v_f}(q - v_f)^2$$

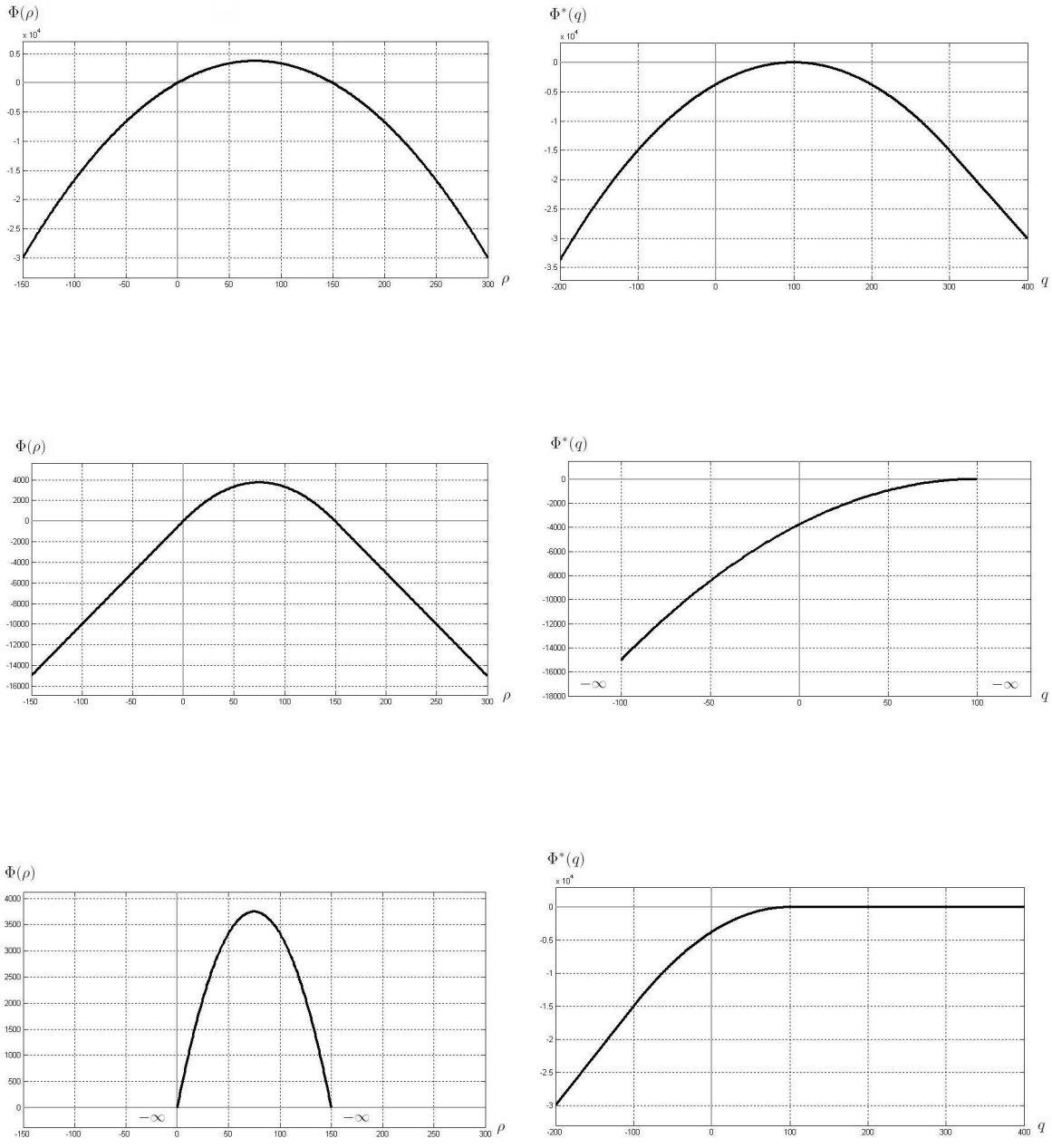

Figure 2.6: Possible extensions of the domain of $\Phi_{GS}(\cdot)$. Up: natural quadratic extension. Middle: linear extension with continuous derivative. Down: natural domain restriction for concave functions.

It is represented graphically in the upper right plot of Figure 2.6 and leads to the following semi-explicit formula for the scalar potential

$$\psi(x,t) = \max_y \left\{ -t\frac{\rho_m}{4v_f}\left(\frac{x-y}{t} - v_f\right)^2 + \int_0^y \rho_I(\zeta)\ \mathrm{d}\zeta \right\}$$

For the trapezoidal flux function as defined in (2.1.3), the Legendre transform is

$$\Phi_{\mathrm{D}}^*(\rho) = \begin{cases} \frac{w\rho_m - \Phi_m}{w} q - \Phi_m & \text{if } \ p \in (-w, 0) \\ \frac{\Phi_m}{v_f} q - \Phi_m & \text{if } \ p \in (0, v_f) \\ -\infty & \text{if } \rho \notin (-w, v_f) \end{cases}$$

and is plotted in Figure 2.7.

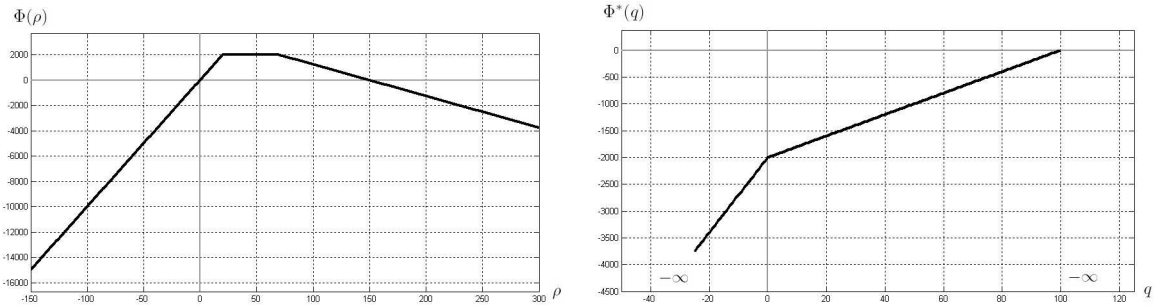

Figure 2.7: The trapezoidal flux function and its Legendre transform.

We can now turn to the selection principle necessary when using the characteristic method to defined the physical solution of the Hamilton-Jacobi Equation (2.2.10). In the characteristic system (2.2.11), the equation $\dot{\sigma} = \Phi'(\eta)\eta - \Phi(\eta)$ can be rewritten

$$\begin{cases} \dot{\sigma} = u\eta - \Phi(\eta) \\ u = \Phi'(u) \end{cases} \tag{2.2.15}$$

which is equivalent to

$$\dot{\sigma} = \inf_{\eta \in \mathbb{R}} \Big\{ u\eta - \Phi(\eta) \Big\} = \Phi^*(u)$$

as the second equation in (2.2.15) is equivalent to $\frac{d}{d\eta}\left(u\eta - \Phi(\eta)\right) = 0$. Moreover, the characteristic speed u is given by $u = \frac{\xi - x_0}{t}$ so $\dot{\sigma} = \Phi^*\left(\frac{\xi - x_0}{t}\right)$ and

$$\sigma(t, x_0) = t\ \Phi^*\left(\frac{\xi - x_0}{t}\right) + \int_0^{x_0} \rho_I(\zeta)\ \mathrm{d}\zeta$$

which is very similar to (2.2.12). The characteristic system (2.2.11) leads to a multivalued solution when several characteristic roots x_i for $i \in \mathcal{I}$ lead to the same projected characteristic value $\xi(t, x_i) = \xi(t, x_j)$ for $(i, j) \in \mathcal{I}^2$ at a given time. In that case, the Hopf-Lax formula tells that the physical solution is selected by setting

$$\psi(\xi(t, x_i), t) = \max_{i \in \mathcal{I}} \big\{ \sigma(t, x_i) \big\}$$

The physical interpretation of this selection principle is that the LWR traffic flow evolves such that the scalar potential ψ is maximized. As illustrated in Figure 2.5, the physical solution (bottom-right) is selected as the upper envelop of the multivalued characteristic surface (bottom-left). Note that this selection principle is consistent with the entropy condition that states for concave flux functions that the density is larger downstream of a shock that upstream of it. As shown on Figure 2.5, a considerable advantage of the Hamilton-Jacobi equation with respect to the LWR conservation law is that its solution is continuous, though possibly not differentiable at the corresponding shock locations. Figure 2.8 (left) shows the solution of the scalar potential $\Psi(x,t)$ for the same initial condition than in Figure 2.5. The isocurves of ψ in Figure 2.8 (right) represent the mean traffic velocity (lagrangian coordinates) as $\nabla\psi$ is orthogonal to $\vec{V}$. We recall here that this mean speed should not be associated to the vehicle trajectories for multilane freeways. We note that the vehicles decelerate abruptly when reaching the shock curve.

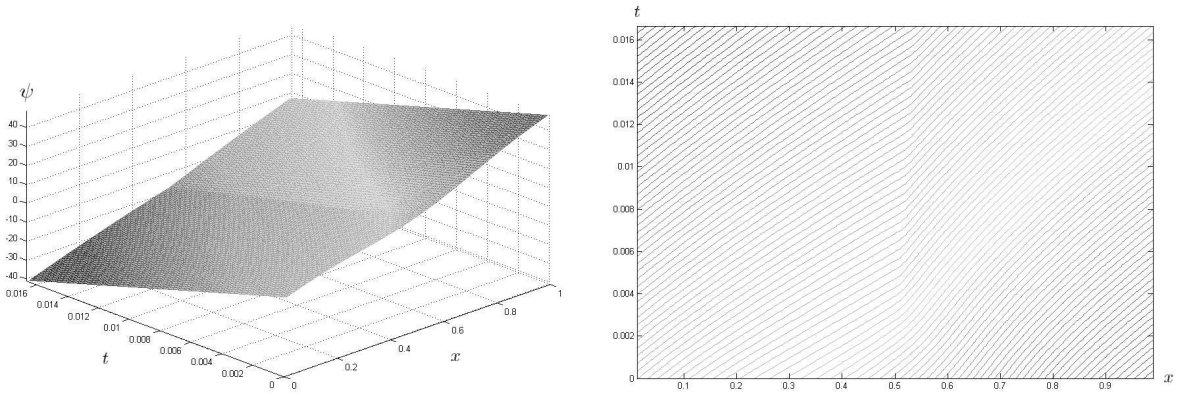

Figure 2.8: Left: the potential surface $\psi(x,t)$. Right: the contour plot of ψ.

In the traffic community, Newell introduced in [Newell, 1993] the so-called "cumulative vehicle" surface $A(x,t)$ and proposed a graphical method to determine the delays using the accumulated flow signals and the freeway capacities only, without postulating an equation of motion. Such an equation is nevertheless necessary to estimate the shock locations which represents the end of the queues. As mentioned by Newell, traffic engineers are often more familiar with the concept of cumulative flow than of instance density at a given location. This observation leads to the expectation that traffic management tools using cumulative vehicle variables will be easier to introduced in traffic operation rooms. In [Newell, 1993], $A(x,t)$ is defined as the solution of

$$\begin{cases} \partial_t A - \Phi(-\partial_x A) = 0 \\ A(x,0) = -\int_0^x \rho_I(\zeta)\ \mathrm{d}\zeta \end{cases}$$

so $A(x,t) = -N(x,t)$ and $A(x,t)$ is the scalar potential associated to the conservative vector field $\vec{F}_A = (-\rho, \phi)$. Daganzo also showed in [Daganzo, 2005] that a variational principle closely related to the Hamilton-Jacobi theory can be used to solve the LWR

problem. Note that from a traffic engineering perspective, the cumulated flow (the integral of the flow measured by sensors) is usually taken to be zero at time $t = 0$. Setting

$$B(x,t) = A(x,t) + \int_0^x \rho_I(\zeta)\ \mathrm{d}\zeta$$

we get

$$\begin{cases} \partial_t B - \Phi(\rho_I(x) - \partial_x B) = 0 \\ B(x,0) = 0 \end{cases}$$

but this Hamilton-Jacobi equation is not convenient neither for analysis nor control.

In the general case of nonconcave flux functions, viscosity solutions were introduced by Lions [Lions, 1982] in the 80's and were retained as the correct physical way to defined nonsmooth solutions. Nevertheless, we will not explore this situation here as traffic flux diagrams are usually taken to be concave.

To conclude this section, the cumulated vehicle approach is appealing as it leads to continuous solutions that are well defined by the theory of Hamilton-Jacobi equations. Nevertheless, when dealing with real field data, one of its drawbacks is to integrate the measurement errors in time as the model use cumulated variables. This is a serious drawback as traffic data are classically of poor quality.

2.3 Treatment of boundary conditions

2.3.1 Formulation to ensure wellposedness

The first wellposedness result for conservation laws with boundary conditions was given in [Bardos et al., 1979] based on an extension of Kruzkov's theory and uses the so-called BLN boundary entropy inequalities. The main feature of boundary conditions in conservation laws is that they cannot be applied strongly for all time, implying that boundary signals are proposed only. Moreover, the set on which they actually apply strongly cannot be defined beforehand as it depends on the solution inside the computational domain. Let consider the initial boundary value problem

$$\begin{cases} \partial_t \rho + \partial_x \Phi(\rho) = g(x,\rho,u) \\ \rho(x,0) = \rho_I(x) \\ \rho(0,t) \sim \rho_0(t) \text{ and } \rho(L,t) \sim \rho_L(t) \end{cases} \tag{2.3.1}$$

where $g(x,\rho,u)$ is a regular source term and $\big(\rho_0(t), \rho_L(t)\big)$ are the boundary signals with $\sim$ meaning that they are only proposed and may not apply for all time. It is shown in [Bardos et al., 1979] that Equation (2.3.1) is wellposed if the traces of the solution at the boundaries, noted $\big(\rho(0,t), \rho(L,t)\big)$, satisfy

$$\sup_{k\in \mathrm{Conv}(\rho(0,t),\rho_0(t))} \ \mathrm{sign}\big(\rho(0,t) - \rho_0(t)\big)\big(\Phi(\rho(0,t)) - \Phi(k)\big) = 0 \tag{2.3.2}$$

$$\inf_{k\in \mathrm{Conv}(\rho(L,t),\rho_L(t))} \ \mathrm{sign}(\rho(L,t) - \rho_L(t))\big(\Phi(\rho(L,t)) - \Phi(k)\big) = 0 \tag{2.3.3}$$

where k is a scalar and $\mathrm{Conv}(a,b)$ is the convex set with extremities a and b, which can be written $\mathrm{Conv}(a,b) = \big(\min(a,b), \max(a,b)\big)$. Equations (2.3.2) and (2.3.3) are called entropy inequalities as they come form the Kruzkov-like formulation

$$\int_0^\infty\int_0^L \Big(|\rho-k|\partial_t\phi+\mathrm{sg}(\rho-k)\big(\Phi(\rho)-\Phi(k)\big)\partial_x\phi-\mathrm{sg}(\rho-k)(x,\rho,u)\phi\Big)\mathrm{d}x\mathrm{d}t+\int_0^L|\rho_0-k|\phi(x,0)\mathrm{d}x$$
$$+\int_0^\infty\Big(\mathrm{sg}(\rho_0-k)\big(\Phi(\rho(0,t)-\Phi(k))\big)\phi(0,t)-\mathrm{sg}(\rho_L-k)\big(\Phi(\rho(L,t)-\Phi(k))\big)\phi(L,t)\Big)\mathrm{d}t\geq 0$$

that characterizes the unique solution to (2.3.1).

2.3.2 Explicit formulation of the boundary conditions

If Equations (2.3.2) and (2.3.3) enables to prove the wellposedness of the initial boundary value problem for scalar conservation laws, it does not provide an explicit formula usable in applications. We propose below to recover the explicit solution behavior at the boundary from these equations. For convenience, we focus on the upstream boundary condition, the downstream boundary condition being analysed in the symmetrical way. To do so, we consider a concave flow function $\Phi(\cdot)$ with maximal flow Φ_m and critical density ρ_c together with an arbitrary proposed upstream boundary condition ρ_0. The upstream trace $\gamma_0\rho$ is not known a priori and the cases $\rho_0 < \rho_c$ and $\rho_0 \geq \rho_c$ are considered separately in (2.3.2).

If $\Phi'(\rho_0) > 0$ at the upstream boundary

$\Phi'(\rho_0) > 0$ means that the characteristics emanating from the boundary go forwards. As depicted on Figure 2.9, two cases should be considered depending on the possible values of $\gamma_0\rho$. We have:

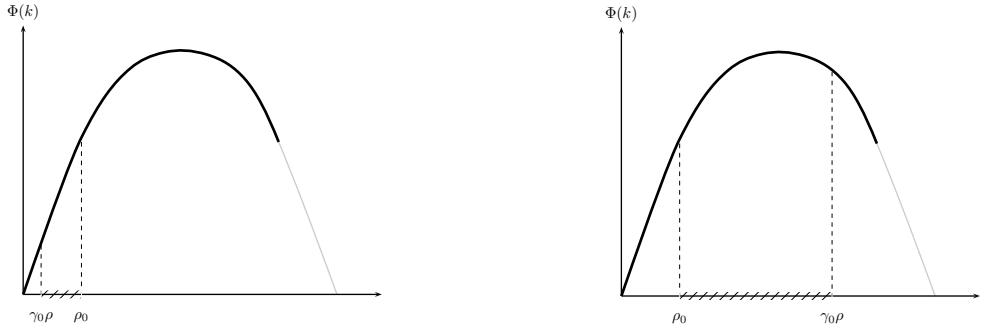

Figure 2.9: Possible configurations with $\Phi'(\rho_0) > 0$ at the upstream boundary.

Case 1: $\gamma_0\rho \leq \rho_0$ so $\mathrm{sign}(\gamma_0\rho - \rho_0) = -1$ and Equation (2.3.2) is equivalent to

$$\sup_{k\in(\gamma_0\rho,\rho_0)} \ \Phi(k) - \Phi(\gamma_0\rho) = 0$$

but

$$\sup_{k\in(\gamma_0\rho,\rho_0)} \ \Phi(k) - \Phi(\gamma_0\rho) = \Phi(\rho_0) \quad \text{for} \quad k = \rho_0$$

which becomes 0 if $\gamma_0\rho = \rho_0$, i.e. if the boundary condition applies strongly.

Case 2: $\gamma_0\rho > \rho_0$ so $\text{sign}(\gamma_0\rho - \rho_0) = 1$ and Equation (2.3.2) is equivalent to

$$\inf_{k\in(\rho_0,\gamma_0\rho)} \ \Phi(k) - \Phi(\gamma_0\rho) = 0$$

We now have 2 possibilities,

- if $\Phi(\gamma_0\rho) > \Phi(\rho_0)$ then

  $$\inf_{k\in(\rho_0,\gamma_0\rho)} \ \Phi(k) - \Phi(\gamma_0\rho) = \Phi(\rho_0) \quad \text{for} \quad k = \rho_0$$

  which becomes 0 if $\gamma_0\rho = \rho_0$, i.e. if the boundary condition applies strongly.
- if $\Phi(\gamma_0\rho) < \Phi(\rho_0)$ then

  $$\inf_{k\in(\rho_0,\gamma_0\rho)} \ \Phi(k) - \Phi(\gamma_0\rho) = 0 \quad \text{for} \quad k = \gamma_0\rho$$

  independently of ρ_0 so the trace $\gamma_0\rho$ is free and the boundary condition does not apply strongly.

The applicability of the upstream boundary condition in the case $\Phi'(\rho_0) > 0$ is summarized in Figure 2.9 where the black curves represent the region for $\gamma_0\rho$ where the boundary condition ρ_0 applies strongly whereas the gray curves represent the region where it does not have any influence, i.e. $\gamma_0\rho$ is given by the inner solution. In Figure 2.9, the stripes represent the interval $\text{Conv}(\rho_0, \gamma_0\rho)$.

If $\Phi'(\rho_0) \leq 0$ at the upstream boundary

$\Phi'(\rho_0) \leq 0$ means that the characteristics emanating from the boundary go backwards so the boundary condition ρ_0 never applies. Figure 2.10 depicts the 2 cases that should be considered in that case. We have:

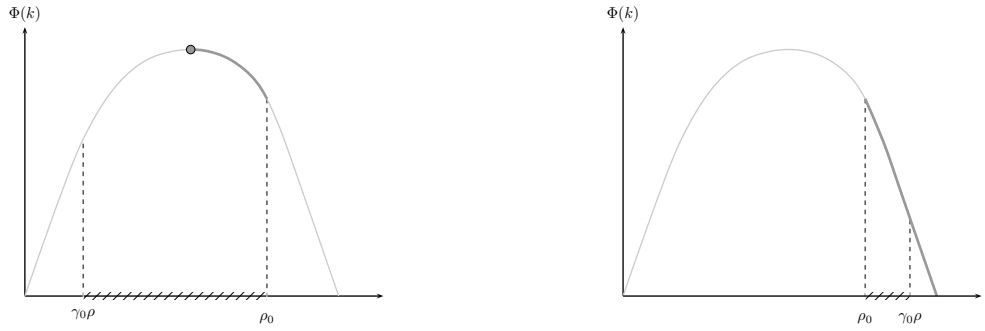

Figure 2.10: Possible configurations with $\Phi'(\rho_0) \leq 0$ at the upstream boundary.

Case 1: $\gamma_0\rho > \rho_0$ so $\text{sign}(\gamma_0\rho - \rho_0) = 1$ and Equation (2.3.2) is equivalent to

$$\inf_{k\in(\rho_0,\gamma_0\rho)} \ \Phi(k) - \Phi(\gamma_0\rho) = 0$$

but

$$\inf_{k\in(\rho_0,\gamma_0\rho)} \ \Phi(k) - \Phi(\gamma_0\rho) = 0 \quad \text{for} \quad k = \gamma_0\rho$$

independently of ρ_0 so the trace $\gamma_0\rho$ is free and no boundary condition applies.

Case 2: $\gamma_0\rho \leq \rho_0$ so $\text{sign}(\gamma_0\rho - \rho_0) = -1$ and Equation (2.3.2) is equivalent to

$$\sup_{k\in(\gamma_0\rho,\rho_0)} \ \Phi(k) - \Phi(\gamma_0\rho) = 0$$

We now have 2 possibilities,

- if $\gamma_0\rho > \rho_c$ then

  $$\sup_{k\in(\gamma_0\rho,\rho_0)} \ \Phi(k) - \Phi(\gamma_0\rho) = 0 \quad \text{for} \quad k = \gamma_0\rho$$

  independently of ρ_0 so the trace $\gamma_0\rho$ is free and no boundary condition applies.

- if $\gamma_0\rho \leq \rho_c$ then

  $$\sup_{k\in(\gamma_0\rho,\rho_0)} \ \Phi(k) - \Phi(\gamma_0\rho) = \Phi(\rho_c) = \Phi_m \quad \text{for} \quad k = \rho_c$$

  which becomes 0 if $\gamma_0\rho = \rho_c$, i.e. if the boundary flow is maximal.

The applicability of the upstream boundary condition is the case $\Phi'(\rho_0) \leq 0$ is summarized in Figure 2.10. In any case, the proposed upstream boundary condition never applies strongly. The dark gray curves in Figure 2.10 show the admissible values for $\gamma_0\rho$ which is given by the inner solution, except in the case marked by a gray dot where the maximal flow Φ_m applies.

Case of the downstream boundary

The case of the downstream boundary is similar and is not treated here as the boundary layer behavior is symmetrical to the one studies in details for the upstream boundary.

2.3.3 Alternative formulations

LeFloch's formulation

In [LeFloch, 1988], the author proposes the following equivalent formulation for the applicability of the boundary conditions when $\Phi(\cdot)$ is concave

$$\begin{cases} \rho(0,t) = \rho_0(t) \text{ and } \Phi'(\rho_0(t)) \geq 0 \\ \Phi'(\rho(0,t)) \leq 0 \text{ and } \Phi'(\rho_0(t)) \leq 0 \\ \Phi'(\rho(0,t)) \leq 0, \Phi'(\rho_0(t)) \geq 0 \text{ and } \Phi(\rho_0(t)) \geq \Phi(\rho(0,t)) \end{cases} \tag{2.3.4}$$

$$\begin{cases} \rho(L,t) = \rho_L(t) \text{ and } \Phi'(\rho_L(t)) \leq 0 \\ \Phi'(\rho(L,t)) \geq 0 \text{ and } \Phi'(\rho_L(t)) \geq 0 \\ \Phi'(\rho(L,t)) \geq 0, \Phi'(\rho_L(t)) \leq 0 \text{ and } \Phi(\rho_L(t)) \geq \Phi(\rho(L,t)) \end{cases} \tag{2.3.5}$$

Though not explicit, this formulation informs on the behavior of the boundary layer. In the first case, the boundary condition applies strongly whereas it has no effect in the two other cases, either because the characteristics leave the computational domain as in the second case or because the shocks are not allowed to enter as in the third case.

As noticed in [LeFloch, 1988], the boundary signals can be modified to simplify the boundary behavior described above. Let consider first the upstream boundary with the proposed boundary signal $\rho_0(t)$. If $\Phi'(\rho_0) \leq 0$ then the associated characteristics go backwards and the boundary condition will never apply. One consequence is that $\rho_0(t)$ may be replaced by

$$\tilde{\rho}_0(t) = \begin{cases} \rho_0(t) & \text{if } \Phi'(\rho_0) > 0 \\ \rho_c(t) & \text{if } \Phi'(\rho_0) \leq 0 \end{cases}$$

with ρ_c the critical density corresponding to maximal flow. An example of such a modification is given in Figure 2.11 for illustration.

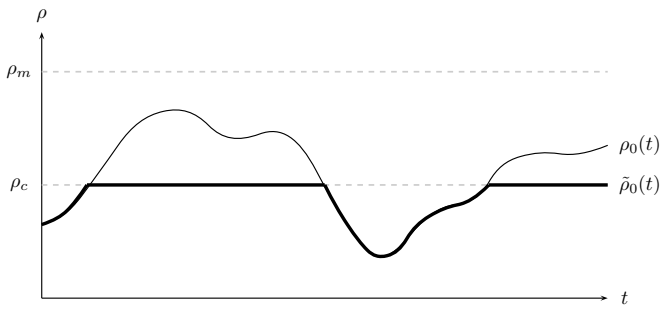

Figure 2.11: Modified boundary signal $\tilde{\rho}_0$ for ρ_0.

The upstream boundary value behavior then becomes

$$\textbf{either } \gamma_0\rho = \tilde{\rho}_0 \textbf{ either } (\Phi'(\gamma_0\rho) \leq 0 \text{ and } \Phi(\gamma_0\rho) \leq \Phi(\tilde{\rho}_0))$$

Similarly, the downstream boundary data may be changed to

$$\tilde{\rho}_L = \begin{cases} \rho_L & \text{if } \Phi'(\rho_L) < 0 \\ \rho_c & \text{if } \Phi'(\rho_L) \geq 0 \end{cases}$$

leading to the admissible downstream boundary values

$$\textbf{either } \gamma_L\rho = \tilde{\rho}_L \textbf{ either } (\Phi'(\gamma_L\rho) \geq 0 \text{ and } \Phi(\gamma_L\rho) \geq \Phi(\tilde{\rho}_L))$$

The Riemann problem formulation

A Riemann problem [LeVeque, 1992; Evans, 1998] for a conservation law is a Cauchy problem with an initial condition given by 2 constant initial states separated by a single discontinuity. Riemann problems can be solved analytically (see the appendix) for scalar conservation laws and give rise to self-similar solutions of the form $\rho(x,t) = \rho(x/t)$. In the boundary condition framework, the equivalent Riemann problem for the upstream boundary writes

$$\begin{cases} \rho(x,0) &=& \rho_I & , \text{ for } x > 0 \text{ and } t = 0 \\ \rho_0(t) &=& \rho_0 & , \text{ for } x = 0 \text{ and } t > 0 \end{cases} \tag{2.3.6}$$

Due to the self-similarity property, the flux $\Phi(\rho(0,t))$ is constant along $x = 0$ and is equal to its value Φ_0 at $t = 0$. Moreover, as $\rho(0,t)$ is necessarily between ρ_0 and ρ_I, we have $\text{sign}\big(\rho(0,t) - \rho_0\big) = \text{sign}\big(\rho_I - \rho_0\big)$. From Equation (2.3.2), the upstream BLN boundary entropy inequality writes, with $\text{Conv}(a,b) = \big(\min(a,b), \max(a,b)\big)$,

$$\sup_{k\in\text{Conv}(\rho_I,\rho_0)} \ \text{sign}\big(\rho_I - \rho_0\big)\big(\Phi_0 - \Phi(k)\big) = 0$$

$$\Updownarrow$$

$$\text{sign}\big(\rho_I - \rho_0\big)\Phi_0 = \inf_{k\in\text{Conv}(\rho_I,\rho_0)} \text{sign}\big(\rho_I - \rho_0\big)\Phi(k)$$

The upstream boundary flux is thus given by [Osher, 1984]

$$\Phi_0 = \begin{cases} \inf_{k\in[\rho_0,\rho_I]} & \Phi(k) & \text{if } \rho_0 \leq \rho_I \\ \sup_{k\in[\rho_I,\rho_0]} & \Phi(k) & \text{if } \rho_I < \rho_0 \end{cases}$$

Similarly, for the downstream Riemann problem

$$\begin{cases} \rho(x,0) &=& \rho_I & , \text{ for } x < L \text{ and } t = 0 \\ \rho_L(t) &=& \rho_L & , \text{ for } x = L \text{ and } t > 0 \end{cases} \tag{2.3.7}$$

the BLN condition writes

$$\inf_{k\in I(\rho_I,\rho_L)} \ \text{sign}\big(\rho_I - \rho_L\big)\big(\Phi_L - \Phi(k)\big) = 0$$

$$\Updownarrow$$

$$\text{sign}\big(\rho_I - \rho_L\big)\Phi_L = \sup_{k\in I(\rho_I,\rho_L)} \text{sign}\big(\rho_I - \rho_L\big)\Phi(k)$$

which gives

$$\Phi_L = \begin{cases} \sup_{k\in[\rho_L,\rho_I]} & \Phi(k) & \text{if } \rho_L \leq \rho_I \\ \inf_{k\in[\rho_I,\rho_L]} & \Phi(k) & \text{if } \rho_I < \rho_L \end{cases}$$

The boundary Riemann problems solved above thus gives an explicit formulation of the boundary fluxes for constant initial and boundary data. Such formulae are interesting when designing numerical schemes as they often require the interface flux only.

The demand/supply formulation

In [Lebacque, 1996; Lebacque & Khoshyaran, 2005], the author uses a demand/supply paradigm to model boundary behaviors. Similarly to the modification of the boundary signals given in [LeFloch, 1988], the proposed upstream boundary flow is given, for a concave flux function $\Phi(\rho)$, by the so-called demand function

$$D(\rho_0) = \begin{cases} \Phi(\rho_0) & \text{if } \Phi'(\rho_0) > 0 \\ \Phi_m & \text{if } \Phi'(\rho_0) \leq 0 \end{cases}$$

and the proposed downstream flow is given by the so-called supply function

$$S(\rho_L) = \begin{cases} \Phi(\rho_L) & \text{if } \Phi'(\rho_L) < 0 \\ \Phi_m & \text{if } \Phi'(\rho_L) \geq 0 \end{cases}$$

where Φ_m is the maximal flow. Figure 2.12 shows an example of the demand and supply functions for the quadratic Greenshield model.

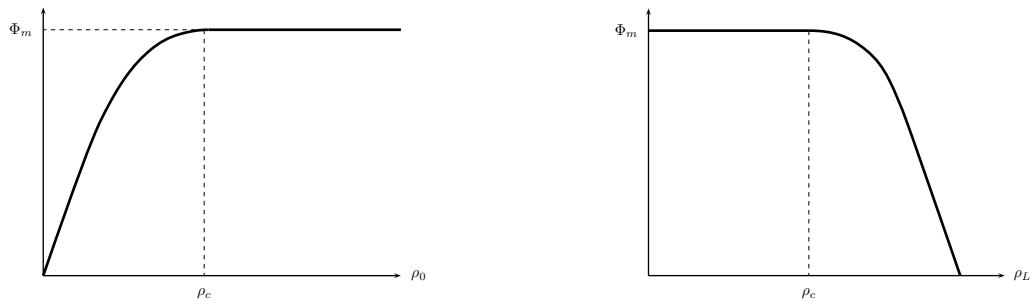

Figure 2.12: Demand (left) and supply (right) functions respectively for the upstream and downstream boundaries.

In this framework introduced in [Lebacque, 1996], the upstream boundary flow of the boundary Riemann problem (2.3.6) is given by

$$\Phi_0 = \min\Big\{D(\rho_0), S(\rho_I)\Big\}$$

whereas the downstream boundary flow of the Riemann problem (2.3.7) is given by

$$\Phi_L = \min\Big\{D(\rho_I), S(\rho_L)\Big\}$$

The great interest of the demand/supply formulation is to be equivalent [Lebacque, 2003*a*; Lebacque & Khoshyaran, 2005] to the BLN formulation introduced above, though being much simpler. This feature have important practical implications when dealing with numerical schemes to simulate the LWR model.

Boundary conditions of Hamilton-Jacobi equations

We recall that the scalar potential $\psi(x,t)$ defined by

$$\psi(x,t) = \int_0^x \rho(\zeta)\ \mathrm{d}\zeta - \int_0^t \phi_0(\tau)\ \mathrm{d}\tau$$

which fulfills

$$\nabla\psi = \begin{pmatrix} \rho \\ -\Phi(\rho) \end{pmatrix}$$

is solution of the homogeneous Hamilton-Jacobi equation

$$\begin{cases} \partial_t\psi + \Phi(\partial_x\psi) = 0 \\ \psi(x,0) = \int_0^x \rho_I(\zeta)\ \mathrm{d}\zeta \end{cases}$$

As discussed in the Cauchy problem section, this Hamilton-Jacobi equation can be solved using a combination of the method of characteristics and a selection principle that keeps the upper envelop as the physical solution. In this framework, it is always possible to add a boundary value or specify the value of $\psi(x,t)$ along a path $\{(x,t) : x = p(t)\}$, i.e. a virtual inner boundary. This last feature is indeed interesting to model accidents or a slow vehicle that constrains the traffic along its trajectory.

Assuming that the vehicle flows is measured upstream and downstream of a freeway section with coordinates $x \in (0,L)$, the specification of these boundary conditions for the scalar potential $\psi(x,t)$ writes simply

$$\begin{cases} \partial_t\psi + \Phi(\partial_x\psi) = 0 \\ \psi(x,0) = \int_0^x \rho_I(\zeta)\ \mathrm{d}\zeta \\ \psi(0,t) = -\int_0^t \phi_0(\tau)\ \mathrm{d}\tau \\ \psi(L,t) = -\int_0^t \phi_L(\tau)\ \mathrm{d}\tau \end{cases}$$

with $\phi_0(t)$ and $\phi_L(t)$ the boundary flows. Written in the cumulated vehicle variable $N(x,t)$, this equation becomes

$$\begin{cases} \partial_t N + \Phi(\partial_x N) = \phi_0(t) \\ N(x,0) = \int_0^x \rho_I(\zeta)\ \mathrm{d}\zeta \\ \psi(0,t) = 0 \\ \psi(L,t) = \int_0^t \phi_0(\tau) - \phi_L(\tau)\ \mathrm{d}\tau \end{cases}$$

These initial boundary value problems can be solved by computing the characteristics from the initial and boundary conditions and then by selecting the minimum value when projected characteristics are crossing.

2.4 Modelling of on/off-ramps

We focus in this section on the solution of the LWR model in the presence of pointwise inhomogeneities created by on and off ramps as well as abrupt changes in the parameter values. An on-ramp is an exogenous flow contribution due to incoming vehicles. This flow may come directly from the demand and its merging with the mainlane traffic or from a metered on-ramp where the inflow is controlled by storing vehicles in the ramp. Off-ramps give rise to a negative flow contribution as vehicles exit the mainlane. This leaving flow can be considered absolutely or as a split ratio of the main lane flow. As shown latter, too large on/off ramp flows may not be applicable. Figure 2.13 gives an example of a freeway with 5 links, 2 on-ramps with ramp flows $\hat{\phi}_3$ and $\hat{\phi}_5$ and 2 off-ramps with splitting ratios β_2 and β_4.

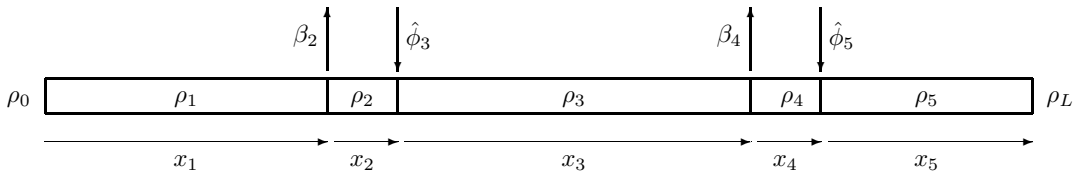

Figure 2.13: Freeway section with on/off-ramps.

In this framework, 3 possible kinds of interfaces are possible:

- **Through interfaces:** they are interfaces without any on or off ramp. The flow is thus transmitted directly from one link to the next one, possibly with different flux functions.

- **On-ramp interfaces:** these interfaces contain an on-ramp. Experimental measurements (See Figure 2.14) show that an on-ramp may become a bottleneck and creates a congestion wave that propagate upstream. We show below that the proposed models share the same feature. The flow contribution of the i^{th} on-ramp is noted $\hat{\phi}_i(t)$.

- **Off-ramp interfaces:** these interfaces contain an off-ramp. As shown later, a sufficiently large off-ramp flow may introduce a free flow in the downstream link though the upstream link stays congested. The flow contribution of the i^{th} off-ramp is given either by its absolute flow $\check{\phi}_i(t)$ or by the split ratio $\beta_i(t)$ that describes the proportion of vehicles leaving the freeway.

Figure 2.14 shows an example of the velocity time series for a sequence of loop detectors installed along a section of the South-Est beltway for Lyon, France. These data were measured during the afternoon rush hours and illustrate the formation and propagation of congestions. Sensor 4, which is installed just before an on-ramp is the first one to measure a velocity decrease, thus informing of the onset of a congestion and

making this on-ramp an active bottleneck. This velocity decrease is then measured on sensors 3, 2 and 1, showing that the congestion wave is propagating upstream. Later, a free flow wave emanates from the upstream boundary and travels forwards until the active bottleneck, thus removing completely the congestion. Models of on/off-ramps should be able to reproduce this type of behavior to be valid and useful for control applications.

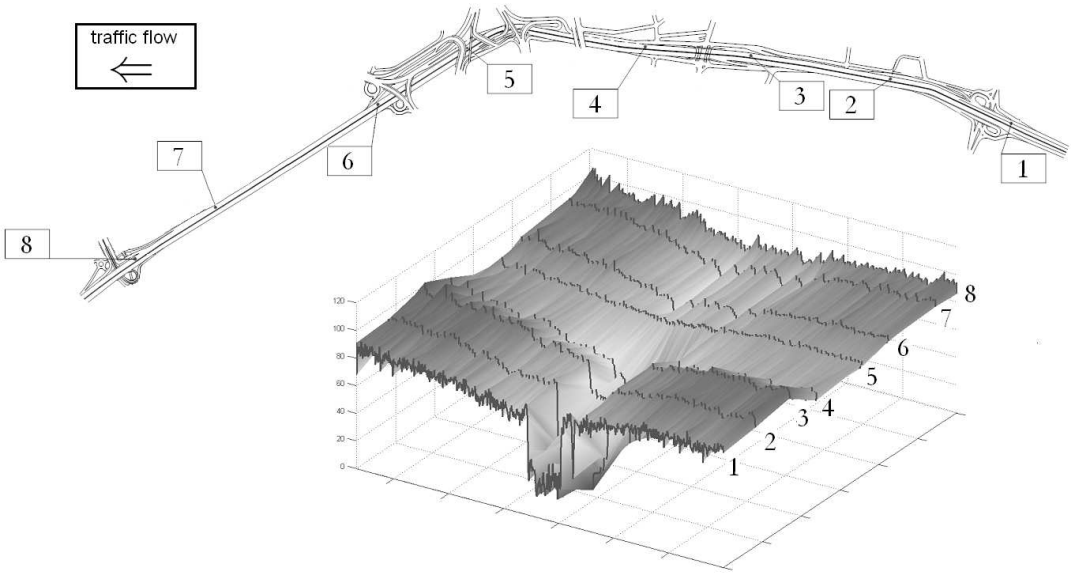

Figure 2.14: Velocity measurements along the South-Est beltway for Lyon, France.

The modelling of through interfaces have already been treated in the literature using the demand/supply paradigm as in [Daganzo, 1994], [Lebacque, 1996] and [Herty & Rascle, 2006]. We focus in this section on on/off-ramps, their particularity being to have a net flow contribution that is usually smaller than the main lane flow. Moreover, we assume that the fundamental diagrams are identical on the left and right of the inhomogeneity, though slight modifications enable to treat more general cases. Five approaches are discussed to model on/off-ramps using respectively discontinuous flux functions, switched interface conditions, the demand/supply paradigm [Daganzo, 1994; Lebacque, 1996; Lebacque & Khoshyaran, 2005], the networked approach [Holden & Risebro, 1995] and singular source terms. Our contributions on this topic concerns the approaches using the discontinuous flux, the switched formulation and the source term. Using the discontinuous flux approach, we provide an entropy condition for the on/off-ramps in order select the unique physical solution when such inhomogeneities are present. Analyzing rigorously the Riemann problem with this entropy condition, we introduce the switched formulation based on the 4 interface states respectively called the *free*, *congested*, *decoupled* and *saturated* states. The *free* and *congested* states are somewhat classical and occur in homogeneous links too. The *decoupled* state appears when an on-ramp becomes a bottleneck or an off-ramp frees a congested state. Finally, the *saturated* state may appear at on-ramps when the inflow is too large to be handled or at off-ramps when more vehicles try to be removed than possible. Based on these 4 states, the interface condition is shown to follow a finite state machine, making the

LWR model with interfaces an hybrid system. Finally, the singular source approach is interesting as it provides a geometric interpretation of the solution using the concept of generalized characteristics.

2.4.1 Using discontinuous flux functions

We restrict our attention to the on-ramp case here, the off-ramp situation being treated similarly. Let consider an on-ramp interface with a ramp flow $\hat{\phi}_i(t) > 0$ connecting 2 links with an identical concave flux function $\Phi(\cdot)$. One way to model this on-ramp is to consider, as represented on Figure 2.15, a discontinuous flow function of the from

$$\hat{\Phi}(x,t,\rho) = \Phi(\rho) + H(-x)\hat{\phi}_i(t) \tag{2.4.1}$$

where $H(\cdot)$ is the Heaviside distribution. This formulation leads to the conservation law

$$\partial_t \rho + \partial_x \hat{\Phi}(x,t,\rho) = 0 \tag{2.4.2}$$

which is equivalent to the LWR model in both link as

$$\begin{aligned} &\text{for } x > 0: && \partial_t \rho + \partial_x \Phi(\rho) = 0 \\ &\text{for } x < 0: && \partial_t \rho + \partial_x \Big(\Phi(\rho) + \hat{\phi}_i(t) \Big) = \partial_t \rho + \partial_x \Phi(\rho) = 0 \end{aligned}$$

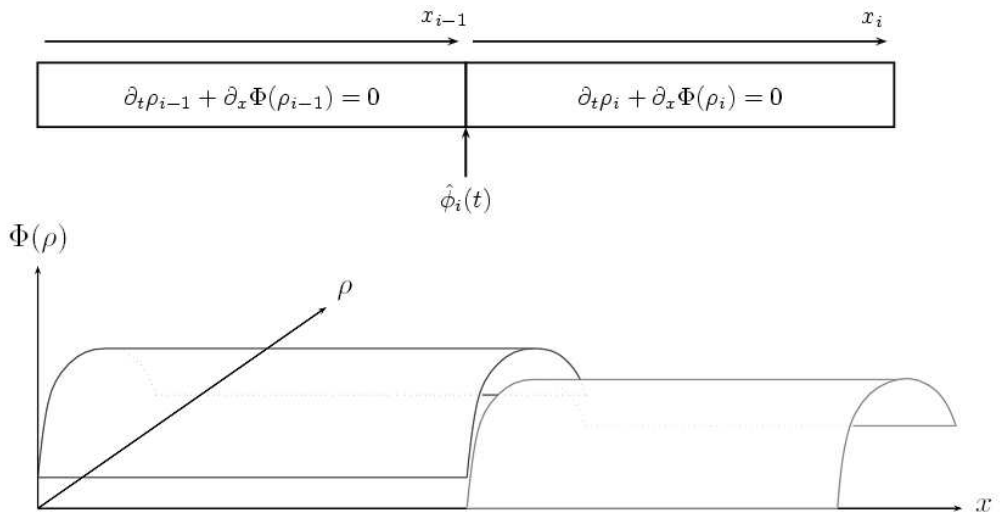

Figure 2.15: Interconnected links through an on-ramp.

Given the finite speed of wave propagation in conservation laws, we can restrict our attention to a local analysis near the interface and forget about the boundary conditions in our analysis. The 2 following theorems are proven in the appendix and generalize Kruzkov's theory [Kružkov, 1970] in the case of a discontinuous flux function as given in (2.4.1).

Theorem 2.4.1 *Given the initial condition $\rho_I \in BV(\mathbb{R}^+ \times \mathbb{R}) \cap L^\infty(\mathbb{R}^+ \times \mathbb{R})$ and a concave flux function $\Phi(\cdot)$, the Cauchy problem with (2.4.2) admits an entropy solution $\rho \in BV(\mathbb{R}^+ \times \mathbb{R}) \cap L^\infty(\mathbb{R}^+ \times \mathbb{R})$ satisfying the following entropy inequalities: $\forall k \in \mathbb{R}$, $\forall \phi \in C_0^2(\mathbb{R}^+ \times \mathbb{R})$ with $\phi \geq 0$,*

$$\int_{\mathbb{R}^+}\int_{\mathbb{R}} \Big(|\rho - k| \partial_t \phi + \operatorname{sign}(\rho - k)\big(\Phi(\rho) - \Phi(k)\big)\partial_x \phi \Big) \mathrm{d}x\mathrm{d}t + \int_{\mathbb{R}^+} \hat{\phi}_i(t)\phi(0,t)\ \mathrm{d}t + \int_{\mathbb{R}} |\rho_I - k|\phi(x,0)\ \mathrm{d}x \ \geq\ 0 \quad (2.4.3)$$

Note that theorem 2.4.1 only provides the existence of such an entropy solution. Though uniqueness can be obtained, it is not necessary here as the entropy inequalities (2.4.3) turns out to be enough to compute the unique solution of the Riemann problem. In particular, (2.4.3) gives the entropy condition stated in the next theorem.

Theorem 2.4.2 *Let ρ_i^l be the left upstream boundary value for the i^{th} link and ρ_{i-1}^r be the right downstream boundary value for the link labelled $i-1$ as in Figure 2.13. Then, a weak solution of (2.4.2) verifying the entropy inequalities (2.4.3) also verifies the following local characterizations:*

- *Rankine-Hugoniot condition:*

$$\Phi(\rho_i^l) = \Phi(\rho_{i-1}^r) + \hat{\phi}_i(t)$$

- *Entropy condition:*

$$\Phi'(\rho_i^l) > 0 \qquad \text{or} \qquad \Phi'(\rho_i^l) \leq 0 \qquad \text{or both}$$

The Rankine-Hugoniot condition is exactly the flow conservation principle and the entropy condition enables to select the only physical solution when there is a lack of uniqueness. This condition will prove to be useful when solving the Riemann problem and have thus important practical consequences when designing numerical schemes. It will be used in the next section to give a switched interpretation of the on-ramp interface behavior. One consequence of this entropy condition is that characteristics cannot emanate from both sides of an inhomogeneity so that an interface cannot provide two boundary conditions ex-nihilo.

2.4.2 Using switched interface conditions

An other way to model on/off ramps in freeways is to consider a concatenation of homogeneous LWR links interconnected through interface conditions. This approach shifts the modelling difficulty to the generalization from boundary conditions to interface conditions, where boundary values are coupled with the ramp flow rather than depending on predefined exogenous signals. Let consider first the on-ramp case. The switched interface approach relies on the two following assumptions:

1. the flow conservation applies at interfaces, i.e.

$$\Phi(\rho_i^l) = \Phi(\rho_{i-1}^r) + \hat{\phi}_i(t) \tag{2.4.4}$$

2. the boundary values should satisfy the BLN condition [Bardos et al., 1979].

Note that Equation (2.4.4) is not enough to describe the interface behavior as $\Phi(\cdot)$ is not invertible and has finite range $[0, \Phi_m]$. Moreover, (2.4.4) does not embedded any causality, i.e. it does not tell which boundary value set the other. The main ingredients to remove these inconsistencies is to look at the characteristic orientations near the interfaces to provide the causality (an incoming characteristic provides a boundary value whereas an outgoing characteristic ask for a boundary value) and to extend Equation (2.4.4) to ensure its solvability. The rigorous formulation of the switched interface formulation relies on the solution of the Riemann problem when an on-ramp is present. This approach is treated in the appendix and we only gives the conclusion of this analysis here. Moreover, we assume that feasible ramp flows are considered only. This condition writes $\hat{\phi}_i \leq \Phi(\rho_i^l)$ and means that the ramp flow leads to the jam density in the upstream link in the worst case. The case $\hat{\phi}_i > \Phi(\rho_i^l)$ would mean that the ramp flow cannot be accommodated in the current condition as there is too less room in the downstream link to absorb the ramp flow. Let introduce a finite state machine where the on-ramp interface may be in 3 possible states:

1. **free**: This state corresponds to the situation where a free flow is crossing the interface and

$$\rho_i^l = \Phi^{-l}\big(\Phi(\rho_{i-1}^r) + \hat{\phi}_i\big) \tag{2.4.5}$$

with $\Phi^{-l}(\cdot)$ the left inverse of $\Phi(\cdot)$. The free state typically occurs when both boundaries are undercritical, i.e. $\rho_{i-1}^r \leq \rho_c$ and $\rho_i^l \leq \rho_c$, and the interface does not act as a bottleneck, i.e. $\Phi(\rho_{i-1}^r) + \hat{\phi}_i < \Phi_m$. This state applies as well when a congestion wave reach the interface from downstream but is not strong enough to unfree the upstream link.

2. **congested**: This state corresponds to the situation where a congested flow is crossing the interface and

$$\rho_{i-1}^r = \Phi^{-r}\big(\Phi(\rho_i^l) - \hat{\phi}_i\big) \tag{2.4.6}$$

with $\Phi^{-r}(\cdot)$ the right inverse of $\Phi(\cdot)$. Note that this last equation should be replaced by $\rho_{i-1}^r = \Phi^{-r}\big(\max\{\Phi(\rho_i^l) - \hat{\phi}_i, 0\}\big)$ if unfeasible ramp flows are allowed. This would imply that $\rho_{i-1}^r = \rho_m$ when $\hat{\phi}_i > \Phi(\rho_i^l)$ and the extra vehicles are stored on the onramp. The congested state typically occurs when both boundaries are overcritical, i.e. $\rho_{i-1}^r > \rho_c$ and $\rho_i^l \geq \rho_c$ or when an upstream free flow wave reaches the interface but does not manage to free the downstream link.

3. **decoupled**: This state corresponds to the situation where the interface is a bottleneck and

$$\begin{cases} \rho_i^l = \rho_c \\ \rho_{i-1}^r = \Phi^{-r}\big(\Phi_m - \hat{\phi}_i\big) \end{cases} \tag{2.4.7}$$

So the upstream boundary is congested (i.e. $\rho_{i-1}^r > \rho_c$) whereas the downstream boundary is at the sonic point ($\rho_i^l = \rho_c$).

In states *free* and *congested*, the on-ramp flow is respectively advected downstream and upstream whereas in state *decoupled*, the flow is maximal downstream of the on-ramp and the ramp flow is advected upstream through a congestion wave. Note that this situation decouples the 2 links as no characteristic cross the interface. Moreover, it leads to a jump discontinuity that is not entropic as the right boundary value $\rho_i^l = \rho_c$ is smaller than left boundary value $\rho_{i-1}^r = \Phi^{-r}\big(\Phi_m - \hat{\phi}_i\big) \geq \rho_c$.

The switched interface condition then takes the form of the Finite State Machine (FSM) as represented in Figure 2.16. In this FSM (see the appendix), the dashed transitions correspond to some shocks crossing the interface independently of the ramp flow. On the contrary, the black transition from the *free* state to the *decoupled* state is due to the ramp flow and have its origin in the range default of the flux function in Equation (2.4.5). This transition thus corresponds to an onramp flow that is large enough to perturb the mainlane state and create a congestion that propagates upstream. The gray transition from the *congested* state only occurs for an unfeasible onramp flow. In this situation, a range default occurs in Equation (2.4.6). It corresponds to a ramp flow that is too large to be absorbed, thus leading to a queuing of the extra vehicles at the ramp.

For illustration purpose, Figures 2.17 and 2.18 illustrate the FSM behavior for an onramp by showing how boundary values $\rho_{i-1}^r < \rho_c$ and $\rho_i^l > \rho_c$ are transmitted at the interface. Figure 2.17 illustrates the *free* and the *decoupled* cases whereas Figure 2.18 illustrates the *congested* case. We refer the reader to the appendix for more details on how the on-ramp interface behavior can be deduced rigorously from the solutions of a set of Riemann problems.

Figure 2.19 shows a trajectory of a LWR model with one on-ramp and virtual initial, boundary and ramp flow data. We recognize the switched dynamics of the on-ramp interface which is initially *free*, then *decoupled* due to the large ramp flow and then *free* again thanks to a free flow wave moving from the upstream boundary.

A similar FSM can be built for off-ramps where the flow conservation principle writes

$$\Phi(\rho_i^l) = \big(1 - \beta_i(t)\big)\ \Phi(\rho_{i-1}^r)$$

and the possible states of the interface are

1. **free**:
$$\rho_i^l = \Phi^{-l}\Big(\big(1 - \beta_i(t)\big)\ \Phi(\rho_{i-1}^r)\Big) \tag{2.4.8}$$

2. **congested**:
$$\rho_{i-1}^r = \Phi^{-r}\left(\frac{\Phi(\rho_i^l)}{\big(1 - \beta_i(t)\big)}\right) \tag{2.4.9}$$

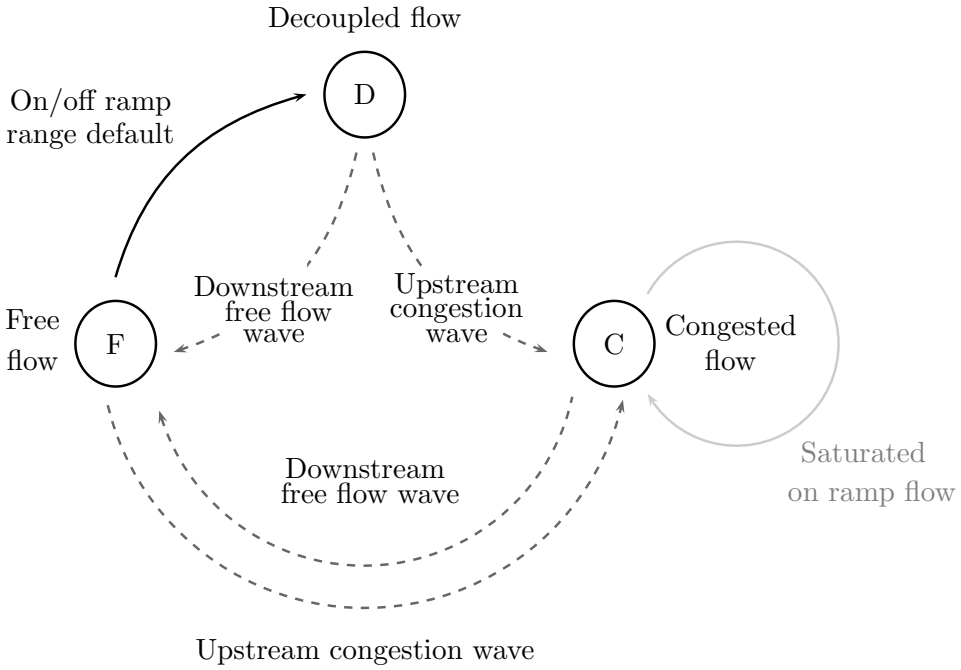

Figure 2.16: FSM of an on-ramp interface.

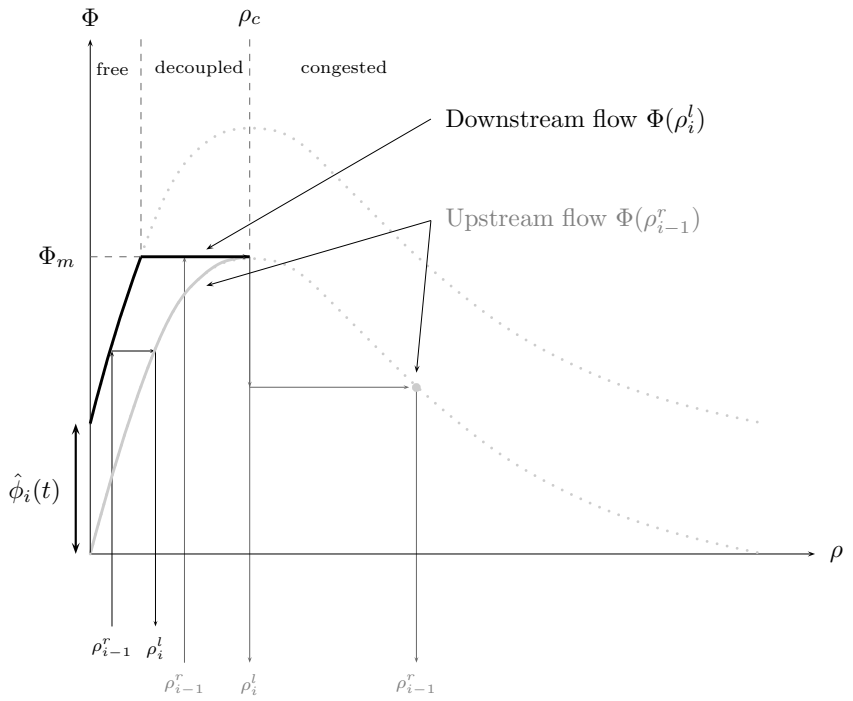

Figure 2.17: The black density computation corresponds to a *free* flow and the gray computation to a transition to *decoupled* flow due to the finite range of $\Phi(\cdot)$.

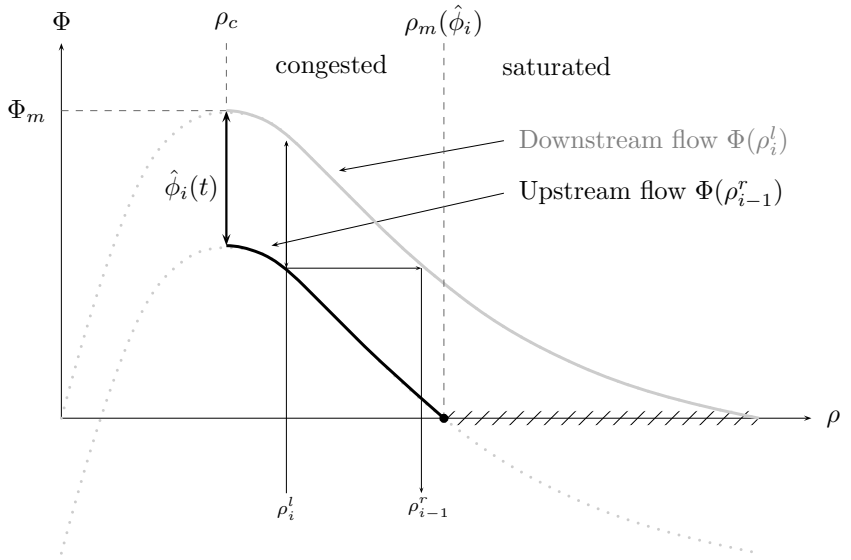

Figure 2.18: Density computation for a *congested* flow.

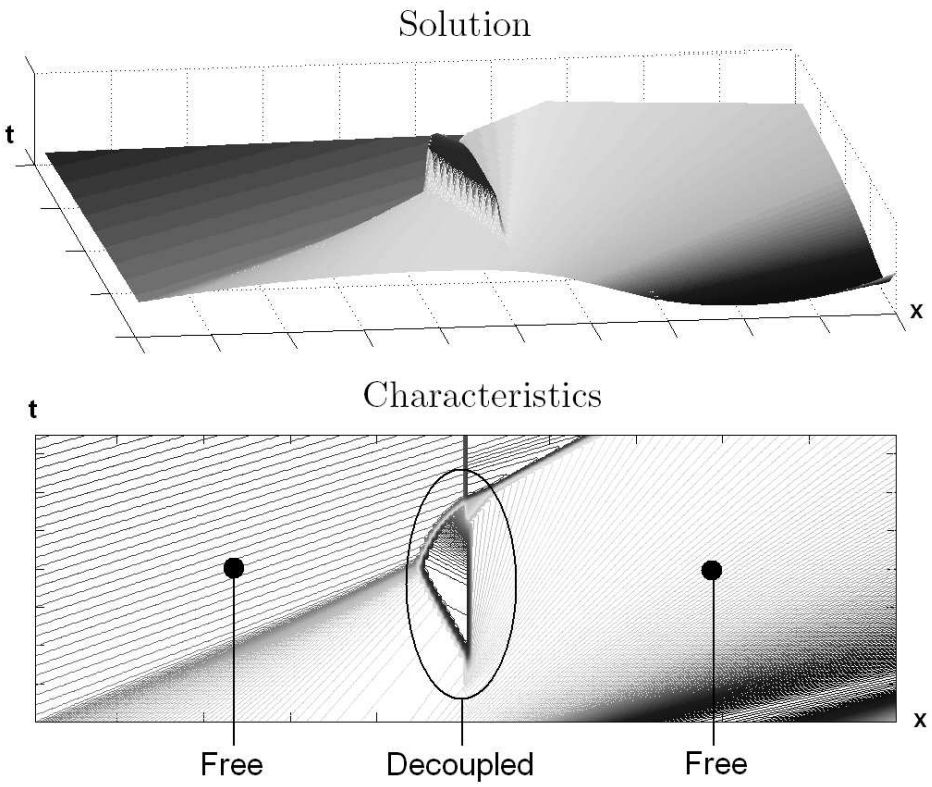

Figure 2.19: A trajectory of a LWR model with an on-ramp.

3. **decoupled**:

$$\begin{cases} \rho_i^l = \big(1 - \beta_i(t)\big)\Phi_m \\ \rho_{i-1}^r = \rho_c \end{cases} \tag{2.4.10}$$

For off-ramps, the upstream link is congested and the downstream link is free in the decoupled state.

A FSM similar to the one represented in Figure 2.16 applies in the offramp case. In this situation, the *decoupled* state occurs when the offramp flow is small enough the free the traffic downstream of the ramp.

2.4.3 Using the demand/supply paradigm

In [Lebacque, 1996], the author uses a demand/supply paradigm similar to [Daganzo, 1994] in order to model freeway inhomogeneities such as a change in the number of lanes or in the maximal velocity. In this setting, the demand function at the downstream boundary of link $i-1$ is defined by the nondecreasing modification of the flux function and writes

$$D(\rho_{i-1}^r) = \begin{cases} \Phi(\rho_{i-1}^r) & \text{for } \rho_{i-1}^r \in (0, \rho_c) \\ \Phi_m & \text{for } \rho_{i-1}^r \in (\rho_c, \rho_m) \end{cases}$$

On the other hand, the supply function at the upstream boundary of link i is defined as the nonincreasing modification of the flux function and writes

$$S(\rho_i^l) = \begin{cases} \Phi_m & \text{for } \rho_i^l \in (0, \rho_c) \\ \Phi(\rho_i^l) & \text{for } \rho_i^l \in (\rho_c, \rho_m) \end{cases}$$

In the demand/supply paradigm for link interconnections, the interface flow is computed by the min formula

$$\phi_{i-1,i} = \min\Big\{D(\rho_{i-1}^r), S(\rho_i^l)\Big\}$$

The validity of this approach can be shown as following. With the above definitions, the characteristics of the demand function $D(\rho_{i-1}^r)$ always have nonnegative speeds whereas the characteristics of supply function $S(\rho_i^l)$ always have nonpositive speeds. This modification of the boundary conditions, which is very similar to the one proposed in [LeFloch, 1988], does not modify the solution of the initial boundary value problem of links $i-1$ and i. The min formula is then a way to ensure that the flow conservation is fulfilled while removing the possible range default problems. However, it gives the boundary flow but not the density values applying at the boundaries. Note that this demand/supply method can be used without any modification when the flow diagrams are different upstream and downstream of the interface [Lebacque, 1996], which makes this approach very efficient for numerical simulations.

In the case of an on-ramp with inflow $\hat{\phi}_i$, the demand function is modified by

$$D^{\hat{\phi}_i}(\rho_{i-1}^r) = \begin{cases} \Phi(\rho_{i-1}^r) + \hat{\phi}_i & \text{for } \rho_{i-1}^r \in (0, \rho_c) \\ \Phi_m + \hat{\phi}_i & \text{for } \rho_{i-1}^r \in (\rho_c, \rho_m) \end{cases}$$

and the interface flow decomes

$$\phi_{i-1,i} = \min\left\{D^{\hat{\phi}_i}(\rho^r_{i-1}), S(\rho^l_i)\right\}$$

Note that when $S(\rho^l_i) < \hat{\phi}_i$, the interface flow $\phi_{i-1,i}$ is lower than $\hat{\phi}_i$, meaning that some vehicles are stored on the on-ramp. In the case of an off-ramp with split ratio β_i, the demand function is modified by

$$D^{\beta_i}(\rho^r_{i-1}) = \begin{cases} (1-\beta_i)\ \Phi(\rho^r_{i-1}) & \text{for } \rho^r_{i-1} \in (0, \rho_c) \\ (1-\beta_i)\ \Phi_m & \text{for } \rho^r_{i-1} \in (\rho_c, \rho_m) \end{cases}$$

and the min formula becomes

$$\phi_{i-1,i} = \min\left\{D^{\beta_i}(\rho^r_{i-1}), S(\rho^l_i)\right\}$$

Figure (2.20) shows the shapes of the demand and supply functions for an on-ramp and an off-ramp. The possible status of the on-ramp are F, D, C and S respectively for *free*, *decoupled*, *congested* and *saturated* and they are F, D and C for the off-ramp. It can be shown that the demand/supply formulation gives the same solution than the explicit Riemann solution.

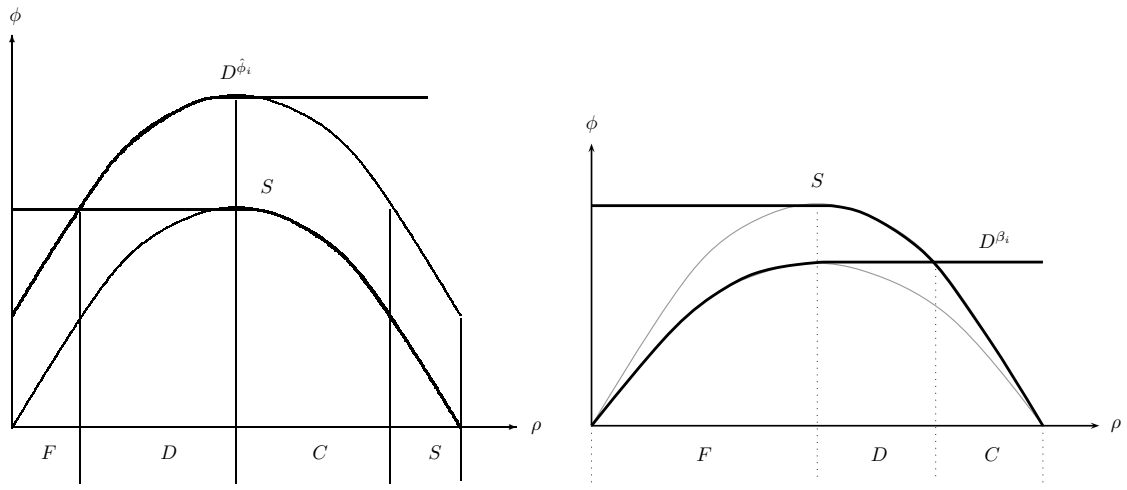

Figure 2.20: Demand/supply paradigm for on-ramps (left) and off-ramps (right).

2.4.4 Using a concatenation of homogeneous links

In [Coclite et al., 2005], the authors analyse a network of LWR links and prove its wellposedness with some additional assumptions for the node behavior. Due to the finite wave propagation in conservation laws, the analysis of a single node is not restrictive. The authors define the node dynamics with

- a set of $n+m$ links with densities ρ_i on intervals (a_i, b_i) and flow functions $\Phi_i(\cdot)$ where $i = 1, ..., n$ identifies incoming links whereas $i = n+1, ..., n+m$ identifies outgoing links,
- a fixed traffic distribution matrix $A = \{\alpha_{ji}\}_{j=n+1,...,n+m}^{i=1,...,n}$ satisfying $\sum_j \alpha_{ji} = 1$ which describes the ratio of vehicle that drives from link i to link j.

The weak solution at a junction is defined by the set of densities ρ_i verifying

$$\sum_{i=1}^{n+m} \int_0^{\infty} \int_{a_i}^{b_i} (\rho_i \partial_t \phi_i + \Phi_i(\rho_i) \partial_x \phi_i) \, \mathrm{d}x \mathrm{d}t = 0$$

for every $\phi_i \in C_0^1(\mathbb{R})$ smooth across the junction, i.e.

$$\phi_i(b_i, 0) = \phi_j(a_i, 0) \quad \text{and} \quad \partial_x \phi_i(b_i, 0) = \partial_x \phi_j(a_i, 0)$$

for $i = 1, ..., n$ and $i = n+1, ..., n+m$. A direct consequence is the Rankine-Hugoniot condition that writes

$$\sum_{i=1}^{n} \Phi_i(\phi_i(b_i, t)) = \sum_{j=n+1}^{n+m} \Phi_j(\phi_j(a_j, t))$$

With the assumptions

- $\Phi_j(\phi_j(a_j, t)) = \sum_{i=1}^{n} \alpha_{ji} \Phi_i(\phi_i(b_i, t))$ for $j = n+1, ..., n+m$,
- $\sum_{i=1}^{n} \Phi_i(\phi_i(b_i, t))$ is maximal,

the authors proved in [Coclite et al., 2005] that the networked LWR model has a unique entropy solution. One particularity of this approach is that the condition $\sum_{i=1}^{n} \Phi_i(\phi_i(b_i, t))$ *is maximal* should be added without any traffic engineering justification. We note that the *discontinuous flux function formulation* analyzed in a previous section enforces such a flow maximization at an onramp interface without mentioning it explicitly in the modelling assumptions.

2.4.5 Using a singular source term

To extent the LWR model and model on/off-ramps, we can come back to its original integral formulation. Let consider a restricted section with an on-ramp as the one represented of Figure 2.21. By adopting a macroscopic point of view, all lanes are abstracted as a unique aggregated lane and the merging area (dark gray) is abstracted as a point.

The principle of vehicle conservation then writes

$$\frac{d}{dt} \int_{x_L}^{x_R} \rho(t, x) dx = \Phi(\rho(t, x_L)) - \Phi(\rho(t, x_R)) + \hat{\phi}_i(t) \tag{2.4.11}$$

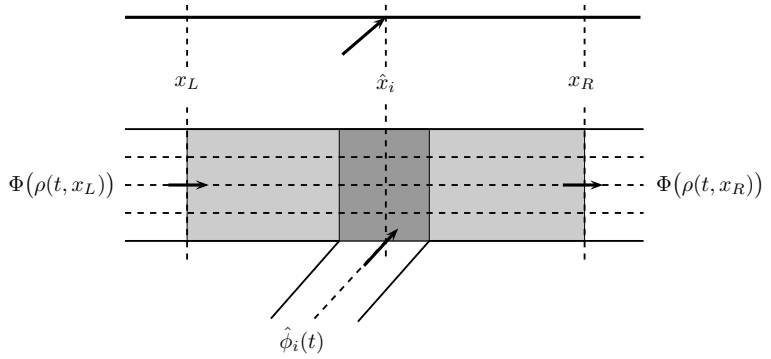

Figure 2.21: Real (down) and abstracted (up) section with one on-ramp.

which can be rewritten like in the homogeneous situation as

$$\int_{x_L}^{x_R} \partial_t \rho(t,x)dx = \int_{x_L}^{x_R} \big(-\partial_x \Phi(\rho(t,x)) + \delta(x-\hat{x}_i)\hat{\phi}_i(t)\big)dx \tag{2.4.12}$$

with $\delta(x-\hat{x}_i)$ the Dirac distribution centered at $\hat{x}_i$. Equation (2.4.12) easily generalizes to several inflows $\hat{\phi}_i(t)$ at $\hat{x}_i$ and outflows $\check{\phi}_i(t)$ at $\check{x}_i$ and can be rewritten in the divergence form

$$\partial_t \rho(t,x) + \partial_x \Phi(\rho(t,x)) = \sum_{i=1}^{N_{\text{on}}} \delta(x-\hat{x}_i)\hat{\phi}_i(t) + \sum_{i=1}^{N_{\text{off}}} \delta(x-\check{x}_i)\check{\phi}_i(t) \tag{2.4.13}$$

We note that in any neighborhood without ramp, this traffic model is strictly equivalent to the LWR model. Using the method of generalized characteristics [Dafermos, 1977*b*], it can be show that (2.4.13) have a solution similar to the one obtained in the *discontinuous flux function* and the *switched* frameworks. For the reader convenience, this analysis can be found in the appendix.

2.4.6 Using cumulated variables and Hamilton-Jacobi equations

As discussed in the boundary condition section, the method of characteristics allows to force the scalar potential $\psi(x,t)$ to assume a specified value along a given space-time curve. The Hamilton-Jacobi equation $\partial_t \psi + \Phi(\partial_x \psi) = 0$ then enables to compute the solution of $\psi(x,t)$ forward in time from the initial and boundary conditions by using the method of characteristics and the *upper envelop selection principle*.

When reaching an on-ramp at $x = \hat{x}_i$ with flow $\hat{\phi}_i(t)$, either from upstream for free flow or from downstream for congested flow, the potential $\psi(x,t)$ is modified at the interface such that

$$\begin{cases} \partial_t \psi(x_i^+,t) = \partial_t \psi(x_i^-,t) - \hat{\phi}_i(t) \\ \partial_t \psi(x_i^+,t) \geq -\Phi_m \end{cases}$$

with Φ_m the capacity in the downstream link. If the first equation can easily be integrated and gives $\psi(x_i^+,t) = \psi(x_i^-,t) - \int_0^t \hat{\phi}_i(\tau)\, d\tau$, the second one is more tricky. The cumulative

vehicle approach is thus usable for free and congested traffic but is not convenient when the traffic is in the decoupled state.

It is the simple hypotheses of which one must be most wary, because these are the ones that have the most chances of passing unnoticed.

Henri Poincaré (1854-1912),
French mathematician, theoretical physicists and philosopher of science.

Chapter 3

The Aw-Rascle-Zhang non-equilibrium model

3.1 Origin and wave system of the ARZ model

There exists mainly two classes of non-equilibrium traffic models for which a second variable is added to the density in order to take into account the observed discrepancies between the measurements and the fundamental diagram. The first one, proposed in [Payne, 1971], is called the Payne-Whitham (PW) model and is very similar to the more recent model developed in [Zhang, 1998]. These models, developed in analogy with the gas dynamics, were severely criticized in [Daganzo, 1995*b*] as small perturbations in the traffic stream may travel faster than the vehicles, implying that drivers may be influenced by the traffic behind them. In response to these obvious limitations, [Aw & Rascle, 2000] and [Zhang, 2002] proposed independently an anisotropic model called the Aw-Rascle-Zhang (ARZ) model, which has been completed with a relaxation term in [Greenberg, 2001]. As a consequence, we restrict our study of non-equilibrium traffic models to the ARZ model as it does not suffer of the isotropy limitation, it has been the subject of many recent studies [Haut & Bastin, 2005; Lebacque et al., 2005; Herty & Rascle, 2006; Herty, Moutari & Rascle, 2006; Garavello & Piccoli, 2006*a*] and is potentially more representative of the traffic behavior in congestions. A theoretical interest of the ARZ model is to be a Temple class [Temple, 1983] system of conservation laws for which more results are available [Colombo & Groli, 2004; Ancona & Coclite, 2005] than for general nonlinear systems. Moreover, an important property of the ARZ model is that its Riemann problem (a Cauchy problem with a piecewise constant initial condition) can be solved analytically [Aw & Rascle, 2000; Lebacque et al., 2005], enabling the direct use of the Godunov scheme [Godunov, 1959; Godlewski & Raviart, 1996] to compute efficiently its numerical solution.

3.1.1 Motivations of the ARZ model

In its general form, the ARZ model takes the form

$$\begin{cases} \partial_t \rho + \partial_x(\rho v) = 0 \\ \partial_t\big(v+P(\rho)\big)+v\partial_x\big(v+P(\rho)\big)=\frac{V(\rho)-v}{\tau} \end{cases} \tag{3.1.1}$$

with $\rho(x,t)$ the vehicle density, $v(x,t)$ the vehicle velocity, $P(\rho)$ a so-called pressure term, $V(\rho)=\Phi(\rho)/\rho$ the equilibrium velocity profile and τ a relaxation parameter. For different pressure terms $P(\rho)$, we get

1. the Aw-Rascle model [Aw & Rascle, 2000] for $P(\rho)=\rho^\gamma$, $\gamma>0$,
2. the Zhang model [Zhang, 2002] for $P(\rho)=-V(\rho)$.

The conservative counterpart of (3.1.1) writes

$$\partial_t \begin{pmatrix} \rho \\ y \end{pmatrix} + \partial_x \begin{pmatrix} y-\rho P(\rho) \\ \frac{y^2}{\rho} - yP(\rho) \end{pmatrix} = \begin{pmatrix} 0 \\ \frac{\Phi(\rho)-y+\rho P(\rho)}{\tau} \end{pmatrix} \tag{3.1.2}$$

with ρ and $y=\rho(v+P(\rho))$ the conserved variables leading to $\phi=\phi(\rho,y)=y-\rho P(\rho)$. We now assume, as proposed in [Zhang, 2002], that $P(\rho)=-V(\rho)$ and following [Lebacque et al., 2005], we define the relative speed variable by $I=v-V(\rho)$. In this situation, a physical interpretation of the so-called relative flow variable $y=\rho(v-V(\rho))=\phi-\Phi(\rho)$ is to be the discrepancy between the current traffic flow and the flow given by the fundamental diagram at the current traffic density. This variable is represented on Figure 3.1 for a specific data point along with other experimental data. The second equation in (3.1.1) rewrites with the relative speed variable as follows

$$\partial_t I + v\partial_x I = -\frac{I}{\tau} \qquad \Leftrightarrow \qquad \dot{I} = -\frac{I}{\tau}$$

meaning that the relative speed I is advected freely at the vehicle velocity for an infinite reaction time $\tau=\infty$ and decreases exponentially to 0 with rate $1/\tau$ along the vehicle trajectories for finite reaction times. For this reason, the variable I is called a Lagrangian marker as it characterize the vehicles in the traffic stream. With $P(\rho)=-V(\rho)$, Equation (3.1.2) becomes

$$\partial_t \begin{pmatrix} \rho \\ y \end{pmatrix} + \partial_x \underbrace{\begin{pmatrix} y+\Phi(\rho) \\ (y+\Phi(\rho))\frac{y}{\rho} \end{pmatrix}}_{F(\rho,y)} = \begin{pmatrix} 0 \\ -\frac{y}{\tau} \end{pmatrix} \tag{3.1.3}$$

with $F(\rho,y)$ the flux vector in the conserved variables $\rho-y$. Note that the choice of the conserved variables have a direct influence on the irregular solution of a conservation law as a nonlinear change of variables may modify the shock speed given by the Rankine-Hugoniot condition [LeVeque, 1992].

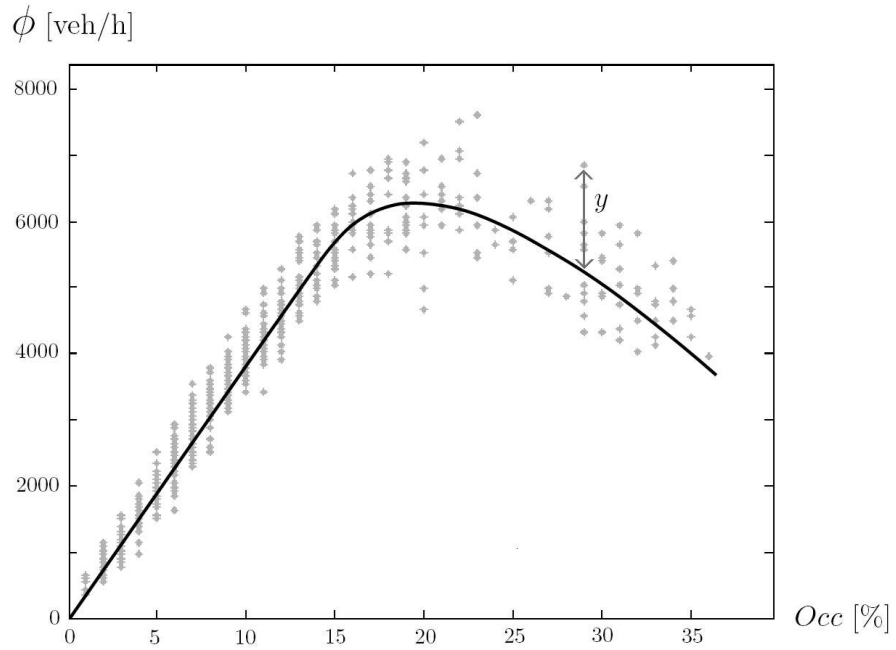

Figure 3.1: Physical interpretation of the y variable.

3.1.2 Wave system of the ARZ model

The analysis of the wave system of the ARZ model can be found in [Aw & Rascle, 2000] and [Lebacque et al., 2005].

Eigenstructure

The Jacobian matrix of $F(\rho, y)$, as defined in Equation (3.1.3), is given by

$$A(\rho, y) = DF(\rho, y) = \begin{pmatrix} \Phi'(\rho) & 1 \\ \Phi'(\rho)\frac{y}{\rho} - (y + \Phi(\rho))\frac{y}{\rho^2} & \frac{2y+\Phi(\rho)}{\rho} \end{pmatrix}$$

Solving $\det(DF(\rho, y) - \lambda I) = 0$, we get the characteristic speeds

$$\lambda_1(\rho, y) = \frac{y}{\rho} + \Phi'(\rho) \qquad \lambda_2(\rho, y) = \frac{y + \Phi(\rho)}{\rho}$$

which, expressed in the phase plane $(\rho, v) = (\rho, (y + \Phi(\rho))/\rho)$, gives

$$\lambda_1(\rho, v) = v + \rho V'(\rho) \leq v \qquad \lambda_2(\rho, v) = v$$

showing that the model is anisotropic as all wave speeds are smaller or equal to the traffic stream average velocity v. An interesting relationship is

$$\lambda_1(\rho, v) = v + \rho V'(\rho) = (v - V(\rho)) + V(\rho) + \rho V'(\rho) = (v - V(\rho)) + \Phi'(\rho)$$

meaning that $\lambda_1(\rho, v)$ is equal to the LWR characteristic speed $\Phi'(\rho)$ plus the relative velocity $I = v - V(\rho)$. The right eigenvectors are defined by $DF(\rho, y)r_i = \lambda_i r_i$. With

the notation $r_i = (a_i, b_i)^T$, the first row of $DF(\rho, y)r_i = \lambda r_i$ gives for the first field

$$b_1 = \frac{y}{\rho}\, a_1$$

so that possible choices are

$$r_1 = \begin{pmatrix} 1 \\ \frac{y}{\rho} \end{pmatrix} \text{ for } a_1 = 1 \qquad \text{or} \qquad r_1 = \begin{pmatrix} \rho \\ y \end{pmatrix} \text{ for } a_1 = \rho$$

Similarly, for the second filed, we get

$$b_2 = \Big(\frac{y + \Phi(\rho)}{\rho} - \Phi'(\rho) \Big)\, a_1$$

so that a possible choice is

$$r_2 = \begin{pmatrix} \rho \\ y + \Phi(\rho) - \rho\Phi'(\rho) \end{pmatrix} = \begin{pmatrix} \rho \\ y - \rho^2 V'(\rho) \end{pmatrix} \quad \text{for } a_1 = \rho$$

Elementary waves

Two classes of waves are present in the ARZ model: the 1-waves for the first field and the 2-waves for the second field that propagate respectively at speed λ_1 and λ_2 in smooth regions. As explained in [Lax, 1973], the 1-field may develop shock and rarefaction waves as it is genuinely nonlinear, i.e. $\nabla\lambda_1 \cdot r_1(\rho, y) \neq 0$ whereas the 2-field may only generate contact discontinuities as it is linearly degenerate, i.e. $\nabla\lambda_2 \cdot r_2(\rho, y) = 0$. Moreover, as $\lambda_1 \leq v$ and $\lambda_2 = v$, 1-waves always have a speed smaller or equal to the traffic velocity whereas 2-waves are always contact discontinuities propagating at the traffic speed. Let now consider the wave interconnection between a constant left state (ρ_-, y_-) and a constant right state (ρ_+, y_+). Due to the wave speeds discussed above, the left state (ρ_-, y_-) is always connected by a 1-wave to an intermediate state (ρ_0, y_0), itself connected by a 2-wave to the right state (ρ_+, y_+). The relationships between (ρ_-, y_-) and (ρ_0, y_0) on one hand and (ρ_0, y_0) and (ρ_+, y_+) on the other hand are given by the following analysis of elementary waves.

- **Shock waves in the 1-field:**

  A shock wave with speed σ connects (ρ_-, y_-) to (ρ_0, y_0) if both states belong to the same Hugoniot locus [LeVeque, 1992] given by

  $$\sigma \begin{bmatrix} \rho \\ y \end{bmatrix} = \begin{bmatrix} y + \Phi(\rho) \\ (y + \Phi(\rho))y/\rho \end{bmatrix} \tag{3.1.4}$$

  Basic manipulations to remove σ from (3.1.4) give the 1-shock jump condition

  $$\frac{y_0}{\rho_0} = \frac{y_-}{\rho_-} \tag{3.1.5}$$

meaning that the relative velocity $I = v - V(\rho)$ is conserved across a shock wave and that the Hugoniot locus in the $\rho - v$ plane is given by the shifted velocity diagram $v_0 = c + V(\rho_0)$ where $c = v_- - V(\rho_-)$. Moreover, plugging (3.1.5) in (3.1.4) gives the shock speed

$$\sigma = \frac{\Phi(\rho_0) - \Phi(\rho_-)}{\rho_0 - \rho_-} + \underbrace{\frac{y_-}{\rho_-}}_{I} \tag{3.1.6}$$

showing that the shock speed in the ARZ model is increased by the relative speed I compared to the LWR model.

- **Rarefaction waves in the 1-field:**

The rarefaction curve connecting (ρ_-, y_-) to (ρ_0, y_0) in the 1-field can be described parametrically by $(\rho(\xi), y(\xi))$, which is solution of the ordinary differential equation

$$\begin{pmatrix} \dot\rho \\ \dot y \end{pmatrix} = \frac{r_1(\rho, y)}{\nabla\lambda_1 \cdot r_1(\rho, y)} \qquad \text{with} \qquad \begin{pmatrix} \rho(0) \\ y(0) \end{pmatrix} = \begin{pmatrix} \rho_- \\ y_- \end{pmatrix}$$

Taking $r_1 = \begin{pmatrix} \rho \\ y \end{pmatrix}$, we have $\nabla\lambda_1 \cdot r_1(\rho, y) = \rho\Phi_e''(\rho)$ and deduce easily

$$\begin{cases} \dot\rho = 1/\Phi_e''(\rho) \\ \dot y = y/(\rho\Phi_e''(\rho)) \end{cases}$$

The condition for (ρ_-, y_-) to be connected to (ρ_0, y_0) by a 1-rarefaction wave is

$$\frac{\dot y}{y} = \frac{\dot\rho}{\rho} \qquad \Leftrightarrow \qquad \frac{y}{\rho} = \text{constant} \qquad \Leftrightarrow \qquad \frac{y_0}{\rho_0} = \frac{y_-}{\rho_-} \tag{3.1.7}$$

We deduce again that the relative velocity $I = y/\rho = v - V(\rho)$ is conserved along 1-rarefaction waves and that the rarefaction curve is again the shifted velocity diagram $v_0 = c + V(\rho_0)$ with $c = v_- - V(\rho_-)$. As the Hugoniot locus and the rarefaction curves coincide, the ARZ model is a Temple class system [Temple, 1983].

- **Contact discontinuities in the 2-field:**

Concerning the contact wave in the 2-field, the second eigenvalue is conserved across the discontinuity, implying that the velocity is conserved across these discontinuities, i.e.

$$\lambda_2(\rho_0, y_0) = \lambda_2(\rho_+, y_+) \quad \Leftrightarrow \quad v_0 = v_+ \quad \Leftrightarrow \quad \frac{y_0 + \Phi(\rho_0)}{\rho_0} = \frac{y_+ + \Phi(\rho_+)}{\rho_+} \tag{3.1.8}$$

3.1.3 Analytical solution of the ARZ Riemann problem

States involved in the solution of the Riemann problem

A Riemann problem is a Cauchy problem with the piecewise constant initial data

$$(\rho, v) = \begin{cases} (\rho_-, y_-) & \text{for} \quad x \leq 0 \\ (\rho_+, y_+) & \text{for} \quad x > 0 \end{cases}$$

Riemann problems are known to give rise to self-similar solutions of the form

$$\big(\rho(x,t), y(x,t)\big) = \big(\rho(x/t), y(x/t)\big)$$

and they can be solved analytically in the scalar case whereas systems usually require an approximate solver as the Roe average method [LeVeque, 1992]. It is a remarkable fact that the Riemann problem of the ARZ model can be solved analytically as for scalar equations, a nice property that will be useful when designing numerical schemes such as the Godunov method [LeVeque, 1992]. Throughout this section, we assume that $\Phi(\rho)$ is strictly concave, which is realistic according to the traffic measurements shown in Figure 3.1. Moreover, for notational convenience, it is often simpler to state the results in the $\rho - v$ plane when solving the Riemann problem. To compute the intermediate state (ρ_0, v_0) connecting (ρ_-, v_-) and (ρ_+, v_+), Equations (3.1.5), (3.1.7) and (3.1.8) give

$$v_0 - V(\rho_0) = v_- - V(\rho_-) \quad \text{and} \quad v_0 = v_+$$

which enables to conclude that

$$\begin{cases} v_0 = v_+ \\ \rho_0 = V^{-1}(v_+ - v_- + V(\rho_-)) \end{cases} \tag{3.1.9}$$

leading to the intermediate relative flow $y_0 = \rho_0(v_0 - V(\rho_0))$. As explained in [Mammar et al., 2005], the mapping $V^{-1}(\cdot)$ may need to be extended to ensure that (3.1.9) always have a solution. To do so, we assume $V^{-1}(\xi) = 0$ for $\xi > \max V(\cdot)$ and $V^{-1}(\xi) = \rho_m$ for $\xi < 0$. With this convention proposed in [Mammar et al., 2005], the Riemann problem of the ARZ model can always be solved analytically.

Elementary wave interconnections in the LWR Riemann problem

The next step is to determine what kind of elementary waves are connecting the states (ρ_-, v_-) and (ρ_0, v_0) involved in the 1-wave. The Lax entropy condition [Lax, 1973] states that a 1-shock occurs when $\lambda_1(\rho_-, v_-) > \lambda_1(\rho_0, v_0)$ whereas a 1-rarefaction wave

develops if $\lambda_1(\rho_-, v_-) \leq \lambda_1(\rho_0, v_0)$. For the 1-shock case, this condition can be rewritten

$$\begin{array}{c} \lambda_1(\rho_-, v_-) > \lambda_1(\rho_0, v_0) \\ \Updownarrow \\ v_- + \rho_- V'(\rho_-) > v_0 + \rho_0 V'(\rho_0) \\ \Updownarrow \\ V(\rho_-) + \rho_- V'(\rho_-) > V(\rho_0) + \rho_0 V'(\rho_0) \\ \Updownarrow \\ \Phi'(\rho_-) > \Phi'(\rho_0) \end{array} \tag{3.1.10}$$

where we used the fact that $v_- - V(\rho_-) = v_0 - V(\rho_0)$ across 1-waves to go from line two to three. We conclude that a 1-shock occurs when $\Phi'(\rho_-) > \Phi'(\rho_0)$ and a 1-rarefaction occurs otherwise. Moreover, with the assumption that $\Phi(\rho)$ is strictly concave, $\Phi'(\rho)$ is monotonic decreasing, leading to the equivalent condition:

- if $\rho_- < \rho_0$, then a 1-shock occurs with shock speed σ given by Equation (3.1.6),
- if $\rho_- > \rho_0$, then a 1-rarefaction wave occurs with minimal and maximal wave speeds $\lambda_1(\rho_-, v_-)$ and $\lambda_1(\rho_0, v_0)$ respectively,
- if $\rho_- = \rho_0$, which is the case when $v_- = v_+ = v_0$ from Equation (3.1.9), then no intermediate state is needed and the solution of the Riemann problem is trivial.

Surprisingly, these conditions are very similar to the entropy condition for the LWR model where the right state is replaced by the intermediate state (ρ_0, v_0). This feature shows the close connection between the ARZ model and the LWR model.

3.2 Treatment of boundary conditions

We consider in this section the upstream case only, the downstream case being treated similarly. As mentioned in [Joseph & LeFloch, 1999], it is a remarkable fact to notice that there is still no unified understanding for the treatment of boundary conditions for systems of conservation laws. We propose here to use the formulation of [Dubois & LeFloch, 1988] where the Dirichlet boundary condition $\mathbf{u}(0,t) = \mathbf{u}_{\text{up}}(t) = (\rho_{\text{up}}(t), y_{\text{up}}(t))$ is replaced by the weaker

$$\mathbf{u}(0,t) \in \mathcal{V}_{\text{up}}(\mathbf{u}_{\text{up}}(t)) = \left\{ w(0+, \mathbf{u}_{\text{up}}(t), \mathbf{u}) : \mathbf{u} \in \mathbb{R}^2_+ \right\} \tag{3.2.1}$$

where $\mathcal{V}_{\text{up}}(\mathbf{u}_{\text{up}}(t))$ is an admissible set of boundary values that depends on the proposed boundary signal $\mathbf{u}_{\text{up}}(t)$. One option discussed in [Dubois & LeFloch, 1988] is to rely on the self-similar solution $w(x/t, \mathbf{u}_{\text{up}}(t), \mathbf{u})$ of the Riemann problem with left and right states $\mathbf{u}_{\text{up}}(t)$ and $\mathbf{u}(0,t)$ respectively to define the set $\mathcal{V}_{\text{up}}(\mathbf{u}_{\text{up}}(t))$. Note that $\mathbf{u}_{\text{up}}(t) \in \mathcal{V}_{\text{up}}(\mathbf{u}_{\text{up}}(t))$ but is not reduced to it.

To compute $\mathcal{V}_{\rm up}(\mathbf{u}_{\rm up}(t))$, all the possible cases should be considered in the underlying Riemann problem. A quick analysis shows that there are at most 5 possible cases as shown in Figure 3.2, each case being identified by the wave present in the genuinely non-linear field: forward shock, forward rarefaction, backward shock, backward rarefaction and sonic rarefaction.

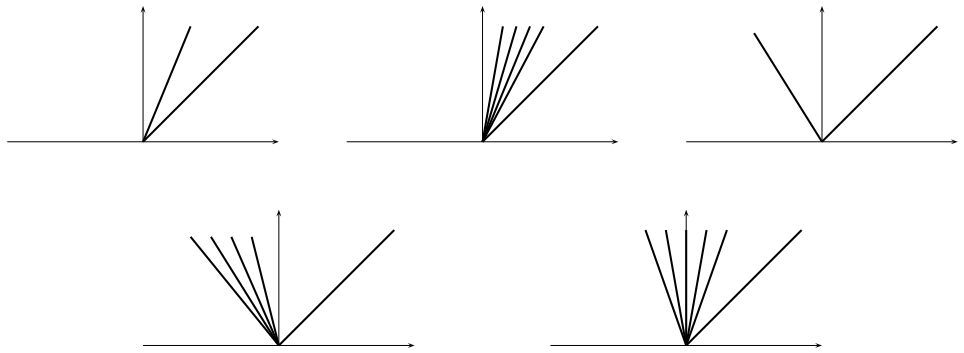

Figure 3.2: Possible wave patterns for the ARZ Riemann problem.

We refer to Figure 3.3 for an explanation of the set $\mathcal{V}_{\rm up}(\mathbf{u}_{\rm up}(t))$. The set of vanishing 1-wave speed $\lambda_1(\rho, v) = 0$ is given by $v = -\rho V'(\rho)$ and is taken to be a straight line by assuming without restriction a linear velocity diagram $V(\rho)$, which ease the exposition. $\mathcal{S}$ and $\mathcal{R}$ denote respectively the shock and rarefaction curves whose expressions are both given by the translated fundamental diagram $v = (v_{\rm up} - V(\rho_{\rm up})) + V(\rho)$. Nevertheless, $\mathcal{S}$ is on the side of decreasing λ_1 whereas $\mathcal{R}$ is on the side of increasing λ_1 with respect to the boundary signal $\mathbf{u}_{\rm up}(t)$. The gray curves are the admissible boundary values and the striped sets correspond to the different boundary behaviors depending on $\mathbf{u}(0, t)$. Note that the striped sets are oriented horizontally as the speed v is constant along 2-waves. When $\lambda_1(\mathbf{u}_{\rm up}(t)) > 0$, the region with horizontal stripes corresponds to a rarefaction wave with all positive 1-wave speeds, the region with oblique stipes to a shock with positive speed and the one with vertical stripes to a shock with negative speed, implying that the inner intermediate state applies at the boundary in that case. In Figure 3.3, $\rho^\star$ is the density value at which the shock speed $\sigma = \sigma_{LWR} + I$ vanishes. When $\lambda_1(\mathbf{u}_{\rm up}(t)) \leq 0$, the gray circle on the rarefaction curve corresponds to a sonic rarefaction wave and occurs in the horizontal stripe set. The region with oblique stipes corresponds to a rarefaction wave with all negative speeds and the one with vertical stripes to a shock with negative speed. In both cases $\lambda_1(\mathbf{u}_{\rm up}(t)) > 0$ and $\lambda_1(\mathbf{u}_{\rm up}(t)) \leq 0$, we note that either the boundary signal $\mathbf{u}_{\rm up}(t)$ applies, either the intermediate state previously noted ρ_0 for the Riemann problem applies.

The downstream boundary case is slightly different as the wave patterns of Figure 3.2 are not symmetrical. Nevertheless, the same approach can be used to determine the set $\mathcal{V}_{\rm do}(\mathbf{u}_{\rm do}(t))$. In practice, boundary conditions are implemented numerically using ghost cells or a supply/demand paradigm similar to the one used for the LWR model.

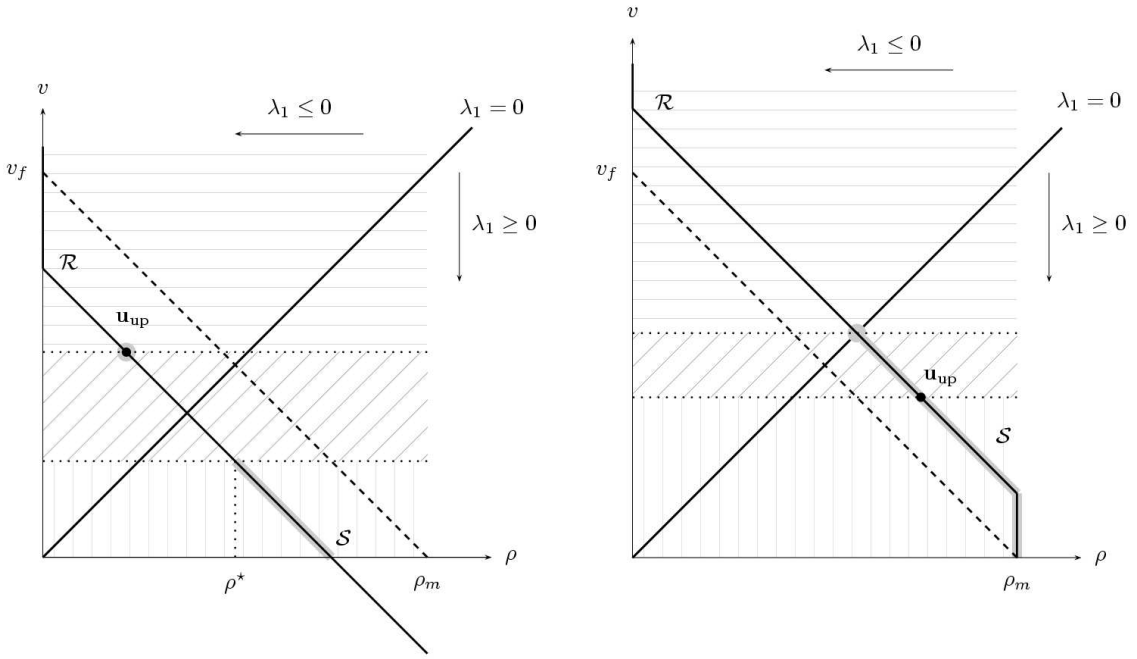

Figure 3.3: Left: Admissible boundary values when $\lambda_1(\mathbf{u}_{\rm up}(t)) > 0$. Right: Admissible boundary values when $\lambda_1(\mathbf{u}_{\rm up}(t)) \leq 0$.

3.3 Modelling of on/off-ramps

3.3.1 Solution of the Riemann problem

We consider on-ramps only in this section as off-ramps behave similarly. Moreover, we assume without restriction that the fundamental diagrams are identical on both sides of the ramp. Related problems have been treated in [Lebacque et al., 2005] for discontinuous fundamental diagrams and in [Herty & Rascle, 2006] for networked ARZ links. We consider here an on-ramp with an incoming flow $\hat{\phi}$ separating 2 links respectively with boundary values $\mathbf{u}_R = (\rho_R, y_R)$ and $\mathbf{u}_L = (\rho_L, y_L)$. As shown in the wave system analysis and the boundary condition analysis, an intermediate state $\mathbf{u}_M = (\rho_M, y_M)$ appears at the boundary of the second link and is connected to the state $\mathbf{u}_R$ by a 2-wave propagating at speed v. One consequence is that $\mathbf{u}_L$ and $\mathbf{u}_M$ are the actual boundary values that should be connected through additional compatible waves. In particular, a static wave that fulfills the flow conservation principle should be incorporated at the ramp location with $\mathbf{u}_-$ and $\mathbf{u}_+$ denoting respectively the traces of the solution upstream and downstream of it. Depending on the solution of the associated Riemann problem, we can have $\mathbf{u}_- = \mathbf{u}_L$ or $\mathbf{u}_+ = \mathbf{u}_M$ or neither of these situations when the onramp is a bottleneck.

The fundamental assumption for the transmission of the boundary conditions is that the Lagrangian marker $I = y/\rho = v - V(\rho)$ is conserved across on-ramps, which means that incoming vehicles adapt to the mainlane relative velocity. With our notations, the

conserved relative speed is I_L and we get the boundary flows

$$\rho_- v_- = \Phi(\rho_-) + I_L \rho_- \quad \text{and} \quad \rho_+ v_+ = \Phi(\rho_+) + I_L \rho_+$$

With the modified fundamental diagram $\Phi_I(\rho) = \Phi(\rho) + I\rho$ as defined in [Lebacque et al., 2005], the flow conservation principle $\rho_- v_- = \rho_+ v_+ + \hat{\phi}$ at the onramp writes

$$\Phi_{I_L}(\rho_+) = \Phi_{I_L}(\rho_-) + \hat{\phi}$$

with $\mathbf{u}_-$ connected or equal to $\mathbf{u}_L$ and $\mathbf{u}_-$ connected or equal to $\mathbf{u}_R$. To solve this wave interconnection problem, we first note that the 1-wave speed is directly related to the slope of the modified diagram as $\Phi_I'(\rho) = \lambda_1(\rho, I)$. There is thus an interest in defining the demand and supply functions as in the LWR model. Second, the ARZ shock speed given by (3.1.6) can be visualized graphically on the modified diagram $\Phi_I(\rho)$ as it is equal to the slope of the straight line connecting the involved states as for the LWR model. Note as well that $\mathbf{u}_M$ can be computed easily from $\mathbf{u}_R$ as it is at the intersection of $\Phi_I(\rho)$ with the straight line connecting $\mathbf{u}_R$ to the origin. These remarks along with the classical assumption that the interface flow should be maximized when there is an ambiguity enable to compute the solution of the Riemann problem. In particular, it should be noticed that two 1-waves can be present in some situations as for the LWR model in the decoupled case.

Solving the ARZ Riemann problem consists in considering all the possible values for $\mathbf{u}_L$ and $\mathbf{u}_R$ and then determine a valid set of waves that enable the interconnection of $\mathbf{u}_L$ to $\mathbf{u}_R$ through intermediate states. The only qualitative difference between the Riemann problem solutions for the LWR and the ARZ model is that the ARZ model has an additional 2-wave that always propagate faster than the other waves. Based on this fact, the cases to be considered for the ARZ Riemann problem are exactly the same than for the LWR, except that the modified fundamental diagram $\Phi_I(\rho)$ should be considered instead of $\Phi(\rho)$. Moreover, $\mathbf{u}_M$ plays the role of the right state in the LWR model and is computed directly from $\mathbf{u}_R$. As the rigorous solution of the LWR Riemann problem is given in the appendix and is similar for the ARZ model, we only provide here three representative solutions of the ARZ Riemann problem as depicted on Figures 3.4, 3.5 and 3.6. As for the LWR model, there exists an upper bound on the feasible ramp flow that depends both on the upstream state through I_L and the downstream state through the intermediate state ρ_M.

3.3.2 The demand/supply paradigm

Following [Lebacque et al., 2005], let define the modified critical density $\rho_c^\star = \text{argmax } \Phi_{I_L}(\rho)$ and the modified maximal flow $\Phi_m^\star = \max \Phi_{I_L}(\rho)$. Then, still following

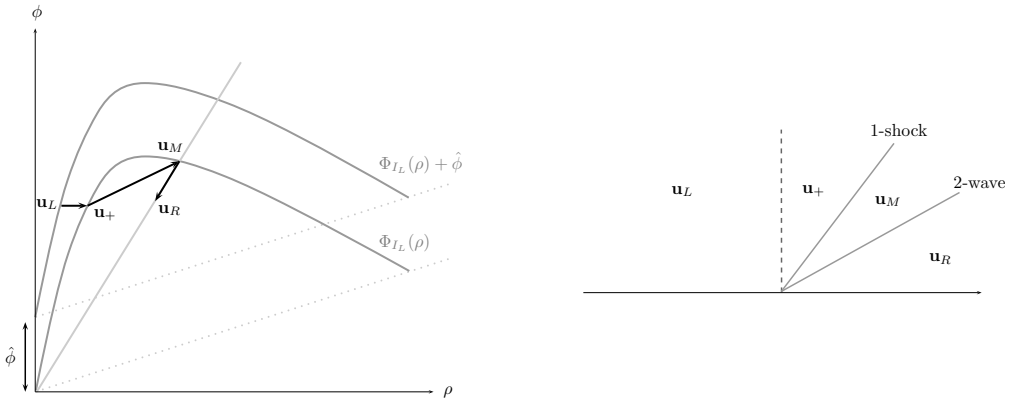

Figure 3.4: Free interface.

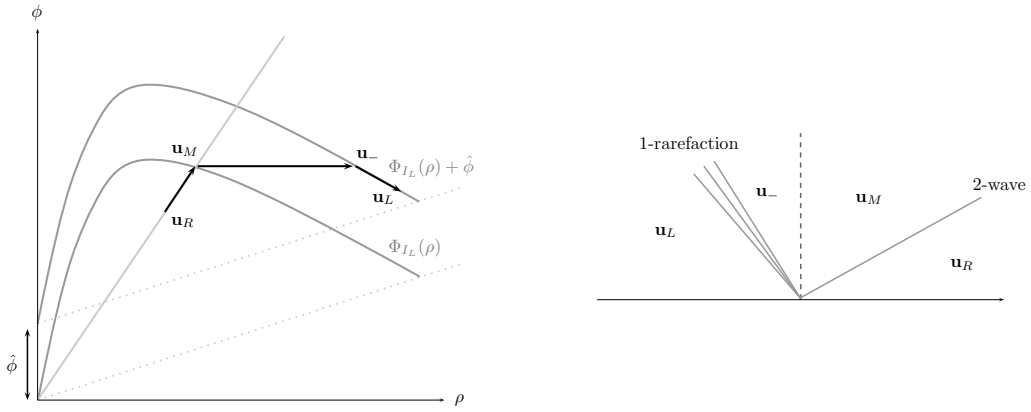

Figure 3.5: Congested interface.

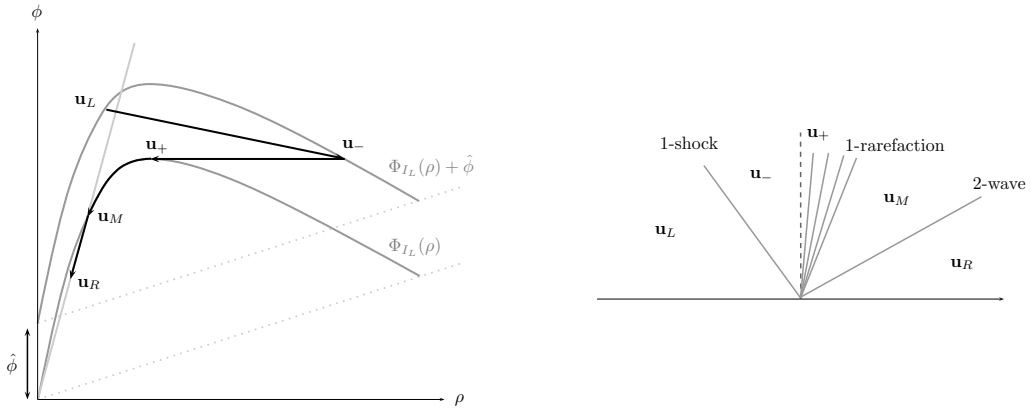

Figure 3.6: Decoupled interface.

[Lebacque et al., 2005], the modified demand and supply functions can be defined by

$$D_{I_L}(\rho) = \begin{cases} \Phi_{I_L}(\rho) + \hat{\phi} & \text{if } \rho \leq \rho_c^\star \\ \Phi_m^\star + \hat{\phi} & \text{if } \rho > \rho_c^\star \end{cases}$$

$$S_{I_L}(\rho) = \begin{cases} \Phi_{I_L}(\rho) & \text{if } \rho \geq \rho_c^\star \\ \Phi_m^\star & \text{if } \rho < \rho_c^\star \end{cases}$$

It can be shown that the flow immediately downstream of the ramp location in the Riemann problem can be computed with the simple formula [Lebacque et al., 2005]

$$F_\rho = \min\big\{D_I(\rho_L), S_I(\rho_M)\big\}$$

where the notation F_ρ was used to show that this formula provides the interface flux for the conserved variable ρ. Similarly, we have $F_y = \rho v I_L = F_\rho I_L$ giving immediately the interface flux for the conserved variable y. F_ρ can then be used to recover the values of the traces $\mathbf{u}_-$ and $\mathbf{u}_+$ using the left and right inverses of $Phi_{I_L}(\rho)$. Though this formulation is very useful for numerical schemes, it is sometime preferable to express the transmission of the boundary conditions in the original variables like ρ and y. This kind of formulation is for instance necessary to compute the sensitivity at onramps.

3.3.3 The switched formulation

We now introduce an interface finite state machine similar to the one used for the LWR model. To do so, 4 states should be defined in the general case, which can be reduced to 3 if we assumed that the ramp are always feasible. For all cases, only the density has to be provided as the velocity can be deduced from

$$v_* = \frac{\Phi_{I_L}(\rho_*)}{\rho_*} = V(\rho_*) + I_L \qquad \text{where } * = L,\ -,\ +\ \text{or } M.$$

Similarly, the conserved variable y can be deduced from

$$y_* = \rho_* I_L \qquad \text{where } * = L,\ -,\ +\ \text{or } M.$$

The 4 possible states are the followings:

1. *Free.* In this state, the left boundary condition is transmitted downstream so that $\mathbf{u}_- = \mathbf{u}_L$ and $\rho_+ = \Phi_{I_L}^{-l}(\Phi_{I_L}(\rho_L) + \hat{\phi})$ with $\Phi_{I_L}^{-l}(\cdot)$ the left inverse of $\Phi_{I_1}(\cdot)$.

2. Congested: In this state, the right boundary condition is transmitted upstream so that $\mathbf{u}_+ = \mathbf{u}_M$ and $\rho_- = \Phi_{I_L}^{-r}(\Phi_{I_L}(\rho_M) - \hat{\phi})$ with $\Phi_{I_L}^{-r}(\cdot)$ the right inverse of $\Phi_{I_1}(\cdot)$.

3. *Decoupled.* In this state, no boundary value set the other and the 2 links can be virtually disconnected. We have $\rho_+ = \rho_c^\star$ and $\rho_- = \Phi_{I_L}^{-r}(\Phi_m^\star - \hat{\phi})$.

4. *Saturated.* This situation occurs when ρ_M and $\hat{\phi}$ are large enough such that the ramp flow is not feasible, i.e. there is no solution ρ to $\Phi_{I_L}(\rho_M) = \Phi_{I_L}(\rho) + \hat{\phi}$.

Similarly to the LWR model, the transition from *Free* to *Decoupled* happens when $\Phi_{I_L}(\rho_L) + \hat{\phi} > \Phi_m^\star$ which again leads to a range default. As a consequence, the same kind of Finite State Machine (FSM) as depicted on Figures 3.7 applies for an onramp interface modelled by the ARZ model. Figure 3.8 shows how these different cases should be interpreted in the $\rho - \rho v$ phase plane for the *free*, *decoupled* and *congested* situations.

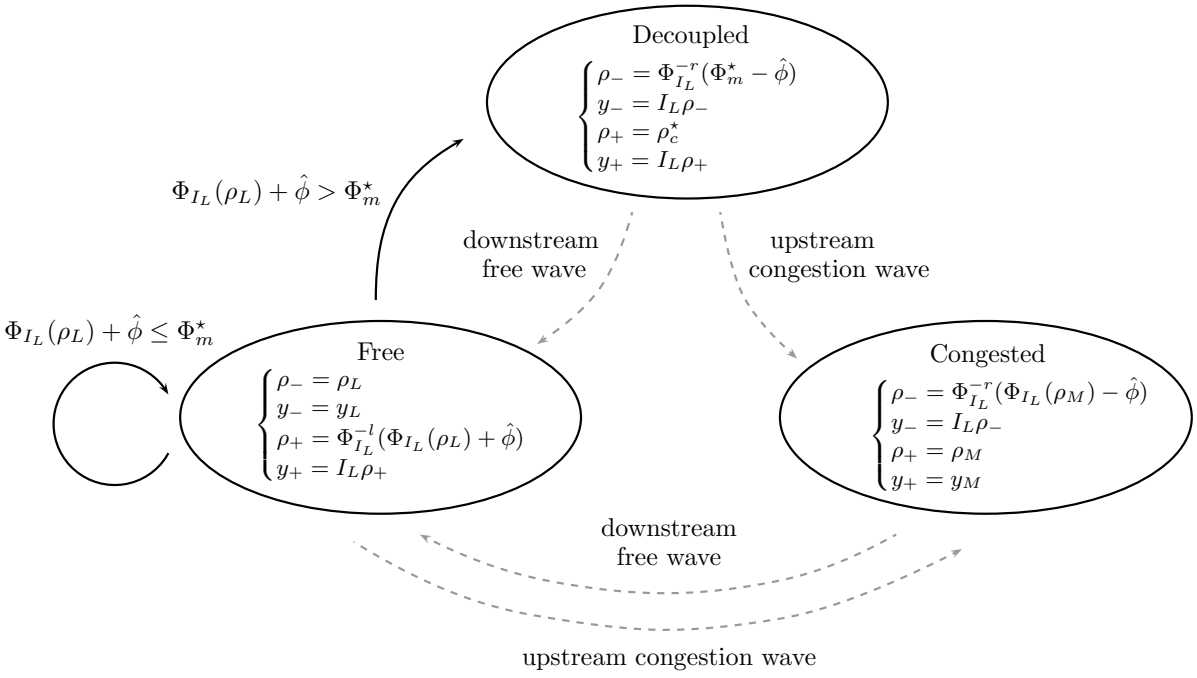

Figure 3.7: Finite state machine applying at onramps for the ARZ model.

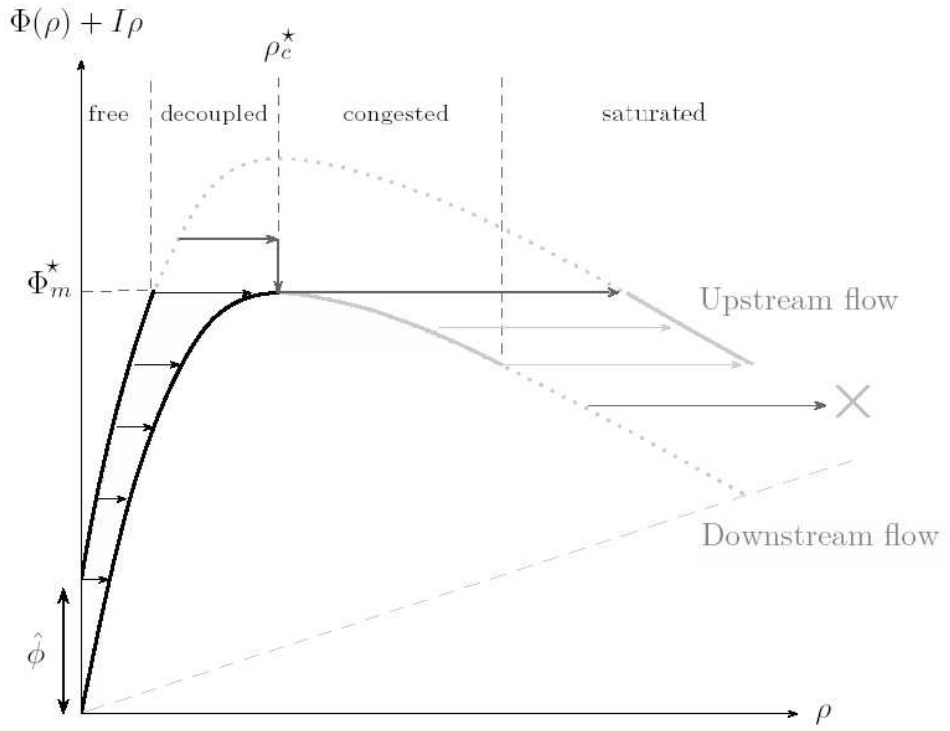

Figure 3.8: Flow arbitration at onramps for the ARZ model.

What is simple is false, what is not is unusable.

Paul Valéry (1871-1945),
French author and Symbolist poet.

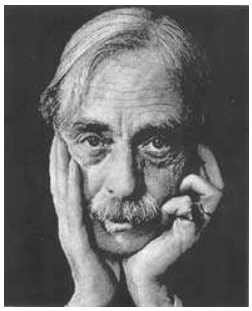

Chapter 4

The Multiclass Origin-Destination model

4.1 Origin and analysis of the Cauchy problem

4.1.1 Motivations of the MOD model

An extension of the LWR model proposed in [Daganzo, 1995*a*], [Lebacque, 1996], [Zhang & Jin, 2002] [Gavage & Colombo, 2003], [Garavello & Piccoli, 2005], [Herty, Kirchner & Moutari, 2006] and [Wong & Wong, 2002] is to consider that the aggregated traffic stream can be decomposed in classes, each class identifying a specificity of the vehicles such as the destination, the path or the vehicle/driver category. The classes considered here are the origin-destination of the vehicles, the targeted application being dynamic assignments and the estimation of origin-destination matrices using a dynamical traffic model.

For illustration purpose, let consider the small freeway section of Figure 4.1 where time series of the traffic counts are plotted for every entries and exits of the network in addition to a plot of the decreasing velocity diagram $V(\rho)$. The goal of the multiclass model studied here is understand and reproduce the dynamics occurring in the links assuming that the origin-destination data are available. In this setting, a direct application is to track the vehicles based on their origin-destination in order to evaluate the delay suffered by the different classes. As mentioned before, an other targeted application application is to use an optimization algorithm to update recursively the origin-destination matrix based of a previous guess using the traffic counts only.

Figure 4.2 provides an abstraction of the network depicted on Figure 4.1. The model is made of a set of origins and destinations, connected by homogeneous links supporting the different possible routes. In this network, the origin-destination data is given by signals α_1 and α_2 that are in the interval $(0, 1)$.

Let consider an homogeneous link where the vehicles are tagged by their route iden-

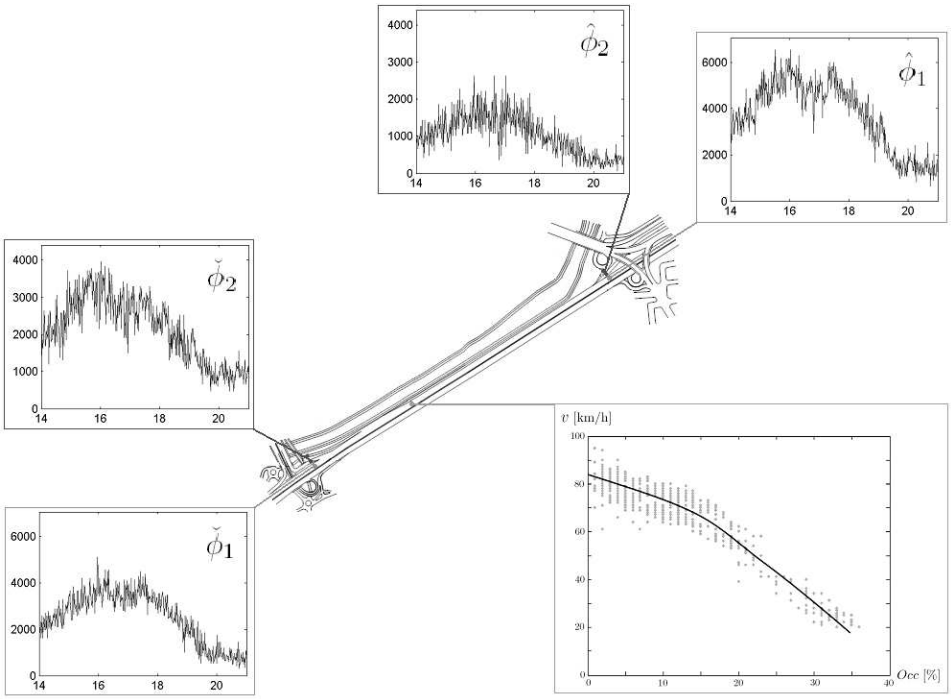

Figure 4.1: Simple network with some vehicle counts and a velocity diagram. Real field data from the South-Est beltway of Lyon, France.

tified by an origin and a destination. The aggregated density is thus decomposed in N_R partial densities noted $\rho_1, ..., \rho_{N_R}$. As a vehicle route is not know by the other vehicles, we can assume that the traffic speed depends only on the aggregated density as in the LWR model, i.e.

$$v(x,t) = V\left(\sum_{k=1}^{N_R} \rho_i(x,t)\right) \tag{4.1.1}$$

This assumption gives for route i the flow $\phi_i = \rho_i v$ and the car conservation principle implies the N_R conservation laws $\partial_t \rho_i + \partial_x \phi_i = 0$. This model can be rewritten compactly as the system of nonlinear conservation laws

$$\partial_t \boldsymbol{\rho} + \partial_x \Big(\boldsymbol{\rho}\ V\left(|\boldsymbol{\rho}|\right) \Big) = 0 \tag{4.1.2}$$

where $\boldsymbol{\rho} = (\rho_1, ..., \rho_{N_R})^T$ is the model state and $|\boldsymbol{\rho}| = \sum_{k=1}^{N_R} \rho_i$.

The quasi-linear form of this system of conservation laws writes

$$\partial_t \boldsymbol{\rho} + A\big(\boldsymbol{\rho}\big)\ \partial_x \boldsymbol{\rho} = 0 \qquad A(\boldsymbol{\rho}) = V(|\boldsymbol{\rho}|)\mathbf{I}_{N_R} + V'(|\boldsymbol{\rho}^{L_j}|)\ \mathbf{1}_{N_j} \cdot \boldsymbol{\rho} \tag{4.1.3}$$

with $\mathbf{I}_{N_R}$ the identity matrix of size N_R, $\mathbf{1}_{N_R}$ the row vector of size N_R filled with ones and $\cdot$ the Kronecker product.

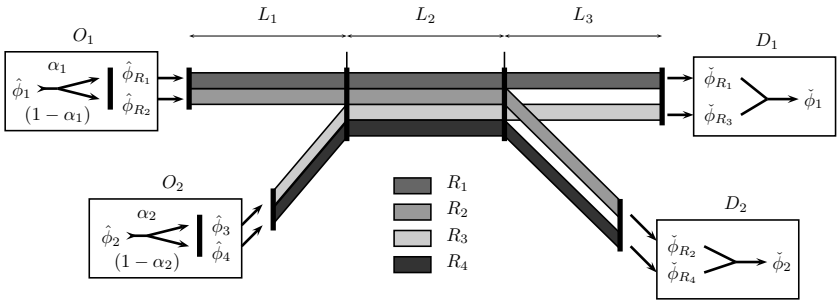

Figure 4.2: Abstraction of the simple network of figure 4.1.

4.1.2 Wave system of the MOD model

Eigenstructure

The nature and structure of the wave system of Equation (4.1.2) is characterized by the following items [Bressan, 2000]:

- Characteristic velocities, i.e. eigenvalues of $A(\boldsymbol{\rho})$

$$\begin{cases} \lambda_1(\boldsymbol{\rho}) &= V(|\boldsymbol{\rho}|) \\ \vdots & \vdots \\ \lambda_{N_R-1}(\boldsymbol{\rho}) &= V(|\boldsymbol{\rho}|) \\ \lambda_{N_R}(\boldsymbol{\rho}) &= V(|\boldsymbol{\rho}|) + |\boldsymbol{\rho}|V'(|\boldsymbol{\rho}|) \end{cases} \tag{4.1.4}$$

  Note that the multiclass model is not strictly hyperbolic because it has $N_R - 1$ identical characteristic speed.

- Matrix $T_r(\boldsymbol{\rho})$ of right eigenvectors of $A(\boldsymbol{\rho})$

$$T_r(\boldsymbol{\rho}) = \begin{pmatrix} | & & | \\ \mathbf{r}_1 & \cdots & \mathbf{r}_{N_R} \\ | & & | \end{pmatrix} = \begin{pmatrix} -1 & -1 & \cdots & -1 & \frac{\rho_1}{\rho_{N_R}} \\ 0 & 0 & \cdots & 1 & \frac{\rho_2}{\rho_{N_R}} \\ \vdots & \vdots & \diagup & \vdots & \vdots \\ 0 & 1 & \cdots & 0 & \frac{\rho_{N_R-1}}{\rho_{N_R}} \\ 1 & 0 & \cdots & 0 & 1 \end{pmatrix} \tag{4.1.5}$$

- Matrix $T_l(\boldsymbol{\rho})$ of left eigenvectors of $A(\boldsymbol{\rho})$

$$T_l(\boldsymbol{\rho}) = \begin{pmatrix} | & & | \\ \mathbf{l}_1 & \cdots & \mathbf{l}_{N_R} \\ | & & | \end{pmatrix} = \begin{pmatrix} -\frac{\rho_{N_R}}{\rho_1} & -\frac{\rho_{N_R-1}}{\rho_1} & \cdots & -\frac{\rho_2}{\rho_1} & 1 \\ 0 & 0 & \cdots & 1 & 1 \\ \vdots & \vdots & \diagup & \vdots & \vdots \\ 0 & 1 & \cdots & 0 & 1 \\ 1 & 0 & \cdots & 0 & 1 \end{pmatrix} \tag{4.1.6}$$

- Characteristic fields: 1 genuinely nonlinear field with wave speed λ_{N_R}, i.e. $\nabla\lambda_{N_R} \cdot \mathbf{r}_{N_R} \neq 0$, and $N_R - 1$ linearly degenerate fields with common wave speed $V(|\boldsymbol{\rho}|)$,

i.e. $\nabla\lambda_{N_k} \cdot \mathbf{r}_{N_k} = 0$, for $k = 1, ..., N_R - 1$. The $N_R - 1$ first characteristic fields may develop contact discontinuities that propagate at the traffic speed $V(|\boldsymbol{\rho}|)$ whereas the last field (corresponding to the underlying LWR model) may develop shock waves and rarefaction waves propagating slower that the traffic as $\lambda_{N_j} \leq V(|\boldsymbol{\rho}|)$.

- Riemann invariants $w_k(\boldsymbol{\rho})$ satisfying $\partial_t w_k(\boldsymbol{\rho}) + \lambda_k(\boldsymbol{\rho}) w_k(\boldsymbol{\rho}) = 0$

$$\left\{ \begin{array}{lcl} w_1(\boldsymbol{\rho}) & = & \frac{\rho_2}{\rho_1} \\ \vdots & & \vdots \\ w_{N_R-1}(\boldsymbol{\rho}) & = & \frac{\rho_{N_R}}{\rho_1} \\ w_{N_R}(\boldsymbol{\rho}) & = & V(|\boldsymbol{\rho}|) \end{array} \right. \tag{4.1.7}$$

Note that, as $\lambda_k(\boldsymbol{\rho}) = V(|\boldsymbol{\rho}|)$ for $k = 1, ...N_R - 1$, the level curves of the traffic ratios $w_k(\boldsymbol{\rho})$ for $k = 1, ...N_R - 1$ are the vehicle trajectories as already noted in [Zhang & Jin, 2002].

Due to the solution of the Riemann problem discussed later, the left and right state are denoted respectively $\boldsymbol{\rho}^0$ and $\boldsymbol{\rho}^+$ for contact discontinuities and $\boldsymbol{\rho}^-$ and $\boldsymbol{\rho}^0$ for shock and rarefaction waves.

Elementary waves

- **Shock waves:**

The Hugoniot curve connecting the left state $\boldsymbol{\rho}^-$ to the right state $\boldsymbol{\rho}^0$ through a shock wave is given by

$$\boldsymbol{\rho}^0 V(|\boldsymbol{\rho}^0|) - \boldsymbol{\rho}^- V(|\boldsymbol{\rho}^-|) = \sigma(\boldsymbol{\rho}^0 - \boldsymbol{\rho}^-) \tag{4.1.8}$$

Summing all rows in Equation (4.1.8), the genuinely nonlinear field develops shock waves having a speed identical to the one present in the LWR model

$$\sigma = \frac{|\boldsymbol{\rho}^0| V(|\boldsymbol{\rho}^0|) - |\boldsymbol{\rho}^-| V(|\boldsymbol{\rho}^-|)}{|\boldsymbol{\rho}^0| - |\boldsymbol{\rho}^-|} \tag{4.1.9}$$

Multiplying (4.1.8) by $(|\boldsymbol{\rho}^0| - |\boldsymbol{\rho}^-|)/(|\boldsymbol{\rho}^0||\boldsymbol{\rho}^-|)$ and using (4.1.9), the left and right states verify

$$\frac{\boldsymbol{\rho}^0}{|\boldsymbol{\rho}^0|} = \frac{\boldsymbol{\rho}^-}{|\boldsymbol{\rho}^-|} \tag{4.1.10}$$

meaning that the traffic composition and thus the density ratio is conserved along shock waves. A shock wave is allowed in the genuinely nonlinear field if it satisfies the Lax entropy condition [Lax, 1973] given by $\lambda_{N_j}(\boldsymbol{\rho}^-) > \sigma > \lambda_{N_j}(\boldsymbol{\rho}^0)$. As in the LWR model, this condition rewrites $|\boldsymbol{\rho}^-| < |\boldsymbol{\rho}^0|$ if the velocity function $V(\cdot)$ is strictly decreasing.

- **Rarefaction waves:**

  A rarefaction wave develops when $\lambda_{N_j}(\boldsymbol{\rho}^-) \leq \lambda_{N_j}(\boldsymbol{\rho}^0)$ and the curve connecting the 2 states is given by the ordinary differential equation

  $$\dot{\boldsymbol{\rho}} = \frac{\mathbf{r}_{N_R}(\boldsymbol{\rho})}{\nabla\lambda_{N_R}(\boldsymbol{\rho}) \cdot \mathbf{r}_{N_R}(\boldsymbol{\rho})} = \frac{\boldsymbol{\rho}}{|\boldsymbol{\rho}|\big(2V'(|\boldsymbol{\rho}|) + |\boldsymbol{\rho}|V''(|\boldsymbol{\rho}|)\big)} \qquad \text{with} \qquad \boldsymbol{\rho}(0) = \boldsymbol{\rho}^-$$

  It implies $\rho_k/|\rho| = \rho_k^-/|\rho^-|$, meaning that the density ratios are conserved along rarefaction waves as for shock curves.

  As Hugoniot locus and rarefaction curves are coinciding straight lines, the multiclass model is a Temple class system [Temple, 1982].

- **Contact discontinuities:**

  The $N_R - 1$ first fields can develop contact discontinuities only with wave speed $V(|\boldsymbol{\rho}^+|) = V(|\boldsymbol{\rho}^0|)$. The left and right states thus satisfy $|\boldsymbol{\rho}^+| = |\boldsymbol{\rho}^0|$, meaning that the total density is conserved along contact discontinuities.

4.2 Treatment of boundary conditions

Boundary conditions are treated similarly than in the ARZ model. Again, the upstream boundary condition writes

$$\boldsymbol{\rho}(0,t) \in \mathcal{V}_{\text{up}}(\boldsymbol{\rho}_{\text{up}}) = \big\{w(0+, \boldsymbol{\rho}_{\text{up}}, \boldsymbol{\rho}) : \boldsymbol{\rho} \in \mathbb{R}^2_+,\ |\rho| < \rho_m\big\}$$

for a 2-class model with possible waves given in Figure 4.3. We refer to Figure 4.3 for the graphical solution of $\mathcal{V}_{\text{Up}}(\boldsymbol{\rho}_{\text{up}}^{L_2})$ where $\mathcal{S}$ and $\mathcal{R}$ denote the shock and rarefaction curves given by straight lines. The ρ_m dashed lines delimits the allowable states whereas the ρ_c dashed lines identifies where λ_{N_R} changes sign. The gray curves are the admissible boundary values and the striped sets identify different boundary behaviors depending on $\boldsymbol{\rho}(0,t)$.

4.3 Modelling of on/off-ramps

The problem is rather non-standard here as each boundary condition depends on the inner state of the interconnected link rather than on a predefined independent boundary signal. For this reason, these boundary conditions are termed interface conditions. Moreover, the sizes of the system of conservation laws on both sides of the interface are different.

The simplified on-ramp and off-ramp interfaces with 2 links L_1 and L_2 depicted on Figure 4.4 are used for our analysis as the other classes in larger systems can be aggregated while conserving the traffic composition. In this section, all the density notations refer to the traces of the variable at the interface. For instance, $\rho_{R_1}^{L_2}$ is the

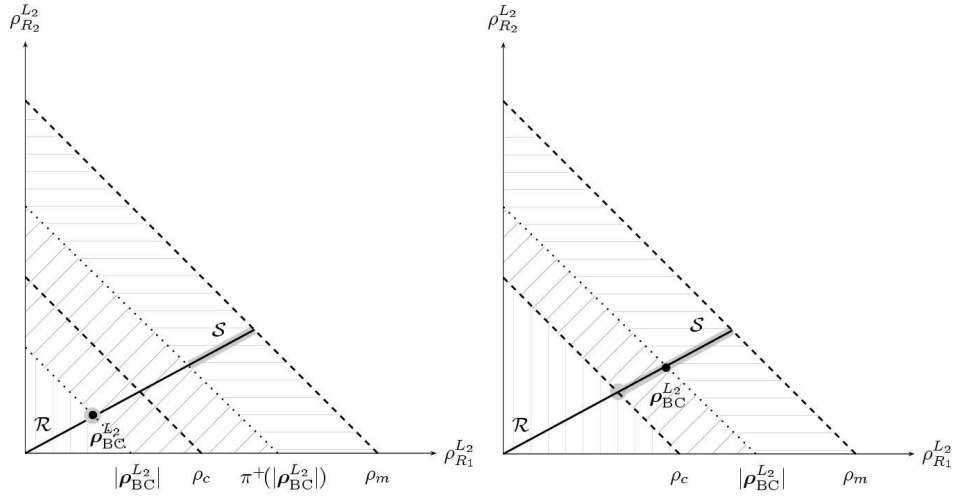

Figure 4.3: Left: Admissible boundary values when $|\boldsymbol{\rho}_{\mathrm{up}}| \leq \rho_c$. The region with horizontal stripes corresponds to a shock with negative speed, the region with oblique stipes to a shock with positive speed and the one with vertical stripes to a rarefaction wave with all positive speeds. Right: Admissible boundary values when $|\boldsymbol{\rho}_{\mathrm{up}}| \leq \rho_c$. The gray circle on the ρ_c dashed line corresponds to a sonic rarefaction wave occurring in the region with vertical stripes. The region with horizontal stripes corresponds to a shock with negative speed and the one with oblique stipes to a rarefaction with all negative speeds.

upstream boundary condition of the density for route R_1 in the downstream link L_2. When only one route is present in a link, $\Phi(\rho) = \rho V(\rho)$ denotes the flow in this link. We first analyse on-ramps and then off-ramps which behave similarly.

Figure 4.4: Two class on-ramp (left) and off-ramp (right) interfaces.

The assumptions for the on-ramp behavior are:

1. The density-flow relationships apply at the boundaries:

$$\begin{cases} \phi_{R_1}^{L_1} = \Phi(\rho_{R_1}^{L_1}) = \rho_{R_1}^{L_1} V(\rho_{R_1}^{L_1}) \\ \phi_{R_1}^{L_2} = \rho_{R_1}^{L_2} V(\rho_{R_1}^{L_2} + \rho_{R_2}^{L_2}) \\ \phi_{R_2}^{L_2} = \rho_{R_2}^{L_2} V(\rho_{R_1}^{L_2} + \rho_{R_2}^{L_2}) \end{cases} \tag{4.3.1}$$

2. The flow conservation principle applies at the interface:

$$\begin{cases} \phi_{R_1}^{L_1} = \phi_{R_1}^{L_2} \\ \phi_{R_2}^{L_2} = \hat{\phi} \end{cases} \tag{4.3.2}$$

For definiteness but without loss of generality, we assume that the following linear velocity relationship, known as the Greenshield model [Pipes, 1967], applies

$$V(\rho) = v_f \left(1 - \frac{\rho}{\rho_m}\right) \tag{4.3.3}$$

where the free velocity and maximal density parameters are taken to be $v_f = 100$ km/h and $\rho_m = 80$ veh/km when necessary.

We show below that the set of Equations (4.3.1) and (4.3.2) involve, for a given on-ramp flow $\hat{\phi}$, some constraints on the traces of the densities at both sides of the interface. These constraints are then used with the applicability of the boundary variable to decide what boundary conditions apply in L_1 and L_2.

4.3.1 Constraints on the boundary values at on-ramps

The flow conservation for route R_2 writes $\rho_{R_2}^{L_2} V(\rho_{R_1}^{L_2} + \rho_{R_2}^{L_2}) = \hat{\phi}$ and can be solved for $\rho_{R_1}^{L_2}$, leading to the relationship plotted in Figure 4.5 whose analytical expression is

$$\rho_{R_1}^{L_2} = \theta_{\hat{\phi}}(\rho_{R_2}^{L2}) = \rho_{\mathrm{m}} - \rho_{R_2}^{L2} - \frac{\hat{\phi}\ \rho_{\mathrm{m}}}{\rho_{R_2}^{L2}\ v_{\mathrm{f}}} \tag{4.3.4}$$

Note that the map $\theta_{\hat{\phi}}(\cdot)$ has a domain defined by

$$\mathrm{Domain}\big\{\theta_{\hat{\phi}}(\cdot)\big\} = [\underline{\rho}_{R_2}^{L_2}, \bar{\rho}_{R_2}^{L_2}] = \left[\frac{\rho_{\mathrm{m}} v_{\mathrm{f}} \pm \sqrt{\rho_{\mathrm{m}} v_{\mathrm{f}}(\rho_{\mathrm{m}} v_{\mathrm{f}} - 4\hat{\phi})}}{2 v_{\mathrm{f}}}\right]$$

where $\underline{\rho}_{R_2}^{L_2}$ is the minimal density able to realize the ramp flow $\hat{\phi}$ whereas $\bar{\rho}_{R_2}^{L_2}$ is the maximal density to ensure feasible densities smaller than ρ_m.

Using this map $\theta_{\hat{\phi}}(\cdot)$, the flow conservation equation for route R_1 writes

$$\phi_{R_1}^{L_1} = \phi_{R_1}^{L_2} = \rho_{R_1}^{L_2} V(\rho_{R_1}^{L_2} + \rho_{R_2}^{L_2}) = \rho_{R_1}^{L_2} V(\theta_{\hat{\phi}}(\rho_{R_2}^{L_2}) + \rho_{R_2}^{L_2})$$

providing the relationship plotted in Figure 4.6 with analytical expression

$$\phi_{R_1}^{L1} = \phi_{R_1}^{L2} = \eta_{\hat{\phi}}(\rho_{R_2}^{L2}) = \frac{-\rho_{\mathrm{m}}\ \hat{\phi}^2 + \rho_{R_2}^{L2}\ \hat{\phi}\ v_{\mathrm{f}}(\rho_{\mathrm{m}} - \rho_{R_2}^{L2})}{v_{\mathrm{f}}(\rho_{R_2}^{L2})^2} \tag{4.3.5}$$

An other useful constraint is the relationship between $\rho_{R_2}^{L_2}$ and the total density $|\rho^{L_2}|$ plotted in Figure 4.7, whose analytical expression is

$$|\rho^{L_2}| = \rho_{R_2}^{L_2} + \theta_{\hat{\phi}}(\rho_{R_2}^{L_2}) = \rho_{\mathrm{m}} - \frac{\hat{\phi}\ \rho_{\mathrm{m}}}{\rho_{R_2}^{L2}\ v_{\mathrm{f}}} \tag{4.3.6}$$

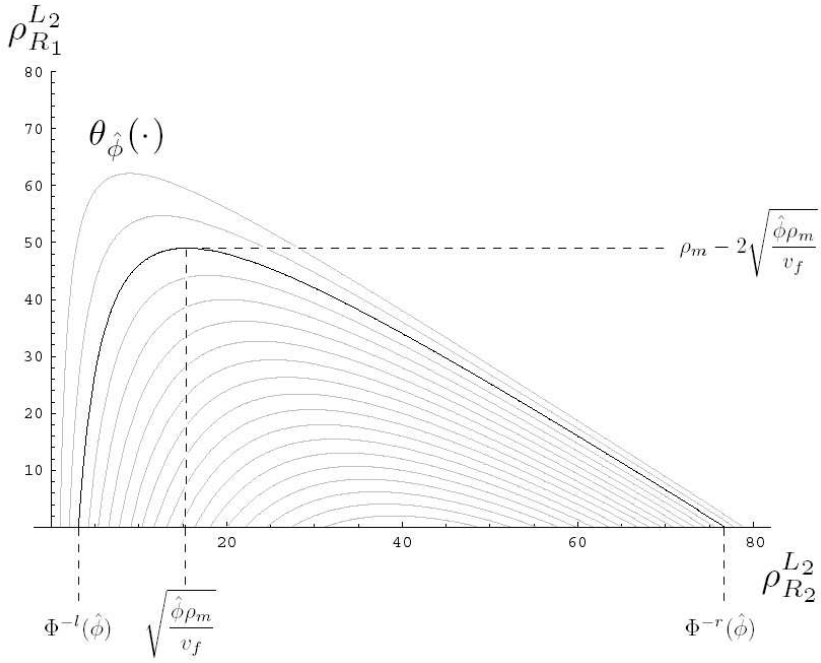

Figure 4.5: Functions $\rho_{R_1}^{L_2} = \theta_{\hat{\phi}}(\rho_{R_2}^{L2})$ for $\hat{\phi} \in [100, 1900]$ with its domain and range. The black curve corresponds to $\hat{\phi} = 300$.

4.3.2 The on-ramp switched behavior

Based on the previous discussions concerning the density constraints and the causality of the boundary conditions at interfaces, the 3 following situations may occur:

1. *Forward.* When $\rho_{R_1}^{L1} \leq \rho_c$ and $\rho_{R_1}^{L2} + \rho_{R_2}^{L2} \leq \rho_c$, the upstream boundary condition should be transmitted downstream as all Riemann invariants and shock/rarefaction waves have positive speed. If $\phi_{R_1}^{L1} \leq \max \eta_{\hat{\phi}}(\cdot)$, the upstream demand can be met and the applying boundary conditions in link L_2 are given by $\rho_{R_2}^{L2} = \eta_{\hat{\phi}}^{-l}(\phi_{R_1}^{L1})$ and $\rho_{R_1}^{L2} = \theta_{\hat{\phi}}(\rho_{R_2}^{L2})$, the left branch inverse of $\eta_{\hat{\phi}}(\cdot)$ being given by

$$\eta_{\hat{\phi}}^{-l}(\phi_{R_1}^{L1}) = \frac{\hat{\phi}\rho_m v_f - \sqrt{\hat{\phi}^2 \rho_m v_f (\rho_m v_f - 4(\hat{\phi} + \phi_{R_1}^{L1}))}}{2v_f(\hat{\phi} + \phi_{R_1}^{L1})}$$

2. *Decoupled.* When $\phi_{R_1}^{L1} > \max \eta_{\hat{\phi}}(\cdot)$ in the *Forward* situation, the upstream boundary condition could be transmitted but saturation occurs as the on-ramp flow is too large. It leads to the decoupled case where the maximal flow offer $\phi_{R_1}^{L1} = \max \eta_{\hat{\phi}}(\cdot)$ applies, giving the downstream and upstream boundary conditions $\rho_{R_1}^{L1} = \Phi^{-r}(\phi_{R_1}^{L1})$, $\rho_{R_2}^{L2} = \text{argmax } \eta_{\hat{\phi}}(\cdot)$ and $\rho_{R_1}^{L2} = \theta_{\hat{\phi}}(\rho_{R_2}^{L2})$ with le right inverse of $\Phi(\cdot)$

$$\Phi^{-r}(\phi) = \frac{\rho_m v_f + \sqrt{\rho_m v_f (\rho_m v_f - 4\phi)}}{2v_f}$$

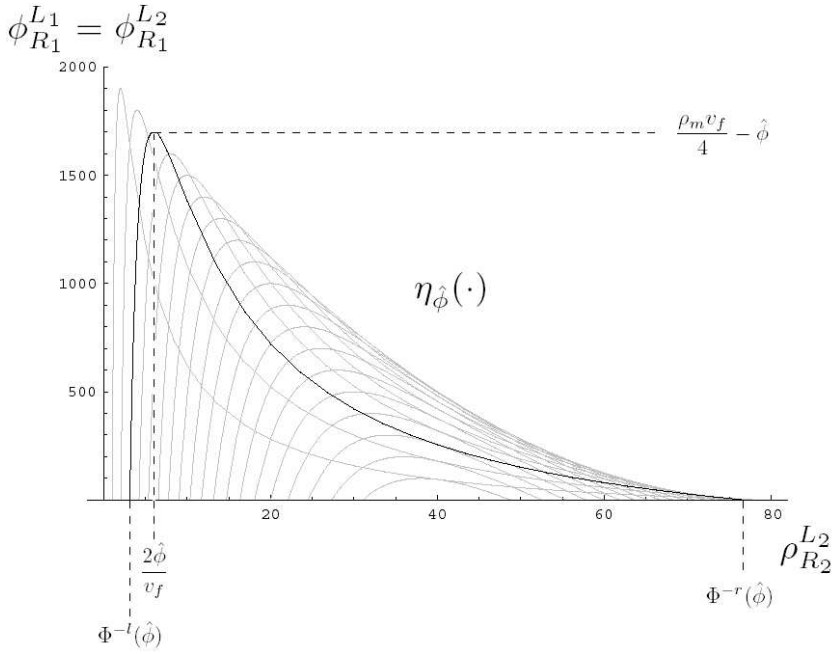

Figure 4.6: Functions $\phi_{R_1}^{L1} = \phi_{R_1}^{L2} = \eta_{\hat{\phi}}(\rho_{R_2}^{L2})$ for $\hat{\phi} \in [100, 1900]$ with its domain and range. The black curve corresponds to $\hat{\phi} = 300$.

This situation which leads to $\rho_{R_1}^{L1} > \rho_c$ and $\rho_{R_1}^{L2} + \rho_{R_2}^{L2} = \rho_c$ is called decoupled as there is no transmission of boundary conditions and the knowledge of $\hat{\phi}$ is enough to set all the boundary conditions.

3. *Backward.* When $\rho_{R_1}^{L2} + \rho_{R_2}^{L2} \geq \rho_c$ and $\rho_{R_1}^{L1} \geq \rho_c$, the downstream boundary condition is transmitted upstream. As $|\rho^{L2}|$ is provided by the inner solution and $\xi_{\hat{\phi}}(\rho_{R_2}^{L2})$ is monotonic, we get that $\rho_{R_2}^{L2} = \xi_{\hat{\phi}}^{-1}(|\rho^{L2}|)$, $\rho_{R_1}^{L2} = \theta_{\hat{\phi}}(\rho_{R_2}^{L2})$ and $\rho_{R_1}^{L1} = \Phi^{-r}(\eta_{\hat{\phi}}(\rho_{R_2}^{L2}))$ where the inverse of $\xi_{\hat{\phi}}(\cdot)$ writes

$$\xi_{\hat{\phi}}^{-1}(|\rho^{L2}|) = \frac{\hat{\phi}\rho_m}{v_f(\rho_m - |\rho^{L2}|)}$$

Note the coherence with the LWR model as we have

$$\rho_{R_1}^{L1} = \Phi^{-r}\Big(\eta_{\hat{\phi}}\big(\xi_{\hat{\phi}}^{-1}(|\rho^{L2}|)\big)\Big) = \Phi^{-r}\big((\Phi(|\rho^{L2}|) - \hat{\phi}\big)$$

4. *Shocked.* This case is of secondary importance and occurs when $\rho_{R_1}^{L1} \leq \rho_c$ and $\rho_{R_1}^{L2} + \rho_{R_2}^{L2} \geq \rho_c$, leading to apparently incompatible boundary values. This situation corresponds to the propagation of a shock wave through the interface and is independent of the value of the on-ramp flow. If $|\Phi'(\rho_{R_1}^{L2} + \rho_{R_2}^{L2})| < |\Phi'(\rho_{R_1}^{L1})|$, the shock moves forward and the *forward* situation applies. If $|\Phi'(\rho_{R_1}^{L2} + \rho_{R_2}^{L2})| > |\Phi'(\rho_{R_1}^{L1})|$, the shock moves backward and the *backward* situation applies.

The finite state machine depicted in Figure 4.8 summarizes the on-ramp interface behavior and demonstrates the hybrid dynamics of the inhomogeneous multiclass model. Simulations provided at the end of the paper illustrate the switching of this finite state machine.

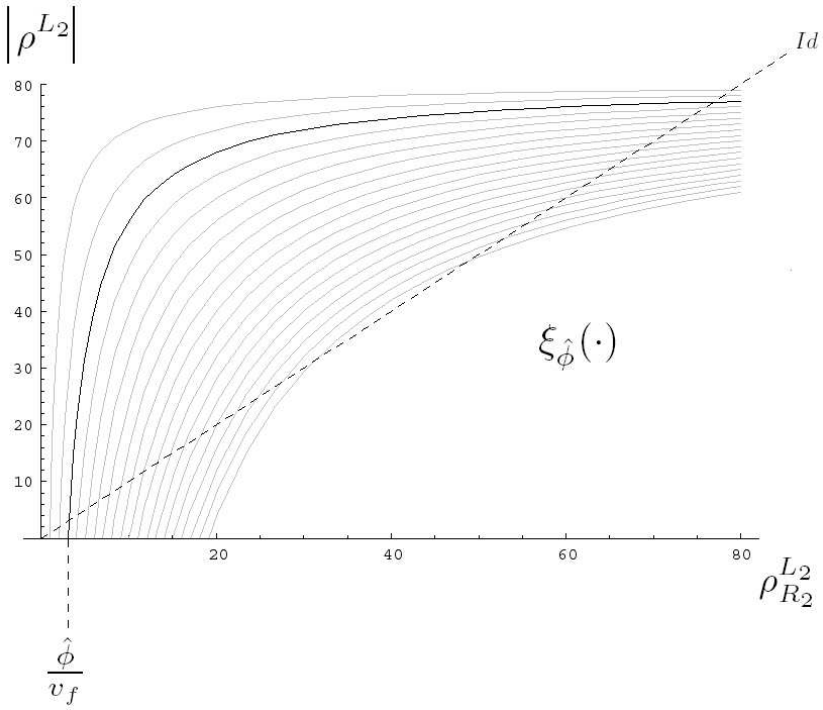

Figure 4.7: Functions $|\rho^{L_2}| = \xi_{\hat{\phi}}(\rho^{L_2}_{R_2})$ for $\hat{\phi} \in [100, 1900]$ with its domain and range. The black curve corresponds to $\hat{\phi} = 300$.

4.3.3 Cases of off-ramps and larger systems

The same kind of density-flow relationship and flow conservation principle applies at off-ramps, leading to

$$\begin{cases} \rho^{L_1}_{R_1} = \theta_{\check{\phi}}(\rho^{L_1}_{R_2}) \\ \phi^{L_1}_{R_1} = \phi^{L_2}_{R_1} = \eta_{\check{\phi}}(\rho^{L_1}_{R_2}) \end{cases} \tag{4.3.7}$$

with maps $\theta_{\cdot}(\cdot)$ and $\eta_{\cdot}(\cdot)$ identical to the one presented for the on-ramp case. The causality have some similarity too and is summarized below:

1. *Backward.* If $\rho^{L2}_{R_1} \geq \rho_c$, $\rho^{L1}_{R_1} + \rho^{L1}_{R_2} \geq \rho_c$ and $\phi^{L2}_{R_1} \leq \max \eta_{\check{\phi}}(\cdot)$, the boundary condition is transmitted upstream with $\rho^{L1}_{R_2} = \eta^{-r}_{\check{\phi}}(\phi^{L2}_{R_1})$ and $\rho^{L1}_{R_1} = \theta_{\check{\phi}}(\rho^{L1}_{R_2})$.

2. *Decoupled.* When $\phi^{L2}_{R_1} > \max \eta_{\check{\phi}}(\cdot)$ in the *backward* situation, the maximal possible demand is met by setting $\phi^{L1}_{R_1} = \phi^{L2}_{R_1} = \max \eta_{\check{\phi}}(\cdot)$, leading to $\rho^{L2}_{R_1} = \Phi^{-l}(\phi^{L2}_{R_1})$, $\rho^{L1}_{R_2} = \text{argmax } \eta_{\check{\phi}}(\cdot)$ and $\rho^{L1}_{R_1} = \theta_{\check{\phi}}(\rho^{L1}_{R_2})$. This case corresponds to a large off-ramp flow that frees the downstream traffic, decoupling the 2 links.

3. *Forward.* If $\rho^{L1}_{R_1} + \rho^{L1}_{R_2} \leq \rho_c$ and $\rho^{L2}_{R_1} \leq \rho_c$, all characteristic speeds are positive so the upstream boundary condition is transferred downwards with $\rho^{L2}_{R_1} = \Phi^{-l}(\eta_{\check{\phi}}(\rho^{L1}_{R_2}))$ and it sets the off-ramp flow to $\check{\phi} = \rho^{L1}_{R_2}.V(|\rho^{L1}|)$.

4. *Shocked.* If we have $\rho^{L1}_{R_1} + \rho^{L1}_{R_2} \leq \rho_c$ and $\rho^{L2}_{R_1} \geq \rho_c$, then a shock wave cross the interface and $|\Phi'(\rho^{L1}_{R_1} + \rho^{L1}_{R_2})| < |\Phi'(\rho^{L2}_{R_1})|$ leads to the *backward* situation whereas

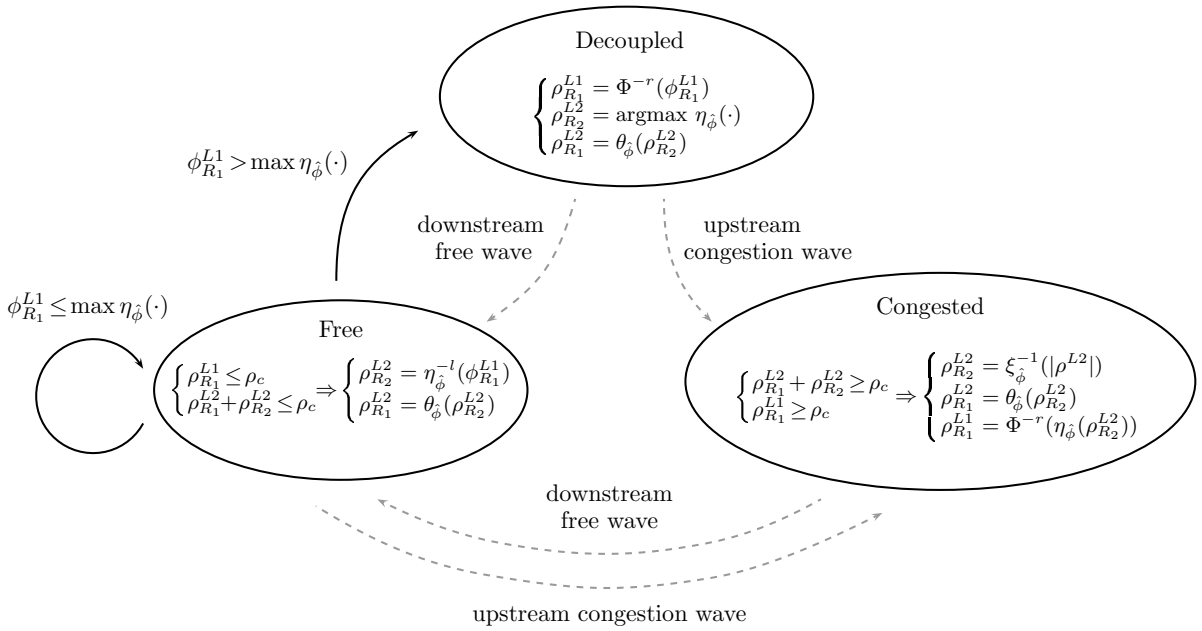

Figure 4.8: Finite state machine defining the on-ramp interface behavior.

$|\Phi'(\rho_{R_1}^{L1} + \rho_{R_2}^{L1})| > |\Phi'(\rho_{R_1}^{L2})|$ to the *forward* situation.

The treatment of general multi-class interface conditions is as follow. The basic assumption is that the traffic composition is conserved at the interfaces which is motivated by the fact that each class behaves similarly as they all have the same velocity function. Consequently, the transmission of the main lane and the ramp interface conditions can be done by treating the aggregated problem as in Figure 4.4 and then redistributing the densities according to the same flow ratio, which is equivalent to the density ratio here as

$$\frac{\phi_{R_i}^{L_j}}{|\phi^{L_j}|} = \frac{\rho_{R_i}^{L_j}}{|\rho^{L_j}|}$$

An expert is a man who has made all the mistakes, which can be made, in a very narrow field.

Niels Henrik David Bohr (1885-1962),
Danish chemist.

Chapter 5

Numerical schemes for macroscopic freeway models

As conservation laws generate irregular flows, they cannot be integrated numerically using standard methods such as finite differences or finite elements, which are known to generate instabilities and/or wrong shock speeds [LeVeque, 1992]. Among the numerical schemes suitable for scalar and systems of conservation laws [LeVeque, 1992; Godlewski & Raviart, 1996], the Godunov method [Godunov, 1959] is a good option as it is a first order scheme, it predicts correctly the propagation of shock waves, is devoid of oscillating behavior and has a nice physical interpretation. In this method, the computational domain is decomposed into cells and the state is assumed to be constant in each of them. As shown in Figure 5.1, it leads to a piecewise approximation of the state, whose

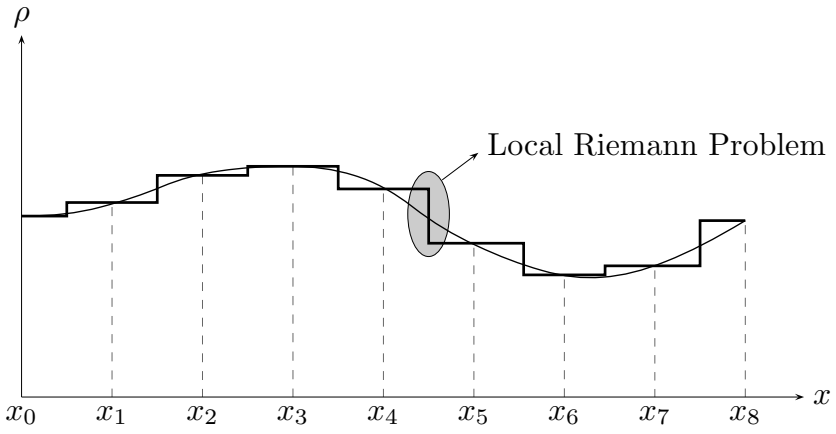

Figure 5.1: Piecewise constant approximation of the state.

evolution can be computed for small time horizons if we know the solution of the Cauchy problems with piecewise constant initial data

$$\rho_I(x) = \begin{cases} \rho_- & \text{for } x < 0 \\ \rho_+ & \text{for } x > 0 \end{cases} \tag{5.0.1}$$

Problems such as (5.0.1) are called Riemann problems in the literature and can be solved analytically for scalar conservation laws [LeVeque, 1992]. In the case of systems, an approximate Riemann solver such as the Roe average method [Godlewski & Raviart, 1996; LeVeque, 1992] is usually necessary as no analytical solution is available in general. Surprisingly, the Riemann problems for the Aw-Rascle-Zhang (ARZ) and the Multiclass-Origin-Destination (MOD) models, which have both been analyzed in the previous chapters, can be solve analytically as already mentioned in [Mammar et al., 2005] and [Zhang & Jin, 2002]. The Godunov scheme, which consists in solving a succession of local Riemann problems, is thus an attractive method for simulating macroscopic traffic models and have been used extensively in the transportation community. As shown in this chapter, the Riemann solvers for the LWR, ARZ and MOD models are very similar, which ease the numerical implementation of these models.

5.1 Numerical scheme for the LWR model

5.1.1 The Godunov scheme for LWR links

With space and time cells of size Δx_i and Δt and indexed by i and n respectively, the Godunov [Godunov, 1959] time stepping for the LWR model writes

$$\rho_i^{n+1} = \rho_i^n + \frac{\Delta t}{\Delta x_i}\Big(\Phi_{num}(\rho_{i-1}^n, \rho_i^n) - \Phi_{num}(\rho_i^n, \rho_{i+1}^n)\Big) \tag{5.1.1}$$

with $\Phi_{num}(\rho_-, \rho_+)$ the numerical flux associated to the interface having density values ρ_- and ρ_+ respectively on the left and right. The numerical flux $\Phi_{num}(\rho_-, \rho_+)$ is given by

$$\Phi_{num}(\rho_-, \rho_+) = \Phi(\rho_*) \tag{5.1.2}$$

with ρ_* the value of the solution to the Riemann problem (5.0.1) at the interface location. Thanks to the self-similarity [LeVeque, 1992] property of the solution to (5.0.1), i.e. $\rho(x,t) = \rho(x/t)$, ρ_* can be computed analytically and is given by Table 5.1.

	$\Phi'(\rho_+) \geq 0$	$\Phi'(\rho_+) < 0$
$\Phi'(\rho_-) \geq 0$	$\rho_* = \rho_-$	$\rho_* = \begin{cases} \rho_- & \text{if } \frac{\Phi(\rho_+)-\Phi(\rho_-)}{\rho_+-\rho_-} > 0 \\ \rho_+ & \text{otherwise} \end{cases}$
$\Phi'(\rho_-) < 0$	$\rho_* = \text{argmax}\big\{\Phi(\cdot)\big\}$	$\rho_* = \rho_+$

Table 5.1: Analytical solution of the Riemann problem (5.0.1).

Proving (5.1.2) consists in analyzing each possibility in Table 5.1, where $\Phi'(\rho)$ gives the orientation of the characteristics, and tracking if the involved wave have positive of negative speed. When $\Phi'(\rho_-) < 0$ and $\Phi'(\rho_+) < 0$, all the characteristics move backwards and thus $\rho_* = \rho_+$. Similarly, all characteristics move forwards for $\Phi'(\rho_-) \geq 0$ and $\Phi'(\rho_+) \geq 0$ and $\rho_* = \rho_-$. When $\Phi'(\rho_-) \geq 0$ and $\Phi'(\rho_+) < 0$, a shock occurs and

the sign of the shock speed is used to decide the value of ρ_*. Finally, $\Phi'(\rho_-) < 0$ and $\Phi'(\rho_+) \geq 0$ gives a rarefaction wave that crosses the origin. In this case, called the sonic point, the maximal flow applies [LeVeque, 1992].

For stability reasons, the time and space cell size should verify the so-called CFL condition [LeVeque, 1992]

$$\Delta x \leq \Delta t \; c_{\max}$$

with $c_{\max}$ the maximal celerity given by

$$c_{\max} = \max_{\rho} \Phi'(\rho)$$

5.1.2 Numerical treatment of boundary conditions

Case of density boundary conditions

Few literature is available about the numerical treatment of boundary conditions, a notable exception being [Kröner, 1997]. The solution of the Riemann problem at the upstream boundary with boundary condition $\rho_0(t)$ should verify the following discrete version of the so-called BLN boundary entropy condition introduced in [Bardos et al., 1979]

$$\text{sign}(\rho_1^n - \rho_0^n)\Phi_{num}^{B_{Up}}(\rho_0^n, \rho_1^n) = \min_{k \in I_n} \; \text{sign}(\rho_1^n - \rho_0^n)\Phi(k)$$

with $\Phi_{num}^{B_{Up}}(\rho_0^n, \rho_1^n)$ the numerical boundary flux applying between time n and $n+1$ and I_n the interval delimited by ρ_0^n and ρ_1^n where ρ_0^n is the proposed boundary value density and ρ_1^n is the density of the first cell. More explicitly, the solution of the Riemann problem at the upstream boundary can be rewritten

$$\Phi_{num}^{B_{Up}}(\rho_0^n, \rho_1^n) = \begin{cases} \inf_{k \in [\rho_0^n, \rho_1^n]} & \Phi(k) & \text{if } \rho_0^n < \rho_1^n \\ \sup_{k \in [\rho_1^n, \rho_0^n]} & \Phi(k) & \text{if } \rho_1^n < \rho_0^n \end{cases}$$

Similarly, at the downstream boundary, the numerical boundary flux writes

$$\Phi_{num}^{B_{Do}}(\rho_N^n, \rho_L^n) = \begin{cases} \sup_{k \in [\rho_L^n, \rho_N^n]} & \Phi(k) & \text{if } \rho_L^n < \rho_N^n \\ \inf_{k \in [\rho_N^n, \rho_L^n]} & \Phi(k) & \text{if } \rho_N^n < \rho_L^n \end{cases}$$

with ρ_L^n the proposed downstream boundary density and ρ_N^n the density in the last cell.

With the following demand/supply functions introduced by [Lebacque, 1996] for concave flux functions

$$D(\rho) = \begin{cases} \Phi(\rho) & \text{if } \rho < \rho_c \\ \Phi_m & \text{if } \rho \geq \rho_c \end{cases} \qquad \text{and} \qquad S(\rho) = \begin{cases} \Phi_m & \text{if } \rho < \rho_c \\ \Phi(\rho) & \text{if } \rho \geq \rho_c \end{cases} \tag{5.1.3}$$

with ρ_c such that $\Phi'(\rho_c) = 0$, these boundary fluxes become simply

$$\Phi_{num}^{B_{Up}}(\rho_0^n, \rho_1^n) = \min \left\{ \; D(\rho_0^n) \; , \; S(\rho_1^n) \; \right\}$$

$$\Phi_{num}^{B_{Do}}(\rho_N^n, \rho_L^n) = \min \left\{ \; D(\rho_N^n) \; , \; S(\rho_L^n) \; \right\}$$

Case of flow boundary conditions

If densities are often considered to be the boundary conditions as in [Bardos et al., 1979], we may want to specify the boundary flows $\phi_0(t)$ and $\phi_L(t)$ instead, which may be more natural in some cases. Nevertheless, careless manipulation of the Godunov scheme in this situation may lead to nonphysical numerical results.

Let consider the downstream boundary $x = L$. When a flow $\phi_L(t)$ is specified, it is assumed to belong to the supply curve in the demand/supply paradigm [Lebacque, 1996]. Consequently, even if the traffic stream is in free flow, a small flow $\phi_L(t)$ will be interpreted as a congested flow, possibly leading to backward congestion waves. To remove this inconsistency, the downstream flow signal $\phi_L(t)$ should be pre-treated using the density information $\rho_L(t)$. In accordance with the demand/supply paradigm of [Lebacque, 1996], the boundary signal $\phi_L(t)$ is modified as

$$\tilde{\phi}_L(t) = \begin{cases} \phi_L(t) & \text{if } \rho_L(t) > \rho_c \\ \Phi_m(t) & \text{if } \rho_L(t) \leq \rho_c \end{cases}$$

Similarly, the upstream flow condition is modified according to

$$\tilde{\phi}_0(t) = \begin{cases} \phi_0(t) & \text{if } \rho_0(t) < \rho_c \\ \Phi_m(t) & \text{if } \rho_0(t) \geq \rho_c \end{cases}$$

Flows $\tilde{\phi}_0$ and $\tilde{\phi}_L$ can then be used directly in the Godunov time stepping (5.1.1).

5.1.3 Numerical treatment of on/off-ramps

The 2 easiest ways to implement interface conditions occurring at on/off-ramps are the demand/supply and the switched interface formulation. The demand/supply paradigm is somehow easier to implement here as the Godunov scheme only uses interface flows in its time stepping. Nevertheless, for control purposes, we may want to keep track of the switches, making the switched formulation interesting too. An other option presented here is to solve analytically the Riemann problem for all possible cases.

Using the demand/supply paradigm

In the demand/supply paradigm [Lebacque, 1996], the demand and supply functions are defined according to (5.1.3). With an on-ramp with flow $\hat{\phi}_i$ between cells i and $i+1$, the flow entering cell $i+1$ writes

$$\hat{\Phi}_{i+1}(\rho_i^n, \rho_{i+1}^n, \hat{\phi}_i^n) = \min\left\{ \; D(\rho_i^n) + \hat{\phi}_i^n \; , \; S(\rho_{i+1}^n) \; \right\}$$

leading to a leaving from cell i of $\hat{\Phi}_i(\rho_i^n, \rho_{i+1}^n, \hat{\phi}_i^n) = \hat{\Phi}_{i+1}(\rho_i^n, \rho_{i+1}^n, \hat{\phi}_i^n) - \hat{\phi}_i^n$. Note that $\hat{\Phi}_{i+1}(\rho_i^n, \rho_{i+1}^n, \hat{\phi}_i^n) < \hat{\phi}_i^n$ if $S(\rho_{i+1}^n) < \hat{\phi}_i^n$, meaning that some vehicles are queuing at the

on-ramp. Similarly, for an off-ramp with splitting ratio β_i between cells i and $i+1$, the flow entering cell $i+1$ is

$$\check{\Phi}_{i+1}(\rho_i^n, \rho_{i+1}^n, \beta_i^n) = \min\left\{ \ (1-\beta_i^n)\ D(\rho_i^n)\ ,\ S(\rho_{i+1}^n)\ \right\}$$

and $\hat{\Phi}_i(\rho_i^n, \rho_{i+1}^n, \beta_i^n) = \hat{\Phi}_{i+1}(\rho_i^n, \rho_{i+1}^n, \beta_i^n)/(1-\beta_i^n)$. Note that with a triangular flux function of the form

$$\Phi(\rho) = \min\{v\rho, w(\rho_m - \rho)\}$$

as proposed in [Daganzo, 1994], these formulae simplify to

$$\hat{\Phi}_{i+1}(\rho_i^n, \rho_{i+1}^n, \hat{\phi}_i^n) = \min\left\{ \ v\rho_i^n + \hat{\phi}_i^n\ ,\ w(\rho_m - \rho_{i+1}^n)\ \right\}$$
$$\check{\Phi}_{i+1}(\rho_i^n, \rho_{i+1}^n, \beta_i^n) = \min\left\{ \ (1-\beta_i^n)\ v\rho_i^n\ ,\ w(\rho_m - \rho_{i+1}^n)\ \right\}$$

Using the switched formulation

The switched formulation consists in identifying the interface status and then transmitting the boundary conditions accordingly. We get for an on-ramp with variables ρ_i^n, ρ_{i+1}^n and $\hat{\phi}_i$ the following behavior:

- Free:
  if $\rho_i^n \le \rho_c$, $\rho_{i+1}^n \le \rho_c$ and $\Phi(\rho_i^n) + \hat{\phi}_i \le \Phi_m$,
  then $\rho_{i+1}^n = \Phi^{-l}(\Phi(\rho_i^n) + \hat{\phi}_i)$ with $\Phi^{-l}(\cdot)$ the left inverse.
- Free but decoupling:
  if $\rho_i^n \le \rho_c$, $\rho_{i+1}^n \le \rho_c$ and $\Phi(\rho_i^n) + \hat{\phi}_i > \Phi_m$,
  then $\rho_{i+1}^n = \rho_c$ and $\rho_i^n = \Phi^{-r}(\Phi_m - \hat{\phi}_i)$ with $\Phi^{r}(\cdot)$ the right inverse.
- Decoupled:
  if $\rho_i^n \ge \rho_c$, $\rho_{i+1}^n = \rho_c$,
  then $\rho_i^n = \Phi^{-r}(\Phi_m - \hat{\phi}_i)$.
- Congested:
  if $\rho_i^n > \rho_c$, $\rho_{i+1}^n > \rho_c$ and $\Phi(\rho_{i+1}^n) \ge \hat{\phi}_i$,
  then $\rho_i^n = \Phi^{-r}(\Phi(\rho_{i+1}^n) - \hat{\phi}_i)$.
- Saturated:
  if $\rho_i^n > \rho_c$, $\rho_{i+1}^n > \rho_c$ and $\Phi(\rho_{i+1}^n) < \hat{\phi}_i$,
  then $\hat{\phi}_i = \Phi(\rho_{i+1}^n)$ and $\rho_i^{n+1} = \rho_m$.
  This state is usually assumed not to occur.
- Congestion passing:
  if $\rho_i^n \le \rho_c$, $\rho_{i+1}^n > \rho_c$ and $\Phi(\rho_i^n) + \hat{\phi}_i > \Phi(\rho_{i+1}^n)$,
  then $\rho_i^n = \Phi^{-r}(\Phi(\rho_{i+1}^n) - \hat{\phi}_i)$.

- Freeing wave passing:
  if $\rho_i^n \leq \rho_c$, $\rho_{i+1}^n > \rho_c$ and $\Phi(\rho_i^n) + \hat{\phi}_i < \Phi(\rho_{i+1}^n)$,
  then $\rho_{i+1}^n = \Phi^{-l}(\Phi(\rho_i^n) + \hat{\phi}_i)$.

In a Godunov scheme, the boundary conditions are first set at each time step according to the above results and a standard time stepping is then performed in each link, keeping these boundary values constant. The saturate case corresponds to an on-ramp flow that would lead to a density above the maximal density in the upstream link if applied. The only possible alternative is to limit this flow to an acceptable value that gives the maximal density. As the consequence, the upstream flow is null and the vehicles are queuing in the upstream link. Nevertheless, this state is usually assumed not to occur. Moreover, note that the case $\rho_i^n > \rho_c$ and $\rho_{i+1}^n < \rho_c$ is not considered as it never occurs if not in the initial condition from the entropy condition.

Using the analytical solution of the Riemann problem

An other interesting option for the numerical treatment of on/off-ramps is to solve the corresponding Riemann problem (5.0.1) for all possible values of the involved variables, i.e. ρ_-, ρ_+, $\hat{\phi}$ and β. This approach is similar to the one used for Table 5.1 but leads to 15 possible cases in the on-ramp case. We refer the reader to the appendix *Justification of the switched formulation for the on-ramp behavior* where all these cases are treated rigorously. An approach was introduced in [Lebacque, 1996] for the LWR model with inhomogeneous parameters. The Godunov scheme can then be used transparently using the analytical Riemann solver proposed in this appendix.

5.1.4 The cell transmission model

The Cell Transmission Model (CTM) proposed in [Daganzo, 1994] can be viewed as a Godunov discretization where the flow function $\Phi(\cdot)$ is assumed to be triangular (or trapezoidal) with maximal flow q_m, slope $v > 0$ for the free flow speed and slope $-w < 0$ for the congestion wave speed, as represented on figure 5.2. In this framework, the Godunov scheme becomes

$$\rho_i(k+1) = \rho_i(k) + \frac{\Delta t}{\Delta x_i}(q_i - q_{i+1})$$

with the interface flow q_i between the cells $i-1$ and i is given by the demand/supply/saturation relationship

$$q_i = \min\left\{v\rho_{i-1}, w(\rho_m - \rho_i), q_m\right\} \tag{5.1.4}$$

As a consequence, 3 modes are possible for a cell interface: the free mode when the demand of cell $i-1$ can be satisfied ($q_i = v\rho_{i-1}$), the congestion mode when the supply of cell i limits the interface flow ($q_i = w(\rho_m - \rho_i)$) and the saturation mode when the infrastructure flow limit is reached ($q_i = q_m$).

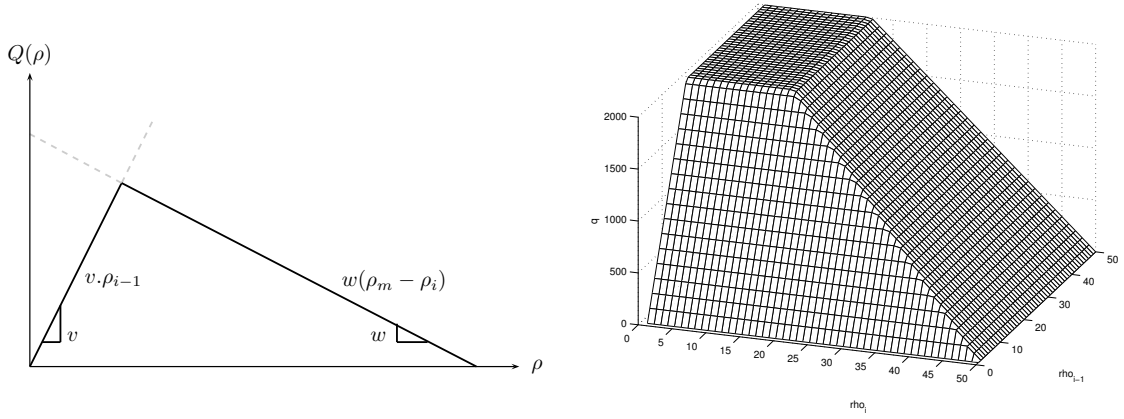

Figure 5.2: Daganzo triangular flow function.

Following this approach, the CTM can be extended to handle on/off ramps with the same demand/supply/saturation paradigm. To do so, we denote q_i^- the flow leaving cell $i-1$, q_i^+ the flow entering in cell i, r_i the on-ramp flow and β_i the off-ramp exit ratio when present. Using $q_i^+ = q_i^- + r_i$ and $q_i^+ \leq q_m$ for on-ramps and $q_i^+ = (1-\beta_i)q_i^-$ and $q_i^- \leq q_m$ for off-ramps, we get the ramp behaviors given in Table 5.2 which are represented as diagrams in Figure 5.3. This table describes a Finite State Machine (FSM) where the

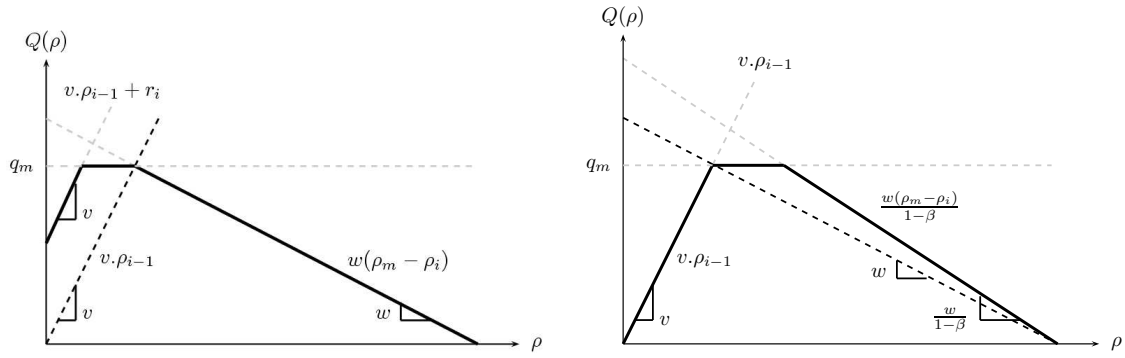

Figure 5.3: Daganzo-like ramp flow function for on (left) and off (right) ramps.

first column identifies the mode given in the second column and the last column describes the interface behavior in that mode. In this setting, the integration scheme should be slightly modified and becomes

$$\rho_i(k+1) = \rho_i(k) + \frac{\Delta t}{\Delta x_i}(q_i^+ - q_{i+1}^-)$$

Two approaches can be used to model the boundary conditions. If the density signals are provided at the boundaries, ghost cells set to the boundary values are inserted before the first cell and after the last one. The above FSM is then used as for standard cells. If the flow signals $q_{\text{Do}}(k)$ and $q_{\text{Do}}(k)$ are provided at the boundaries, then table 5.3 is used to compute the values of $q_1(k)$ and $q_{N+1}(k)$.

Through interface		
Condition	Mode	Interface flow
$v.\rho_{i-1}(k) \leq w(\rho_m - \rho_i(k))$	Free	$q_i(k) = q_i(k)^- = q_i(k)^+ = v.\rho_{i-1}(k)$
$v.\rho_{i-1}(k) > w(\rho_m - \rho_i(k))$	Congested	$q_i(k) = q_i(k)^- = q_i(k)^+ = w(\rho_m - \rho_i(k))$
On-ramp interface		
Condition	Mode	Interface flow
$v.\rho_{i-1}(k) + r_i(k) \leq w(\rho_m - \rho_i(k)) < q_m$	Free	$q_i(k)^- = v.\rho_{i-1}(k)$ $q_i(k)^+ = v.\rho_{i-1}(k) + r(k)$
$q_m > v.\rho_{i-1}(k) + r_i(k) > w(\rho_m - \rho_i(k))$	Congested	$q_i(k)^- = w(\rho_m - \rho_i(k)) - r(k)$ $q_i(k)^+ = w(\rho_m - \rho_i(k))$
$v.\rho_{i-1}(k) + r_i(k) > q_m$	Decoupled	$q_i(k)^- = q_m - r(k)$ $q_i(k)^+ = q_m$
Off-ramp interface		
Condition	Mode	Interface flow
$(1-\beta_i(k))v.\rho_{i-1}(k) \leq w(\rho_m - \rho_i(k)) \leq q_m$	Free	$q_i(k)^- = v.\rho_{i-1}(k)$ $q_i(k)^+ = (1-\beta_i(k))v.\rho_{i-1}(k)$
$q_m \geq (1-\beta_i(k))v.\rho_{i-1}(k) > w(\rho_m - \rho_i(k))$	Congested	$q_i(k)^- = \frac{w(\rho_m - \rho_i(k))}{1-\beta_i}$ $q_i(k)^+ = w(\rho_m - \rho_i(k))$
$q_m(1-\beta_i(k)) < w(\rho_m - \rho_i(k))$	Decoupled	$q_i(k)^- = q_m$ $q_i(k)^+ = (1-\beta)q_m$

Table 5.2: Behavior of CTM through, on-ramp and off-ramp interfaces.

Upstream boundary		
Condition	Mode	Upstream boundary flow
$q_{\mathrm{Up}}(k) \geq w(\rho_m - \rho_i(k))$	Free	$q_1(k) = q_{\mathrm{Up}}(k)$
$q_{\mathrm{Up}}(k) < w(\rho_m - \rho_i(k))$	Congested	$q_1(k) = w(\rho_m - \rho_i(k))$
Downstream boundary		
Condition	Mode	Downstream boundary flow
$v.\rho_{i-1}(k) \geq q_{\mathrm{Do}}(k)$	Free	$q_{N_c+1}(k) = v.\rho_{N_c}(k)$
$v.\rho_{i-1}(k) < q_{\mathrm{Do}}(k)$	Congested	$q_{N_c+1}(k) = q_{\mathrm{Do}}(k)$

Table 5.3: Boundary behaviors for the CTM model.

5.1.5 Simulation example

In this section, we simulate the section of the South-Est beltway of Lyon, France as depicted on Figure 5.4. From the measurements, we clearly see that the on-ramp close to the counting station number 4 is responsible of a congestion that propagates upstream until the boundary. The first step in applying the numerical methods described above

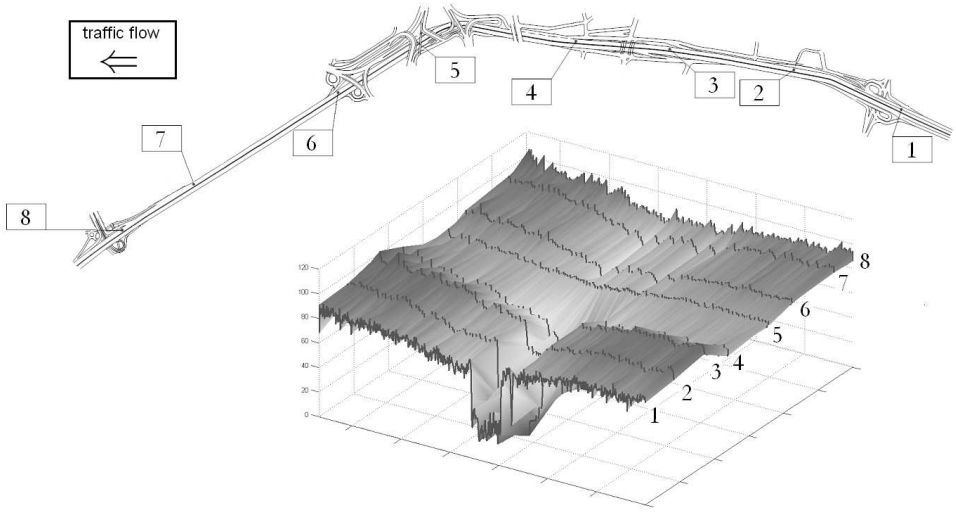

Figure 5.4: Section of the South-Est beltway of Lyon, France used in the study case.

is to estimate the parameters of the model. To do so, we rely on the experimental measurements of the fundament diagrams from the counting stations numbered 1 to 8 as given in Figure 5.5. The identified CTM parameters for each counting station are

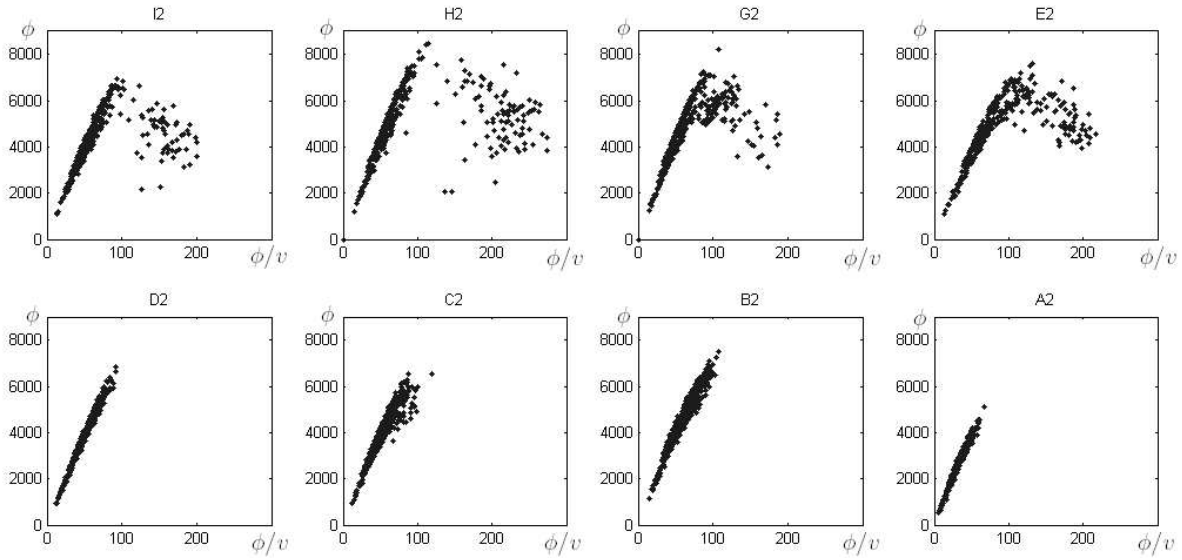

Figure 5.5: Measurements used to identify the model parameters.

$$
\begin{aligned}
1: &\quad [v, w, \rho_c, \phi_m] = [75, 35, 92, NA] \\
2: &\quad [v, w, \rho_c, \phi_m] = [82, 32, 105, NA] \\
3: &\quad [v, w, \rho_c, \phi_m] = [85, 35, 85, 6350] \\
4: &\quad [v, w, \rho_c, \phi_m] = [75, 25, 95, 6200] \\
5: &\quad [v, w, \rho_c, \phi_m] = [75, NA, NA, NA] \\
6: &\quad [v, w, \rho_c, \phi_m] = [78, NA, NA, NA] \\
7: &\quad [v, w, \rho_c, \phi_m] = [78, NA, NA, NA] \\
8: &\quad [v, w, \rho_c, \phi_m] = [81, NA, NA, NA]
\end{aligned}
$$

with NA meaning that the corresponding parameters is irrelevant. Note that triangular fluxes are used for 1 and 2, making the parameter ϕ_m irrelevant. No congestion is observed on stations 5, 6, 7, 8. As a consequence, no critical density, congestion wave speed and maximal flow can be identified. These parameters are interpolated linearly between counting stations, giving rise to a flux tube represented in Figure 5.6. Providing

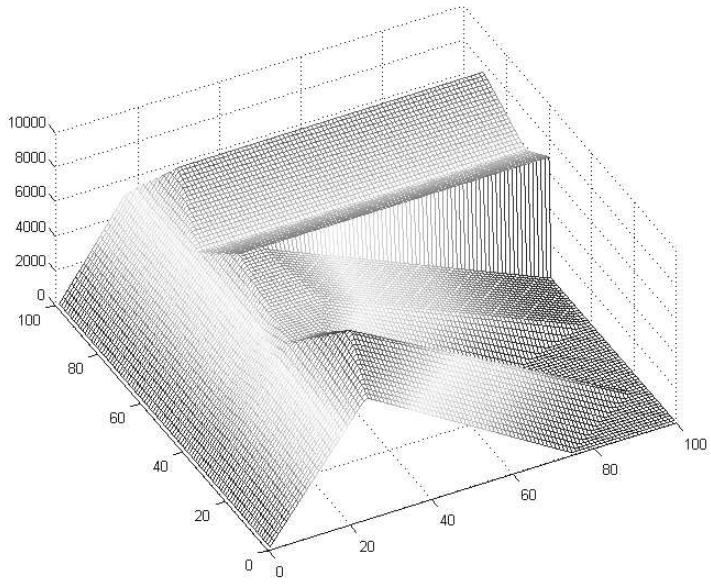

Figure 5.6: Flux tube coming from the spacial dependance of the fundamental diagram.

interpolated initial and boundary conditions along with the measured ramp flow, the internal state is computed with the CTM scheme. Figures 5.7 and 5.8 show the simulation result respectively for the density and the velocity along with the measured data. We see that the model predict the congestion quite accurately.

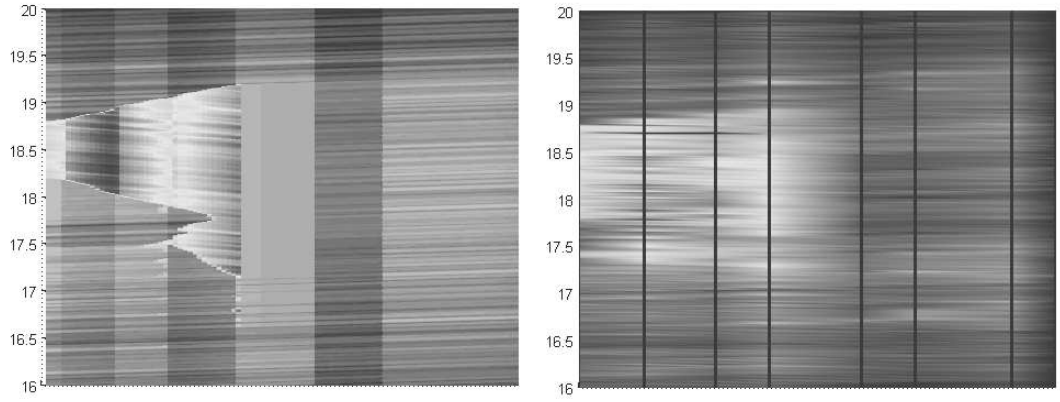

Figure 5.7: Comparaison of the simulated and observed density.

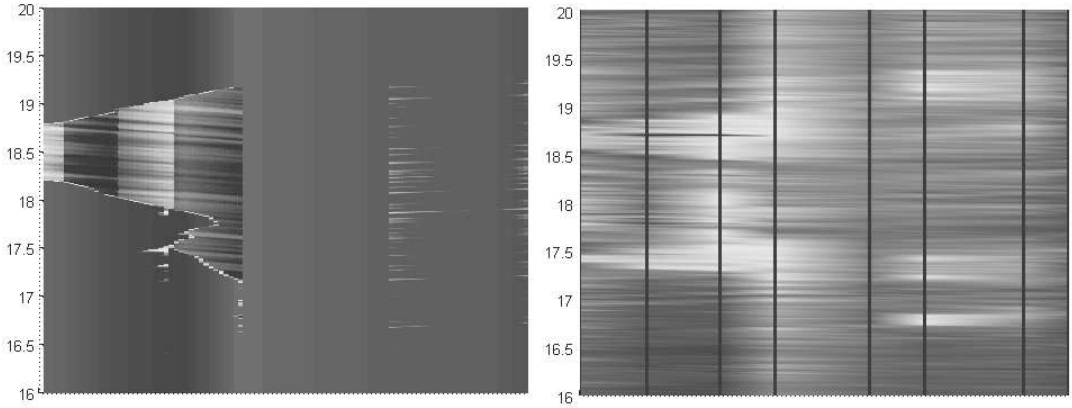

Figure 5.8: Comparaison of the simulated and observed velocity.

5.2 Numerical scheme for the ARZ model

5.2.1 The Godunov method for ARZ links

The Godunov method can be used for systems of conservation laws such as the ARZ model as in [Mammar et al., 2005; Lebacque et al., 2005]. It recursively approximates the state by a piecewise constant function and solves a series of Riemann problem to determine the state of the next time iteration. With the system of conservation laws

$$\partial_t \mathbf{u} + \partial_x \mathbf{F}(\mathbf{u}) = 0$$

the Godunov scheme takes the form

$$\mathbf{u}_i^{n+1} = \mathbf{u}_i^n + \frac{\Delta t}{\Delta x}\left(\mathbf{F}(\mathbf{u}_{i-1/2}^n) - \mathbf{F}(\mathbf{u}_{i+1/2}^n)\right)$$

where $\mathbf{u}_{i+1/2}^n$ is the solution of the Riemann problem at the origin with left and right data $\mathbf{u}_i^n$ and $\mathbf{u}_{i+1}^n$ respectively. To use the Godunov scheme, $\mathbf{u}_{i-1/2}^n$ and $\mathbf{u}_{i+1/2}^n$ should be computed only making simplified Riemann solver as the one before sufficient.

In the case of systems, the CFL condition writes

$$\Delta x \leq \Delta t \; c_{\max}$$

with $c_{\max}$ the maximal wave speed given by

$$c_{\max} = \max_{i,\rho} \lambda_i(\mathbf{u})$$

where $\lambda_i(\mathbf{u})$ are the eigenvalues of $\mathbf{F}(\mathbf{u})$.

In using the Godunov method to numerically solve the ARZ model, we are only interested by the value of the Riemann problem solution at the initial discontinuity location $x = 0$, denoted (ρ_R, v_R). We describe below some simplifications that can be done to give a simplified analytical Riemann solver with ρ_- and ρ_+ the left and right states in the initial condition.

1. Case of shocks: A 1-shock occurs when $\Phi_e'(\rho_-) > \Phi_e'(\rho_0)$, which is equivalent to $\rho_- < \rho_0$ with $\Phi_e(\rho)$ a strict concave function. Moreover, this strict concavity and the fact that $\rho_- < \rho_0$ imply

$$\Phi_e'(\rho_0) < \frac{\Phi_e(\rho_0) - \Phi_e(\rho_-)}{\rho_0 - \rho_-} < \Phi_e'(\rho_-)$$

Using

$$\frac{y_0}{\rho_0} = v_0 - V_e(\rho_0) = v_- - V_e(\rho_-)$$

and

$$\sigma = \frac{\Phi_e(\rho_0) - \Phi_e(\rho_-)}{\rho_0 - \rho_-} + \frac{y_0}{\rho_0} \tag{5.2.1}$$

we obtain

$$\begin{gathered}
\Phi_e'(\rho_0) + v_0 - V_e(\rho_0) < \sigma < \Phi_e'(\rho_-) + v_- - V_e(\rho_-) \\
\Updownarrow \\
v_0 + \rho_0 V_e'(\rho_0) < \sigma < v_- + \rho_- V_e'(\rho_-) \\
\Updownarrow \\
\lambda_1(\rho_0, v_0) < \sigma < \lambda_1(\rho_-, v_-)
\end{gathered}$$

We conclude that in the case of shocks, the value of (ρ_R, v_R) can be determined by examining the signs of $\lambda_1(\rho_0, v_0)$ and $\lambda_1(\rho_-, v_-)$ only.

2. Case of sonic rarefaction waves: When $\lambda_1(\rho_-, y_-) < 0 < \lambda_1(\rho_0, y_0)$, the fan generated by the rarefaction wave spreads across the origin. The traffic state at $x = 0$, called the sonic point, is denoted (ρ_*, y_*) and solves $\lambda_1(\rho_*, y_*) = 0$. This sonic state verifies in the $\rho - v$ variables

$$\begin{cases}
\lambda_1(\rho_*, y_*) = v_* + \rho_*.V_e'(\rho_*) = 0 & \text{as it is the sonic point} \\
v_* - V_e(\rho_*) = v_- - V_e(\rho_-) & \text{as it is on the rarefaction curve}
\end{cases}$$

We conclude that ρ_* solves

$$V_e(\rho_*) + \rho_* V_e'(\rho_*) + v_- - V_e(\rho_-) = 0$$

which gives

$$\begin{cases} \Phi_e'(\rho_*) = -(v_- - V_e(\rho_-)) \\ v_* = V_e(\rho_*) + (v_- - V_e(\rho_-)) \end{cases} \tag{5.2.2}$$

It is interesting to make a parallel with the LWR model for which $\Phi_e'(\rho_*) = 0$.

3. Case of non-sonic rarefaction waves: The minimal speed in a rarefaction wave is $\lambda_1(\rho_-, v_-)$ whereas the maximal speed is $\lambda_1(\rho_0, v_0)$. When $\lambda_1(\rho_-, v_-) \geq 0$ or $\lambda_1(\rho_0, v_0) \leq 0$, the value of (ρ_R, v_R) can again be determined by examining the signs of $\lambda_1(\rho_0, v_0)$ and $\lambda_1(\rho_-, v_-)$ only.

The analytical solution of the simplified Riemann problem is summarized in table 5.4 and can be used directly in a Godunov scheme.

	$\lambda_1(\rho_-, y_-) \geq 0$	$\lambda_1(\rho_-, y_-) < 0$
$\lambda_1(\rho_0, y_0) \geq 0$	$(\rho_R, v_R) = (\rho_-, y_-)$	$(\rho_R, v_R) = (\rho_*, y_*)$ with (5.2.2)
$\lambda_1(\rho_0, y_0) < 0$	$(\rho_R, v_R) = \begin{cases} (\rho_-, y_-) & \text{if } \sigma > 0 \\ (\rho_0, y_0) & \text{if } \sigma < 0 \end{cases}$ with (5.2.1)	$(\rho_R, v_R) = (\rho_0, y_0)$

Table 5.4: Simplified solution of the Riemann problem

5.2.2 The demand/supply formulation for ARZ links

We propose in this section a demand/supply paradigm which proven to be a powerful tool for the LWR model [Lebacque, 1996]. The notions of demand and supply were first proposed for the ARZ model in [Lebacque et al., 2005] and [Herty & Rascle, 2006]. Using the notations

$$\begin{aligned} \Phi(\rho) &= \rho V(\rho) \\ I &= v - V(\rho) \\ y &= \rho I \\ \phi &= \rho v = y + \phi(\rho) \end{aligned}$$

let rewrite the ARZ flux function

$$F(\rho, v) = \begin{pmatrix} F(\rho, v) \\ G(\rho, v) \end{pmatrix} = \begin{pmatrix} \rho v \\ \rho v(v - V(\rho)) \end{pmatrix} \tag{5.2.3}$$

and consider the Riemann problem with initial condition (5.0.1). Due to the conservation of the relative speed in the whole region $x < vt$ including $x = 0$, the relative velocity variable $I = I_- = I_0$ can be considered as a constant parameter which only depends on the initial condition. As $G(\rho, v) = F(\rho, v)(v - V(\rho))$ in (5.2.3), we deduce that $G(\rho, v)$

can be computed immediately from $F(\rho, v)$ in the region $x < vt$. As in [Lebacque et al., 2005], let introduce the modified fundamental diagram

$$\hat{\Phi}(\rho) = \Phi(\rho) + I_- \rho \tag{5.2.4}$$

in $x < vt$, implying that $F_1(\rho, v) = \rho v = \hat{\Phi}(\rho) = F_1(\rho)$ in this region. Still following [Lebacque et al., 2005], let define the demand function

$$D(\rho) = \begin{cases} \hat{\Phi}(\rho) & \text{if } \rho \leq \rho_c \\ \hat{\Phi}_m & \text{if } \rho > \rho_c \end{cases} \tag{5.2.5}$$

and an supply of supply function

$$S(\rho) = \begin{cases} \hat{\Phi}_m & \text{if } \rho \leq \rho_c \\ \hat{\Phi}(\rho) & \text{if } \rho > \rho_c \end{cases} \tag{5.2.6}$$

with $\rho_c = \text{argmax } \hat{\Phi}(\rho)$ and $\hat{\Phi}_m = \max\ \hat{\Phi}(\rho)$. Figure 5.9 shows an example of demand and supply functions. From their definition, the corresponding modified fundamental diagram is defined as the concave envelop of these 2 concave functions.

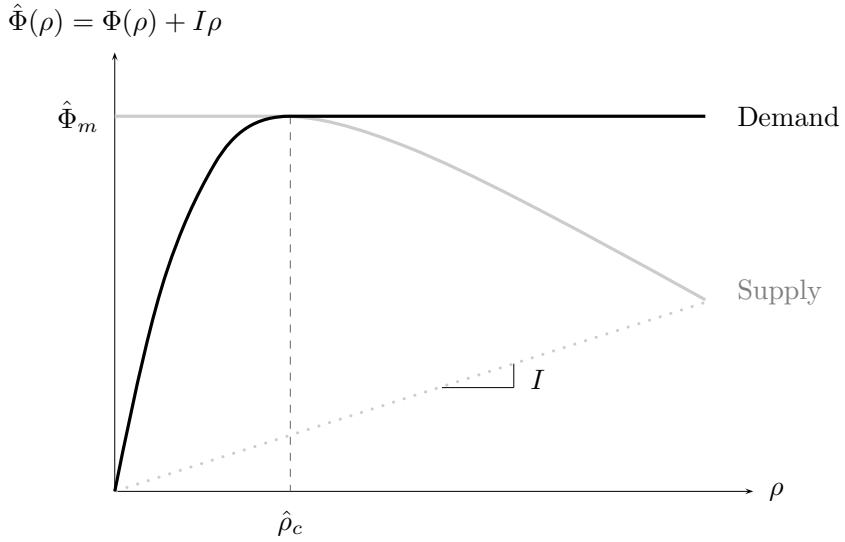

Figure 5.9: Modified fundamental diagram and demand/supply functions.

One of the main step in formulating a Cell Transmission Model as in [Daganzo, 1994] for the ARZ model is to prove the following theorem

Theorem 5.2.1 *Let (ρ_-, I_-) and (ρ_+, I_+) be respectively the left and right state of a Riemann problem for the ARZ model. Then the flux at the initial discontinuity location is constant for all $t > 0$ and is given with notations (5.2.3) by*

$$F(\rho_-, \rho_0) = \min\left\{D(\rho_-), S(\rho_0)\right\} \tag{5.2.7}$$

and

$$G(\rho_-, \rho_0, I_-) = F(\rho_-, \rho_0)\ I_- \tag{5.2.8}$$

with

$$\rho_0 = V^{-1}(I_+ + V(\rho_+) - I_-) \tag{5.2.9}$$

Proof. As shown in Table 5.4, $\lambda_1(\rho) = \Phi'(\rho) + I_- = \hat{\Phi}'(\rho)$, which is the slope of the modified fundamental diagram $\hat{\Phi}(\rho)$, plays a fundamental role in defining the solution of the Riemann problem. The proof of Theorem 5.2.1 consists in analysing the 4 possible cases in Table 5.4 and showing that Equation (5.2.7) is always fulfilled with Equation (5.2.9) giving the intermediate state. Equation (5.2.9) is then immediately deduced from (5.2.3).

- The case $\lambda_1(\rho_-) < 0$ and $\lambda_1(\rho_0) < 0$ implies that $\rho_- > \rho_c$ and $\rho_0 > \rho_c$. From (5.2.5) and (5.2.6), $F(\rho_-, \rho_0) = \min\{D(\rho_-), S(\rho_0)\} = S(\rho_0) = \hat{\Phi}(\rho_0)$ which equivalent to the solution $\rho_R = \rho_0$ given by Table 5.4.

- The case $\lambda_1(\rho_-) \geq 0$ and $\lambda_1(\rho_0) \geq 0$ is similar but with $\rho_- \leq \rho_c$ and $\rho_0 \leq \rho_c$ and leads respectively to $F(\rho_-, \rho_0) = D(\rho_-) = \hat{\Phi}(\rho_-)$ and $\rho_R = \rho_-$ from Equation (5.2.7) and Table 5.4.

- The case $\lambda_1(\rho_-) \geq 0$ and $\lambda_1(\rho_0) < 0$ implies that $\rho_- \leq \rho_c$ and $\rho_0 > \rho_c$ leading to $D(\rho_-) = \hat{\Phi}(\rho_-)$ and $S(\rho_0) = \hat{\Phi}(\rho_0)$. According to Table 5.4, this case gives rise to a shock where the shock speed corresponds to the slope of the straight line connecting $(\rho_-, \hat{\Phi}(\rho_-))$ and $(\rho_0, \hat{\Phi}(\rho_0))$. As a consequence, $\sigma < 0$, which gives $\rho_R = \rho_0$ in Table 5.4, implies $\hat{\Phi}(\rho_-) > \hat{\Phi}(\rho_0)$ so $F(\rho_-, \rho_0) = \hat{\Phi}(\rho_0)$ according to (5.2.7), which is the correct result. Similarly, $\sigma \geq 0$ gives respectively $\rho_R = \rho_-$ and $F(\rho_-, \rho_0) = \hat{\Phi}(\rho_-)$ according to Table 5.4 and Equation (5.2.7) as $\hat{\Phi}(\rho_-) \leq \hat{\Phi}(\rho_0)$ in this case.

- The case $\lambda_1(\rho_-) < 0$ and $\lambda_1(\rho_0) \geq 0$ implies that $\rho_- \geq \rho_c$ and $\rho_0 < \rho_c$ and thus lead to $D(\rho_-) = S(\rho_+) = \hat{\Phi}_m$. Equation (5.2.7) then gives $F(\rho_-, \rho_0) = \hat{\Phi}_m$, meaning that the flow is maximal at the original discontinuity location. This claim is verified by Table 5.4 and Equation (5.2.2) which imply that $\Phi'(\rho_R) + I_- = 0$ which is equivalent to $\hat{\Phi}(\rho_R) = \hat{\Phi}_m$.

□

A direct consequence of Theorem 5.2.1 is that the Godunov scheme can be implemented with

$$F_{i-1}^n = \min\left\{D\big(\rho_{i-1}^n\big), S\big(V^{-1}(I_i^n + V(\rho_i^n) - I_{i-1}^n)\big)\right\} \tag{5.2.10}$$

$$F_i^n = \min\left\{D\big(\rho_{i-1}^n\big), S\big(V^{-1}(I_i^n + V(\rho_i^n) - I_{i-1}^n)\big)\right\} \tag{5.2.11}$$

$$\rho_i^{n+1} = \rho_i^n + \frac{\Delta t}{\Delta x}\big(F_{i-1}^n - F_i^n\big) \tag{5.2.12}$$

$$y_i^{n+1} = y_i^n + \frac{\Delta t}{\Delta x}\big(F_{i-1}^n I_{i-1}^n - F_i^n I_i^n\big) \tag{5.2.13}$$

where F_i^n is the flow leaving cell i.

This demand/supply paradigm extends in a straightforward way when an on-ramp or an off-ramp is present at the interface.

5.2.3 ARZ Cell Transmission Models

With a triangular fundamental diagram

We now turn to the special case where the fundamental diagram is assumed to be a triangular function as represented in Figure 5.10. Compared to experimental data, this assumption does not appear to be too restrictive in most cases, thus justifying this assumption. As in [Daganzo, 1994] and using the same terminology, the parameters of this fundamental diagram are the free flow speed v_f, the congestion wave speed w and the maximal density ρ_m. The triangular flow diagram of Figure 5.10 can be written

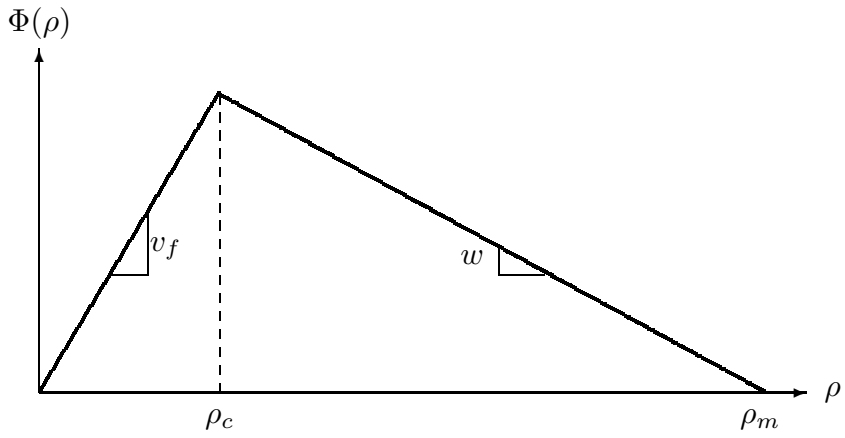

Figure 5.10: Triangular flow diagram.

$$\Phi(\rho) = \min\left\{ \; v_f\rho \; , \; w(\rho_m - \rho) \; \right\}$$

which leads, according to (5.2.4), to the modified fundamental diagram

$$\hat{\Phi}(\rho) = \min\left\{ \; v_f\rho + I_-\rho \; , \; w(\rho_m - \rho) + I_-\rho \; \right\}$$

when consider a Riemann problem with initial condition (5.0.1). Similarly, the demand and supply functions in (5.2.5) and (5.2.6) become

$$D(\rho_-) = \min\left\{ \; v_f\rho_- + I_-\rho_- \; , \; \hat{\Phi}_m \; \right\} \quad \text{and} \quad S(\rho_0) = \min\left\{ \; w(\rho_m - \rho_0) + I_-\rho_0 \; , \; \hat{\Phi}_m \; \right\}$$

Using theorem 5.2.1, we conclude that

$$F(\rho_-, \rho_0) = \min\left\{ \; v_f\rho_- + I_-\rho_- \; , \; w(\rho_m - \rho_0) + I_-\rho_0 \; , \; \hat{\Phi}_m \; \right\}$$

giving the 3 following possible states for the interface

$$\begin{array}{lll} \textit{free} & \text{if} & F(\rho_-,\rho_0) = v_f\rho_- + I_-\rho_- \\ \textit{congested} & \text{if} & F(\rho_-,\rho_0) = w(\rho_m - \rho_0) + I_-\rho_0 \\ \textit{decoupled} & \text{if} & F(\rho_-,\rho_0) = \hat{\Phi}_m \end{array}$$

Due to the triangular nature of the fundamental diagram, the velocity function can be written

$$V(\rho) = \frac{\Phi(\rho)}{\rho} = \min\left\{ v_f \ , \ \frac{w(\rho_m - \rho)}{\rho} \right\}$$

which gives for $v \in [0, v_f]$ the inverse mapping

$$V^{-1}(v) = \frac{w\rho_m}{w+v}$$

Plugging this formula of $V^{-1}(\cdot)$ in the intermediate state equation, we get

$$\begin{aligned} \rho_0 &= \frac{w\rho_m}{w + I_+ + V(\rho_+) - I_-} \\ &= \max\left\{ \frac{w\rho_m}{w + I_+ + v_f - I_-} \ , \ \frac{w\rho_m\rho_+}{w\rho_+ + I_+\rho_+ + w(\rho_m - \rho_+) - I_-\rho_+} \right\} \end{aligned}$$

To summarize, the Cell Transmission Model for the ARZ model in the $\rho - I$ variables is given by the set of equations

$$S_i^n = \max\left\{ \frac{w\rho_m}{w + I_i^n + v_f - I_{i-1}^n}, \frac{w\rho_m\rho_i^n}{w\rho_i^n + I_i^n\rho_i^n + w(\rho_m - \rho_i^n) - I_{i-1}^n\rho_i^n} \right\} \tag{5.2.14}$$

$$S_{i+1}^n = \max\left\{ \frac{w\rho_m}{w + I_{i+1}^n + v_f - I_i^n}, \frac{w\rho_m\rho_{i+1}^n}{w\rho_{i+1}^n + I_{i+1}^n\rho_{i+1}^n + w(\rho_m - \rho_{i+1}^n) - I_i^n\rho_i^n} \right\} \tag{5.2.15}$$

$$F_{i-1}^n = \min\left\{ v_f\rho_{i-1}^n + I_{i-1}^n\rho_{i-1}^n \ , \ S_i^n \ , \ \hat{\Phi}_m \right\} \tag{5.2.16}$$

$$F_i^n = \min\left\{ v_f\rho_i^n + I_i^n\rho_i^n \ , \ S_{i+1}^n \ , \ \hat{\Phi}_m \right\} \tag{5.2.17}$$

$$\rho_i^{n+1} = \rho_i^n + \frac{\Delta t}{\Delta x}\left(F_{i-1}^n - F_i^n\right) \tag{5.2.18}$$

$$y_i^{n+1} = y_i^n + \frac{\Delta t}{\Delta x}\left(F_{i-1}^n I_{i-1}^n - F_i^n I_i^n\right) \tag{5.2.19}$$

With a quadratic fundamental diagram

The main difference of the ARZ-CTM using a triangular fundamental diagram with its LWR counterpart [Daganzo, 1994] is that some nonlinear operations are involved in (5.2.14), (5.2.14) and (5.2.19) in addition to the min/max operations. An important consequence is that relaxations of optimization problems involving the ARZ-CTM would not lead to linear programming as in [Gomes & Horowitz, 2006] for the LWR case. One potential possibility to remove this nonlinearity would be to assume an affine velocity function

$$V(\rho) = v_f\left(1 - \frac{\rho}{\rho_m}\right)$$

known as the Greenshield model [Pipes, 1967], leading to the linear inverse

$$V^{-1}(v) = \rho_m \left(1 - \frac{v}{v_f}\right)$$

Nevertheless, the flow function $\Phi(\rho) = \rho V(\rho)$ loose its piecewise affine property in this case and becomes the quadratic function

$$\Phi(\rho) = \rho v_f - \frac{v_f}{\rho_m}\rho^2$$

The CTM equations then become

$$S_i^n = \frac{-\rho_m I_i^n + v_f \rho_i^n + \rho_m I_{i-1}^n}{v_f} \tag{5.2.20}$$

$$S_{i+1}^n = \frac{-\rho_m I_{i+1}^n + v_f \rho_{i+1}^n + \rho_m I_i^n}{v_f} \tag{5.2.21}$$

$$F_{i-1}^n = \min\left\{ D(\rho_{i-1}^n) \ , \ S(\rho_i^n) \right\} \tag{5.2.22}$$

$$F_i^n = \min\left\{ D(\rho_i^n) \ , \ S(\rho_{i+1}^n) \right\} \tag{5.2.23}$$

$$\rho_i^{n+1} = \rho_i^n + \frac{\Delta t}{\Delta x}\left(F_{i-1}^n - F_i^n\right) \tag{5.2.24}$$

$$y_i^{n+1} = y_i^n + \frac{\Delta t}{\Delta x}\left(F_{i-1}^n I_{i-1}^n - F_i^n I_i^n\right) \tag{5.2.25}$$

Optimization problems involving this model still need to use nonlinear programming but all the constraints are clearly either linear, either bilinear, either convex in this situations.

With an hybrid fundamental diagram

Finally, we propose an hybrid formulation where the velocity function writes

$$V(\rho) = \min\{v_f, z(\rho_m - \rho)\}$$

leading to the fundamental diagram

$$\Phi(\rho) = \min\{v_f \rho, z(\rho_m \rho - \rho^2)\}$$

The interest of this formulation is to remove some nonlinearities in the Cell Transmission Model, which writes in that case

$$S_i^n = \frac{-\rho_m I_i^n + v_f \rho_i^n + \rho_m I_{i-1}^n}{v_f} \tag{5.2.26}$$

$$S_{i+1}^n = \frac{-\rho_m I_{i+1}^n + v_f \rho_{i+1}^n + \rho_m I_i^n}{v_f} \tag{5.2.27}$$

$$F_{i-1}^n = \min\left\{ v_f \rho_{i-1}^n + I_- \rho_{i-1}^n \ , \ S(\rho_i^n) \right\} \tag{5.2.28}$$

$$F_i^n = \min\left\{ v_f \rho_i^n + I_- \rho_i^n \ , \ S(\rho_{i+1}^n) \right\} \tag{5.2.29}$$

$$\rho_i^{n+1} = \rho_i^n + \frac{\Delta t}{\Delta x}\left(F_{i-1}^n - F_i^n\right) \tag{5.2.30}$$

$$y_i^{n+1} = y_i^n + \frac{\Delta t}{\Delta x}\left(F_{i-1}^n I_{i-1}^n - F_i^n I_i^n\right) \tag{5.2.31}$$

5.3 Numerical scheme for the MOD model

5.3.1 The Godunov scheme

We propose to use again the Godunov scheme to simulate the MOD model. To this end, let consider the Riemann problem with initial condition

$$\boldsymbol{\rho}(x,0) = \begin{cases} \boldsymbol{\rho}_- & \text{if } x < 0 \\ \boldsymbol{\rho}_+ & \text{if } x \geq 0 \end{cases}$$

As shown in the analysis of the wave system, $\lambda_{N_R}(\boldsymbol{\rho}) \leq \lambda_k(\boldsymbol{\rho})$ for $k = 1, ..., N_r$ and thus contact discontinuities always propagate faster than the shock or rarefaction waves. As a consequence, the left state $\boldsymbol{\rho}_-$ is always connected to an intermediate state $\boldsymbol{\rho}_0$ by a 1-wave, itself connected to the right state by a superposition of $N_R - 1$ contact discontinuities. As illustrated on Figure 5.11, the following interconnection of elementary waves are possible

$$\begin{aligned} |\boldsymbol{\rho}_+| \geq |\boldsymbol{\rho}_-| \ &: \ \boldsymbol{\rho}_- \ -[\text{shock}]\rightarrow \ \boldsymbol{\rho}_0 \ -[\text{contact}]\rightarrow \boldsymbol{\rho}_+ \\ |\boldsymbol{\rho}_+| < |\boldsymbol{\rho}_-| \ &: \ \boldsymbol{\rho}_- \ -[\text{raref.}]\rightarrow \ \boldsymbol{\rho}_0 \ -[\text{contact}]\rightarrow \boldsymbol{\rho}_+ \end{aligned}$$

with the intermediate state $\boldsymbol{\rho}_0$ components given by

$$\boldsymbol{\rho}_k^0 = \boldsymbol{\rho}_k^- \frac{|\boldsymbol{\rho}_+|}{|\boldsymbol{\rho}_-|}$$

Thanks to this analytical solution of the Riemann problem, the Godunov method [Godlewski & Raviart, 1996] can be used to integrate numerically the MOD model. For an homogeneous link, the spacial domain is decomposed in N cells indexed by i and the

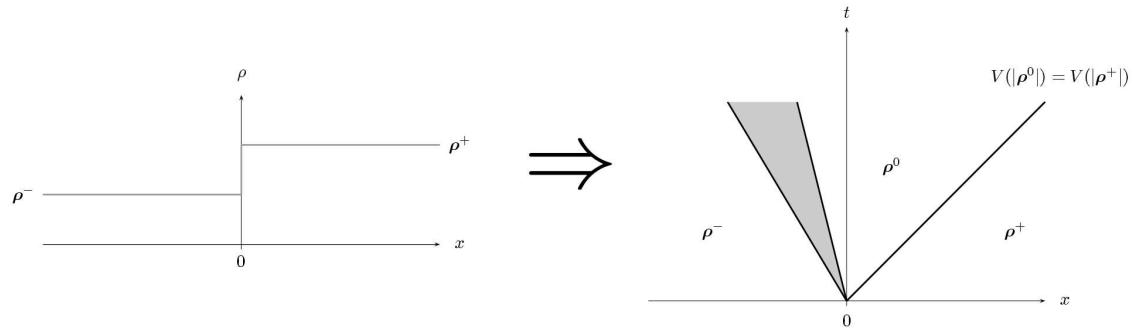

Figure 5.11: Wave interconnection in the solution of the Riemann problem.

time domain in M cells indexed by n. The time stepping of the Godunov scheme writes in this case

$$\boldsymbol{\rho}_i^{n+1} = \boldsymbol{\rho}_i^n + \frac{\Delta t}{\Delta x}\left(F(\boldsymbol{\rho}_{i-1}^n, \boldsymbol{\rho}_i^n) - F(\boldsymbol{\rho}_i^n, \boldsymbol{\rho}_{i+1}^n)\right)$$

with $F(\boldsymbol{\rho}_-, \boldsymbol{\rho}_+)$ the numerical flow function corresponding to the solution of the Riemann problem with left and right states $\boldsymbol{\rho}_-$ and $\boldsymbol{\rho}_+$ respectively. Let define the aggregated flow function

$$f(\boldsymbol{\rho}) = |\boldsymbol{\rho}| V(|\boldsymbol{\rho}|)$$

the shock speed function

$$\sigma(\boldsymbol{\rho}_L, \boldsymbol{\rho}_R) = (f(\boldsymbol{\rho}_R) - f(\boldsymbol{\rho}_L))/(|\boldsymbol{\rho}_R| - |\boldsymbol{\rho}_L|)$$

and the aggregated celerity function

$$c(\boldsymbol{\rho}) = V(|\boldsymbol{\rho}|) + |\boldsymbol{\rho}| V'(|\boldsymbol{\rho}|)$$

As for the LWR and the ARZ models, the numerical flux function $F(\boldsymbol{\rho}_-, \boldsymbol{\rho}_+)$ can be written $F(\boldsymbol{\rho}_-, \boldsymbol{\rho}_+) = f(\boldsymbol{\rho}_*)$ with the interface state $\boldsymbol{\rho}_*$ given by the table

If	$c(\boldsymbol{\rho}_L) > 0$	$c(\boldsymbol{\rho}_L) \leq 0$
$c(\boldsymbol{\rho}_R) \geq 0$	$\boldsymbol{\rho}_* = \boldsymbol{\rho}_L$	$\boldsymbol{\rho}_* = \boldsymbol{\rho}_L . \rho_c / \lvert\boldsymbol{\rho}_L\rvert$
$c(\boldsymbol{\rho}_R) < 0$	$\boldsymbol{\rho}_* = \begin{cases} \boldsymbol{\rho}_L & \text{if } \sigma(\boldsymbol{\rho}_L, \boldsymbol{\rho}_R) > 0 \\ \boldsymbol{\rho}_M & \text{if } \sigma(\boldsymbol{\rho}_L, \boldsymbol{\rho}_R) < 0 \end{cases}$	$\boldsymbol{\rho}_* = \boldsymbol{\rho}_M$

where ρ_c is the critical density corresponding to maximal flow, i.e. $f'(\rho_c) = 0$, and $\boldsymbol{\rho}_M$ is the intermediate state of the corresponding Riemann problem.

In the MOD model, the on and off ramp are implemented using the switched interface formulation.

5.3.2 Simulation examples

We provide in Figure 5.12 a simulation example that illustrate the dynamical behavior of the multiclass model in the presence of one on-ramp and one off-ramp. The top

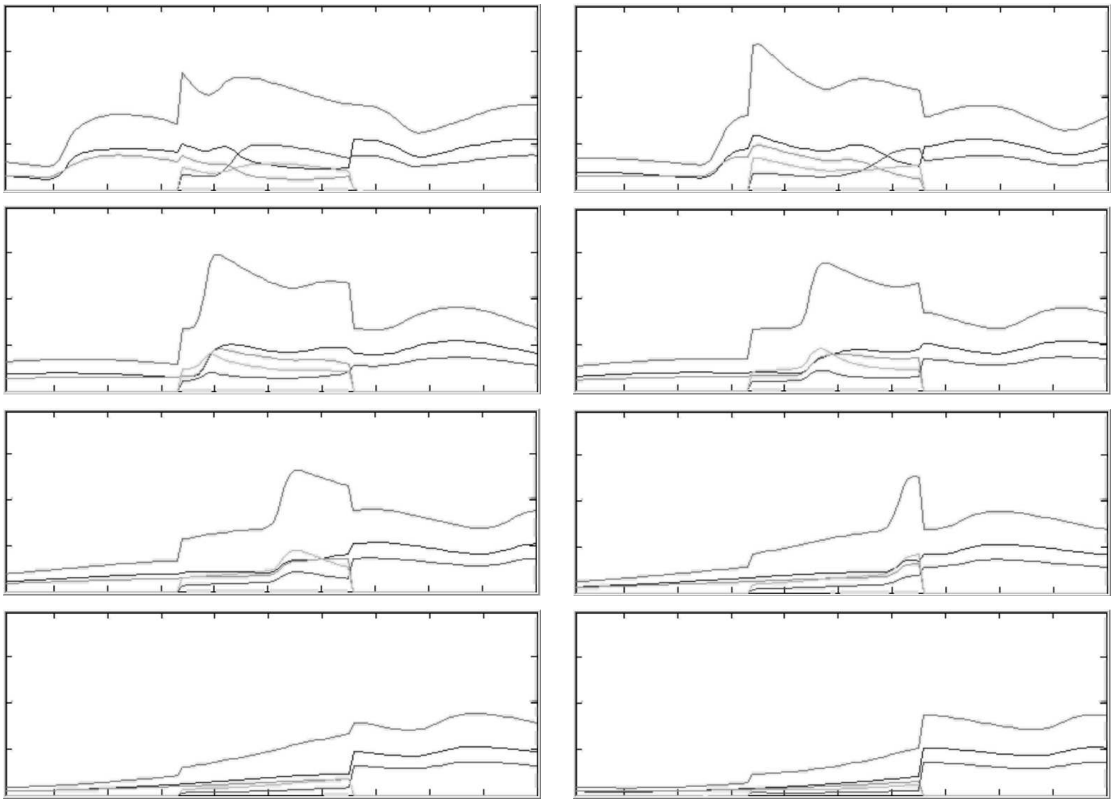

Figure 5.12: Simulation of a simple network with one on-ramp and one off-ramp in the *Forward* case only.

curve is the aggregated density whereas the other curves are affected to the different routes. We restrict to the *Forward* case only both at the on-ramp and the off-ramp. As a consequence, we observe the forward propagation of all density waves. Note the discontinuities at the ramp locations and the birth and then propagation of a shock wave (smoothed due to the numerical integration).

Part II

Control of Conservation Laws and Traffic Applications

A mathematician is a device for turning coffee into theorems.

Paul Erdös (1913-1996),
Hungarian famously eccentric mathematician.

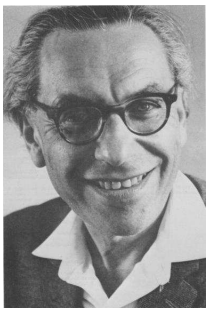

Chapter 6

Optimal Control of Distributed Conservation Laws

As discussed in the first chapters, macroscopic freeway models are hyperbolic partial differential equation, implying that information propagates at a finite speed in these systems. This physical argument motivates the use of receding horizon techniques as local control actions have a spacial influence that increases with time. A sufficiently long prediction horizon thus allows to control a relevant portion of the spacial domain. This chapter addresses this problem and presents an optimization-based receding horizon strategy with applications in ramp metering, missing data reconstruction and origin-destination volume estimation. Given the smoothness usually required to design optimization algorithms, the irregularity of the solutions to conservation laws apparently forbids the immediate use of classical techniques such as linearization, adjoint calculus and gradient computation. We show in this chapter that they indeed extend quite straightforwardly at the price of some acceptable complications. This remarkable fact enables to treat both the scalar and the system cases in a unified way with respect to the theory developed for more regular systems. Before presenting how conservation law trajectories can be optimized, we briefly introduce several physical systems for which the general theory can be applied.

6.1 Physical systems modelled by conservation laws

For systems where the state is composed of distributed quantities

$$y(x,t) = (y_1(x,t), ..., y_m(x,t)) \in \mathbb{R}$$

along a one-dimensional manifold $x \in \mathbb{R}$, the conservation principle states that the evolution of each aggregated conserved quantity in any arbitrary region $(x_L, x_R) \subset \mathbb{R}$ depends only on the flows at the boundaries and the contribution of exogenous flows. In physical systems, a constitutive relationships $f(y) = (f_1(y), ..., f_m(y))$ are used to express the flows at x in terms of the conserved quantities y at the same location. The

exogenous flows are assumed to have the form $g(x,y,u) = (g_1(x,y,u),...,g_m(x,y,u))$ with u a finite dimensional control variable. In 1-dimension, systems considered in this chapter are driven by nonlinear balance equations of the vector form

$$\frac{\mathrm{d}}{\mathrm{d}t}\int_{x_L}^{x_R} y(x,t)\ \mathrm{d}x = f(y(x_L,t)) - f(y(x_R,t)) + \int_{x_L}^{x_R} g(x,y,u)\ \mathrm{d}x \quad , \quad \forall\ (x_L,x_R) \subset \mathbb{R} \tag{6.1.1}$$

with the initial condition $y(x,t) = y_I(x)$. If Equation (6.1.1) is to be considered on a bounded domain $(x,t) \in \Omega = (0,L)\times(0,T)$ as in all practical problems, appropriate boundary conditions should be provided at $x = 0$ and $x = L$, either in the form of the flow signals $f_0(t)$ and $f_L(t)$ or the conserved quantity signals $y_0(t)$ and $y_L(t)$. Note that Equation 6.1.1 is an infinite set of integral equations so that the state only requires to be locally measurable, i.e. in $y \in L^1_{\mathrm{loc}}()$.

In 1-dimension and under appropriate assumptions, the basic manipulations

$$\frac{\mathrm{d}}{\mathrm{d}t}\int_{x_L}^{x_R} y(x,t)\ \mathrm{d}x = \int_{x_L}^{x_R} \partial_t y(x,t)\ \mathrm{d}x \quad \text{and} \quad f(y(x_L,t)) - f(y(x_R,t)) = -\int_{x_L}^{x_R} \partial_x y(x,t)\ \mathrm{d}x$$

transforms Equation (6.1.1) in the unique divergence form partial differential equation

$$\begin{cases} \partial_t y + \partial_x f(y) = g(x,y,u) \\ y(x,t=0) = y_I(x) \\ y(0,t) = y_0(t) \text{ and } y(L,t) = y_L(t) \end{cases} \tag{6.1.2}$$

In the scalar case, Equation (6.1.2) can be rewritten

$$\mathrm{div}_{t,x}\begin{pmatrix} y \\ f(y) \end{pmatrix} = g(x,y,u) \quad \Leftrightarrow \quad \begin{pmatrix} f'(y) \\ 1 \end{pmatrix} \cdot \nabla_{t,x} y = g(x,y,u) \tag{6.1.3}$$

showing that the directional derivative of y along $(f'(y),1)$ is locally equal to the contribution of the source term, thus recovering the method of characteristics [Evans, 1998]. We recall that the main difficulties in analyzing conservation laws are:

Gradient catastrophe Partial differential equations can be analyzed using the method of characteristics [Evans, 1998], which constructs solutions of (6.1.3) by computing a family of integral curves (called projected characteristics) that are tangent to $(f'(y),1)$ and along which the source term is integrated. For nonlinear conservation laws such as (6.1.3), this method fails to provide a solution for all times as these characteristics may intersect in finite time, even for smooth initial and boundary conditions. It can be shown that characteristic crossings correspond to gradient catastrophes [Lax, 1973; LeFloch, 2002] where $\partial_x y \to \infty$.

Overprescribed boundary conditions Specifying explicit Dirichlet boundary conditions at $x = 0$ and $x = L$ for quasi-linear equations such as (6.1.3) generally leads to ill-posed initial boundary value problems [Bardos et al., 1979]. The reason is that enforcing the boundary condition when characteristics leave the computational

domain would lead to an overprescribed boundary value. Note that characteristics cannot be defined beforehand in (6.1.3) as $(f'(y), 1)$ depends on y, making the analytical treatment of boundary conditions tedious for nonlinear conservation laws.

We give below several examples of physical system modelled by conservation laws:

- An unperturbed fluid simply transported by itself with velocity $y(x,t)$ leads to the well-known Burgers equation

$$\partial_t y + \partial_x \left(\frac{y^2}{2} \right) = 0$$

- An homogeneous freeway section with vehicle density ρ and flow function $\Phi(\rho)$ may be modelled by the Lighthill-Whitham-Richards (LWR) equation [Lighthill & Whitham, 1955]

$$\partial_t \rho + \partial_x \Phi(\rho) = 0$$

- An incompressible two-phase immiscible flow in a porous medium like oil and water in petroleum engineering satisfies the Buckley-Leverett equation [LeVeque, 1992]

$$\partial_t y + \partial_x \left(\frac{y^2}{y^2 + a(1-y^2)^2} \right) = 0$$

with y the reduced water saturation in petroleum applications.

- Any Hamilton-Jacobi [Melikyan, 1998] equation $\partial_t z + H(\partial_x z) = 0$ can be transformed to the conservation law $\partial_t y + \partial_x H(y) = 0$ by setting $y = \partial_x z$. For instance, the curve $S(t) = \{(x, v(x,t)) \in \mathbb{R}^2\}$ delimiting a burning region $y \leq v(x,t)$ verifies

$$\partial_t y + \partial_x (-c\sqrt{1+y^2}) = 0 \tag{6.1.4}$$

with $y = \partial_x v$ and c the burning speed.

- The Euler equation for compressible gaz dynamics [Dafermos, 2000] writes

$$\partial_t \begin{pmatrix} \rho \\ \rho v \\ e \end{pmatrix} + \partial_x \begin{pmatrix} \rho v \\ \rho v^2 + p \\ (e+p)v \end{pmatrix} = 0 \tag{6.1.5}$$

- The shallow water equations with topography $B(x,y)$, which may model open air channels or Tsunamis [George & LeVeque, 2006], writes

$$\begin{cases} \partial_t h + \partial_x (hu) + \partial_y (hv) = 0 \\ \partial_t (hu) + \partial_x (hu^2 + \frac{1}{2} gh) + \partial_y (huv) = -gh \partial_x B(x,y) \\ \partial_t (hv) + \partial_x (huv) + \partial_y (hv^2 + \frac{1}{2} gh) = -gh \partial_y B(x,y) \end{cases} \tag{6.1.6}$$

- Non-equilibrium traffic can be modelled by the Payne model [Payne, 1971]

$$\begin{cases} \partial_t \rho + \partial_x(\rho v) = 0 \\ \partial_t v + v\partial_x v + \frac{c^2}{\rho}\partial_x \rho = \frac{V(\rho)-v}{\tau} \end{cases} \tag{6.1.7}$$

  or the Aw-Rascle-Zhang model [Aw & Rascle, 2000; Zhang, 2002]

$$\begin{cases} \partial_t \rho + \partial_x(\rho v) = 0 \\ \partial_t\big(v + P(\rho)\big) + v\partial_x\big(v + P(\rho)\big) = \frac{V(\rho)-v}{\tau} \end{cases} \tag{6.1.8}$$

  with ρ and v respectively the traffic density and velocity, $V(\rho)$ the equilibrium velocity and $P(\rho)$ a pressure term.

- Magneto-hydrodynamic (MHD) systems as plasma can be modelled by

$$\partial_t \begin{pmatrix} \rho \\ \rho\mathbf{u} \\ \mathbf{B} \\ E \end{pmatrix} + \partial_x \begin{pmatrix} \rho\mathbf{u} \\ \rho\mathbf{u}\mathbf{u} + I((p + \frac{1}{2}\mathbf{B}^2) - \mathbf{B}\mathbf{B}) \\ \mathbf{u}\mathbf{B} - \mathbf{B}\mathbf{u} \\ (E + p + \frac{1}{2}\mathbf{B}^2)\mathbf{u} - \mathbf{B}(\mathbf{u}\cdot\mathbf{B}) \end{pmatrix} = 0 \tag{6.1.9}$$

- Acoustic propagation in an heterogeneous medium verifies

$$\begin{aligned} &\partial_t p(x,t) + K(x)\partial_x u(x,t) = 0 \\ &\rho(x)\partial_t u(x,t) + \partial_x p(x,t) = 0 \end{aligned} \tag{6.1.10}$$

  with ρ the density, K the bulk modulus, u the velocity and p the pressure.

- The kinetic formulation of chromatography systems for Langmuir isotherms writes [James, Peng & Perthame, 1995]

$$\partial_t u_i + \partial_x \frac{k_i u_i}{D} = 0 \tag{6.1.11}$$

  with $1 \le i \le N$, $0 < k_1 < ... < k_N$ and $D = 1 + u_1 + ... + u_N$.

- The dynamics of a nonlinear elastic string can be modelled by

$$\partial_t \begin{pmatrix} \mathbf{u} \\ \mathbf{v} \end{pmatrix} + \partial_x \begin{pmatrix} \mathbf{v} \\ \mathbf{T} \end{pmatrix} = 0 \tag{6.1.12}$$

  where $\mathbf{u}$ is tangent to the string, $-\mathbf{v}$ is the velocity of a string element and $\mathbf{T}$ is the tension with the stress-stain relation of the form $\mathbf{T} = \mathbf{T}(\mathbf{u}) = T(|\mathbf{u}|)\mathbf{u}/|\mathbf{u}|$.

6.2 The general adjoint-based optimization method

The optimal control theory of partial differential equations was initiated in the early 70's by Pierre Louis Lions with his seminal book [Lions, 1971]. The proposed approached consists in computing the necessary conditions of optimality in the form of the system equation, an adjoint equation of the same kind and a vanishing first variation condition. This analytic approach that was successfully applied to linear elliptic, parabolic and second order hyperbolic equations can be extended to nonlinear systems using gradient-based recursive algorithms. An abondent literature is available on this method with applications in airfoil design ([Jameson, 1995], [Jameson, 2003], [Jameson, Martinelli & Pierce, 1998]), fluid steering ([Bewley, Temam & Ziane, 2000], [Hinze & Kunisch, 2001], [Collis, Ghayour, Heinkenschloss, Ulbrichf & Ulbrich, 2002], [Ghattas & Bark, 1997]), gaz steering [Giles & Pierce, 2001], control of water wave ([Sanders & Katopodes, 2000], [Chen & Georges, 1999]), air traffic control ([Bayen, Raffard & Tomlin, 2004]) and many others. We present in this section an overview of the adjoint-based optimization method and refer the reader to the appendix for the notations and the notions of functional analysis.

Let consider the following abstract Banach space optimization problem

$$\begin{aligned} &\underset{y\in\mathcal{Y}}{\textbf{Min}} \quad \mathcal{J}_{\text{obs}}(y) \\ &\textbf{Subj. to} \quad \begin{cases} \mathcal{C}(y,u)=0 \\ \\ u\in\mathcal{U}_{\text{ad}} \end{cases} \end{aligned} \tag{6.2.1}$$

where $\mathcal{J}_{\text{obs}}(y)$ is the cost function, $\mathcal{C}(y,u)$ is the implicit dynamical system equation, y is the system state living in $\mathcal{Y}$ and u is the control variable living in the constrained set $\mathcal{U}_{\text{ad}} \subset \mathcal{U}$. The constrained set $\mathcal{U}_{\text{ad}}$ is assumed to be a convex and to be defined by a set of inequalities $f_i(u) \geq 0$ with $i = 1, ..., N_i$.

The constraint $\mathcal{U}_{\text{ad}}$ is classically handled using a barrier technique [Boyd & Vandenberghe, 2004] that moves the constraint to the objective function at the cost of requiring some iterations to find the solution of the original problem. Following this approach, let consider the new optimization problem

$$\begin{aligned} &\underset{\substack{y\in\mathcal{Y}\\ u\in\mathcal{U}}}{\textbf{Min}} \quad \mathcal{J}(y,u) \\ &\textbf{Subj. to} \quad \mathcal{C}(y,u)=0 \end{aligned} \tag{6.2.2}$$

where $\mathcal{J}(y,u) = \mathcal{J}_{\text{obs}}(y) + \mathcal{J}_{\text{bar}}(u)$ is the generalized cost function and $u \in \mathcal{U}$ is now free. In the barrier technique, the inequalities $f_i(u) \geq 0$ are replaced by the terms $\frac{1}{M}\int \log(f_i(u))$ included in $\mathcal{J}_{\text{bar}}(u)$ to ensure that $u \in \mathcal{U}_{\text{ad}}$. Then, solving (6.2.2) for different values of M as $M \to \infty$ leads to the solution of the original problem (6.2.1).

We assume here the existence of all the manipulated mathematical objects, a more rigorous approach being followed later in the applications of interest. Assuming that

there exists $\bar{y}$ and $\bar{u}$ such that $\mathcal{C}(\bar{y},\bar{u})=0$, that $\mathcal{C}$ is continuously Fréchet differentiable in neighborhoods of $\bar{y}$ and $\bar{u}$ and that $D_y\mathcal{C}[\bar{y},\bar{u}]$ is continuously invertible, the implicit function theorem states that $y=y(u)$ locally. Moreover, the sensitivity operator $D_u y[\bar{u}]$ is the unique solution of

$$D_y\mathcal{C}[y(\bar{u}),\bar{u}]\circ D_u y[\bar{u}] + D_u\mathcal{C}[y(\bar{u}),\bar{u}] = 0 \tag{6.2.3}$$

Under a uniqueness assumption of y with respect to u, which is given by the wellposedness of the system equation $\mathcal{C}(y,u)=0$, Problem (6.2.2) can be replaced by the equivalent reduced problem

$$\underset{u\in\mathcal{U}}{\mathbf{Min}}\ \mathcal{J}_{\mathrm{red}}(u) \triangleq \mathcal{J}(y(u),u)$$

Assuming $\mathcal{J}_{\mathrm{red}}(u)$ is Fréchet differentiable, the necessary conditions for (y^*,u^*) to be optimal are

$$\begin{cases} \mathcal{C}(y^*,u^*)=0 \\ D_u\mathcal{J}_{\mathrm{red}}[u^*]=\mathbf{0} \end{cases} \tag{6.2.4}$$

with $\mathbf{0}\in\mathcal{L}(\mathcal{U})$ the null operator. The Chain rule then gives

$$\langle D_u\mathcal{J}_{\mathrm{red}}[\bar{u}],\tilde{u}\rangle_{\mathcal{U}^*,\mathcal{U}} = \langle D_u\mathcal{J}[\bar{y},\bar{u}],\tilde{u}\rangle_{\mathcal{U}^*,\mathcal{U}} + \langle D_y\mathcal{J}[\bar{y},\bar{u}], D_u y[\bar{u}](\tilde{u})\rangle_{\mathcal{Y}^*,\mathcal{Y}}$$

with $D_u y[\bar{u}]\in\mathcal{L}(\mathcal{U},\mathcal{Y})$ the solution to the sensitivity equation (6.2.3). Using its adjoint $D_u y[\bar{u}]^\star$, we obtain

$$\langle D_u\mathcal{J}_{\mathrm{red}}[\bar{u}],\tilde{u}\rangle_{\mathcal{U}^*,\mathcal{U}} = \langle D_u\mathcal{J}[\bar{y},\bar{u}],\tilde{u}\rangle_{\mathcal{U}^*,\mathcal{U}} + \langle D_u y[\bar{u}]^\star\circ D_y\mathcal{J}[\bar{y},\bar{u}],\tilde{u}\rangle_{\mathcal{U}^*,\mathcal{U}}$$

From Equation (6.2.3), we deduce that

$$D_u y[\bar{u}]^\star = -D_u\mathcal{C}[\bar{y},\bar{u}]^\star\circ\left(D_y\mathcal{C}[\bar{y},\bar{u}]^\star\right)^{-1}$$

leading to the gradient formula

$$D_u\mathcal{J}_{\mathrm{red}}[\bar{u}] = D_u\mathcal{J}[\bar{y},\bar{u}] - D_u\mathcal{C}[\bar{y},\bar{u}]^\star\circ D_y\mathcal{C}[\bar{y},\bar{u}]^{-\star}\circ D_y\mathcal{J}[\bar{y},\bar{u}]$$

To simplify the computation, the adjoint variable $\lambda = -D_y\mathcal{C}[\bar{y},\bar{u}]^{-\star}\circ D_y\mathcal{J}[\bar{y},\bar{u}]$ is introduced, splitting the derivative computation in two steps

$$D_y\mathcal{C}[\bar{y},\bar{u}]^\star\lambda = -D_y\mathcal{J}[\bar{y},\bar{u}] \tag{6.2.5}$$

$$D_u\mathcal{J}_{\mathrm{red}}[\bar{u}] = D_u\mathcal{C}[\bar{y},\bar{u}]^\star\lambda + D_u\mathcal{J}[\bar{y},\bar{u}] \tag{6.2.6}$$

and giving an alternative to (6.2.4). Indeed, the necessary conditions for (y^*,u^*) to be optimal is that there exists an adjoint variable λ^* such that

$$\begin{cases} \mathcal{C}(y^*,u^*)=0 & \text{(SE)} \\ D_y\mathcal{C}[y^*,u^*]^\star\lambda^* = -D_y\mathcal{J}[y^*,u^*] & \text{(AE)} \\ D_u\mathcal{C}[y^*,u^*]^\star\lambda^* + D_u\mathcal{J}[y^*,u^*]=0 & \text{(DE)} \end{cases} \tag{6.2.7}$$

where SE stands for State Equation, AE for Adjoint Equation and DE for Decision Equation. Solving the optimality system (6.2.7) analytically is in general hopeless and

the alternative is to develop an iterative gradient-based method that convergences to u^*. From the Riesz representation theorem, if $\mathcal{U}$ is an Hilbert space, the gradient $\nabla_u \mathcal{J}_{\text{red}}[u]$ can be identified with the Fréchet derivative $D_u \mathcal{J}_{\text{red}}[u]$ given in (6.2.6). Nevertheless, as the gradient expression depends on the definition of the inner product in general, the inner product definition can be viewed as a design parameter. The adjoint method can thus be used to compute the gradient $\nabla_u \mathcal{J}_{\text{red}}[u]$ of the cost functional with reasonable effort. Moreover, it can be shown that the adjoint variable λ corresponds to the Lagrange multiplier of the optimization problem.

If infinite dimensional computations were possible, Algorithm 2 could be used to solve (6.2.2) iteratively. Nevertheless, as the computations in $\mathcal{Y}$, $\mathcal{U}$ and $\mathcal{Y}^*$ cannot be done by a computer, numerical approximations are unavoidable. Note that this method only provides a local minimum in general and may fail to converge if $\mathcal{U}_{\text{ad}}$ is not compact.

Algorithm 2 General steepest descent algorithm with barrier iterations.

Require: $u := u_{\text{init}} \in \mathcal{U}_{\text{ad}}$, $M := M_{\text{init}} > 0$, $\epsilon_i > 0$, $\epsilon_o > 0$, $\Delta M > 0$
  while $\mathcal{J}_{\text{bar}}(u)/\mathcal{J}_{\text{obs}}(\rho) > \epsilon_o$ **do**
    while $\|\nabla_u \mathcal{J}_{\text{red}}\| > \epsilon_i$ **do**
      Compute $y := y(u)$, $\lambda := \lambda(y)$
      Update $u := u - t\nabla_u \mathcal{J}_{\text{red}}$, $t \in (0,1)$ such that $u \in \mathcal{U}_{\text{ad}}$
    end while
    M := M.ΔM
  end while

6.3 Preliminaries

The main technical ingredients of the adjoint method are the linearization of the system dynamics and the integrations by parts used to compute the adjoint operator. Due to the irregularity of the flows generated by conservation laws, these equations cannot be linearized in the classical sense in general. The next section relates the different solutions proposed in the mathematical community to get around this complication. Next, we provide some generalizations of the integration by parts for piecewise-C^1 and BV fields. These formula are restricted to $\mathbb{R}^2$ as 1-dimensional conservation laws will be treated only.

6.3.1 Linearization of conservation laws

6.3.2 Integration by parts for piecewise-C^1 fields

As shown in [Dafermos, 1977*b*] using the method of Generalized Characteristics, the flow generated by conservation laws can be considered to be piecewise-C^1 practically. Though

not suited for the wellposedness analysis of such equations, the following integration by parts formula is given for this functional space.

Theorem 6.3.1 (Integration by parts for piecewise-C^1 fields in $\mathbb{R}^2$) *Let $\Omega \subset \mathbb{R}^2$ with components (x,t) be an open and bounded domain with Lipschitz boundary $\partial\Omega$ and let $u : \Omega \to \mathbb{R}^2$ be piecewise-C^1 with singularities in both components occurring along N_s continuously differentiable curves $\Gamma_i \subset \Omega$ parameterized by $\Gamma_i = \{(x,t) : x = s_i(t),\ t \in [t_i^I, t_i^F]\}$. With $u = (u_1, u_2)$, $\phi \in C^1(\mathbb{R}^2)$ and ν the outward normal to $\partial\Omega$, the following integration by parts formula applies*

$$\int_\Omega u \cdot \nabla\phi \ \mathrm{d}\mathcal{L}^2 = -\int_{\Omega\setminus\cup_i\Gamma_i} \phi \ \mathrm{div} u \ \mathrm{d}\mathcal{L}^2 + \int_{\partial\Omega} u\cdot\nu \ \phi \ \mathrm{d}\mathcal{H}^1 + \sum_{i=1}^{N_s} \int_{t_i^I}^{t_i^F} \dot{s}_i(t)[u_2\phi]_{|_{x=s_i(t)}} - [u_1\phi]_{|_{x=s_i(t)}} dt \quad (6.3.1)$$

where $[\xi]_{|_{x=s_i(t)}} = \lim_{x\downarrow s_i(t)} \xi - \lim_{x\uparrow s_i(t)}$ is the jump in ξ at $(s_i(t),t) \in \Gamma_i$.

Proof. Let first decompose Ω into N distinct subsets Ω_j with boundaries $\partial\Omega_j$ such that the restrictions of u to Ω_j are C^1. As the Lebesgue measure is unchanged when the integration domain is modified by a set of measure 0, we can write

$$\int_\Omega u \cdot \nabla\phi \ \mathrm{d}\mathcal{L}^2 = \sum_{j=1}^{N} \int_{\Omega_j} u \cdot \nabla\phi \ \mathrm{d}\mathcal{L}^2$$

Applying a standard integration by parts on Ω_j gives

$$\int_{\Omega_j} u \cdot \nabla\phi \ \mathrm{d}\mathcal{L}^2 = -\int_{\Omega_j} \phi \ \mathrm{div} u \ \mathrm{d}\mathcal{L}^2 + \int_{\partial\Omega_j} u\cdot\nu_j \ \phi \ \mathrm{d}\mathcal{H}^1$$

with ν_j the normal vector to $\partial\Omega_j$. The third term in the above equation have contributions coming either from a virtual boundary $\partial\Omega_j$ where u is C^1, a portion of $\partial\Omega$ or a portion of a curve Γ_i. In the first case, the contributions annihilate when summing over all Ω_i. In the second case, the contribution writes simply

$$\int_{\partial\Omega_j\cap\partial\Omega} u\cdot\nu \ \phi \ \mathrm{d}\mathcal{H}^1$$

The third case requires more analysis and is treated as follows. A tangent vector to Γ_i being $(\dot{s}_i(t) \quad 1)$, a normal vector to Γ_i writes $(-1 \quad \dot{s}_i(t))$. If this vector is an outward normal to Ω_j, the contribution is

$$\int_{\partial\Omega_j\cap\Gamma_i} \frac{1}{\sqrt{1+\dot{s}_i(t)^2}} \begin{pmatrix} -1 \\ \dot{s}_i(t) \end{pmatrix} \big(u \ \phi\big)^+ \ \mathrm{d}\mathcal{H}^1 = \int_{t_i^I}^{t_i^F} \begin{pmatrix} -1 \\ \dot{s}_i(t) \end{pmatrix} \big(u \ \phi\big)^+ \ \mathrm{d}t$$

with $\big(u \ \phi\big)^+ = \lim_{x\downarrow s_i(t)} \big(u \ \phi\big)$. If the vector $(-1 \quad \dot{s}_i(t))$ is an inward normal to Ω_j, then the contribution is

$$\int_{\partial\Omega_j\cap\Gamma_i} \frac{1}{\sqrt{1+\dot{s}_i(t)^2}} \begin{pmatrix} -1 \\ \dot{s}_i(t) \end{pmatrix} \big(-u \ \phi\big)^- \ \mathrm{d}\mathcal{H}^1 = \int_{t_i^I}^{t_i^F} \begin{pmatrix} -1 \\ \dot{s}_i(t) \end{pmatrix} \big(-u \ \phi\big)^- \ \mathrm{d}t$$

with $\big(u\ \phi\big)^- = \lim_{x\uparrow s_i(t)}\ \big(u\ \phi\big)$.

Summing the contributions for all subsets Ω_j gives the theorem. □

6.3.3 Integration by parts for BV fields

As the wellposedness of conservation laws ([Kružkov, 1970],[Bressan, Crasta & Piccoli, 2000]) was established in the space BV of functions with bounded variations, we propose below a version of the integration by parts formula that can be used in the computation of adjoint operators. This result is quite general as BV functions are differentiable in essentially the weakest measure theoretic sense. We refer the reader to the appendix and [Evans & Gariepy, 1991] for more details about this functional space.

Theorem 6.3.2 (Integration by parts for BV fields in $\mathbb{R}^n$) *Let $\Omega \subset \mathbb{R}^n$ be open and bounded with Lipschitz boundary $\partial\Omega$ and $u \in BV(\Omega, \mathbb{R}^n)$. Then, with $\phi \in C^1(\mathbb{R}^n)$, the following integration by parts formula applies*

$$\int_\Omega u \cdot \nabla\phi \ \mathrm{d}\mathcal{L}^n = -\int_{\Omega\setminus\cup_i\Gamma_i} \phi\ \mathrm{div}u \ \mathrm{d}\mathcal{L}^n + \int_{\partial\Omega} u\cdot\nu\ \phi\ \mathrm{d}\mathcal{H}^{n-1} - \sum_{i=1}^n \int_\Omega \phi\ \mathrm{d}[D_{x_i}u_i]_\mathrm{s}$$

where $[D_{x_i}u_i]_\mathrm{s}$ is the singular part associated to the scalar measure $[D_{x_i}u_i]$.

Proof. The Green-Gauss theorem (see appendix) states that,

$$\int_\Omega u\ \mathrm{div}\phi\ \mathrm{d}\mathcal{L}^n = -\int_\Omega \phi\cdot \mathrm{d}[Du] + \int_{\partial\Omega} (\phi\cdot\nu)\ Tu\ \mathrm{d}\mathcal{H}^{n-1}$$

for all $u \in BV(\Omega)$ and $\phi \in C^1(\mathbb{R}^n, \mathbb{R}^n)$ with $T : BV(\Omega) \to L^1(\partial\Omega, \mathcal{H}^{n-1})$ the trace operator and $[Du]$ the vector measure for the gradient of u. Let take $u = (u_1, ..., u_n)$ with $u_i \in BV(\Omega)$ and $\phi \in C^1(\mathbb{R}^n)$. Taking $\psi = (0, ..., \phi, ..., 0)$ with the i^{th} component being the only non vanishing entry, the Green-Gauss theorem gives

$$\int_\Omega u_i\ \mathrm{div}\psi\ \mathrm{d}\mathcal{L}^n = \int_\Omega u_i\ \partial_{x_i}\phi\ \mathrm{d}\mathcal{L}^n = -\int_\Omega \phi\ \mathrm{d}[D_{x_i}u_i] + \int_{\partial\Omega} (\phi\ \nu_i)\ Tu_i\ \mathrm{d}\mathcal{H}^{n-1}$$

Repeating the same procedure for all i and summing give

$$\int_\Omega u\cdot\nabla\phi\ \mathrm{d}\mathcal{L}^n = -\int_\Omega \phi\ \mathrm{d}[\mathrm{Div}u] + \int_{\partial\Omega} Tu\cdot\nu\ \phi\ \mathrm{d}\mathcal{H}^{n-1}$$

where the measure $[\mathrm{Div}u]$ is given by

$$[\mathrm{Div}u] = \sum_{i=1}^n [D_{x_i}u_i] = \sum_{i=1}^n [D_{x_i}u_i]_\mathrm{ac} + \sum_{i=1}^n [D_{x_i}u_i]_\mathrm{s}$$

The fact that $[D_{x_i}u_i]_\mathrm{ac} = \mathcal{L}^n \llcorner \partial_{x_i}u_i$ implies

$$\int_\Omega \phi\ \sum_{i=1}^n \mathrm{d}[D_{x_i}u_i]_\mathrm{ac} = \int_{\Omega\setminus\cup_i\Gamma_i} \phi\ \sum_{i=1}^n \partial_{x_i}u_i\ \mathrm{d}\mathcal{L}^n = \int_{\Omega\setminus\cup_i\Gamma_i} \phi\ \mathrm{div}u\ \mathrm{d}\mathcal{L}^n$$

leading to

$$\int_\Omega \phi \ \mathrm{d}[\mathrm{Div}u] = \int_{\Omega\setminus\cup_i\Gamma_i} \phi \ \mathrm{div}u \ \mathrm{d}\mathcal{L}^n + \sum_{i=1}^n \int_\Omega \phi \ \mathrm{d}[D_{x_i}u_i]_\mathrm{s}$$

For notational purpose, omitting the trace operator when evaluating the boundary conditions gives the theorem. □

We give below a version in $\mathbb{R}^2$ suitable for 1-dimensional conservation laws.

Theorem 6.3.3 (Integration by parts for BV fields in $\mathbb{R}^2$) *Let $\Omega \subset \mathbb{R}^2$ with components (x,t) be open and bounded with Lipschitz boundary $\partial\Omega$ and let $u = (u_1, u_2) \in BV(\Omega, \mathbb{R}^2)$ have singularities along N_s Lipschitz curves $\Gamma_i \subset \Omega$ parameterized by $\Gamma_i = \{(x,t) : x = s_i(t),\ t \in [t_i^I, t_i^F]\}$. Then, with $\phi \in C^1(\mathbb{R}^2)$ and ν the outward normal to $\partial\Omega$, the following integration by parts formula applies*

$$\int_\Omega u\cdot\nabla\phi \ \mathrm{d}\mathcal{L}^2 = -\int_{\Omega\setminus\cup_i\Gamma_i} \phi \ \mathrm{div}u \ \mathrm{d}\mathcal{L}^2 + \int_{\partial\Omega} u\cdot\nu \ \phi \ \mathrm{d}\mathcal{H}^1 + \sum_{i=1}^{N_s} \int_{t_i^I}^{t_i^F} \dot{s}_i(t)[u_2\phi]_{|_{x=s_i(t)}} - [u_1\phi]_{|_{x=s_i(t)}} dt \quad (6.3.2)$$

Proof. A structural property of BV functions [DiPerna, 1975; DiPerna, 1979] is that, if $u \in BV(\Omega)$, then the domain $\Omega \in \mathbb{R}^2$ is a disjoint union of

- an open set A of points of approximate continuity, i.e.

$$x \in A \ \Leftrightarrow \ \exists\ \bar{u} \in \mathbb{R} \ : \ \lim_{r\to 0} \frac{1}{r^2} \int_{B(x,r)} |u(y) - \bar{u}| \mathrm{d}y = 0$$

- a closed set Γ, which is an at most countable union of Lipschitz surfaces of dimension $n-1$, of points of approximate jump discontinuity with distinguished direction ν, i.e.

$$x \in \Gamma \ \Leftrightarrow \ \exists\ \bar{u}^- \neq \bar{u}^+ \ : \ \lim_{r\to 0} \frac{1}{r^2} \int_{B(x,r)\cap\{y:(y-x)\cdot\pm\nu\geq 0\}} |u(y) - \bar{u}^\pm| \mathrm{d}y = 0$$

- and a closed set I with vanishing $\mathcal{H}^1$ measure of irregular points so that $\Omega = A \cup \Gamma \cup I$.

This structure enables the disjoint decomposition $\Omega = \bigcup_{j=1}^N \Omega_j$ where u is continuous on all Ω_j, implying $[D_{x_i}u_i]_\mathrm{s} = 0$ for all i over all Ω_j. The remaining of the proof follows the piecewise-C^1 case using the trace operator and noting that the set I is never taken into account as it has vanishing $\mathcal{H}^1$ measure. □

From the above theorems, BV fields are very similar to piecewise-C^1 fields when applying integrations by parts. For this reason, piecewise-C^1 functions and measure theoretically piecewise-C^1 measures will be treated similarly throughout the book.

6.4 Optimal control of scalar conservation laws

6.4.1 Problem formulation

In this section, we consider the class of 1-dimensional scalar conservation laws on $\Omega = (0, L) \times (0, T)$ where $x \in (0, L)$ is a bounded spacial domain and $t \in (0, T)$ a finite time horizon. They take the form

$$\begin{cases} \partial_t y + \partial_x f(y) = g(x, y, u) \\ y(x, t = 0) = y_I(x) \\ y(0, t) = y_0(t) \text{ and } y(L, t) = y_L(t) \end{cases} \tag{6.4.1}$$

where $y(x, t) \in BV(\Omega)$ is the system state, $u(t) \in \mathcal{U}$ is a finite dimensional control variable, $f : \mathbb{R} \to \mathbb{R}$ a smooth flux function and $g : \mathbb{R} \times BV(\Omega) \times \mathcal{U}$ a source term. Note that we restrict to problems where the control affects the system evolution through the source term only. We recall that y may have N_s curves of discontinuity parameterized by $\Gamma_i = \{(x, t) : x = s_i(t),\ t \in [t_i^I, t_i^F]\}$ where $s(t) = (s_1(t), ..., s_{N_s}(t))$ is the vector of shock locations at time t.

Coming back the notations adopted in section 6.2 dealing with the general adjoint method, Equation (6.4.1) corresponds to the operator

$$\mathcal{C} : \mathcal{Y} \times \mathcal{U} \to \mathcal{M}$$
$$\mathcal{C}(y, u) = \partial_t y + \partial_x f(y) - g(x, y, u)$$

with

$$\mathcal{Y} = \{y \in BV(\Omega) : y(x, t = 0) = y_I(x),\ y(0, t) = y_0(t) \text{ and } y(L, t) = y_L(t)\}$$

and $\mathcal{M}$ the space of signed Radon measures.

The class of optimal control problems we are considering is

$$\begin{aligned} \underset{y_I, u}{\textbf{Min}} \quad & \mathcal{J}(y, s, u) = \mathcal{J}_{\text{obs}}(y) + \mathcal{J}_{\text{s}}(s) + \mathcal{J}_{\text{bar}}(u) \\ & = \textstyle\int_\Omega \mathcal{P}(y(x, t))\, \mathrm{d}x\mathrm{d}t + \sum_{i=1}^{N_s} \int_{t_i}^T \mathcal{Q}_i(s_i(t))\, \mathrm{d}t + \int_0^T \mathcal{R}(u(t))\, \mathrm{d}t \\ \textbf{Subj. to} \quad & \begin{cases} \partial_t y + \partial_x f(y) = g(x, y, u) \\ y(x, t = 0) = y_I(x) \\ y(0, t) = y_0(t) \text{ and } y(L, t) = y_L(t) \\ y_I \in BV(\mathbb{R}) \text{ and } u \in \mathcal{U}_{\text{ad}} \end{cases} \end{aligned} \tag{6.4.2}$$

where $\mathcal{J}_{\text{obs}}(y)$ weights the value of the distributed state y, $\mathcal{J}_{\text{s}}(s)$ weights the shock locations s and $\mathcal{J}_{\text{bar}}(u)$ weights the control variable $u = (u_1, ..., u_{N_u})$. In (6.4.2), the decision variables are the initial condition y_I and the control variable u present in the source term, allowing to treat control and estimation problems in a unified way. Convex constraints

on u are handled by introducing standard barrier terms [Boyd & Vandenberghe, 2004] in $\mathcal{J}_{\text{bar}}(u)$ to restrict the control variable to the admissible subset $\mathcal{U}_{\text{ad}} \subset \mathcal{U}$. A nonstandard feature of Problem (6.4.2) is the possible weights on the shock locations to take into account the shock sensitivities with respect to the decision variables.

6.4.2 Linearization of scalar conservation laws

This section is dedicated to the study of the first variation of (6.4.1). The equation fulfilled by the perturbed initial condition, control and distributed state is given with unchanged boundary conditions and an explicit formula is proposed for its measure solution.

Theorem 6.4.1 (Linearization of scalar conservation laws) *The linearized dynamics of (6.4.1) along the reference trajectory $(\bar{y}_I, \bar{u}, \bar{y})$ with perturbations $(\tilde{y}_I, \tilde{u}, \tilde{y})$ is given by*

$$\begin{cases} \partial_t \tilde{y} + \partial_x\big(f'(\bar{y})\tilde{y}\big) = \partial_y g(x,\bar{y},\bar{u})\tilde{y} + \partial_u g(x,\bar{y},\bar{u})\tilde{u} \\ \tilde{y}(0,x) = \tilde{y}_I \\ \tilde{y}(t,0) = 0 \text{ and } \tilde{y}(t,L) = 0 \end{cases} \tag{6.4.3}$$

interpreted in the weak sense as for (6.4.1).

Proof. The perturbed control $u = \bar{u} + \tilde{u}$ and initial condition $y_I = \bar{y}_I + \tilde{y}_I$ lead to a perturbed state $y = \bar{y} + \tilde{y}$ where $(\bar{u}, \bar{y})$ and (u, y) should verify (6.4.1). As (6.4.1) should be interpreted in the weak sense, we have

$$\int_\Omega y\partial_t\phi + f(y)\partial_x\phi + g(x,y,u)\phi \,\mathrm{d}x\mathrm{d}t + \int_{(0,L)} y_I\phi_{|_{t=0}} \,\mathrm{d}x = 0$$
$$+ \int_{(0,T)} \Big(y_0\phi_{|_{x=0}} - y_L\phi_{|_{x=L}}\Big) \,\mathrm{d}x = 0$$

for all $\phi \in C^1(\Omega)$ with $\phi_{|_{t=T}} = 0$. Replacing $u = \bar{u} + \tilde{u}$ and $y = \bar{y} + \tilde{y}$ in the above equation, taking the Taylor expansion of f and g and removing the nonlinear terms that vanish as $\tilde{u} \to 0$, $\tilde{y}_I \to 0$ and $\tilde{y} \to 0$, we obtain (6.4.3) in its weak form. □

remark 6.4.1 *Note that it makes sense that the first variation of a nonlinear conservation law is itself a conservation law as the conservation principle should always be fulfilled. Nevertheless, care should be taken in the analysis of (6.4.3) as its coefficients are discontinuous at the shock locations in the reference trajectory.*

Linear transport equations such as (6.4.3) have been proven to have a unique measure valued solution in [Poupaud & Rascle, 1997] without needing any entropy condition. Other possible alternatives are the space of distributions of the Sobolev space H^{-1} as solutions to (6.4.3) are composed to a piecewise-C^1 field and singular measures centered at every shock locations in the reference trajectory.

Theorem 6.4.2 *Equation (6.4.3) has a unique weak solution in the space of measures or distributions given by*

$$\tilde{y} = \tilde{y}_s + \sum_{i=1}^{N_s} \kappa_i \delta_{\Gamma_i} \tag{6.4.4}$$

with $\Gamma_i = \{(\bar{s}_i(t), t) : t \in [t_i^I, T]\}$ *the* N_s *shock curves present in* $\bar{y}$, $\tilde{y}_s$ *the strong solution, defined in* $\Omega \backslash \cup_i \Gamma_i$, *of the partial differential equation*

$$\begin{array}{ll} \text{(DE)} & \left\{ \begin{array}{l} \partial_t \tilde{y}_s + \partial_x\big(f'(\bar{y})\tilde{y}_s\big) = \partial_y g(x,\bar{y},\bar{u})\tilde{y}_s + \partial_u g(x,\bar{y},\bar{u})\tilde{u} \\ \tilde{y}_s|_{t=0} = \tilde{y}_I \\ \tilde{y}_s|_{x=0} = 0 \quad \text{and} \quad \tilde{y}_s|_{x=L} = 0 \quad \text{when applicable} \end{array} \right. \\ \text{(IC)} & \\ \text{(BC)} & \end{array} \tag{6.4.5}$$

and κ_i, *for* $i = \{1, \ldots, N_s\}$, *the solutions of the ordinary differential equations*

$$\begin{array}{ll} \text{(DE)} & \left\{ \begin{array}{l} \frac{d\kappa_i}{dt} = \kappa_i \partial_y g(x,\bar{y},\bar{u})_{|_{x=\bar{s}_i(t)}} - [f'(\bar{y})\tilde{y}_s]_{|_{x=\bar{s}_i(t)}} + \dot{\bar{s}}_i[\tilde{y}_s]_{|_{x=\bar{s}_i(t)}} \\ \kappa_i(t_i^I) = 0 \end{array} \right. \\ \text{(IC)} & \end{array} \tag{6.4.6}$$

where κ_i *is linked to the shock displacement* $\tilde{s}_i$ *by* $\kappa_i = -\tilde{s}_i[\bar{y}]_{|_{x=\bar{s}_i(t)}}$.

Proof. The main ingredient of the proof is to use the integration by parts of theorem 6.3.1 or theorem 6.3.3 that apply respectively to piecewise-C^1 and BV fields. No distinction is made here as they propose the same formula.

Assuming that $\tilde{y}$ is piecewise-C^1, Equation (6.4.3) writes in the weak sense

$$\int_\Omega \begin{pmatrix} f'(\bar{y})\tilde{y} \\ \tilde{y} \end{pmatrix} \cdot \nabla\phi \, \mathrm{d}x\mathrm{d}t + \int_\Omega \big(\partial_y g(x,\bar{y},\bar{u})\tilde{y} + \partial_u g(x,\bar{y},\bar{u})\tilde{u}\big)\phi \, \mathrm{d}x\mathrm{d}t + \int_{(0,L)} \tilde{y}_I \phi_{|_{t=0}} \, \mathrm{d}x = 0$$

with $\phi \in C^1(\Omega)$ and $\phi(x, t = T) = 0$. Applying an integration by parts gives

$$\int_{\Omega\backslash\cup_i\Gamma_i} \Big(-\partial_t\tilde{y} - \partial_x\big(f'(\bar{y})\tilde{y}\big) + \partial_y g(x,\bar{y},\bar{u})\tilde{y} + \partial_u g(x,\bar{y},\bar{u})\tilde{u}\Big)\phi \, \mathrm{d}x\mathrm{d}t$$
$$\int_{(0,L)} \Big(\tilde{y}_I - \tilde{y}_{|t=0}\Big)\phi_{|t=0} \, \mathrm{d}x + \sum_{i=1}^{N_s} \int_{t_i^I}^T \Big(\dot{\bar{s}}[\tilde{y}]_{|_{x=\bar{s}_i(t)}} - [f'(\bar{y})\tilde{y}]_{|_{x=\bar{s}_i(t)}}\Big)\phi_{|_{x=\bar{s}_i(t)}} \, \mathrm{d}t$$

where we used the fact that ϕ is continuous and vanishes at $t = T$. If $\tilde{y}$ is the strong solution of (6.4.3) in $\Omega \backslash \cup_i \Gamma_i$, the first and last terms are set to 0 and the only way to cancel the remaining terms is to assume that $\tilde{y}$ is the superposition of a piecewise-C^1 field and some singular measures defined on the set $\cup_i \Gamma_i$ as in (6.4.4). The same solution structure have been proposed in [Bardos & Pironneau, 2003] and [Godlewski & Raviart, 1999] using different approaches.

Plugging this solution structure

$$\tilde{y}(x,t) = \tilde{y}_s(x,t) + \sum_{i=1}^{N_s} \kappa_i(t) \; \delta(x = \bar{s}_i(t))$$

into the weak form of (6.4.3) and applying an integration by part on the piecewise-C^1 field $\tilde{y}_s$ leads to

$$\int_{\Omega\backslash\cup_i\Gamma_i}\Big(-\partial_t\tilde{y}_s-\partial_x\big(f'(\bar{y})\tilde{y}_s\big)+\partial_y g(x,\bar{y},\bar{u})\tilde{y}_s+\partial_u g(x,\bar{y},\bar{u})\tilde{u}\Big)\phi\,\mathrm{d}x\mathrm{d}t$$
$$+\int_{(0,L)}\Big(\tilde{y}_I-\tilde{y}_{s|_{t=0}}\Big)\phi_{|_{t=0}}\mathrm{d}x+\sum_{i=1}^{N_s}\int_{t_i^I}^{T}\Big(\dot{\bar{s}}[\tilde{y}_s]_{|_{x=\bar{s}_i(t)}}-[f'(\bar{y})\tilde{y}_s]_{|_{x=\bar{s}_i(t)}}\Big)\phi_{|_{x=\bar{s}_i(t)}}\mathrm{d}t$$
$$+\int_\Omega\sum_{i=1}^{N_s}\kappa_i\delta_{\Gamma_i}\big(\partial_t\phi+f'(\bar{y})\partial_x\phi+\partial_y g(x,\bar{y},\bar{u})\phi\big)\,\mathrm{d}x\mathrm{d}t$$

Setting $\tilde{y}_s$ to be the strong solution of (6.4.3) in $\Omega\backslash\cup_i\Gamma_i$ as in (6.4.5) set the first 2 terms to 0. On the other hand, the last term can be rewritten as follows

$$\int_\Omega\sum_{i=1}^{N_s}\kappa_i\delta_{\Gamma_i}\Big(\partial_t\phi+f'(\bar{y})\partial_x\phi+\partial_y g(x,\bar{y},\bar{u})\phi\Big)\,\mathrm{d}x\mathrm{d}t= \tag{6.4.7}$$
$$\sum_{i=1}^{N_s}\int_{t_i^I}^{T}\kappa_i\Big(\partial_t\phi+f'(\bar{y})\partial_x\phi+\partial_y g(x,\bar{y},\bar{u})\phi\Big)_{|_{x=\bar{s}_i(t)}}\mathrm{d}t= \tag{6.4.8}$$
$$\sum_{i=1}^{N_s}\int_{t_i^I}^{T}\kappa_i\left(\frac{\mathrm{d}}{\mathrm{d}t}\phi_{|_{x=\bar{s}_i(t)}}+\partial_y g(x,\bar{y},\bar{u})_{|_{x=\bar{s}_i(t)}}\phi_{|_{x=\bar{s}_i(t)}}\right)\mathrm{d}t= \tag{6.4.9}$$
$$\sum_{i=1}^{N_s}\int_{t_i^I}^{T}\Big(-\frac{\mathrm{d}\kappa_i}{\mathrm{d}t}+\kappa_i\,\partial_y g(x,\bar{y},\bar{u})_{|_{x=\bar{s}_i(t)}}\Big)\phi_{|_{x=\bar{s}_i(t)}}\mathrm{d}t+\kappa_{i|_{t=t_i^I}}\phi_{|_{x=\bar{s}_i(t_i^I)}} \tag{6.4.10}$$

where the full derivative $\frac{\mathrm{d}}{\mathrm{d}t}\phi_{|_{x=\bar{s}_i(t)}}$ of ϕ along Γ_i is given by

$$\frac{\mathrm{d}}{\mathrm{d}t}\phi_{|_{x=\bar{s}_i(t)}}=\partial_t\phi_{|_{x=\bar{s}_i(t)}}+f'(\bar{y})_{|_{x=\bar{s}_i(t)}}\partial_x\phi_{|_{x=\bar{s}_i(t)}}=\partial_t\phi_{|_{x=\bar{s}_i(t)}}+\dot{\bar{s}}_i\partial_x\phi_{|_{x=\bar{s}_i(t)}}$$

If the pointwise values $\bar{y}$ at $x=\bar{s}_i(t)$ are not well defined a priori, the curves Γ_i constitute regular discontinuities of the field $f'(\bar{y})$ according to Filippov's theory [Filippov, 1988]. As a consequence and following [Dafermos, 1977*b*], setting $f'(\bar{y})=\dot{\bar{s}}_i$ whenever $x=\bar{s}_i(t)$ enables to define such pointwise values while giving the same generalized characteristics $\xi(t)$, which are continuous curves solving $\dot{\xi}=f'(\bar{y})$ and sliding along Γ_i when reached.

Adding all the terms defined on the curves Γ_i gives

$$\sum_{i=1}^{N_s}\int_{t_i^I}^{T}\Big(-\frac{\mathrm{d}\kappa_i}{\mathrm{d}t}+\kappa_i\partial_y g(x,\bar{y},\bar{u})_{|_{x=\bar{s}_i(t)}}+\dot{\bar{s}}[\tilde{y}_s]_{|_{x=\bar{s}_i(t)}}-[f'(\bar{y})\tilde{y}_s]_{|_{x=\bar{s}_i(t)}}\Big)\phi_{|_{x=\bar{s}_i(t)}}\mathrm{d}t$$
$$+\sum_{i=1}^{N_s}\kappa_{i|_{t=t_i^I}}\phi_{|_{x=\bar{s}_i(t_i^I)}}=0$$

which is verified by the set of ordinary differential equations (6.4.6).

The interpretation of the κ_i are as follows. Let consider without restriction a reference solution of the form $\bar{y}=\bar{y}^1+(\bar{y}^2-\bar{y}^1)H(x-\bar{s}(t))$ where $\bar{y}^1$ and $\bar{y}^2$ are two C^1 functions

and $H(\cdot)$ is the Heaviside distribution. A differentiation in the sense of distributions tells that infinitesimal perturbations write

$$\tilde{y} = \tilde{y}^1 + (\tilde{y}^2 - \tilde{y}^1)H(x - \bar{s}(t)) - \tilde{s}(\bar{y}^2 - \bar{y}^1)\delta(x - \bar{s}(t))$$

with $\tilde{s}_i$ the infinitesimal discontinuity displacement. We conclude that the singular part of $\tilde{y}$ is defined by $\kappa_i = -\tilde{s}_i[\bar{y}]_{|_{x=\bar{s}_i(t)}}$, thus informing on the shock sensitivities. □

The following important remarks should be made here.

remark 6.4.2 *For practical purpose, the solution of (6.4.5) should be computed first, for instance using the method of characteristics or any suited numerical scheme as it is interpreted in the strong sense in $\Omega\backslash(\cup_i\Gamma_i)$. Then, the κ_i are deduced from (6.4.6) using the solution $\tilde{y}_s$ computed in the previous step.*

remark 6.4.3 *Even if (6.4.3) has a unique solution, $\bar{y} \in BV(\Omega)$ whereas $\tilde{y} \in \mathcal{M}$. As a consequence, $y = \bar{y} + \tilde{y}$ is not necessarily in $BV(\Omega)$, in particular if shocks are present in $\bar{y}$. This fact prevents Equation (6.4.3) to be called a linearization in the usual sense.*

remark 6.4.4 *The formula given in theorem 6.4.2 enables to recover the results proposed in [Bardos & Pironneau, 2003] for the homogeneous burgers equation, i.e. $f(y) = y^2/2$ and $g(x, y, u) = 0$, where y_I is only allowed to vary in a parametric manner. Moreover, it is coherent with the results presented in [Bouchut & James, 1998], [Bouchut & James, 1999] and [Godlewski & Raviart, 1999] as well.*

6.4.3 Adjoint equation of scalar linear conservation laws

We now turn to the computation of the adjoint operator of (6.4.3), which is needed in the adjoint method. To simplify the exposition, let set

$$\begin{cases} \alpha(x,t) = f'(\bar{y}) \\ \beta(x,t) = \partial_y g(x, \bar{y}, \bar{u}) \\ \gamma(x,t) = \partial_u g(x, \bar{y}, \bar{u}) \end{cases} \tag{6.4.11}$$

underlining the fact that the coefficients involved in (6.4.3) are only space and time varying constant fields, possibly discontinuous. With these notations, the linearized dynamics rewrites

$$\begin{cases} \partial_t \tilde{y}_s + \partial_x \alpha(x,t)\tilde{y}_s = \beta(x,t)\tilde{y}_s + \gamma(x,t)\tilde{u} \\ \tilde{y}_s(x,0) = \tilde{y}_I,\ \tilde{y}_s(0,t) = 0 \text{ and } \tilde{y}_s(L,t) = 0 \text{ when applicable} \\ \dot{\kappa}_i = \beta(\bar{s}_i(t),t)\kappa_i - [\alpha(\bar{s}_i(t),t)\tilde{y}_s(\bar{s}_i(t),t)] + \dot{\bar{s}}_i(t)[\tilde{y}_s(\bar{s}_i(t),t)] \\ \kappa_i(0) = 0 \end{cases} \tag{6.4.12}$$

The following theorem applies.

Theorem 6.4.3 *The adjoint equation of the linear transport equation (6.4.12) without control action, i.e. $\tilde{u} = 0$, is given by*

$$\begin{array}{ll} (\mathrm{DE_{ODE}}) & \left\{ \begin{array}{l} \dot{\mu}_i = -\beta_{|_{x=\bar{s}_i(t)}} \mu_i \\ \mu(T) = 0 \\ \lambda^-{}_{|_{x=\bar{s}_i(t)}} = \lambda^+{}_{|_{x=\bar{s}_i(t)}} = \mu_i \\ -\partial_t \lambda - \alpha(x,t)\partial_x \lambda = \beta(x,t)\lambda \\ \lambda(x,T) = 0 \\ \lambda(0,t) = 0 \text{ and } \lambda(L,t) = 0 \text{ when applicable} \end{array} \right. \\ (\mathrm{FC_{ODE}}) & \\ (\mathrm{SIC}) & \\ (\mathrm{DE_{PDE}}) & \\ (\mathrm{FC_{PDE}}) & \\ (\mathrm{BC_{PDE}}) & \end{array} \tag{6.4.13}$$

Proof. Defining two dual variables $\mu(t) = (\mu_1(t), \dots, \mu_{N_s}(t))$ and $\lambda(x,t)$, respectively for $\kappa(t) = (\kappa_1(t), \dots, \kappa_{N_s}(t))$ and $\tilde{y}_s$, the adjoint identity writes

$$\Big\langle \lambda, (6.4.5)_{\mathrm{DE}} \Big\rangle + \Big\langle \mu, (6.4.6)_{\mathrm{DE}} \Big\rangle = \Big\langle \mathrm{ADJ}_1(\lambda), \tilde{y}_s \Big\rangle + \Big\langle \mathrm{ADJ}_2(\mu), \kappa \Big\rangle$$

with $\mathrm{ADJ}_1(\lambda)$ and $\mathrm{ADJ}_2(\mu)$ two adjoint operators to be defined with possibly additional constraints on λ and μ and $\langle \cdot, \cdot \rangle$ the duality pairing. Using an integration by parts, we get

$$\begin{aligned} &\int_\Omega \lambda\big(\partial_t \tilde{y}_s + \partial_x(\alpha \tilde{y}_s) - \beta \tilde{y}_s\big)\mathrm{d}x\mathrm{d}t \\ &\quad + \sum_{i=1}^{N_s} \int_{t_i}^T \mu_i \left(\dot{\kappa}_i - \beta_{|_{x=\bar{s}_i(t)}} \kappa_i + [\alpha \tilde{y}_s]_{|_{x=\bar{s}_i(t)}} - \dot{\bar{s}}_i(t) [\tilde{y}_s]_{|_{x=\bar{s}_i(t)}} \right) \mathrm{d}t \quad = \\ &\int_{\Omega \setminus \cup_i \Gamma_i} \tilde{y}_s\big(-\partial_t \lambda - \alpha \partial_x \lambda - \beta \lambda\big)\mathrm{d}x\mathrm{d}t + \int_0^L \lambda \tilde{y}_s \big|_0^T \mathrm{d}x + \int_0^T \lambda \alpha(x,t) \tilde{y}_s \big|_0^L \mathrm{d}t \\ &\quad + \sum_{i=1}^{N_s} \int_{t_i}^T \Big(-[\lambda \alpha \tilde{y}_s]_{|_{x=\bar{s}_i(t)}} + \dot{\bar{s}}_i(t) [\lambda \tilde{y}_s]_{|_{x=\bar{s}_i(t)}} \Big) \mathrm{d}t + \sum_{i=1}^{N_s} \int_{t_i}^T -\kappa_i \Big(\dot{\mu}_i + \beta_{|_{x=\bar{s}_i(t)}} \mu_i \Big) \mathrm{d}t \\ &\quad + \sum_{i=1}^{N_s} \mu_i \kappa_i \big|_{t_i}^T + \sum_{i=1}^{N_s} \int_{t_i}^T \left([\mu_i \alpha \tilde{y}_s]_{|_{x=\bar{s}_i(t)}} - \dot{\bar{s}}_i(t) [\mu_i \tilde{y}_s]_{|_{x=\bar{s}_i(t)}} \right) \mathrm{d}t \end{aligned}$$

Rearranging and identifying gives the theorem. □

remark 6.4.5 *In the adjoint equation (6.4.13),* $(\mathrm{DE_{ODE}})$ *and* $(\mathrm{FC_{ODE}})$ *are respectively the dynamical equation and the final condition associated to the ordinary differential equations,* $(\mathrm{DE_{PDE}})$, $(\mathrm{FC_{PDE}})$ *and* $(\mathrm{BC_{PDE}})$ *are respectively the dynamical equation, the final condition and the boundary conditions associated to the partial differential equation and* (SIC) *are the shock interface conditions that link the two dynamical equations.*

remark 6.4.6 *The reverse initial boundary value problem (6.4.13) is well posed as boundary data on ∂_Ω and inside Ω are only prescribed when characteristics enter the domain or leave shock curves.*

remark 6.4.7 *For practical purposes,* $(\mathrm{DE_{ODE}})$ *should be solved first with final condition* $(\mathrm{FC_{ODE}})$*. Then, the shock interface condition* (SIC) *provide additional boundary data along with* $(\mathrm{FC_{PDE}})$ *and* $(\mathrm{BC_{PDE}})$ *to solve* $(\mathrm{DE_{PDE}})$*.*

6.4.4 Adjoint-based gradient evaluation for scalar equations

The following theorem applies to evaluate gradients of the cost functional involved in optimal control problems such as (6.4.2).

Theorem 6.4.4 *The gradients of $\mathcal{J}(y,s,u)$ in (6.4.2) with respect to the decision variables u and y_I in problem and along the reference trajectory $(\bar{y},\bar{u})$ are given by*

$$\nabla_u \mathcal{J} = \mathcal{R}'(\bar{u}) + \int_0^L \gamma(x,t)\lambda(x,t)\mathrm{d}x \tag{6.4.14}$$

$$\nabla_{y_I} \mathcal{J} = \lambda(x,0) \tag{6.4.15}$$

with λ the solution of

$$\begin{array}{ll} (\mathrm{DE_{ODE}}) & \dot{\mu}_i = -\beta_{|_{x=\bar{s}_i(t)}}\mu_i + \frac{\mathcal{Q}_i'(\bar{s}_i)}{[\bar{y}]_{|_{x=\bar{s}_i(t)}}} \\ (\mathrm{FC_{ODE}}) & \mu(T) = 0 \\ (\mathrm{SIC}) & \lambda^-{}_{|_{x=\bar{s}_i(t)}} = \lambda^+{}_{|_{x=\bar{s}_i(t)}} = \mu_i \\ (\mathrm{DE_{PDE}}) & -\partial_t\lambda - \alpha(x,t)\partial_x\lambda = \beta(x,t)\lambda + \mathcal{P}'(\bar{y}) \\ (\mathrm{FC_{PDE}}) & \lambda(x,T) = 0 \\ (\mathrm{BC_{PDE}}) & \lambda(0,t) = 0 \text{ and } \lambda(L,t) = 0 \text{ when applicable} \end{array} \tag{6.4.16}$$

Proof. The proof is very similar to the one used to compute the adjoint operator of scalar linear conservation laws.

On one hand, the first variation of $\mathcal{J}(y,s,u)$ around the reference trajectory $(\bar{y},\bar{s},\bar{u})$ and with perturbations $(\tilde{y},\tilde{s},\tilde{u})$ is

$$\begin{array}{rcl} \tilde{\mathcal{J}} & = & \int_\Omega \mathcal{P}'(\bar{y})\tilde{y} + \sum_{i=1}^{N_s}\int_{t_i}^T \mathcal{Q}_i'(\bar{s}_i)\tilde{s}_i + \int_0^T \mathcal{R}'(\bar{u})\tilde{u} \\ & = & \int_\Omega \mathcal{P}'(\bar{y})\tilde{y} - \sum_{i=1}^{N_s}\int_{t_i}^T \mathcal{Q}_i'(\bar{s}_i)\frac{\kappa_i}{[\bar{y}]_{|\Gamma_i}} + \int_0^T \mathcal{R}'(\bar{u})\tilde{u} \end{array} \tag{6.4.17}$$

One the other hand, dual calculus using integration by parts gives

$$\begin{array}{l} \displaystyle\int_\Omega \lambda\big(\partial_t\tilde{y}_s + \partial_x(\alpha\tilde{y}_s) - \beta\tilde{y}_s - \gamma\tilde{u}\big)\mathrm{d}x\mathrm{d}t \\ \quad \displaystyle + \sum_{i=1}^{N_s}\int_{t_i}^T \mu_i\left(\dot{\kappa}_i - \beta_{|_{x=\bar{s}_i(t)}}\kappa_i + [\alpha\tilde{y}_s]_{|_{x=\bar{s}_i(t)}} - \dot{\bar{s}}_i(t)[\tilde{y}_s]_{|_{x=\bar{s}_i(t)}}\right)\mathrm{d}t \quad = \\ \displaystyle\int_{\Omega\setminus\cup_i\Gamma_i} \underbrace{\tilde{y}_s\big(-\partial_t\lambda - \alpha\partial_x\lambda - \beta\lambda\big)}\,\mathrm{d}x\mathrm{d}t - \int_\Omega \gamma\lambda\tilde{u}\,\mathrm{d}x\mathrm{d}t + \int_0^L \lambda\tilde{y}_s\big|_0^T\mathrm{d}x + \int_0^T \lambda\alpha(x,t)\tilde{y}_s\big|_0^L\mathrm{d}t \\ \quad \displaystyle + \sum_{i=1}^{N_s}\int_{t_i}^T\Big(-[\lambda\alpha\tilde{y}_s]_{|_{x=\bar{s}_i(t)}} + \dot{\bar{s}}_i(t)[\lambda\tilde{y}_s]_{|_{x=\bar{s}_i(t)}}\Big)\mathrm{d}t + \sum_{i=1}^{N_s}\underbrace{\int_{t_i}^T -\kappa_i\Big(\dot{\mu}_i + \beta_{|_{x=\bar{s}_i(t)}}\mu_i\Big)}\mathrm{d}t \\ \quad \displaystyle + \sum_{i=1}^{N_s}\mu_i\kappa_i\big|_{t_i}^T + \sum_{i=1}^{N_s}\int_{t_i}^T\left([\mu_i\alpha\tilde{y}_s]_{|_{x=\bar{s}_i(t)}} - \dot{\bar{s}}_i(t)[\mu_i\tilde{y}_s]_{|_{x=\bar{s}_i(t)}}\right)\mathrm{d}t \quad = \quad 0 \end{array}$$

where the above equation vanished as $\tilde{y}_s$ and κ_i satisfy the linearized dynamics given by (6.4.5) and (6.4.6). Identifying the terms underlined by brackets to the ones in Equation (6.4.17) leads to the theorem. □

As the original optimal control problem is nonlinear, we propose to use algorithm 3 to seek iteratively for a local minimum of (6.4.2). When barrier functions [Boyd & Vandenberghe, 2004] are used in (6.4.2), an additional loop should be added in algorithm 3 to iterate on the barrier parameter.

Algorithm 3 General steepest descent algorithm with barrier iterations.

Require: $\bar{u} := u^{\text{init}} \in \mathcal{U}_{\text{ad}}$, $\bar{y}_I = y_I^{\text{init}}$, $\epsilon > 0$
  while $|\nabla_u \mathcal{J} + \nabla_{y_I} \mathcal{J}| > \epsilon$ **do**
    Solve for $\bar{y}$ with $\bar{u}$ and $\bar{y}_I$ using (6.4.1)
    Compute μ_i from (DE_{ODE}) and (DE_{ODE}) in (6.4.16)
    Compute λ from (DE_{PDE}), (FC_{PDE}), (BC_{PDE}) and (SIC) in (6.4.16)
    Compute $\tilde{u} = -\nabla_u \mathcal{J}$ and $\tilde{y}_I = -\nabla_{y_I} \mathcal{J}$ from (6.4.14) and (6.4.15)
    Update $\bar{u} := \bar{u} + t_1 \tilde{u}$ and $\bar{y}_I := \bar{y}_I + t_2 \tilde{y}_I$ with $t_1 \in (0, 1)$ such that $u \in \mathcal{U}_{\text{ad}}$
  end while

As the solution of (6.4.1) and the evaluations of $\nabla_u \mathcal{J}$ and $\nabla_{y_I} \mathcal{J}$ in theorem 6.4.3 require to solve some partial and ordinary differential equations, numerical integration methods are unavoidable. We propose to use the 1^{st} order Godunov scheme [LeVeque, 1992] for conservation laws, the 1^{st} order upwind-downwind method [LeVeque, 1992] for the adjoint equation and the simple euler scheme for the ordinary differential equations. As the number N_s of shocks in the reference trajectory cannot be determined beforehand and may vary during the interactive process of gradient descent used in algorithm 3, a numerical shock detection procedure should be used. With convex or concave flux function, which is the case in traffic flow models for example, the shocks present in the solution always have the same jump sign, i.e. $[y] \geq 0$ and $[y] \leq 0$ respectively for the concave and convex cases. As a consequence, a large gradient seeking method is enough as large gradients in the solution will develop in shock making this approach robust enough.

An interesting interpretation, called here the marginal cost interpretation, of the adjoint based gradient evaluation is the following. $\mathcal{P}'(\bar{y})$ and $\mathcal{Q}'(\bar{s}_i)$ are used to trigger the adjoint variables where improvements are possible in the cost function. Then, the adjoint variables are transported backwards in time with the adjoint equation until reaching a region where some decision variables are available. In this interpretation, the fact that $\mu(t = T) = 0$, $\lambda(x, T) = 0$, $\lambda(0, t) = 0$ and $\lambda(L, t) = 0$ make sense as no improvement may come from the final condition of the fixed boundary value. Moreover, the coupling between μ and λ given by (SIC) in (6.4.16) enables the shock sensitivity to be incorporated in the gradient computation. Such coupling is thus necessary to take into account the influence of the decision variables on the shock locations.

6.4.5 Simulation experiments with the Burgers equation

The Burgers equation is often used as a basic example when dealing with scalar conservation laws as it is simple and contains all the properties of this class of equations such as shocks, rarefaction waves and weak formulations of the boundary conditions.

Solution of the linearized Burgers equation

Let consider for illustration purpose the Burgers equation given by

$$\begin{cases} \partial_t y + \partial_x \left(\frac{y^2}{2}\right) = 0 & \text{in } (0,1)\times(0,1) \\ y(x,t=0) = y_I(x) & \text{in } (0,1) \\ y(0,t) = y_0(x) \text{ and } y(L,t) = y_L(x) & \text{in } (0,1) \end{cases} \tag{6.4.18}$$

Following (6.4.3), its first variation is

$$\begin{cases} \partial_t \tilde{y} + \partial_x (\bar{y}\tilde{y}) = 0 & \text{in } (0,1)\times(0,1) \\ \tilde{y}(x,t=0) = \tilde{y}_I(x) & \text{in } (0,1) \\ \tilde{y}(0,t) = 0 \text{ and } \tilde{y}(L,t) = 0 & \text{in } (0,1) \end{cases} \tag{6.4.19}$$

whose solution, according to (6.4.4), (6.4.5) and (6.4.6) can be written

$$\tilde{y} = \tilde{y}_s + \sum \kappa_i \delta_{\Gamma_i} \tag{6.4.20}$$

$$\text{with} \quad \begin{cases} \partial_t \tilde{y}_s + \partial_x (\bar{y}\tilde{y}_s) = 0 & \text{in } (0,1)\times(0,1)\backslash \cup_i \Gamma_i \\ \tilde{y}_s(x,t=0) = \tilde{y}_I(x) & \text{in } (0,1) \\ \tilde{y}_s(0,t) = 0 \text{ and } \tilde{y}_s(L,t) = 0 & \text{in } (0,1) \\ \dot{\kappa}_i = -[\bar{y}\tilde{y}_s] + \dot{\tilde{s}}[\tilde{y}_s] & \text{in } (t_i^I, 1) \\ \kappa_i(0) = 0 \end{cases} \tag{6.4.21}$$

which have some similarities with the results presented in [Bardos & Pironneau, 2003].

To illustrate the behavior of the linearized Burgers equation with a single shock, let consider the following initial and boundary data for the reference and perturbed trajectories

$$\begin{cases} y_I = 0.5 - 0.7\ H(x-0.5) + 0.4\sin(2\pi x) \\ y_0(t) = 0.5 \text{ and } y_L(t) = -0.2 \\ \tilde{y}_I = 0.1\sin(\pi x) \end{cases} \tag{6.4.22}$$

Results are given in the Figures 6.1, 6.2 and 6.3 where we note the good matching (Figure 6.3) between the computed and measured values of κ which is linked to the shock displacement by $\kappa = -\tilde{s}\ [y]_{x=s(t)}$.

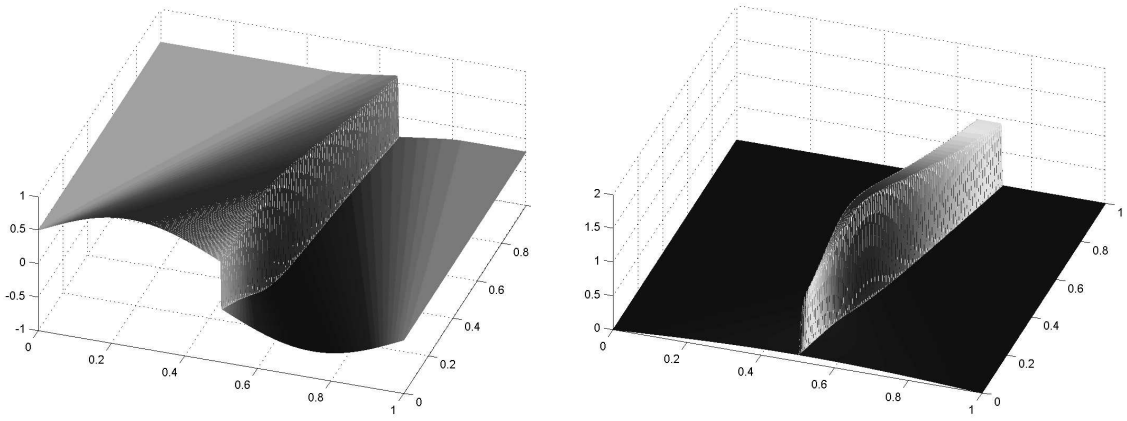

Figure 6.1: Left: solution of the homogeneous Burgers equation (6.4.18). Right: difference between the perturbed $y(\bar{y}_I + \tilde{y}_I)$ and unperturbed $y(\bar{y}_I)$ solutions.

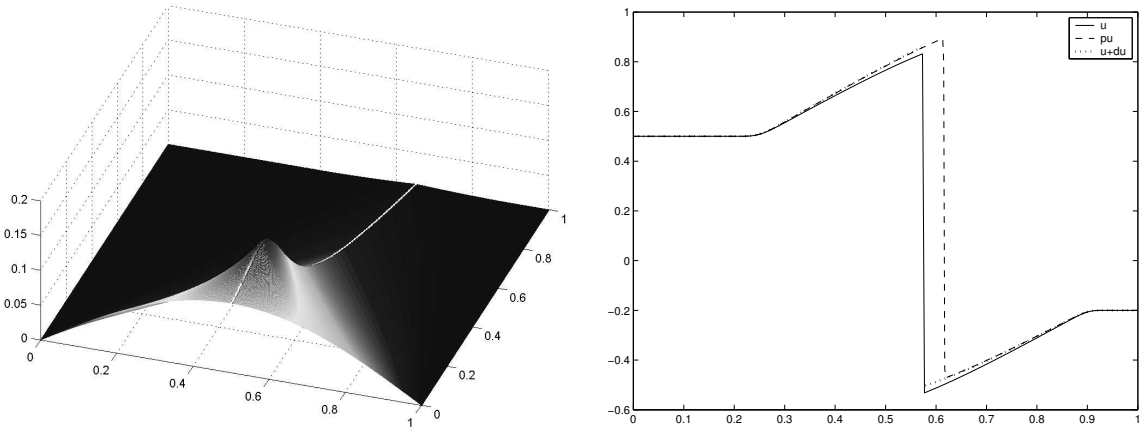

Figure 6.2: Left: regular part $\tilde{y}_s$. Right: 1^{st} order approximation with $\tilde{y}_s$ only.

Optimal control of the Burgers equation

Let consider the source controlled Burgers equation

$$\begin{cases} \partial_t y + \partial_x \left(\frac{y^2}{2}\right) = \tilde{\delta}_{\frac{1}{3}} u & \text{in } (0,1)\times(0,1) \\ y(x, t=0) = y_I(x) & \text{in } (0,1) \\ y(0,t) = y_0(x) \text{ and } y(L,t) = y_L(x) & \text{in } (0,1) \end{cases} \tag{6.4.23}$$

where $\tilde{\delta}_{\frac{1}{3}}$ is the following approximation of the Dirac measure

$$\tilde{\delta}_{\frac{1}{3}}(x) = \frac{1}{\pi}\frac{\epsilon}{\epsilon^2 + (x-1/3)^2} \ \in C^\infty \quad , \quad \epsilon > 0 \tag{6.4.24}$$

Let consider the following optimal control problem

$$\begin{array}{l} \underset{y}{\textbf{Min}} \quad \int_0^1\int_0^1 \frac{1}{2}y^2 \mathrm{d}x\mathrm{d}t + \sum_{i=1}^{N_s}\int_{t_i}^T \frac{1}{2}(s_i(t)-L)^2\mathrm{d}t + \frac{1}{M}\int_0^T \ln((u-u_{\min})(u_{\max}-u))\mathrm{d}t \\ \textbf{Subj. to} \quad (6.4.23) \end{array} \tag{6.4.25}$$

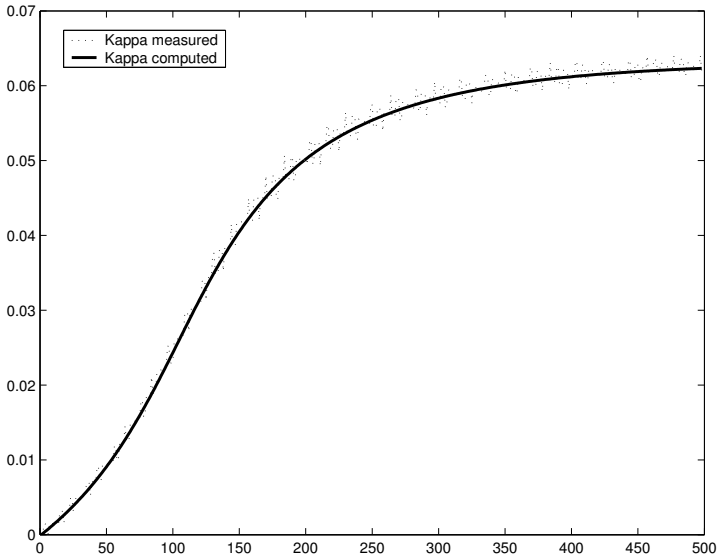

Figure 6.3: Comparaison of the measured and computed values of κ.

where the first term of the cost functional is used to steer the state to 0, the second to move possible shocks as forward as possible and the last one to force the control variable u to take its values in $(u_{\min}, u_{\max})$ with M the barrier parameter.

With the notations introduced in the last section where $(\bar{y}_I, \bar{y}, \bar{u})$ is a reference trajectory for (6.4.23), we have

$$\begin{cases} \alpha = f'(\bar{y}) = \bar{y} \\ \beta = \partial_y g = 0 \\ \gamma = \partial_u g = \tilde{\delta}_{\frac{1}{3}} \\ \mathcal{P}'(\bar{y}) = \bar{y} \\ \mathcal{Q}_i'(\bar{s}_i) = \bar{s}_i(t) - L \\ \mathcal{R}'(\bar{u}) = -\frac{1}{M}\left(\frac{1}{\bar{u}-u_{\min}} - \frac{1}{u_{\max}-\bar{u}}\right) \end{cases}$$

which leads, following (6.4.16), to the adjoint equation

$$\begin{cases} \dot{\mu}_i = \frac{\bar{s}_i(t)-L}{[\bar{y}]_{|x=\bar{s}_i(t)}} \\ \mu(T) = 0 \\ \lambda^-(\bar{s}_i(t), t) = \lambda^+(\bar{s}_i(t), t) = \mu_i \\ -\partial_t \lambda - \bar{y}\partial_x \lambda = \bar{y} \\ \lambda(x, T) = 0 \\ \lambda(0, t) = 0 \text{ and } \lambda(L, t) = 0 \text{ when applicable} \end{cases} \tag{6.4.26}$$

and, following (6.4.14) and (6.4.15), to the gradient formulae

$$\nabla_u \mathcal{J} = \int_0^L \tilde{\delta}_{\frac{1}{3}}(x,t)\lambda(x,t)\,\mathrm{d}x - \frac{1}{M}\left(\frac{1}{\bar{u}-u_{\min}} - \frac{1}{u_{\max}-\bar{u}}\right)$$
$$\nabla_{y_I} \mathcal{J} = \lambda(x,0)$$

As a numerical example, we consider the same initial and boundary data as is (6.4.22) where the initial condition is assumed to be fixed, i.e. $\tilde{y}_I = 0$ and the control variable is initially zero. The results are as follow. Before the optimization, $u = 0$ and the solution is depicted in Figure 6.1. After the first gradient iteration, the cost is reduced from 0.7203 to 0.6569 and Figure 6.4 shows the corresponding adjoint variable λ and new control variable u. Figure 6.5 shows the new solution with the new control and the difference between the updated and the non-updated states after one gradient iteration. The spike that can be observed on (6.5) is a numerical approximation of the singular measure present in the solution of the linearized dynamics.

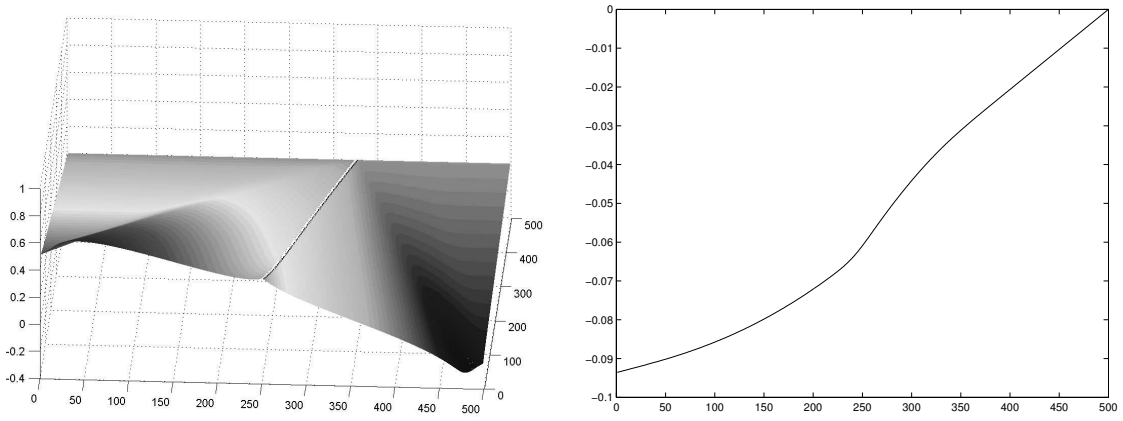

Figure 6.4: Left: solution of the distributed adjoint variable λ with reference trajectory computed from data (6.4.22). Right: new control after one gradient iteration.

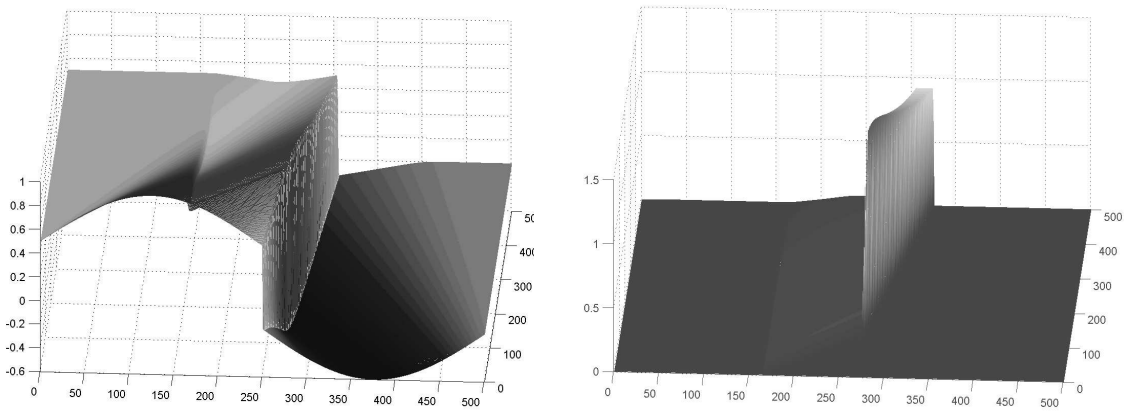

Figure 6.5: Left: updated state. Right: difference between the updated and the non-updated states.

6.5 Optimal control of systems of conservation laws

We follow in this section the same program as in section 6.4 but for systems of conservation laws. As could be expected, the results are less powerful in this case as the available knowledge is thinner for systems.

6.5.1 Problem formulation

We consider in this section systems of m conservation laws on a bounded domain $\Omega = (0, L) \times (0, T)$ taking the form

$$\begin{cases} \partial_t \mathbf{y} + \partial_x \mathbf{f}(\mathbf{y}) = \mathbf{g}(x, \mathbf{y}, \mathbf{u}) \\ \mathbf{y}(x, t = 0) = \mathbf{y}_I(x) \\ \mathbf{y}(0, t) = \mathbf{y}_0(t) \text{ and } \mathbf{y}(L, t) = \mathbf{y}_L(t) \end{cases} \tag{6.5.1}$$

with $\mathbf{y} \in BV(\Omega, \mathbb{R}^m)$ the system state, $\mathbf{u} \in \mathcal{U}$ the control signal, $\mathbf{f}$ a smooth vector flux function and $\mathbf{g}$ a vector source term. As in the scalar case, only control variables in the source term are considered.

Based (6.5.1), the class of optimal control problems we are considering is

$$\begin{aligned} \underset{\mathbf{y}_I, \mathbf{u}}{\textbf{Min}} \quad & \mathcal{J}(\mathbf{y}, \mathbf{u}) = \mathcal{J}_{\text{obs}}(\mathbf{y}) + \mathcal{J}_{\text{bar}}(\mathbf{u}) \\ & \qquad = \int_\Omega \mathcal{P}(\mathbf{y}) \, \mathrm{d}x\mathrm{d}t + \int_0^T \mathcal{R}(u(t)) \, \mathrm{d}t \\ \textbf{Subj. to} \quad & \begin{cases} \partial_t \mathbf{y} + \partial_x \mathbf{f}(\mathbf{y}) = \mathbf{g}(x, \mathbf{y}, \mathbf{u}) \\ \mathbf{y}(x, t = 0) = \mathbf{y}_I(x) \\ \mathbf{y}(0, t) = \mathbf{y}_0(t) \text{ and } \mathbf{y}(L, t) = \mathbf{y}_L(t) \\ \mathbf{y}_I \in BV(\mathbb{R}, \mathbb{R}^m) \text{ and } u \in \mathcal{U}_{\text{ad}} \end{cases} \end{aligned} \tag{6.5.2}$$

where $\mathcal{J}_{\text{obs}}(\mathbf{y})$ define the objective on the distributed state variable $\mathbf{y}$ and $\mathcal{J}_{\text{bar}}(\mathbf{u})$ embed some barrier functions [Boyd & Vandenberghe, 2004] to ensure $u \in \mathcal{U}_{\text{ad}}$.

The program to solve Problem (6.5.2) is similar to the one followed in section 6.4. First, we perform a linearization of (6.5.2). Then, we compute the adjoint system, taking into account the piecewise-C^1 structure of the solution. Finally, the adjoint identity is used to evaluate gradients of the cost functional $\mathcal{J}(\mathbf{y}, \mathbf{u})$ with respect to the decision variables $\mathbf{y}_I$ and $\mathbf{u}$. Note that the shock locations are not taken into account in the objective function of (6.5.2) contrary to the scalar case.

6.5.2 First variation of systems of conservation laws

Theorem 6.5.1 (Linearization of systems of conservation laws) *The linearized dynamics of the system of conservation laws (6.5.1) is given by*

$$\begin{cases} \partial_t \tilde{\mathbf{y}} + \partial_x \left(D\mathbf{f}(\bar{\mathbf{y}})\tilde{\mathbf{y}} \right) = D_{\mathbf{y}}\mathbf{g}(x, \bar{\mathbf{y}}, \bar{\mathbf{u}})\tilde{\mathbf{y}} + D_{\mathbf{u}}\mathbf{g}(x, \bar{\mathbf{y}}, \bar{\mathbf{u}})\tilde{\mathbf{u}} \\ \tilde{y}(0, x) = 0 \\ \tilde{y}(0, t) = 0 \text{ and } \tilde{y}(L, t) = 0 \end{cases} \tag{6.5.3}$$

and is wellposed.

Proof. As in the scalar case, the perturbed variables $\mathbf{u} = \bar{\mathbf{u}} + \tilde{\mathbf{u}}$ and $\mathbf{y} = \bar{\mathbf{y}} + \tilde{\mathbf{y}}$ are plugged in the weak formulation of the conservation law (6.5.1) and the nonlinear terms are removed after some Taylor expansions. The wellposedness of (6.5.3) is established in [Poupaud & Rascle, 1997] and its solution may have singular measures where the reference trajectory $\bar{\mathbf{y}}$ have discontinuities. □

remark 6.5.1 *The homogeneous boundary conditions in (6.5.3) apply only when necessary, i.e. when there are some incoming characteristics computed form the eigenvalue decomposition of $D\mathbf{f}(\bar{\mathbf{y}})$ as in classical linear conservation laws [Godlewski & Raviart, 1996].*

6.5.3 Adjoint equation of system of linear conservation laws

Theorem 6.5.2 *The adjoint equation of the linear system of transport equation (6.5.3) without control action, i.e. $\tilde{\mathbf{u}} = 0$, is given by*

$$\begin{cases} -\partial_t \lambda - D\mathbf{f}(\bar{\mathbf{y}})^T \partial_x \lambda = D_{\mathbf{y}}\mathbf{g}(\bar{\mathbf{y}}, \bar{\mathbf{u}})^T \lambda \\ \lambda(x, T) = 0 \\ \lambda(0, t) = 0 \text{ and } \lambda(L, t) = 0 \text{ when applicable} \\ \lambda_{|_{x=\bar{s}_i(t)}} = 0 \end{cases} \tag{6.5.4}$$

Proof. The adjoint operator $\mathrm{PDE}^\star(\lambda) = 0$ of (6.5.3) with λ the adjoint variable is computed using the adjoint identity $\langle \lambda, \mathrm{PDE}(y) \rangle = \langle \mathrm{PDE}^\star(\lambda), y \rangle$ where $\langle \cdot, \cdot \rangle$ is the duality pairing. Using several integration by parts for measure theoretically piecewise-C^1 field, we get

$$\begin{aligned} &\langle \lambda, \partial_t \tilde{\mathbf{y}} + \partial_x \left(D\mathbf{f}(\bar{\mathbf{y}})\tilde{\mathbf{y}} \right) - D_{\mathbf{y}}\mathbf{g}(\bar{\mathbf{y}}, \bar{\mathbf{u}})\tilde{\mathbf{y}} \rangle = \\ &\quad \left\langle \tilde{\mathbf{y}}, -\partial_t \lambda - D\mathbf{f}(\bar{\mathbf{y}})^T \partial_x \lambda - D_{\mathbf{y}}\mathbf{g}(\bar{\mathbf{y}}, \bar{\mathbf{u}})^T \lambda \right\rangle + \int_0^L \lambda^T \tilde{\mathbf{y}} \big|_0^T \mathrm{d}x + \underbrace{\int_0^T \lambda^T D\mathbf{f}(\bar{\mathbf{y}})\tilde{\mathbf{y}} \big|_0^L \mathrm{d}t} \\ &\quad + \sum_{i=1}^{N_s} \int_{t_i^I}^T \dot{s}_i \left[\lambda^T (\tilde{\mathbf{y}} - D\mathbf{f}(\bar{\mathbf{y}})\tilde{\mathbf{y}}) \right]_{|_{x=s_i(t)}} \mathrm{d}t \end{aligned} \tag{6.5.5}$$

Let call $-\partial_t \lambda - D\mathbf{f}(\bar{\mathbf{y}})^T \partial_x \lambda = D_{\mathbf{y}}\mathbf{g}(\bar{\mathbf{y}}, \bar{\mathbf{u}})^T \lambda$ the adjoint equation. To remove the underbraced term in (6.5.5), the applicability of the boundary conditions should be

studied both for the linearized dynamics (6.5.3) and the adjoint equation and we refer to [Godlewski & Raviart, 1996] for further details on this topic. In non-conservative form, these equations can be rewritten $\partial_t \tilde{\mathbf{y}} + D\mathbf{f}(\bar{\mathbf{y}})\partial_x \tilde{\mathbf{y}} = \mathbf{S}_\mathbf{y}$ for the linearized dynamics and $\partial_\tau \lambda - D\mathbf{f}(\bar{\mathbf{y}})^T \partial_x \lambda = \mathbf{S}_\lambda$ for the adjoint equation with $\mathbf{S}_\mathbf{y}$ and $\mathbf{S}_\lambda$ some source terms and $\tau = -t$ the reversed time. In any case, the source terms does not modify the applicability of the boundary conditions and can be forgotten.

Let note $D\mathbf{f}(\bar{\mathbf{y}}) = T\Lambda T^{-1}$ the eigenvalue decomposition of $D\mathbf{f}(\bar{\mathbf{y}})$. The splitting of the operator $\Lambda = \Lambda^- + \Lambda^+$ in its negative and positive eigenvalues tells which characteristic variable can be assigned at the boundaries. Using this operator spitting, we can write

$$\lambda^T D\mathbf{f}(\bar{\mathbf{y}})\tilde{\mathbf{y}} = \lambda^T T\Lambda T^{-1}\tilde{\mathbf{y}} = \lambda^T T\Lambda^- T^{-1}\tilde{\mathbf{y}} + \lambda^T T\Lambda^+ T^{-1}\tilde{\mathbf{y}}$$

We only treat the case $x = 0$ here, the treatment of the other boundary being similar. As homogeneous boundary conditions apply to the linearized equation, we have $\Lambda^+ T^{-1}\tilde{\mathbf{y}}|_{x=0} = 0$ where Λ^+ selects the appropriate entering characteristic variables. The remaining term for $x = 0$ in the underbraced term of (6.5.5) becomes

$$\lambda_{|_{x=0}}{}^T D\mathbf{f}(\bar{\mathbf{y}})\tilde{\mathbf{y}}_{|_{x=0}} = \lambda_{|_{x=0}}{}^T T\Lambda^- T^{-1}\tilde{\mathbf{y}}_{|_{x=0}} = \tilde{\mathbf{y}}_{|_{x=0}}{}^T T^{-T}\Lambda^- T^T \lambda_{|_{x=0}}$$

Let note $-D\mathbf{f}(\bar{\mathbf{y}})^T = P\Pi P^{-1}$. With appropriate eigenvalue ordering and eigenvector normalization, we have $\Pi = -\Lambda$, implying $\Pi^- = \Lambda^+$, $\Pi^+ = \Lambda^-$ and $T^T = P^{-1}$. Setting homogeneous boundary conditions to the reversed time adjoint equation implies

$$\Pi^+ P^{-1}\lambda|_{x=0} = \Lambda^- T^T \lambda|_{x=0} = 0$$

and leads to $\lambda^T D\mathbf{f}(\bar{\mathbf{y}})\tilde{\mathbf{y}} = 0$ at $x = 0$. The same procedure applies to $x = L$ and we conclude that homogeneous boundary conditions in the adjoint equation set the underbraced term in (6.5.5) to 0. Moreover, this analysis shows that the subsets of $(0, T)$ where the boundary conditions are active for the linearized and adjoint equations are complementary.

To conclude the proof, we note that setting $\lambda(x, T) = 0$ and $\lambda(\bar{s}_i(t), t) = 0$ along all shock curves present in $\bar{\mathbf{y}}$ remove all the terms in the left hand side of (6.5.5) except the adjoint equation. □

6.5.4 Adjoint-based gradient evaluation for systems

Theorem 6.5.3 *The gradients of $\mathcal{J}(\mathbf{y}, \mathbf{u})$ in (6.5.2) with respect to the decision variables $\mathbf{y}_I$ and $\mathbf{u}$ and along the reference trajectory $(\bar{u}, \bar{y})$ are*

$$\nabla_\mathbf{u}\mathcal{J}(\bar{\mathbf{u}}, \bar{\mathbf{y}}) = \mathcal{R}'(\bar{u}) + D_\mathbf{u}\mathbf{s}(\bar{\mathbf{y}}, \bar{\mathbf{u}})^\star \lambda \tag{6.5.6}$$

$$\nabla_{\mathbf{u}_I}\mathcal{J}(\bar{\mathbf{u}}, \bar{\mathbf{y}}) = \lambda(x, 0) \tag{6.5.7}$$

with the adjoint variable λ defined by

$$\begin{cases} -\partial_t \lambda - D\mathbf{f}(\bar{\mathbf{y}})^T \partial_x \lambda = D_\mathbf{y}\mathbf{g}(\bar{\mathbf{y}}, \bar{\mathbf{u}})^T \lambda + \mathbf{g}'(\bar{\mathbf{y}}) \\ \lambda(x, T) = 0 \\ \lambda(0, t) = 0 \text{ and } \lambda(L, t) = 0 \quad \text{when applicable} \\ \lambda_{|_{x=\bar{s}_i(t)}} = 0 \end{cases} \tag{6.5.8}$$

Proof. On one hand, the first variation of the cost functional in (6.5.2) writes

$$\tilde{\mathcal{J}} = \int_\Omega \mathcal{P}'(\bar{\mathbf{y}})\ \mathrm{d}x\mathrm{d}t + \int_0^T \mathcal{R}'(\bar{u})\tilde{u}\ \mathrm{d}t \tag{6.5.9}$$

On the other hand, the adjoint identity applied to the linearized dynamics (6.5.3) with control action $\tilde{\mathbf{u}}$ implies

$$\begin{aligned}\int_\Omega \lambda\left(\partial_t\tilde{\mathbf{y}} + \partial_x\left(D\mathbf{f}(\bar{\mathbf{y}})\tilde{\mathbf{y}}\right) - D_{\mathbf{y}}\mathbf{g}(\bar{\mathbf{y}},\bar{\mathbf{u}})\tilde{\mathbf{y}} - D_{\mathbf{u}}\mathbf{g}(\bar{\mathbf{y}},\bar{\mathbf{u}})\tilde{\mathbf{u}}\right)\mathrm{d}x\mathrm{d}t = \\ \int_\Omega \tilde{\mathbf{y}}\left(-\partial_t\lambda - D\mathbf{f}(\bar{\mathbf{y}})^T\partial_x\lambda - D_{\mathbf{y}}\mathbf{g}(\bar{\mathbf{y}},\bar{\mathbf{u}})^T\lambda\right)\mathrm{d}x\mathrm{d}t - \int_0^T \tilde{\mathbf{u}}^T D_{\mathbf{u}}\mathbf{g}(\bar{\mathbf{y}},\bar{\mathbf{u}})^\star\lambda\ \mathrm{d}t \\ + \int_0^L \lambda^T\tilde{\mathbf{y}}\big|_0^T\mathrm{d}x + \int_0^T \lambda^T D\mathbf{f}(\bar{\mathbf{y}})\tilde{\mathbf{y}}\big|_0^L\mathrm{d}t + \sum_{i=1}^{N_s}\int_{t_i^I}^T \dot{s}_i\left[\lambda^T(\tilde{\mathbf{y}} - D\mathbf{f}(\bar{\mathbf{y}})\tilde{\mathbf{y}})\right]_{\big|x\,=\,s_i(t)}\mathrm{d}t = 0\end{aligned}$$

Setting

$$-\partial_t\lambda - D\mathbf{f}(\bar{\mathbf{y}})^T\partial_x\lambda - D_{\mathbf{y}}\mathbf{g}(\bar{\mathbf{y}},\bar{\mathbf{u}})^T\lambda = \mathcal{P}'(\bar{y})$$

with the same boundary conditions than the adjoint equation (6.5.4) and identifying with $\tilde{\mathcal{J}}$ in (6.5.9) gives the theorem. □

remark 6.5.2 *In the gradient formula (6.5.6), $D_{\mathbf{u}}\mathbf{g}(\bar{\mathbf{y}},\bar{\mathbf{u}})^\star = D_{\mathbf{u}}\mathbf{g}(\bar{\mathbf{y}},\bar{\mathbf{u}})^T$ for smooth matrices $D_{\mathbf{u}}\mathbf{g}(\bar{\mathbf{y}},\bar{\mathbf{u}})$. When Dirac distributions are present in $D_{\mathbf{u}}\mathbf{g}(\bar{\mathbf{y}},\bar{\mathbf{u}})$, then $D_{\mathbf{u}}\mathbf{s}(\bar{\mathbf{y}},\bar{\mathbf{u}})^\star$ is the transpose of $D_{\mathbf{u}}\mathbf{s}(\bar{\mathbf{y}},\bar{\mathbf{u}})$ where Dirac distributions are replaced by pointwise evaluations.*

Pure mathematicians sometimes are satisfied with showing that the non-existence of a solution implies a logical contradiction, while engineers might consider a numerical result as the only reasonable goal. Such one sided views seem to reflect human limitations rather than objective values. In itself mathematics is an indivisible organism uniting theoretical contemplation and active application.

Richard Courant (1888-1972),
German-American mathematician.
in Variational Methods for the solution of problems of equilibrium and vibrations, Bulletin of American Mathematical Society, 49, 1943.

Chapter 7

Optimal Control Applications in Freeway Management

Three freeway management applications are discussed in this chapter, the ramp metering problem, the missing data estimation problem and the origin-destination estimation problem. The optimal control theory developed in the previous chapter is successively applied to these 3 problems, showing the generality of the approach. Several simulation experiments are provided to illustrate the effectiveness of the optimal control method and analyse its limitations or drawbacks.

7.1 Practical considerations

Taking into account the real time constraint and the adaptation requirement of real applications, the gradient evaluation methods proposed in (6.4) and (6.5) respectively for scalar and system of nonlinear conservation laws can be used in at least two ways:

- **Receding horizon**: At time t, $\nabla_u \mathcal{J}$ is used iteratively to find the local minimum of the optimal control problem on the finite time horizon $[t, t+T_1]$. Then the optimal control strategy u^* is applied in the time window $[t, t+T_2]$ with $T_2 \leq T_1$. At time $t+T_2$, the same procedure is repeated.

- **Instantaneous control:** At time t, $\nabla_u \mathcal{J}$ is computed for an horizon T and the updated control $u_{[t,t+T]} = u_{[t-T,t]} - \nabla_u \mathcal{J}$ with respect to a first guess is applied instantaneously.

Note that both of these methods are inherently open-loop in the control terminology. Though receding horizon techniques may be used to emulate feedback, we prefer to use these strategies for optimal trajectory generation and then use a feedback controller to robustly track these references.

7.2 The ramp metering problem

Meaningful objectives in the design of ramp metering strategies are

- maximize the Vehicle-Miles-Travelled (VMT), i.e.

$$\textbf{Min} \quad \mathcal{J}_{\text{VMT}}(\phi) = -\int_0^T \int_0^L \phi(x,t)\ \mathrm{d}x\mathrm{d}t \tag{7.2.1}$$

- minimize the Total-Travel-Time (TTT), i.e.

$$\textbf{Min} \quad \mathcal{J}_{\text{TTT}}(\rho) = \int_0^T \int_0^L \rho(x,t)\ \mathrm{d}x\mathrm{d}t \tag{7.2.2}$$

In the ramp metering problem, the initial condition is assumed to be known and the only decision variables are the metering rates u_i, $i = 1, ..., N_u$ that control the flow allowed to enter the freeway at N_u on-ramps.

We propose below 3 control designs respectively for the LWR model, the Payne model and the ARZ model, all of them using the VMT objective. In all cases, the metering rates u_i are constrained to be in the interval $(0, 1)$, value 0 corresponding to a constant red light, 1 to a constant green light and intermediate values to modulations of these 2 states. The constraint $u_i \in (0, 1)$ is handled by the classical barrier term

$$\mathcal{J}_{\text{bar}}(u) = -\frac{1}{M} \sum_{i=1}^{N_u} \int_0^T \ln\big(u_i(1-u_i)\big)\ \mathrm{d}t \tag{7.2.3}$$

whose an example is given in Figure 7.1 for several values of M.

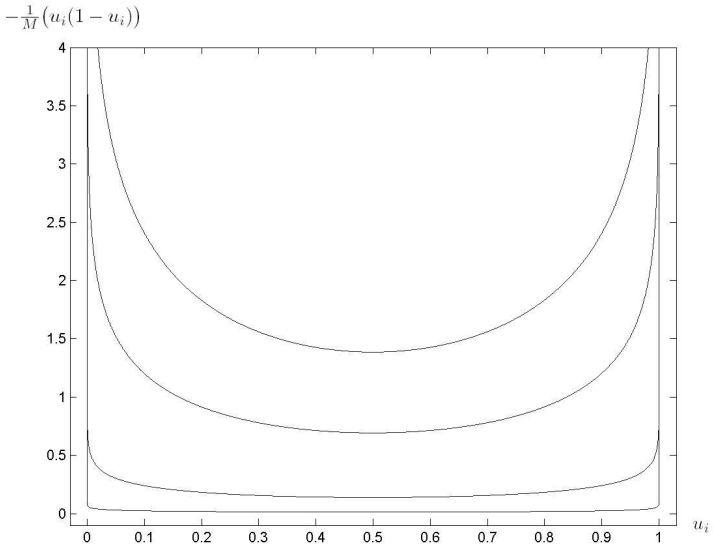

Figure 7.1: Barrier term $\frac{1}{M}\ln\big(u_i(1-u_i)\big)$ with $M = \{1, 2, 10, 100\}$.

In the ramp metering application, the contributions of on/off-ramps are modelled by a source term such that

- on-ramp flows are proportional to metering rates u_i,
- on-ramp flows are smoothly saturated by the main lane density,
- the density on the mainlane is always less than the maximal density ρ_{m},
- off-ramp flows are modelled by a splitting ratio $\beta_i \in (0,1)$.

To fulfil these requirements, the i^{th} on-ramp flow $\hat{\phi}_i$ at $x = \hat{x}_i$ is written

$$\hat{\phi}_i(t) = u_i(t)\ \Psi_i(\rho(\hat{x}_i, t)) \tag{7.2.4}$$

with $\Psi_i(\cdot)$ a smooth saturation function, as the one depicted in Figure 7.2, that limits the on-ramp flow for large mainlane densities. Some properties that should be fulfilled by the map $\Psi_i(\cdot)$ are

- $\Psi_i(\xi) = \bar{\phi}_i$ for $\xi \in (0, \gamma)$, where $\bar{\phi}_i$ is the maximal possible on-ramp flow,
- $\Psi_i'(\cdot) \leq 0$ as the allowed on-ramp flow decreases with the mainlane density,
- $\Psi_i(\rho_m) = 0$ as no vehicle is allowed to enter at maximal mainlane density.

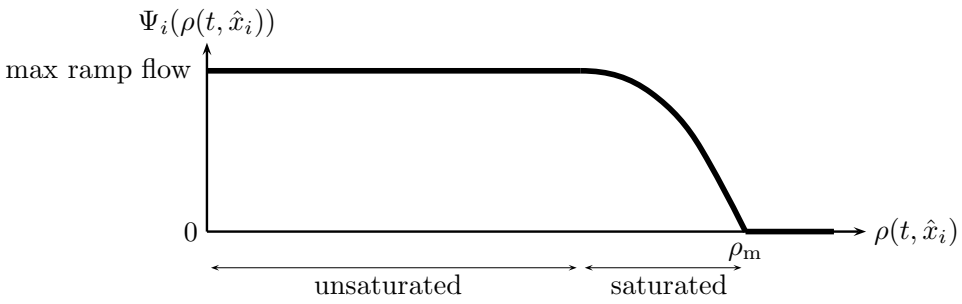

Figure 7.2: Smooth saturation at on-ramp i.

The j^{th} off-ramp flow $\check{\phi}_j$ at $x = \check{x}_j$ is written

$$\check{\phi}_j(t) = \beta_j(t)\ \phi(\check{x}_j, t) \tag{7.2.5}$$

with $\phi(\check{x}_j, t) = \Phi(\rho(\check{x}_j, t))$ is the case of the LWR model.

With N_u on-ramps and N_β off-ramps, the density source term g_ρ writes

$$g_\rho(x, \rho, u) = \sum_{i=1}^{N_u} \delta_{\hat{x}_i}(x)\ u_i(t)\ \Psi_i(\rho(x,t)) - \sum_{j=1}^{N_\beta} \delta_{\check{x}_j}(x)\ \beta_j\ \phi(x,t) \tag{7.2.6}$$

where $\delta_{\hat{x}_i}(x)$ and $\delta_{\check{x}_i}(x)$ set the spacial influence of the on/off-ramps. The distributions $\delta_{\hat{x}_i}$ and $\delta_{\check{x}_i}$ can be considered either to be Dirac measures or smooth approximations of them to avoid possible yet unresolved wellposedness issues for some models.

7.2.1 With the LWR model

With the source term (7.2.6), the LWR model writes

$$\partial_t \rho + \partial_x \Phi(\rho) = \underbrace{\sum_{i=1}^{N_u} \delta_{\hat{x}_i}(x)\ u_i(t)\ \Psi_i(\rho(x,t)) - \sum_{j=1}^{N_\beta} \delta_{\check{x}_j}(x)\ \beta_j\ \Phi(\rho(x,t))}_{g(x,\rho,u)} \tag{7.2.7}$$

completed by the initial condition $\rho_I(x)$ and the boundary signals $\rho_0(t)$ and $\rho_L(t)$. To apply the adjoint method described in the previous chapter to the VMT optimization problem (7.2.1), the following derivatives, along the reference trajectory $(\bar{\rho}, \bar{u})$, are needed

$$\begin{aligned}
&D_\rho \Phi(\rho) = \Phi'(\rho) \\
&D_\rho g[x, \bar{\rho}, \bar{u}] = \sum_{i=1}^{N_u} \delta_{\hat{x}_i} \bar{u}_i \Psi_i'(\bar{\rho}) - \sum_{i=j}^{N_\beta} \delta_{\check{x}_j} \beta_j \Phi'(\bar{\rho}) \\
&D_u g[x, \bar{\rho}, \bar{u}] = \left(\delta_{\hat{x}_1} \Psi_1(\bar{\rho}), ..., \delta_{\hat{x}_{N_u}} \Psi_{N_u}(\bar{\rho})\right) \\
&D_\rho \mathcal{J}[\bar{\rho}, \bar{u}] = D_\rho \mathcal{J}_{\mathrm{VMT}}[\bar{\rho}] = -\Phi'(\rho) \\
&D_u \mathcal{J}[\bar{\rho}, \bar{u}] = D_u \mathcal{J}_{\mathrm{bar}}[\bar{u}] = -\frac{1}{M}\left(\frac{1}{\bar{u}_1} - \frac{1}{1-\bar{u}_1}, ..., \frac{1}{\bar{u}_{N_u}} - \frac{1}{1-\bar{u}_{N_u}}\right)
\end{aligned}$$

The gradient of the VMT objective (7.2.1) with the barrier term (7.2.3) is

$$\nabla_u \mathcal{J} = \begin{pmatrix} -\Psi_1(\bar{\rho}(\cdot, \hat{x}_1))\ \lambda(\cdot, \hat{x}_1) - \frac{1}{M}\left(\frac{1}{\bar{u}_1} - \frac{1}{1-\bar{u}_1}\right) \\ \vdots \\ -\Psi_{N_u}(\bar{\rho}(\cdot, \hat{x}_{N_u}))\ \lambda(\cdot, \hat{x}_{N_u}) - \frac{1}{M}\left(\frac{1}{\bar{u}_{N_u}} - \frac{1}{1-\bar{u}_{N_u}}\right) \end{pmatrix} \tag{7.2.8}$$

where the adjoint variable λ is solution of the adjoint equation

$$\begin{cases}
-\partial_t \lambda - \Phi'(\bar{\rho})\partial_x \lambda = \Phi'(\bar{\rho}) + \sum_{i=1}^{N_u} \delta_{\hat{x}_i} \bar{u}_i \Psi_i'(\bar{\rho})\lambda - \sum_{i=1}^{N_w} \delta_{\check{x}_i} \beta_i \Phi'(\bar{\rho})\lambda \\
\lambda(x, T) = 0 \\
\lambda(0, t) = 0 \text{ when } \Phi'(\bar{\rho}(0,t)) < 0 \\
\lambda(L, t) = 0 \text{ when } \Phi'(\bar{\rho}(L,t)) > 0 \\
\lambda_{|\Gamma_i} = 0 \text{ with } \Gamma_i = \{(x,t) : [\bar{\rho}(x,t)] \neq 0\}
\end{cases} \tag{7.2.9}$$

For a practical implementation, the spacial domain is discretized in N cells of length Δx and the time horizon discretized with period Δt. The Godunov scheme can be used to simulate the LWR model (7.2.7), the source term being integrated with a simple Euler method. Concerning the adjoint equation, we propose the following backwards hybrid upwind/downwind scheme [LeVeque, 1992]

$$\lambda_i^{n-1} = \lambda_i^n + \frac{\Delta t}{\Delta x}\Phi'\left(\rho_i^n\right) \begin{cases} \lambda_i^n - \lambda_{i-1}^n & \text{if } \Phi'(\rho_i^n) < 0 \\ \lambda_{i+1}^n - \lambda_i^n & \text{if } \Phi'(\rho_i^n) > 0 \end{cases} + \Delta t\Big[\Phi'\left(\rho_i^n\right) \ + \ u_{\hat{\delta}(i)}^n \Psi_{\hat{\delta}(i)}'(\rho_i^n)\lambda_i^n \ - \ \beta_{\check{\delta}(i)}^n \Phi'(\rho_i^n)\lambda_i^n\Big]$$

where $\hat{\delta}$ and $\check{\delta}$ map cell indices to on/off-ramp indices when applicable. Both schemes require $\Delta x/\Delta t > \max|\Phi'(\rho)|$ to have a stable convective part and a Runge-Kutta method may be necessary to stabilize the source terms. With $\iota(i)$ the cell index corresponding to the i^{th} on-ramp, the numerical gradient for the VMT objective is evaluated as

$$(\nabla_{u_i}\mathcal{J})^n = -\Psi_i\left(\rho^n_{\iota(i)}\right)\lambda^n_{\iota(i)} - \tfrac{1}{M}\left(\tfrac{1}{u^n_{\iota(i)}} - \tfrac{1}{1-u^n_{\iota(i)}}\right)$$

We propose to include this gradient evaluation method in the steepest descent numerical scheme presented in Algorithm 4, which solves (7.2.1) iteratively with the LWR model (7.2.7) and the barrier function (7.2.3).

Algorithm 4 Steepest descent algorithm to solve the ramp metering problem with the LWR model and constraints on the metering rate.

Require: $u_i := u_i^{\text{init}} \in (0,1)$, $M := M_{\text{init}}$, ϵ_i, ϵ_o, ΔM
  while $\mathcal{J}_{\text{bar}}(u)/\mathcal{J}_{\text{obs}}(\rho) > \epsilon_o$ **do**
    while $\|\nabla_u\mathcal{J}\| > \epsilon_i$ **do**
      Compute ρ from (7.2.7)
      Compute λ from (7.2.9)
      Compute $\nabla_{u_i}\mathcal{J}$ from (7.2.8)
      Update $u_i := u_i - t\nabla_{u_i}\mathcal{J}_{\text{aug}}$, $t \in (0,1)$ such that $u \in (0,1)$
    end while
    M := M.ΔM
  end while

We now give 2 simulation experiments that illustrate the effectiveness of the approach. Let consider first the virtual network of 12 km depicted in Figure 7.3. A time horizon

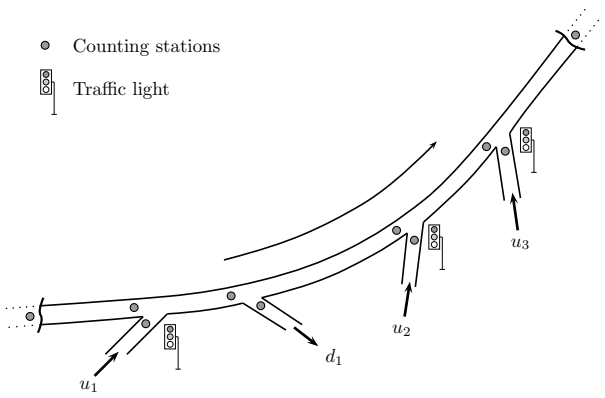

Figure 7.3: Virtual freeway considered for illustration.

of 1.5 hours at the beginning of the afternoon rush hours is considered with real field initial and boundary data courtesy of DDE Isère. The Greenshield model is used for the flux function $\Phi(\cdot)$ with parameters v_{f} =109 km/h and ρ_{m} =75 veh/km obtained by least square fitting using these data. Figure 7.7 shows the iterations of the observation and augmented costs where the steps in $\mathcal{J}$ are due to the iterations in the barrier

parameter M. An improvement of around 10 % is observed on $\mathcal{J}_{\text{obs}}$ which is relevant for traffic management applications. Figure 7.5 shows the 3 optimal on-ramp flows and the distributed flow improvement in the computational domain $(0, L) \times (0, T)$. We note that the metering rates are decreased when the afternoon congestion builds up. Finally, Table 7.1 gives the simulation parameters and results.

simulation parameters	
Number of space points	150 for 12 km
Number of time points	2700 for 1.5 h
Total number of points	675000
v_{f} form least square fitting of Φ_{GS}	109 km/h
ρ_{m} form least square fitting of Φ_{GS}	75 veh/km
Optimization computational time	35 s
Number of outer iterates	12
Last relative $\mathcal{J}_{\text{obs}}$ variation	5.6695e-007
Last relative $\mathcal{J}$ variation	-2.3012e-005
Last $\mathcal{J}_{\text{bar}}$	-0.4661
Last $\mathcal{J}_{\text{obs}}$	-1.1870e+005

Table 7.1: Simulation parameters.

In the second experiment, we consider a section of Grenoble (France) beltway as depicted on Figure 7.6. with real field data courtesy of DDE Isère.

Figures 7.7 and 7.8 shows the optimization results for a time horizon of 1.5 hour at the beginning of the afternoon rush hours. Again, the metering rates decrease (Figure 7.8) to cope with the congestion but as shown on Figure 7.7, the improvement is only of few percents (between 1 % and 2 %) in that case.

From the above experiments, the following comments can be made

1. The proposed optimization method is effective as a decrease in the cost functional is observed and the control variable is kept in its admissible set in both cases.

2. The improvement obtained by this method depends highly on the freeway state before optimization. As notice in the second experiment, the improvement may be small and no guarantee can be given on a lower bound of it. Nevertheless, this shortcoming is not dependent on the method as a traffic state can be very close to the optimal without performing any optimization.

3. A weakness of the proposed method is that it requires the knowledge of the initial condition ρ_I and the boundary conditions ρ_{up} and ρ_{do}, the optimum being possibly quite sensitive to these partially unknown data. Receding horizon techniques may help to avoid propagation of errors in the estimates of ρ_I, ρ_{up} and ρ_{do}. In addition, performing an a priori defined maximum number of steps in the gradient descent may avoid over-optimization with erroneous data.

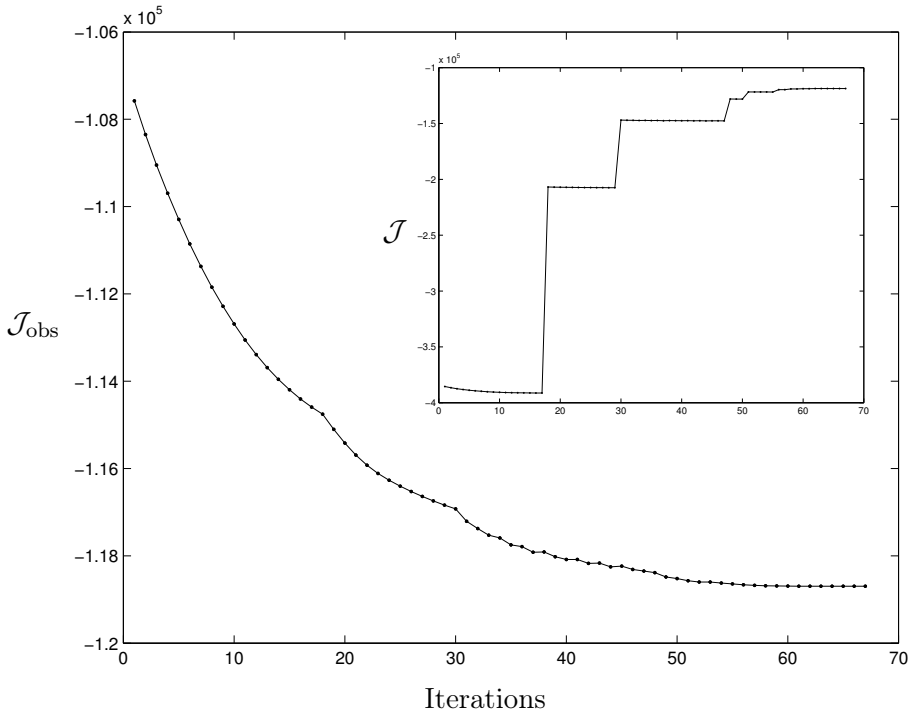

Figure 7.4: Decreases int the costs $\mathcal{J}_{\text{obs}}$ and $\mathcal{J}$.

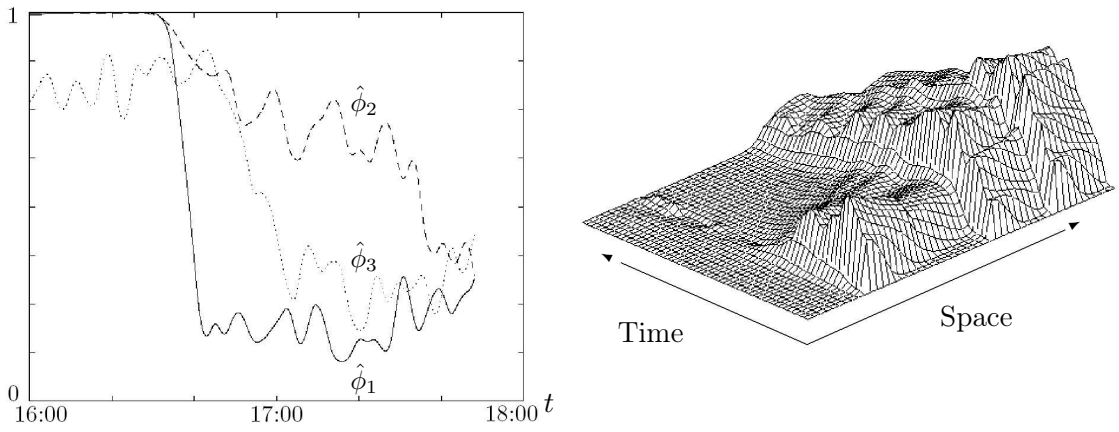

Figure 7.5: Optimal metering rates and distributed flow improvement in time and space.

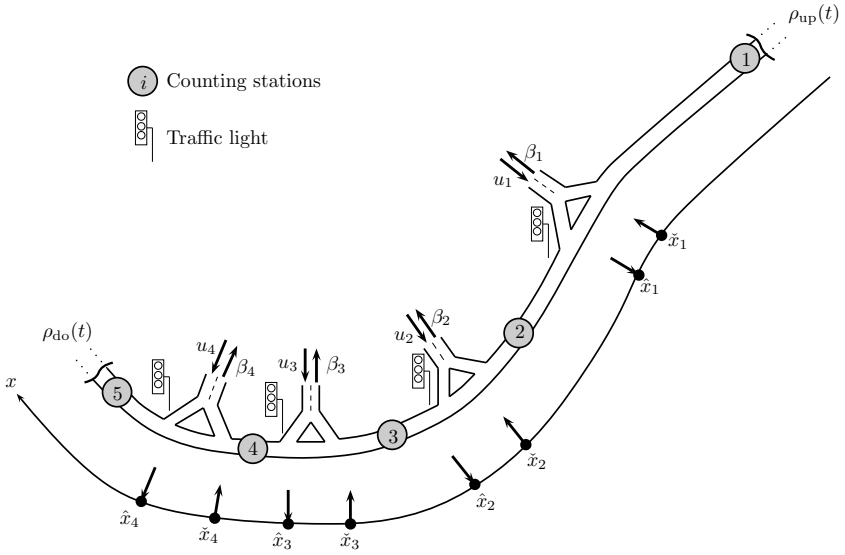

Figure 7.6: Beltway of Grenoble (France) considered for the study case.

7.2.2 With the Payne model

The Payne model [Payne, 1971] with the source term discussed above writes

$$\partial_t \begin{pmatrix} \rho \\ \phi \end{pmatrix} + \partial_x \begin{pmatrix} \phi \\ \frac{\phi^2}{\rho} + c^2\rho \end{pmatrix} = \begin{pmatrix} \sum_{i=1}^{N_u} \delta_{\hat{x}_i} u_i \Psi_i(\rho) - \sum_{i=1}^{N_\beta} \delta_{\check{x}_i} \beta_i \phi \\ \frac{\Phi(\rho)-\phi}{\tau} \end{pmatrix} \tag{7.2.10}$$

with ρ and $\phi = \rho v$ the conserved variables and c, τ and $\Phi(\cdot)$ the model parameters.

For this model, the linearized dynamics writes

$$\begin{cases} D\mathbf{f}(\bar{\rho}, \bar{\phi}) = \begin{pmatrix} 0 & 1 \\ c^2 - \frac{\bar{\phi}^2}{\bar{\rho}^2} & \frac{2\bar{\phi}}{\bar{\rho}} \end{pmatrix} \\ D_{\mathbf{y}}\mathbf{g}(\bar{\rho}, \bar{\phi}, \bar{u}) = \begin{pmatrix} \sum \delta_{\hat{x}_i} \bar{u}_i \Psi_i'(\bar{\rho}) & -\sum \delta_{\check{x}_i} \beta_i \\ \frac{\Phi'(\bar{\rho})}{\tau} & -\frac{1}{\tau} \end{pmatrix} \\ D_{\mathbf{u}}\mathbf{g}(\bar{\rho}, \bar{\phi}, \bar{u}) = \begin{pmatrix} \delta_{\hat{x}_1} \Psi_1(\bar{\rho}) & \cdots & \delta_{\hat{x}_{N_u}} \Psi_{N_u}(\bar{\rho}) \\ 0 & \cdots & 0 \end{pmatrix} \end{cases}$$

Using the results stated above, the gradient evaluation of the VMT objective with the barrier term (7.2.3) writes

$$\nabla_{u_i} \mathcal{J}_{\text{VMT}} = \Psi_i(\bar{\rho}(\hat{x}_i, t))\lambda_1(\hat{x}_i, t) - \frac{1}{M}\left(\frac{1}{\bar{u}_i} - \frac{1}{1-\bar{u}_i}\right) \tag{7.2.11}$$

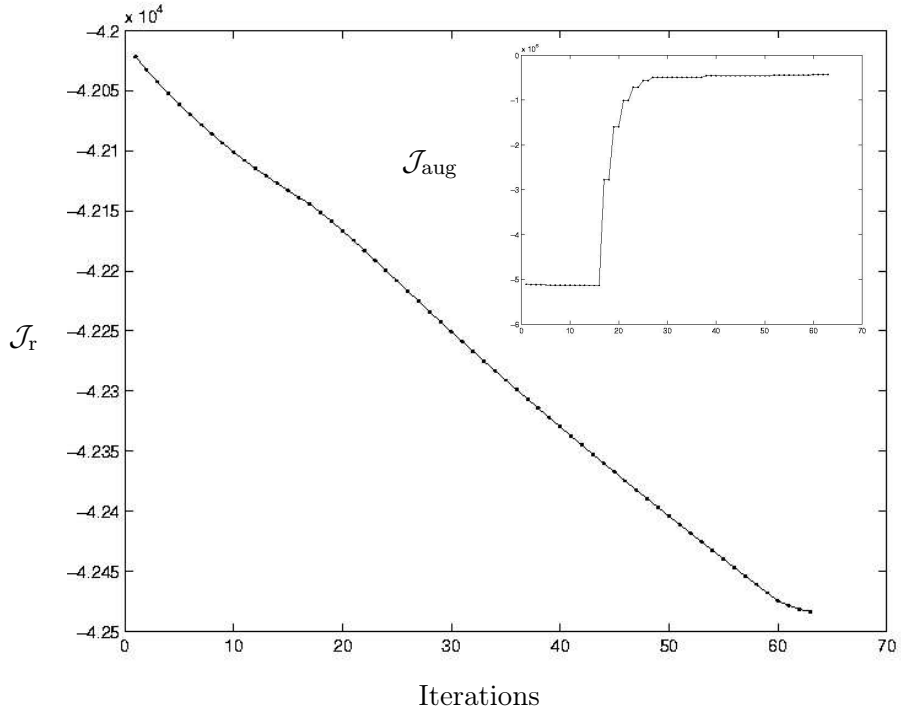

Figure 7.7: Reduction of the costs $\mathcal{J}_{\mathrm{r}}$ and $\mathcal{J}_{\mathrm{aug}}$

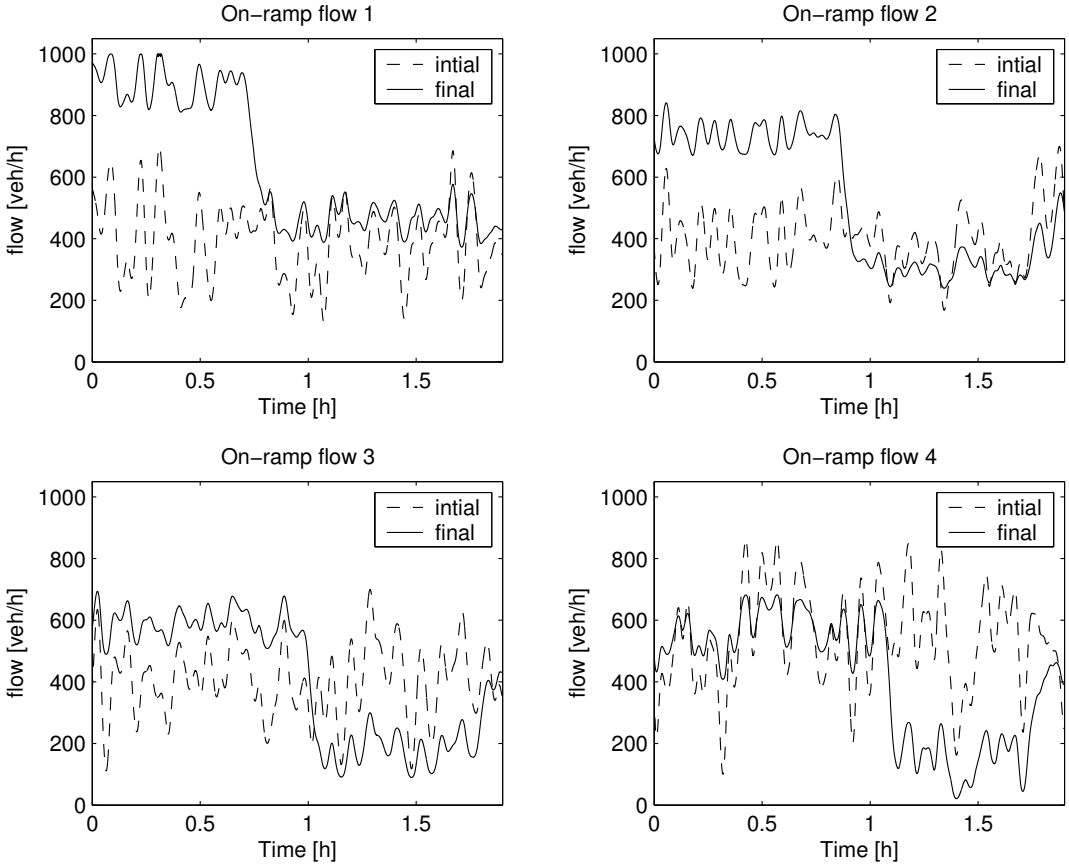

Figure 7.8: Optimal on-ramp flows before and after optimization.

with $\lambda = (\lambda_1 \;\; \lambda_2)$ the adjoint variable, solution of the adjoint equation

$$\begin{cases} -\partial_t \lambda_1 - \left(c^2 - \frac{\bar{\phi}^2}{\bar{\rho}^2}\right) \partial_x \lambda_2 = \sum \delta_{\hat{x}_i} \bar{u}_i \Psi_i'(\bar{\rho}) \lambda_1 + \frac{\Phi'(\bar{\rho})}{\tau} \lambda_2 \\ -\partial_t \lambda_2 - \partial_x \lambda_1 - \frac{2\bar{\phi}}{\bar{\rho}} \partial_x \lambda_2 = -\sum \delta_{\bar{x}_i} \beta_i \lambda_1 - \frac{1}{\tau} \lambda_2 - 1 \\ \lambda_1(x,T) = 0 \text{ and } \lambda_2(x,T) = 0 \\ \lambda_1(0,t) = 0, \;\; \lambda_1(L,t) = 0, \;\; \lambda_2(0,t) = 0 \text{ and } \lambda_2(L,t) = 0 \\ \lambda_{1_{|\Gamma_i}} = 0 \text{ and } \lambda_{2_{|\Gamma_i}} = 0 \text{ with } \Gamma_i = \{(x,t) : [\bar{\rho}(x,t)] \neq 0\} \end{cases} \tag{7.2.12}$$

Equation (7.2.12) is a linear hyperbolic system that can be solved numerically using the schemes proposed in [Godlewski & Raviart, 1996]. The gradient keeps the same form as (7.2.11) for the TTT objective and only the source term in the adjoint equations (7.2.12) is slightly modified as $\mathbf{g}' = (-1 \;\; 0)^T$ in the TTT case.

We now focus on the numerical implementation of the optimization scheme. Several specific methods have been proposed to integrate systems of conservation laws such as (7.2.10) and we propose to use the Roe average method [Bermudez & Vazquez, 1994] for the Payne model. The time stepping of the Roe average method is given by

$$\mathbf{y}_i^{n+1} = \mathbf{y}_i^n - \frac{\Delta t}{\Delta x} \Big(\tilde{\mathbf{f}}(\mathbf{y}_i^n, \mathbf{y}_{i+1}^n) - \tilde{\mathbf{f}}(\mathbf{y}_{i-1}^n, \mathbf{y}_i^n) \Big) + \Delta t \, \tilde{\mathbf{g}}(\mathbf{y}_{i-1}^n, \mathbf{y}_i^n, \mathbf{y}_{i+1}^n)$$

with $\tilde{\mathbf{f}}(\cdot)$ the numerical flux given by

$$\tilde{\mathbf{f}}(\mathbf{y}_i^n, \mathbf{y}_{i+1}^n) = \frac{1}{2} \Big(\mathbf{f}(\tilde{\mathbf{y}}_{i+1/2}) - |D\mathbf{f}(\tilde{\mathbf{y}}_{i+1/2})| (\mathbf{y}_{i+1} - \mathbf{y}_i) \Big)$$

and $\tilde{\mathbf{g}}(\cdot)$ the numerical source term given by

$$\begin{aligned} \tilde{\mathbf{g}}(\mathbf{y}_{i-1}^n, \mathbf{y}_i^n, \mathbf{y}_{i+1}^n) = {} & \frac{1}{2} \Big(I + D\mathbf{f}(\tilde{\mathbf{y}}_{i-1/2}) |D\mathbf{f}(\tilde{\mathbf{y}}_{i-1/2})| \Big) \frac{\mathbf{g}_{i-1}^n + \mathbf{g}_i^n}{2} \\ & + \frac{1}{2} \Big(I - D\mathbf{f}(\tilde{\mathbf{y}}_{i+1/2}) |D\mathbf{f}(\tilde{\mathbf{y}}_{i+1/2})| \Big) \frac{\mathbf{g}_i^n + \mathbf{g}_{i+1}^n}{2} \end{aligned}$$

where $|A| = T \; \mathrm{diag}(|\lambda_i|) \; T^{-1}$ with $A = T \Lambda T^{-1}$ and $\tilde{\mathbf{y}}_{i+1/2}$ is the Roe average at the cell interface $i/i+1$ given, for the Payne model, by

$$\begin{cases} \tilde{\rho}_{i+1/2} = \sqrt{\rho_i \rho_{i+1}} \\ \tilde{v}_{i+1/2} = \frac{\sqrt{\rho_i} v_i + \sqrt{\rho_{i+1}} v_{i+1}}{\sqrt{\rho_i} + \sqrt{\rho_{i+1}}} \\ \tilde{\phi}_{i+1/2} = \tilde{\rho}_{i+1/2} \tilde{v}_{i+1/2} \end{cases}$$

Concerning the backwards in time linear adjoint equation (7.2.12), we propose to use the upwind method

$$\begin{aligned} \lambda_i^{n-1} = \lambda_i^n - {} & \frac{\Delta t}{\Delta x} \Big(- D\mathbf{f}(\bar{\mathbf{y}}_i^n)^T \Big)^+ (\lambda_i^n - \lambda_{i-1}^n) \\ & - \frac{\Delta t}{\Delta x} \Big(- D\mathbf{f}(\bar{\mathbf{y}}_i^n)^T \Big)^- (\lambda_{i+1}^n - \lambda_i^n) + \Delta t \; \mathbf{S}_\lambda \end{aligned} \tag{7.2.13}$$

where $A^+ = T\Lambda^+T^{-1}$, $A^- = T\Lambda^-T^{-1}$ and $\mathbf{S}_\lambda$ is the adjoint equation source term. The boundary conditions of the adjoint system are implemented using ghost cells set to 0, their applicability being directly handled by the discretization methods.

We provide below a simulation example with the VMT objective for a single on-ramp that creates a congestion with a constant inflow of 400 veh/h during 5 min on a 5 km freeway section. The optimizer gives the flow improvement depicted in Figure 7.9 with the ramp flow of Figure 7.10 computed in 20 iterations. The new metering rate releases slowly the vehicle and enables to delay the flow drop upstream of the on-ramp. The improvement is rather local in space due to the finite speed of propagation.

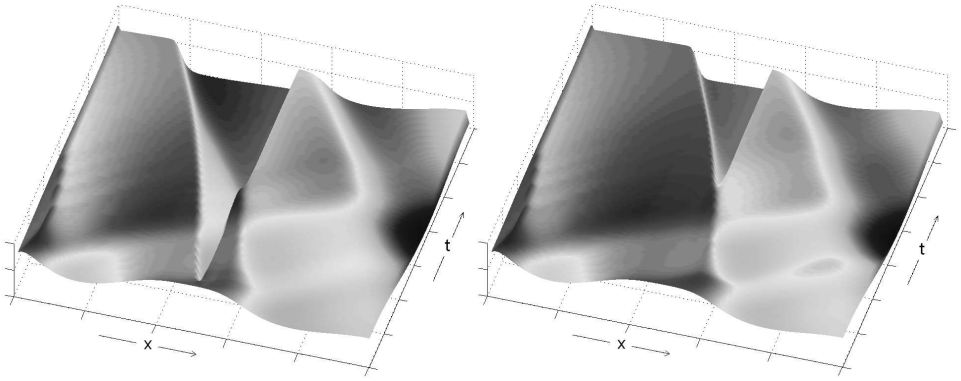

Figure 7.9: Initial (left) and optimized (right) flows with 20 iterations.

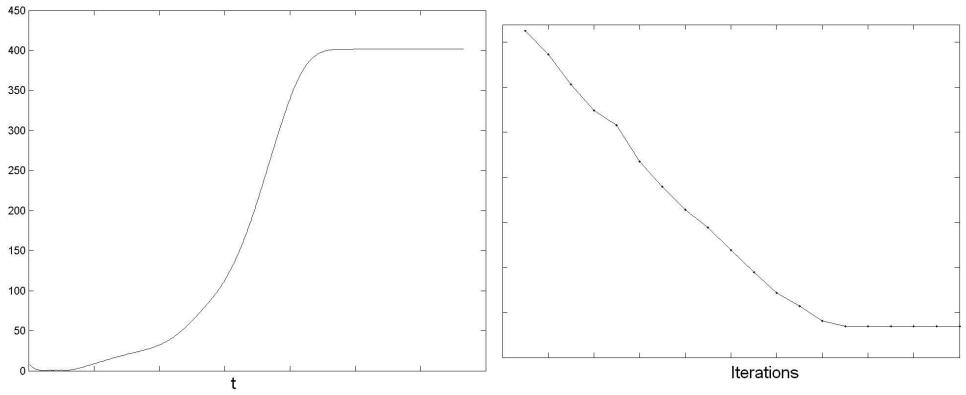

Figure 7.10: Optimized control (left) and $\mathcal{J}_{\text{obs}}$ (right).

7.2.3 With the ARZ model

The ARZ model introduced in [Aw & Rascle, 2000] and [Zhang, 2002] with the density source term (7.2.6) writes

$$\partial_t \begin{pmatrix} \rho \\ \omega \end{pmatrix} + \partial_x \begin{pmatrix} \omega - \rho P(\rho) \\ \frac{\omega^2}{\rho} - \omega P(\rho) \end{pmatrix} = \begin{pmatrix} \sum_{i=1}^{N_u} \delta_{\hat{x}_i} u_i \Psi_i(\rho) - \sum_{i=1}^{N_\beta} \delta_{\check{x}_i} \beta_i (\omega - \rho P(\rho)) \\ \frac{\Phi(\rho) - \omega + \rho P(\rho)}{\tau} \end{pmatrix} \quad (7.2.14)$$

with ρ and $\omega = \rho(v + P(\rho))$ the conserved variables, leading to the dependant flow variable $\phi = \phi(\rho, \omega) = \omega - \rho P(\rho)$. The parameters of the ARZ model are the relaxation term τ and the term $P(\cdot)$, which is taken to be $-V(\rho)$ in [Zhang, 2002].

The linearized dynamics of the ARZ model writes

$$\begin{cases} D\mathbf{f}(\bar{\rho}, \bar{\omega}) = \begin{pmatrix} -P(\bar{\rho}) - \bar{\rho}P'(\bar{\rho}) & 1 \\ -\frac{\bar{\omega}^2}{\bar{\rho}^2} - \bar{\omega}P'(\bar{\rho}) & \frac{2\bar{\omega}}{\bar{\rho}} - P(\bar{\rho}) \end{pmatrix} \\ D_{\mathbf{y}}\mathbf{g}(\bar{\rho}, \bar{\omega}, \bar{u}) = \begin{pmatrix} \sum \delta_{\hat{x}_i} \bar{u}_i \Psi'(\bar{\rho}) - \sum \delta_{\check{x}_i} \beta_i (-P(\bar{\rho}) - \rho P'(\bar{\rho})) & -\sum \delta_{\check{x}_i} \beta_i \\ \frac{\Phi'(\bar{\rho}) + P(\bar{\rho}) + \bar{\rho}P'(\bar{\rho})}{\tau} & -\frac{1}{\tau} \end{pmatrix} \\ D_{\mathbf{u}}\mathbf{g}(\bar{\rho}, \bar{\omega}, \bar{u}) = \begin{pmatrix} \delta_{\hat{x}_1} \Psi_1(\bar{\rho}) & \cdots & \delta_{\hat{x}_{N_u}} \Psi_{N_u}(\bar{\rho}) \\ 0 & \cdots & 0 \end{pmatrix} \end{cases}$$

leading to a VMT gradient with barrier term (7.2.3) given by

$$\nabla_{u_i} \mathcal{J}_{\text{VMT}} = \Psi_i(\bar{\rho}(\hat{x}_i, t))\lambda_1(\hat{x}_i, t) - \frac{1}{M}\left(\frac{1}{\bar{u}_i} - \frac{1}{1 - \bar{u}_i}\right) \tag{7.2.15}$$

where the ARZ adjoint system is

$$\begin{cases} -\partial_t \lambda_1 + \big(P(\bar{\rho}) + \bar{\rho}P'(\bar{\rho})\big)\partial_x \lambda_1 + \left(\frac{\bar{\omega}^2}{\bar{\rho}^2} + \bar{\omega}P'(\bar{\rho})\right)\partial_x \lambda_2 = \\ \qquad \sum \delta_{\hat{x}_i} \bar{u}_i \Psi'(\bar{\rho})\lambda_1 - \sum \delta_{\check{x}_i} \beta_i (-P(\bar{\rho}) - \rho P'(\bar{\rho}))\lambda_1 \\ \qquad + \frac{\Phi'(\bar{\rho}) + P(\bar{\rho}) + \bar{\rho}P'(\bar{\rho})}{\tau}\lambda_2 - P(\bar{\rho}) - \bar{\rho}P(\bar{\rho}) \\ -\partial_t \lambda_2 - \partial_x \lambda_1 - \left(\frac{2\bar{\omega}}{\bar{\rho}} - P(\bar{\rho})\right)\partial_x \lambda_2 = -\sum \delta_{\check{x}_i} \beta_i \lambda_1 - \frac{1}{\tau}\lambda_2 - 1 \\ \lambda_1(x, T) = 0 \text{ and } \lambda_2(x, T) = 0 \\ \lambda_1(0, t) = 0,\ \lambda_1(L, t) = 0,\ \lambda_2(0, t) = 0 \text{ and } \lambda_2(L, t) = 0 \\ \lambda_{1_{|\Gamma_i}} = 0 \text{ and } \lambda_{2_{|\Gamma_i}} = 0 \text{ with } \Gamma_i = \{(x, t) : [\bar{\rho}(x, t)] \neq 0\} \end{cases} \tag{7.2.16}$$

The gradient keeps the same form as (7.2.15) for the TTT objective and only the source term in the adjoint equations (7.2.16) is slightly modified as $\mathbf{g}' = (-1 \ \ 0)^T$ in the this case. For the numerical implementation of the optimization method, we propose to use the Godunov scheme for the ARZ equation and the upwind scheme (7.2.13) for the backwards in time linear adjoint equation (7.2.16).

7.3 The missing data reconstruction problem

Using the LWR model, let consider in this section the problem of estimating the current traffic state $\rho(0, x)$ based on the density measurements $\xi_i(t)$ with $t \in (-T, 0)$ given by a set of sensor (loop detectors) installed at a finite set of locations $\{\tilde{x}_i\}_{i=1}^{N_m}$. As nonlinear conservation laws are not invertible (cannot be integrated backwards) due to the entropy

condition, iterations on the final condition of the time horizon $(-T, 0)$ would not be valid to estimate $\rho(0, x)$. The alternative is to search for the initial condition that minimizes the square error at the sensor locations and then to deduce the final state form the one-to-one correspondance provided by the state equation.

In the state estimation problem, the on-ramp flows $\hat{\phi}$ and off-ramp flows $\check{\phi}$ are assumed to be measured and the decision equation is the initial condition ρ_I. The corresponding optimization problem writes

$$\underset{\rho_I}{\textbf{Min}} \quad \mathcal{J}_{\text{obs}}(\rho) = \sum_i^{N_m} \tfrac{1}{2} \int_0^T (\rho(\cdot, \tilde{x}_i) - \xi_i)^2 = \sum_i^{N_m} \tfrac{1}{2} \int_0^T \int_0^L \delta_{\tilde{x}_i} (\rho - \xi_i)^2$$

$$\textbf{Subj. to} \begin{cases} \partial_t \rho + \partial_x \Phi(\rho) = \sum_i \delta_{\hat{x}_i} \hat{\phi} - \sum_j \delta_{\check{x}_j} \beta_j \check{\phi} \\ \rho(0, x) = \rho_I(x) \\ \rho(0, t) = \rho_0(t) \text{ and } \rho(L, t) = \rho_L(t) \end{cases} \tag{7.3.1}$$

Using the adjoint based gradient evaluation method, we deduce

$$\nabla_{\rho_I} \mathcal{J}_{\text{obs}} = \lambda(x, 0) \tag{7.3.2}$$

with λ the solution of the adjoint equation

$$\begin{cases} -\partial_t \lambda - \Phi'(\bar{\rho}) \partial_x \lambda = \delta_{\tilde{x}_i} (\rho - \xi_i) \\ \lambda(x, T) = 0 \\ \lambda(0, t) = 0 \text{ when } \Phi'(\bar{\rho}(0, t)) < 0 \\ \lambda(L, t) = 0 \text{ when } \Phi'(\bar{\rho}(L, t)) > 0 \\ \lambda_{|\Gamma_i} = 0 \text{ with } \Gamma_i = \{(x, t) : [\bar{\rho}(x, t)] \neq 0\} \end{cases} \tag{7.3.3}$$

The marginal cost interpretation gives some insight on the limitations of the method. As characteristics linking the sensor locations to the initial condition in $(-T, 0)$ are the only ones to provide information in the descent method, a lack of such characteristics would lead to a poor estimation. Nevertheless, this is a structural limitation of the system that cannot be overcome by any method.

Algorithm 5 is proposed to compute numerically a local optimal of Problem (7.3.1) and is used in a numerical experiment conducted for the freeway of Figure 7.6 with 5 sensors. Figure 7.11 shows the congestion wave created by the initial condition and the residual error in the trajectory with the estimated initial condition. Figure 7.12 shows the good estimation property of the method when compared to a linear interpolation between available data. An improvement of 90 % is obtained on the cost function $\mathcal{J}_{\text{obs}}$.

7.4 The origin-destination estimation problem

In this section, it is proposed to use a Prediction Error Minimization (PEM) method to estimate the Origin-Destination flows on a stretch of freeway. Though no node are present

Algorithm 5 Steepest descent algorithm for the missing data reconstruction problem.

Require: $\rho_I := \rho_I^{\text{init}} \in (0, \rho_{\text{m}})$, ϵ
  while $\|\nabla_{\rho_I} \mathcal{J}_{\text{o}}\| > \epsilon$ **do**
    Compute ρ from (7.3.1)
    Compute λ from (7.3.3)
    Compute $\nabla_{\rho_I} \mathcal{J}_{\text{obs}}$ from (7.3.2)
    Update $\rho_I := \rho_I - \nabla_{\rho_I} \mathcal{J}_{\text{obs}}$
  end while

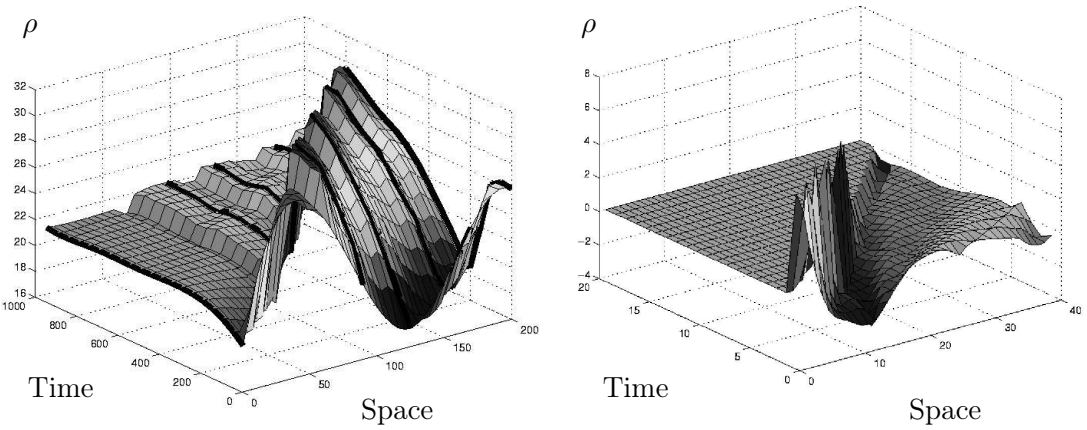

Figure 7.11: Left: actual density distribution to be estimated with sensor data (black lines). Right: residual error after optimization.

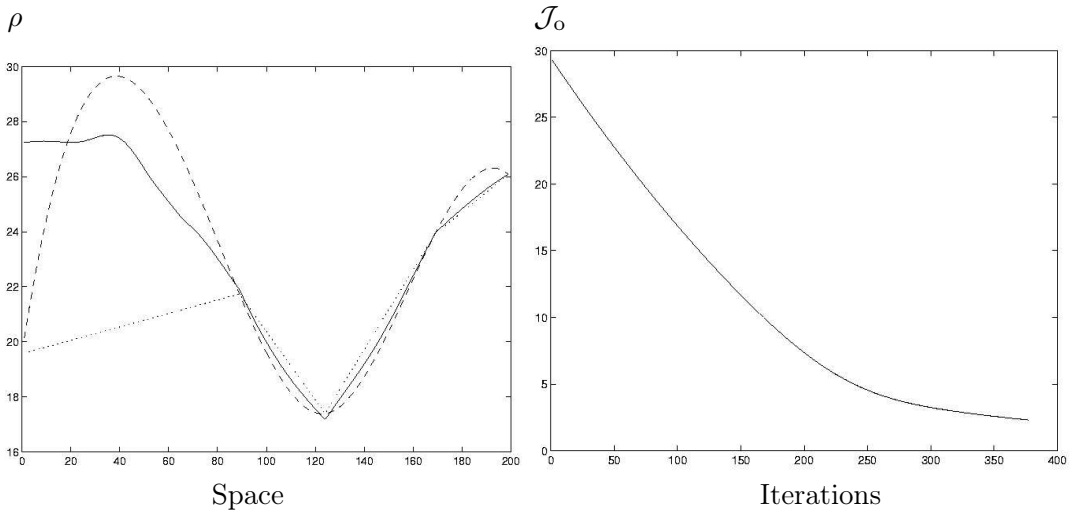

Figure 7.12: Left: estimated initial condition (dashed: actual, plain: estimated, dot: linear interpolation of measurements). Right: evolution of the cost function $\mathcal{J}_{\text{obs}}$.

in this case, we call this problem the OD matrix estimation. To simplify the exposition of the problem and its solution, we restrict to the treatment of the small network depicted in Figure 7.13 using the multiclass model presented in a previous chapter where free flow is assumed all along the freeway. In this model, we recall that the traffic state is the

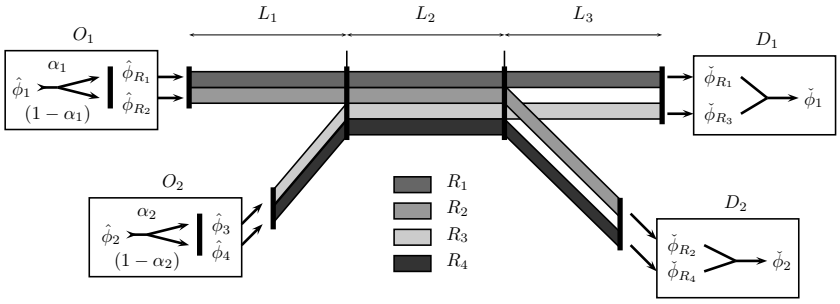

Figure 7.13: Network used for illustration.

vector $\boldsymbol{\rho}$ of partial flows tagged with their Origin-Destination information. The free flow assumption is not true in general and the traffic may be free, i.e. ($|\boldsymbol{\rho}| < \rho_c$), or congested, i.e. ($|\boldsymbol{\rho}| < \rho_c$), both in a time and space varying way. The 2 main consequences of such behavior are:

1. The interface conditions modelling the on/off-ramps vary with time following a finite state machine (FSM). In the general case, the sensitivity analysis should follow this FSM.

2. The actuated and observed boundaries may vary in time, leading to difficulties in the problem setting and the treatment of boundary conditions.

With the free flow assumption, the OD estimation objective weighting the deviation of the predicted and measured flows writes

$$\underset{\alpha_1,\alpha_2}{\mathbf{Min}}\ \mathcal{J}(\boldsymbol{\rho}^{L_2},\boldsymbol{\rho}^{L_3}) = \int_0^T \frac{1}{2}\Big[(\gamma_{\mathrm{Do}}\rho_{R_1}^{L_3}+\gamma_{\mathrm{Do}}\rho_{R_3}^{L_3})V(\gamma_{\mathrm{Do}}|\boldsymbol{\rho}^{L_3}|)-\check{\phi}_1\Big]^2 + \frac{1}{2}\Big[(\gamma_{\mathrm{Do}}\rho_{R_2}^{L_2}+\gamma_{\mathrm{Do}}\rho_{R_4}^{L_2})V(\gamma_{\mathrm{Do}}|\boldsymbol{\rho}^{L_2}|)-\check{\phi}_2\Big]^2 \quad (7.4.1)$$

with the constraints

$$
\textbf{Subj. to}\quad
\begin{cases}
\partial_t \boldsymbol{\rho}^{L_1} + \partial_x \mathbf{f}(\boldsymbol{\rho}^{L_1}) = 0 \\
\partial_t \boldsymbol{\rho}^{L_2} + \partial_x \mathbf{f}(\boldsymbol{\rho}^{L_2}) = 0 \\
\partial_t \boldsymbol{\rho}^{L_3} + \partial_x \mathbf{f}(\boldsymbol{\rho}^{L_3}) = 0 \\
\boldsymbol{\rho}^{L_1}(t{=}0) = \boldsymbol{\rho}_I^{L_1},\ \boldsymbol{\rho}^{L_2}(t{=}0) = \boldsymbol{\rho}_I^{L_2},\ \boldsymbol{\rho}^{L_3}(t{=}0) = \boldsymbol{\rho}_I^{L_3} \\
\gamma_{\mathrm{Up}}\rho_{R_1}^{L_1} = \alpha_1 \Phi^{-l}(\hat{\phi}_1) \ \text{ and } \ \gamma_{\mathrm{Up}}\rho_{R_2}^{L_1} = (1-\alpha_1)\Phi^{-l}(\hat{\phi}_1) \\
\gamma_{\mathrm{Up}}\rho_{R_1}^{L_2} = I_{R_1}^{\hat{\phi}_2}(\gamma_{\mathrm{Do}}\boldsymbol{\rho}^{L_1}) \\
\qquad = \frac{\gamma_{\mathrm{Do}}\rho_{R_1}^{L_1}}{\gamma_{\mathrm{Do}}|\boldsymbol{\rho}^{L_1}|}\ \theta_{\hat{\phi}_2}\Big(\eta_{\hat{\phi}_2}^{-l}\big(\gamma_{\mathrm{Do}}|\boldsymbol{\rho}^{L_1}|V(\gamma_{\mathrm{Do}}|\boldsymbol{\rho}^{L_1}|)\big)\Big) \\
\gamma_{\mathrm{Up}}\rho_{R_2}^{L_2} = I_{R_2}^{\hat{\phi}_2}(\gamma_{\mathrm{Do}}\boldsymbol{\rho}^{L_1}) \\
\qquad = \frac{\gamma_{\mathrm{Do}}\rho_{R_2}^{L_1}}{\gamma_{\mathrm{Do}}|\boldsymbol{\rho}^{L_1}|}\ \theta_{\hat{\phi}_2}\Big(\eta_{\hat{\phi}_2}^{-l}\big(\gamma_{\mathrm{Do}}|\boldsymbol{\rho}^{L_1}|V(\gamma_{\mathrm{Do}}|\boldsymbol{\rho}^{L_1}|)\big)\Big) \\
\gamma_{\mathrm{Up}}\rho_{R_3}^{L_2} = I_{R_3}^{\hat{\phi}_2}(\gamma_{\mathrm{Do}}\boldsymbol{\rho}^{L_1}; \alpha_2) \\
\qquad = \alpha_2\ \eta_{\hat{\phi}_2}^{-l}\big(\gamma_{\mathrm{Do}}|\boldsymbol{\rho}^{L_1}|V(\gamma_{\mathrm{Do}}|\boldsymbol{\rho}^{L_1}|)\big) \\
\gamma_{\mathrm{Up}}\rho_{R_4}^{L_2} = I_{R_4}^{\hat{\phi}_2}(\gamma_{\mathrm{Do}}\boldsymbol{\rho}^{L_1}; \alpha_2) \\
\qquad = (1-\alpha_2)\ \eta_{\hat{\phi}_2}^{-l}\big(\gamma_{\mathrm{Do}}|\boldsymbol{\rho}^{L_1}|V(\gamma_{\mathrm{Do}}|\boldsymbol{\rho}^{L_1}|)\big) \\
\gamma_{\mathrm{Up}}\rho_{R_1}^{L_3} = I_{R_1}^{\check{\phi}_2}(\gamma_{\mathrm{Do}}\boldsymbol{\rho}^{L_2}) \\
\qquad = \frac{\gamma_{\mathrm{Do}}\rho_{R_1}^{L_2}}{\gamma_{\mathrm{Do}}\rho_{R_1}^{L_2}+\gamma_{\mathrm{Do}}\rho_{R_3}^{L_2}}\Phi^{-l}\Big(\eta_{\check{\phi}_2}\big(\gamma_{\mathrm{Do}}\rho_{R_2}^{L_2}+\gamma_{\mathrm{Do}}\rho_{R_4}^{L_2}\big)\Big) \\
\gamma_{\mathrm{Up}}\rho_{R_3}^{L_3} = I_{R_3}^{\check{\phi}_2}(\gamma_{\mathrm{Do}}\boldsymbol{\rho}^{L_2}) \\
\qquad = \frac{\gamma_{\mathrm{Do}}\rho_{R_3}^{L_2}}{\gamma_{\mathrm{Do}}\rho_{R_1}^{L_2}+\gamma_{\mathrm{Do}}\rho_{R_3}^{L_2}}\Phi^{-l}\Big(\eta_{\check{\phi}_2}\big(\gamma_{\mathrm{Do}}\rho_{R_2}^{L_2}+\gamma_{\mathrm{Do}}\rho_{R_4}^{L_2}\big)\Big) \\
\alpha_1 \in (0,1) \text{ and } \alpha_2 \in (0,1)
\end{cases}
\tag{7.4.2}
$$

where γ_{Up} and γ_{Do} are the trace operators for the upstream and downstream boundaries respectively. In the free flow case, $\hat{\phi}_1$ and $\hat{\phi}_2$ are the actuated boundaries whereas $\check{\phi}_1$ and $\check{\phi}_2$ are the observed boundaries. As we can see, writing all the interface conditions is tedious, even for such a small network.

The linearized dynamics of (7.4.2) writes formally

$$\begin{cases} \partial_t \tilde{\boldsymbol{\rho}}^{L_1} + \partial_x\big(D\mathbf{f}(\bar{\boldsymbol{\rho}}^{L_1})\tilde{\boldsymbol{\rho}}^{L_1}\big) = 0 \\ \partial_t \tilde{\boldsymbol{\rho}}^{L_2} + \partial_x\big(D\mathbf{f}(\bar{\boldsymbol{\rho}}^{L_2})\tilde{\boldsymbol{\rho}}^{L_2}\big) = 0 \\ \partial_t \tilde{\boldsymbol{\rho}}^{L_3} + \partial_x\big(D\mathbf{f}(\bar{\boldsymbol{\rho}}^{L_3})\tilde{\boldsymbol{\rho}}\big) = 0 \\ \tilde{\boldsymbol{\rho}}^{L_1}(t{=}0) = 0,\ \tilde{\boldsymbol{\rho}}^{L_2}(t{=}0) = 0,\ \tilde{\boldsymbol{\rho}}^{L_3}(t{=}0) = 0 \\ \gamma_{\mathrm{Up}}\tilde{\boldsymbol{\rho}}_{L_1} = \begin{pmatrix} \Phi^{-l}(\hat{\phi}_1) \\ -\Phi^{-l}(\hat{\phi}_1) \end{pmatrix} \tilde{\alpha}_1 \\ \gamma_{\mathrm{Up}}\tilde{\boldsymbol{\rho}}_{L_2} = \begin{pmatrix} \nabla I_{R_1}^{\hat{\phi}_2}(\gamma_{\mathrm{Do}}\bar{\boldsymbol{\rho}}^{L_1}) \\ \nabla I_{R_2}^{\hat{\phi}_2}(\gamma_{\mathrm{Do}}\bar{\boldsymbol{\rho}}^{L_1}) \\ \nabla_\rho I_{R_3}^{\hat{\phi}_2}(\gamma_{\mathrm{Do}}\bar{\boldsymbol{\rho}}^{L_1},\bar{\alpha}_2) \\ \nabla_\rho I_{R_4}^{\hat{\phi}_2}(\gamma_{\mathrm{Do}}\bar{\boldsymbol{\rho}}^{L_1},\bar{\alpha}_2) \end{pmatrix} \gamma_{\mathrm{Do}}\tilde{\boldsymbol{\rho}}^{L_1} + \begin{pmatrix} 0 \\ 0 \\ \nabla_\alpha I_{R_3}^{\hat{\phi}_2}(\gamma_{\mathrm{Do}}\bar{\boldsymbol{\rho}}^{L_1},\bar{\alpha}_2) \\ \nabla_\alpha I_{R_4}^{\hat{\phi}_2}(\gamma_{\mathrm{Do}}\bar{\boldsymbol{\rho}}^{L_1},\bar{\alpha}_2) \end{pmatrix} \tilde{\alpha}_2 \\ \gamma_{\mathrm{Up}}\tilde{\boldsymbol{\rho}}_{L_3} = \begin{pmatrix} \nabla I_{R_1}^{\hat{\phi}_2}(\gamma_{\mathrm{Do}}\bar{\boldsymbol{\rho}}^{L_2}) \\ \nabla I_{R_1}^{\hat{\phi}_2}(\gamma_{\mathrm{Do}}\bar{\boldsymbol{\rho}}^{L_2}) \end{pmatrix} \gamma_{\mathrm{Do}}\tilde{\boldsymbol{\rho}}^{L_2} \end{cases}$$

Due to the complex expression of some gradients in the above equation, numerical differentiation may be needed to ease practical implementations. Nevertheless, these computations only need to be done one time.

The OD estimation problem requires some more analysis that the general case studied before due to the multiple boundary conditions. The first variation of the cost functional (7.4.1) writes

$$\tilde{\mathcal{J}} = \int_0^T \Big(\nabla_{\boldsymbol{\rho}^{L_3}}\mathcal{J}(\gamma_{\mathrm{Do}}\bar{\boldsymbol{\rho}}^{L_3})\ \gamma_{\mathrm{Do}}\tilde{\boldsymbol{\rho}}^{L_3} + \nabla_{\boldsymbol{\rho}^{L_2}}\mathcal{J}(\gamma_{\mathrm{Do}}\bar{\boldsymbol{\rho}}^{L_2})\ \gamma_{\mathrm{Do}}\tilde{\boldsymbol{\rho}}^{L_2}\Big)\mathrm{d}t \tag{7.4.3}$$

We now introduce 3 adjoint variables $\boldsymbol{\lambda}_1$, $\boldsymbol{\lambda}_2$, $\boldsymbol{\lambda}_3$ and compute the adjoint system as following

$$\begin{aligned} 0 =& < \boldsymbol{\lambda}_1, \partial_t \tilde{\boldsymbol{\rho}}^{L_1} + \partial_x\big(D\mathbf{f}(\bar{\boldsymbol{\rho}}^{L_1})\tilde{\boldsymbol{\rho}}^{L_1}\big) > \\ &+ < \boldsymbol{\lambda}_2, \partial_t \tilde{\boldsymbol{\rho}}^{L_2} + \partial_x\big(D\mathbf{f}(\bar{\boldsymbol{\rho}}^{L_2})\tilde{\boldsymbol{\rho}}^{L_2}\big) > \\ &+ < \boldsymbol{\lambda}_3, \partial_t \tilde{\boldsymbol{\rho}}^{L_3} + \partial_x\big(D\mathbf{f}(\bar{\boldsymbol{\rho}}^{L_3})\tilde{\boldsymbol{\rho}}\big) > \\ =& < \tilde{\boldsymbol{\rho}}^{L_1}, -\partial_t\boldsymbol{\lambda}_1 - D\mathbf{f}(\bar{\boldsymbol{\rho}}^{L_1})^T\partial_x\boldsymbol{\lambda}_1 > + \int_{\mathrm{Up}}^{\mathrm{Do}} [\boldsymbol{\lambda}_1^{\mathrm{T}}\tilde{\boldsymbol{\rho}}^{L_1}]_0^T \mathrm{d}x \\ &+ < \tilde{\boldsymbol{\rho}}^{L_1}, -\partial_t\boldsymbol{\lambda}_2 - D\mathbf{f}(\bar{\boldsymbol{\rho}}^{L_2})^T\partial_x\boldsymbol{\lambda}_2 > + \int_{\mathrm{Up}}^{\mathrm{Do}} [\boldsymbol{\lambda}_2^{\mathrm{T}}\tilde{\boldsymbol{\rho}}^{L_2}]_0^T \mathrm{d}x \\ &+ < \tilde{\boldsymbol{\rho}}^{L_1}, -\partial_t\boldsymbol{\lambda}_3 - D\mathbf{f}(\bar{\boldsymbol{\rho}}^{L_3})^T\partial_x\boldsymbol{\lambda}_3 > + \int_{\mathrm{Up}}^{\mathrm{Do}} [\boldsymbol{\lambda}_3^{\mathrm{T}}\tilde{\boldsymbol{\rho}}^{L_3}]_0^T \mathrm{d}x \\ &+ \int_0^T [\boldsymbol{\lambda}_1^{\mathrm{T}} D\mathbf{f}(\bar{\boldsymbol{\rho}}^{L_1})\tilde{\boldsymbol{\rho}}^{L_1}]_{\mathrm{Up}}^{\mathrm{Do}}\mathrm{d}t + \int_0^T [\boldsymbol{\lambda}_2^{\mathrm{T}} D\mathbf{f}(\bar{\boldsymbol{\rho}}^{L_2})\tilde{\boldsymbol{\rho}}^{L_2}]_{\mathrm{Up}}^{\mathrm{Do}}\mathrm{d}t \\ &+ \int_0^T [\boldsymbol{\lambda}_3^{\mathrm{T}} D\mathbf{f}(\bar{\boldsymbol{\rho}}^{L_3})\tilde{\boldsymbol{\rho}}^{L_3}]_{\mathrm{Up}}^{\mathrm{Do}}\mathrm{d}t + \sum_{k=1}^{3}\sum_{\Gamma_i}\int_{t_i}^T \sigma_i \boldsymbol{\lambda}_{\Gamma_i}^{\mathrm{T}}[\tilde{\boldsymbol{\rho}}^{L_k} - D\mathbf{f}(\bar{\boldsymbol{\rho}}^{L_k})\tilde{\boldsymbol{\rho}}^{L_k}]_{\Gamma_i}\mathrm{d}t \end{aligned}$$

Setting all the gray variables to 0 leads to a linear hyperbolic initial boundary value problem where the boundary values are coupled through

$$\int_0^T \Big(- \gamma_{\mathrm{Up}} \boldsymbol{\lambda}_1{}^{\mathrm{T}} D\mathbf{f}(\gamma_{\mathrm{Up}} \bar{\boldsymbol{\rho}}^{L_1}) \gamma_{\mathrm{Up}} \tilde{\boldsymbol{\rho}}^{L_1} + \gamma_{\mathrm{Do}} \boldsymbol{\lambda}_3{}^{\mathrm{T}} D\mathbf{f}(\gamma_{\mathrm{Do}} \bar{\boldsymbol{\rho}}^{L_3}) \gamma_{\mathrm{Do}} \tilde{\boldsymbol{\rho}}^{L_3}$$
$$+ (\gamma_{\mathrm{Do}} \boldsymbol{\lambda}_1{}^{\mathrm{T}} D\mathbf{f}(\gamma_{\mathrm{Do}} \bar{\boldsymbol{\rho}}^{L_1}) \gamma_{\mathrm{Do}} \tilde{\boldsymbol{\rho}}^{L_1} - \gamma_{\mathrm{Up}} \boldsymbol{\lambda}_2{}^{\mathrm{T}} D\mathbf{f}(\gamma_{\mathrm{Up}} \bar{\boldsymbol{\rho}}^{L_2}) \gamma_{\mathrm{Up}} \tilde{\boldsymbol{\rho}}^{L_2})$$
$$+ \ (\gamma_{\mathrm{Do}} \boldsymbol{\lambda}_2{}^{\mathrm{T}} D\mathbf{f}(\gamma_{\mathrm{Do}} \bar{\boldsymbol{\rho}}^{L_2}) \ \gamma_{\mathrm{Do}} \tilde{\boldsymbol{\rho}}^{L_2} - \gamma_{\mathrm{Up}} \boldsymbol{\lambda}_3{}^{\mathrm{T}} D\mathbf{f}(\gamma_{\mathrm{Up}} \bar{\boldsymbol{\rho}}^{L_3}) \ \gamma_{\mathrm{Up}} \tilde{\boldsymbol{\rho}}^{L_3}) \Big) \mathrm{d}t = 0$$

Noting $\gamma_{\mathrm{Up}} \tilde{\boldsymbol{\rho}}^{L_1} = B_{0/1} \tilde{\alpha}_1$, $\gamma_{\mathrm{Up}} \tilde{\boldsymbol{\rho}}^{L_2} = A_{1/2} \gamma_{\mathrm{Do}} \tilde{\boldsymbol{\rho}}^{L_1} + B_{1/2} \tilde{\alpha}_2$ and $\gamma_{\mathrm{Up}} \tilde{\boldsymbol{\rho}}^{L_3} = A_{2/3} \gamma_{\mathrm{Do}} \tilde{\boldsymbol{\rho}}^{L_2}$, we can write

$$\begin{aligned} 0 = \int_0^T & - \gamma_{\mathrm{Up}} \boldsymbol{\lambda}_1{}^{\mathrm{T}} D\mathbf{f}(\gamma_{\mathrm{Up}} \bar{\boldsymbol{\rho}}^{L_1}) B_{0/1} \tilde{\alpha}_1 - \gamma_{\mathrm{Up}} \boldsymbol{\lambda}_2{}^{\mathrm{T}} D\mathbf{f}(\gamma_{\mathrm{Up}} \bar{\boldsymbol{\rho}}^{L_2}) B_{1/2} \ \tilde{\alpha}_2 \\ & + \underbrace{\Big(\gamma_{\mathrm{Do}} \boldsymbol{\lambda}_1{}^{\mathrm{T}} D\mathbf{f}(\gamma_{\mathrm{Do}} \bar{\boldsymbol{\rho}}^{L_1}) - \gamma_{\mathrm{Up}} \boldsymbol{\lambda}_2{}^{\mathrm{T}} D\mathbf{f}(\gamma_{\mathrm{Up}} \bar{\boldsymbol{\rho}}^{L_2}) A_{1/2} \Big)}_{=\ 0} \ \gamma_{\mathrm{Do}} \tilde{\boldsymbol{\rho}}^{L_1} \\ & + \underbrace{\Big(\gamma_{\mathrm{Do}} \boldsymbol{\lambda}_2{}^{\mathrm{T}} D\mathbf{f}(\gamma_{\mathrm{Do}} \bar{\boldsymbol{\rho}}^{L_2}) - \gamma_{\mathrm{Up}} \boldsymbol{\lambda}_3{}^{\mathrm{T}} D\mathbf{f}(\gamma_{\mathrm{Up}} \bar{\boldsymbol{\rho}}^{L_3}) A_{2/3} \Big)}_{= \nabla_{\boldsymbol{\rho}^{L_2}} \mathcal{J}(\gamma_{\mathrm{Do}} \bar{\boldsymbol{\rho}}^{L_2})} \ \gamma_{\mathrm{Do}} \tilde{\boldsymbol{\rho}}^{L_2} \\ & + \underbrace{\gamma_{\mathrm{Do}} \boldsymbol{\lambda}_3{}^{\mathrm{T}} D\mathbf{f}(\bar{\boldsymbol{\rho}}^{L_3})}_{= \nabla_{\boldsymbol{\rho}^{L_3}} \mathcal{J}(\gamma_{\mathrm{Do}} \bar{\boldsymbol{\rho}}^{L_3})} \ \gamma_{\mathrm{Do}} \tilde{\boldsymbol{\rho}}^{L_3} \end{aligned}$$

So $\tilde{\mathcal{J}} = <\gamma_{\mathrm{Up}} \boldsymbol{\lambda}_1{}^{\mathrm{T}} D\mathbf{f}(\bar{\boldsymbol{\rho}}^{L_1}) B_{0/1}, \tilde{\alpha}_1> + <\gamma_{\mathrm{Up}} \boldsymbol{\lambda}_2{}^{\mathrm{T}} D\mathbf{f}(\bar{\boldsymbol{\rho}}^{L_2}) B_{1/2}, \tilde{\alpha}_2>$ and the gradients of the optimization problem (7.4.1)-(7.4.2) become

$$\begin{cases} \nabla_{\alpha_1} \tilde{\mathcal{J}} = \gamma_{\mathrm{Up}} \boldsymbol{\lambda}_1{}^{\mathrm{T}} D\mathbf{f}(\gamma_{\mathrm{Up}} \bar{\boldsymbol{\rho}}^{L_1}) \ B_{0/1} \\ \nabla_{\alpha_2} \tilde{\mathcal{J}} = \gamma_{\mathrm{Up}} \boldsymbol{\lambda}_2{}^{\mathrm{T}} D\mathbf{f}(\gamma_{\mathrm{Up}} \bar{\boldsymbol{\rho}}^{L_2}) \ B_{1/2} \end{cases} \tag{7.4.4}$$

with $\boldsymbol{\lambda}_1$ and $\boldsymbol{\lambda}_2$ the solutions of the adjoint equation

$$\begin{cases} -\partial_t \boldsymbol{\lambda}_1 - D\mathbf{f}(\bar{\boldsymbol{\rho}}^{L_1})^T \partial_x \boldsymbol{\lambda}_1 = 0 \\ -\partial_t \boldsymbol{\lambda}_2 - D\mathbf{f}(\bar{\boldsymbol{\rho}}^{L_2})^T \partial_x \boldsymbol{\lambda}_2 = 0 \\ -\partial_t \boldsymbol{\lambda}_3 - D\mathbf{f}(\bar{\boldsymbol{\rho}}^{L_3})^T \partial_x \boldsymbol{\lambda}_3 = 0 \\ \boldsymbol{\lambda}_1(x,T) = \boldsymbol{\lambda}_2(x,T) = \boldsymbol{\lambda}_3(x,T) = 0 \\ \gamma_{\mathrm{Do}} \boldsymbol{\lambda}_3^{\mathrm{T}} = \nabla_{\boldsymbol{\rho}^{L_3}} \mathcal{J}(\gamma_{\mathrm{Do}} \bar{\boldsymbol{\rho}}^{L_3}) D\mathbf{f}(\gamma_{\mathrm{Do}} \bar{\boldsymbol{\rho}}^{L_3})^{-1} \\ \gamma_{\mathrm{Do}} \boldsymbol{\lambda}_2^{\mathrm{T}} = \Big(\gamma_{\mathrm{Up}} \boldsymbol{\lambda}_3^{\mathrm{T}} D\mathbf{f}(\bar{\boldsymbol{\rho}}^{L_3}) A_{2/3} + \nabla_{\boldsymbol{\rho}^{L_2}} \mathcal{J}(\gamma_{\mathrm{Do}} \bar{\boldsymbol{\rho}}^{L_2}) \Big) D\mathbf{f}(\gamma_{\mathrm{Do}} \bar{\boldsymbol{\rho}}^{L_2})^{-1} \\ \gamma_{\mathrm{Do}} \boldsymbol{\lambda}_1^{\mathrm{T}} = \gamma_{\mathrm{Up}} \boldsymbol{\lambda}_2^{\mathrm{T}} D\mathbf{f}(\gamma_{\mathrm{Up}} \bar{\boldsymbol{\rho}}^{L_2}) A_{1/2} D\mathbf{f}(\gamma_{\mathrm{Do}} \bar{\boldsymbol{\rho}}^{L_1})^{-1} \end{cases} \tag{7.4.5}$$

Note that to completely solve the OD estimation problem and remove the free flow assumption, these computations should be done for every possible free/congested/decoupled configuration.

Based on the gradient evaluation formula given above, the following iterative optimization method is proposed to update an OD matrix based on the on/off-ramps vehicle counts:

1. A first guess is given for the decision variables $\alpha_k(t)$.
2. The model (7.4.2) is *exited* using the current decision variables and the measured flows through a set of actuated boundaries ensuring the wellposedness of the initial boundary value problem. This prediction provides some computed values at the observed boundaries, which are the duals of the actuated boundaries.
3. The gradients (7.4.4) are computed using the adjoint equation (7.4.5).
4. A steepest descent method modify the decision variables to decrease the cost.
5. The previous steps are repeated iteratively until a local minimum is reached.

Thus, be it understood, to demonstrate a theorem, it is neither necessary nor even advantageous to know what it means.

Henri Poincaré (1854-1912),
French mathematician, theoretical physicists and philosopher of science.

Chapter 8

Dissipativity Methods for Feedback Control of Freeways

In this chapter, a new methodology is proposed to design feedback controllers that stabilize one-dimensional scalar conservation laws such as the LWR freeway model. The control problem we address can be formulated as follows: *how to design a feedback controller that uses pointwise inflows along the spacial domain to track a reference for the internal distributed state?* We restrict here to conservation laws with a concave flux function, which is not restrictive for the LWR model.

Very few attempts have been made to stabilize conservation laws using feedback control. The main reasons are the following. First, contrary to linear finite dimensional systems, there is no constructive method to design controllers for nonlinear infinite dimensional systems. Second, the presence of shock waves complicates the design as it leads to irregular states which are not common in the standard analysis. Design methodologies for partial differential equations can be organized in 2 classes: the first one consists in designing a controller for the infinite dimensional system directly whereas the second consists in discretizing the equation and then use finite dimensional techniques to compute the controller. Available contributions in the direct design approach for hyperbolic partial differential equations are [de Halleux, Prieur, Coron, d'Andréa Novel & Bastin, 2003] and [Coron, d'Andréa Novel & Bastin, 2004] where the authors proposed a feedback controller for open channels. Nevertheless, they considered smooth solutions only, thus removing the difficulty due to the presence of shock waves. In [Krstic, 1999], the author proposed a feedback design for the Burgers equation with a small viscosity parameter. However, as the control law is inversely proportional to this parameters, this approach would lead to a blow up of the control action in the inviscid case. On the other hand, many contributions are available concerning the design of controllers for finite dimensional discretizations of partial differential equations. For instance, [Balogh & Krstic, 2004] proposed a controller for parabolic partial differential equations based on a finite difference approximation. However, such an approach cannot be applied to hyperbolic equations as finite difference schemes are not valid for this class of equations, mainly because of the presence of shock waves. We propose in this chapter a specific Go-

dunov discretization scheme [LeVeque, 1992] that can be used for conservation laws and lead to a valid finite dimensional approximation. The particularity of the obtained finite dimensional model is to be a switched affine system which is not the case for parabolic or elliptic equations. Other discretization methods could be used as the Lax-Friedrichs scheme [LeVeque, 1992] but it would lead to a nonlinear discrete system for which no constructive control methods are available.

Specific schemes such as the Godunov method [Godunov, 1959], which is an efficient first order method, can be used to discretize conservation laws but they do not lead to a closed-form expression in general. An other useful tool is the front tracking method [Holden et al., 1988] which uses a piecewise affine approximation of the nonlinear flux function and track all the elementary waves to compute an approximate solution of a conservation law. Combining these two schemes leads to a discrete piecewise affine (PWA) system suitable for controller design. Several constructive methods have been proposed in [Johansson & Rantzer, 1998] and [Cuzzola & Morari, 2002; P. Biswas & Morari, 2005] to compute a set of static feedback gains that can be used in a switched controller structure to stabilize PWA systems. This methodology leads to a set of Linear Matrix Inequalities (LMI) parameterized with the controller gain that can be solved efficiently using widely available softwares. The originality of our approach is thus to use a specific discretization scheme that transforms the original partial differential equation into a discrete PWA system and then use transparently control methods for this class of systems. As an illustrative example, we perform a controller design for the ramp metering application when one on-ramp can be actuated only. The cases of coordinated ramp metering and stabilization of ramp queues are left for further investigation but can be treated in this setting as well.

Based on the CTM model of [Daganzo, 1994], a switched formulation with a discrete state associated to each cell was introduced in [Gomes & Horowitz, 2003] and [Munoz, Sun, Horowitz & Alvarez, 2003; Munoz, Sun, Horowitz & Alvarez, 2006] for control and estimation purposes. To reduced the complexity which grows exponentially with the system size, the discrete state was allowed to take a small number of values in [Munoz et al., 2003; Munoz et al., 2006] by assuming that only one shock front was present along the considered freeway section. Following the numerical schemes described earlier, our model associates the discrete states to the cell interfaces and the discrete state space is allowed to be as large as needed. Several techniques will be discussed later to reduce this space to its minimum in order to maintain the complexity of feedback controller design at a reasonable level.

8.1 Piecewise affine approximation of the LWR model

8.1.1 The homogeneous case

Let consider first the homogeneous LWR model which writes

$$\partial_t \rho + \partial_x \Phi(\rho) = 0$$

The Godunov scheme [LeVeque, 1992] for the LWR model, with space and time discretization Δx_i and Δt respectively, writes

$$\rho_i[k+1] = \rho_i[k] + \frac{\Delta t}{\Delta x_i}\left(\Phi_n(\rho_{i-1}[k], \rho_i[k]) - \Phi_n(\rho_i[k], \rho_{i+1}[k])\right) \tag{8.1.1}$$

where $i = 1, ..., N$ is the space index, $k = 1, ..., M$ the time index and $\Phi_n(\rho_L, \rho_R)$ is the numerical flux function given by the solution of the Riemann problem with left and right initial states ρ_L and ρ_R. The analytical solution for $\Phi_n(\rho_L, \rho_R)$ is known [LeVeque, 1992] and can be written $\Phi_n(\rho_L, \rho_R) = \Phi(\rho^*)$ with ρ^* given by

	$\Phi'(\rho_R) \geq 0$	$\Phi'(\rho_R) < 0$
$\Phi'(\rho_L) \geq 0$	$\rho^* = \rho_L$	$\rho^* = \begin{cases} \rho_L & \text{if } \frac{\Phi(\rho_R)-\Phi(\rho_L)}{\rho_R-\rho_L} > 0 \\ \rho_R & \text{otherwise} \end{cases}$
$\Phi'(\rho_L) < 0$	$\rho^* = \text{argmax } \Phi(\cdot)$	$\rho^* = \rho_R$

As the numerical computations should be done on a bounded spacial domain, two boundary signal $\rho_0[k]$ and $\rho_{N+1}[k]$ are assumed to be known and to apply in ghost cells indexed by $i = 0$ and $i = N + 1$. The same technique as above is then used to compute the boundary fluxes by assuming that the fundamental diagrams parameters are identical in cells $i = 0$ and $i = 1$ as well as in cells $i = 0$ and $i = 1$. The Godunov scheme can thus be written in the form of the switched nonlinear system

$$\begin{cases} \rho_{k+1} &= f_{\alpha_k}(\rho_k) \\ \alpha_k &= g(\rho_k) \end{cases}$$

where $\rho_k = (\rho_1[k], ...\rho_n[k])$ is the continuous state and $\alpha_k = (\alpha_0[k], ..., \alpha_N[k])$ is a discrete state that determines the behavior of the cell interfaces in the time interval k to $k + 1$. The discrete state α_k only depends on the continuous state ρ_k at time k through the nonlinear function $g(\cdot)$ which tells which entry should be selected in the above table for each interface. In this switched formulation, the dynamics $f_{\alpha_k}(\cdot)$ of the continuous state depends on the current configuration α_k and is determined by the time stepping given in Equation (8.1.1).

We now show how this switched nonlinear system can be put in the more convenient form of a piecewise affine (PWA) system. We restrict here to concave flux functions as

we are interested in freeway traffic models. Every piecewise affine approximation of a concave function $\Phi(\cdot)$ can be written

$$\Phi_{PWA}(\rho) = \min \ \{a_i \rho + b_i\}_{i=1,...,p}$$

where a_i and b_i are two sets of p reals defining the approximation. We assume that $a_m = 0$ so that b_m is the maximal flow. Figure 8.1 gives an example of such a piecewise affine approximation $\tilde{f}(\cdot)$ for a concave function $f(\cdot)$.

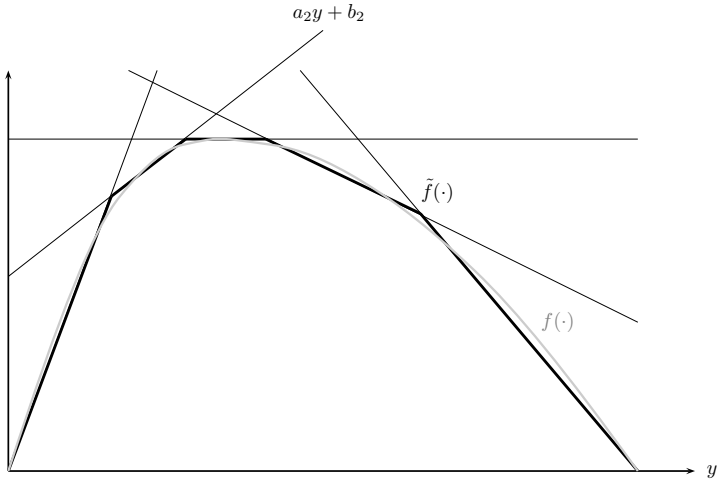

Figure 8.1: Piecewise affine approximation of a concave flux function f.

Combining the Godunov scheme with a piecewise affine approximation of the flux function $\Phi(\rho)$, the proposed discretization scheme for the homogeneous LWR model becomes Equation (8.1.1) with the numerical flux function given by

$$\Phi_n(\rho_L, \rho_R) = \min \ \{ \ a_1 \ \rho_L + b_1 \ , \ ... \ , \ a_{m-1} \ \rho_L + b_{m-1} \ , \ b_m \ , \ a_{m+1} \ \rho_R + b_{m+1} \ , \ ... \ , \ a_p \ \rho_R + b_p \ \} \tag{8.1.2}$$

Note that Equations (8.1.1) and (8.1.2) generalize the CTM discretization proposed in [Daganzo, 1994] and discussed in the chapter *Numerical schemes for macroscopic freeway models*. With $\alpha_k = (\alpha_0[k], ..., \alpha_N[k])$ selecting which entry in (8.1.2) applies in the time interval $[k, k+1]$ for each cell interface, this formulation can easily be put in the form of the piecewise affine system

$$\begin{cases} \rho_{k+1} &= A_{\alpha_k} \rho_k + a_{\alpha_k} \\ \alpha_k &= g(\rho_k) \end{cases}$$

Explicit expressions of the matrices A_{α_k} are given later for the ramp metering application. Note that, in practice, the discrete state α_k does not suffer of chartering as it is often constant and varies slowly when a congestion or free flow wave is traveling along the freeway section.

8.1.2 The inhomogeneous case

As a macroscopic approach was selected to model homogeneous links, ramps are abstracted by pointwise flow contributions as illustrated on Figure 8.2. In this setting,

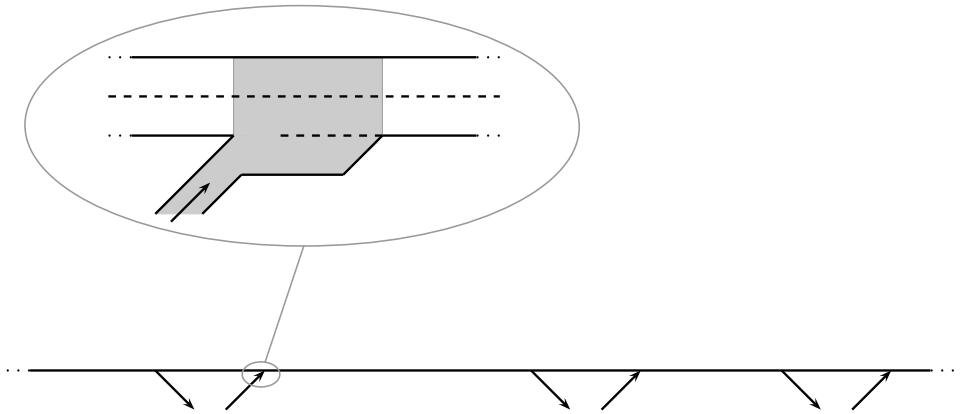

Figure 8.2: Abstraction of onramps and offramps by pointwise inhomogeneities.

the freeway is decomposed in a series of cells interconnected through interfaces that can be with an onramp, with an offramp or without any ramp, as depicted on Figure 8.3. Moreover, the inhomogeneities in the flux function parameters can be handled and these changes should occur at the cell interfaces. In this discretization, $i = 1, ..., N$ is the

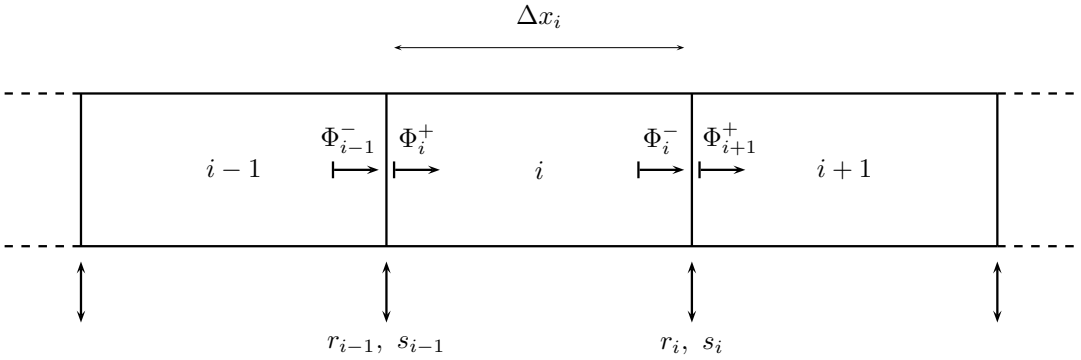

Figure 8.3: Decomposition of the freeway in cells.

cell index and Δ_i the length of the i^{th} cell. r_i and s_i are respectively the onramp and offramp flows at the interface between cells i and $i+1$. For notational convenience, these flows are added to all interfaces and set to 0 when not present. In particular, r_i and s_i cannot be both nonzero for the same index i. With a time step of Δt, the Godunov discretization writes

$$\rho_i[k+1] = \rho_i[k] + \Delta_i \left(\ \Phi_i^+[k] \ - \ \Phi_i^-[k] \ \right) \tag{8.1.3}$$

with $\rho_i[k]$ the density in cell i at time k, $\Phi_i^+[k]$ the flow entering in cell i between time k and $k+1$, $\Phi_i^-[k]$ the flow leaving cell i between time k and $k+1$, and $\Delta_i = \Delta t / \Delta x_i$

a discretization parameter. Note that, contrary to the classical Godunov discretization, the flows at the left and right of the interfaces should be differentiated due to the possible presence of an onramp or an offramp. Indeed, the flow conservation implies

$$\Phi_i^+[k] = \Phi_{i-1}^-[k] + r_{i-1}[k] - s_{i-1}[k] \tag{8.1.4}$$

For the inhomogeneous LWR model, we restrict to trapezoidal fundamental diagram $\Phi_i(\rho_i)$ for each cell i as depicted in Figure 8.4. This trapezoidal flux function is rather standard in the transportation community [Daganzo, 1994] and seems to be an acceptable approximation with respect to field data. The parameters of this fundamental diagram are v_i, w_i, $\bar{\rho}_i$ and $\bar{\Phi}_i$ which are respectively the free flow speed, the congestion wave speed, the maximal density and the maximal flow, also called capacity, for cell i.

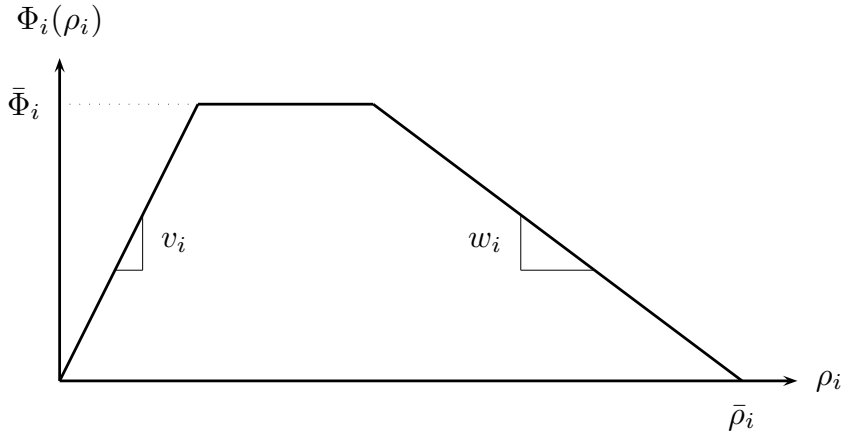

Figure 8.4: Trapezoidal fundamental diagram.

Following [Lebacque, 1996], we define the demand function for cell $i-1$ by

$$D_{i-1}[k] = \min\left\{ v_{i-1}\rho_{i-1}[k] + r_{i-1}[k] - s_{i-1}[k] \ , \ \bar{\Phi}_{i-1} + r_{i-1}[k] - s_{i-1}[k] \right\} \tag{8.1.5}$$

which tells how much vehicles want to enter the next cell between time k and $k+1$. It is computed as the flow of leaving vehicles from cell $i-1$ plus the possible onramp flow and minus the possible offramp flow if present at the interface between cells $i-1$ and i. Similarly, the supply function for cell i is defined by

$$S_i[k] = \min\left\{ w_i(\bar{\rho}_i - \rho_i[k]) \ , \ \bar{\Phi}_i \right\} \tag{8.1.6}$$

and tells how much vehicles can enter cell i between time k and $k+1$ given the current congestion status of this cell. Following [Lebacque, 1996], the interface flow is then given by the formula

$$\Phi_i^+[k] = \min\left\{ D_{i-1}[k] \ , \ S_i[k] \right\} \tag{8.1.7}$$

which is equivalent to the Godunov formulation. Plugging (8.1.5) and (8.1.6) in (8.1.9), we finally get

$$\Phi_i^+[k] = \min\left\{ v_{i-1}\rho_{i-1}[k] + r_{i-1}[k] - s_{i-1}[k] \ , \ w_i(\bar{\rho}_i - \rho_i[k]) \ , \ \bar{\Phi}_{i-1} + r_{i-1}[k] - s_{i-1}[k] \ , \ \bar{\Phi}_i \right\} \tag{8.1.8}$$

The flow conservation given by Equation (8.1.4) then gives

$$\Phi_{i-1}^{-}[k] = \min\left\{v_{i-1}\rho_{i-1}[k]\ ,\ w_i(\bar{\rho}_i-\rho_i[k])-r_{i-1}[k]+s_{i-1}[k]\ ,\ \bar{\Phi}_{i-1}\ ,\ \bar{\Phi}_i-r_{i-1}[k]+s_{i-1}[k]\right\} \tag{8.1.9}$$

To get a positive flow $\Phi_i^+[k]$, it is assumed that the flow $s_{i-1}[k]$ is always smaller than $v_{i-1}\rho_{i-1}[k]$ and $\bar{\Phi}_{i-1}$ and that $\rho_i[k]$ is always smaller than $\bar{\rho}_i$. This first assumption means that the offramp flow $s_i[k]$ should be feasible in the sense that no more vehicles are removed than available or than the capacity. In practice, $s_i[k]$ should be checked to fulfill this constraint at time k before being applied. If it is not the case, it is set to the maximal feasible value. The second assumption $\rho_i[k] \leq \bar{\rho}_i$ is classical in freeway models and is not restrictive. To get a positive flow $\Phi_{i-1}^-[k]$, it is assumed than $r_{i-1}[k]$ is always smaller than $\bar{\Phi}_i$ and $w(\bar{\rho}_i - \rho_i[k])$. The capacity constraint $r_{i-1}[k] \leq \bar{\Phi}_i$ is classical and not restrictive. The constraint $r_{i-1}[k] \leq w(\bar{\rho}_i-\rho_i[k])$ means that the onramp flow should be feasible in the sense that no more vehicles can be discharged from an onramp than the maximal available room on the mainlane. Again, $r_{i-1}[k]$ should be checked to fulfill these constraints before being applied in the numerical scheme. Nevertheless, practical situations usually not suffer of such constraint violations.

In equations (8.1.8) and (8.1.9), each selection of a specific item in the minimum formula have a physical meaning. For instance, in the case of $\Phi_i^+[k]$, the selection of $v_{i-1}\rho_{i-1}[k]+r_{i-1}[k]-s_{i-1}[k]$ means that a free flow is crossing the interface whereas the selection of $w_i(\bar{\rho}_i-\rho_i[k])$ means that a congested flow is crossing it due to a shortage of supply in cell i. The selection of $\bar{\Phi}_{i-1}+r_{i-1}[k]-s_{i-1}[k]$ means that the flow leaving cell $i-1$ reaches its maximal value, i.e. the upstream capacity, whereas the selection of $\bar{\Phi}_i$ means that the flow entering cell i reaches the downstream capacity due to an excess of demand. This last situation typically occurs when an onramp becomes a bottleneck. We can thus associate a discrete state $\alpha_i[k]$ to each interface telling in which state is the interface between times k and $k+1$. The values that can be taken by $\alpha_i[k]$ are

$\mathbf{F}$:	when free flow is selected,
$\mathbf{C}$:	when congested flow is selected,
$\mathbf{D_d}$:	when the maximal decoupling demand is selected,
$\mathbf{D_s}$:	when the maximal decoupling supply is selected.

Note that we assumed that the upstream capacity $\bar{\Phi}_{i-1}$ can be different from the downstream capacity $\bar{\Phi}_i$ in general, thus creating 2 possible decoupling discrete states $\mathbf{D_d}$ and $\mathbf{D_s}$. Nevertheless, these 2 states can often be merged into a unique decoupled state $\mathbf{D}$ as when no ramp is present at the interface, i.e. $r_i[k] = s_i[k] = 0$ or when the fundamental diagrams have identical capacities upstream and downstream, i.e. when $\bar{\Phi}_{i-1} = \bar{\Phi}_i$. In these cases, there are only 3 terms in (8.1.8) and (8.1.9) and the 2 states $\mathbf{D_d}$ and $\mathbf{D_s}$ are replaced by a single state $\mathbf{D}$. Nevertheless, there are some situations when these 2 decoupling states should be considered independently, typically when the capacity is different upstream and downstream of an onramp or an offramp. Such situations occurs when the number of lanes are different upstream and downstream of a ramp. For

instance, on-ramps have sometimes an additional lane downstream of it that may end further by merging with the mainlane.

For a discretization in N cells, two virtual cells indexed respectively by 0 and $N+1$ can be added for the upstream and downstream boundary conditions. In this situation, the interfaces are numbered from 0 to N, interface i being the leaving interface of cell i. If the boundary conditions are given in the form of the density signals $\rho_0[k]$ and $\rho_{N+1}[k]$, respectively for the upstream and downstream boundaries, then the numerical fluxes at these interfaces are given by

$$\Phi_1^+[k] = \min\left\{v_1\rho_0[k],\ S_1[k]\right\} = \min\left\{v_1\rho_0[k],\ w_i(\bar{\rho}_1 - \rho_1[k]),\ \bar{\Phi}_1\right\} \tag{8.1.10}$$

and

$$\Phi_N^+[k] = \min\left\{D_N[k],\ w_N(\bar{\rho}_N - \rho_{N+1}[k])\right\} = \min\left\{v_N\rho_N[k],\ w_N(\bar{\rho}_N - \rho_{N+1}[k]),\ \bar{\Phi}_N\right\} \tag{8.1.11}$$

Note that we assumed in (8.1.10) and (8.1.11) that the fundamental diagram parameters are the same in the virtual boundary cells and in the neighboring cells, which is reasonable. The possible values of $\alpha_0[k]$ at the upstream boundary are $\mathbf{F}$, $\mathbf{C}$ and $\mathbf{D_s}$ whereas the possible values of $\alpha_{N+1}[k]$ at the downstream boundary are $\mathbf{F}$, $\mathbf{C}$ and $\mathbf{D_d}$.

We now turn to the piecewise affine formulation of the discretized model in the inhomogeneous case. To do so, the onramp flows $r_i[k]$ will be assumed to be control signals as the targeted application is ramp metering. On the other hand, the offramp flows $s_i[k]$ and the boundary signals $\rho_0[k]$ and $\rho_N[k]$ will be considered as exogenous signals possibly subject to measurement or prediction errors. To ease the writing of the different involved matrices, let define the following describing functions:

- $\mathbf{F}(\alpha) = 1$ when $\alpha = \mathbf{F}$ and 0 otherwise,
- $\mathbf{C}(\alpha) = 1$ when $\alpha = \mathbf{C}$ and 0 otherwise,
- $\mathbf{D_d}(\alpha) = 1$ when $\alpha = \mathbf{D_d}$ and 0 otherwise,
- $\mathbf{D_s}(\alpha) = 1$ when $\alpha = \mathbf{D_s}$ and 0 otherwise.

With these definitions, combining (8.1.3), (8.1.8) and (8.1.9) gives for the inner cells indexed by $i = 2, ..., N-1$

$$\begin{aligned}
\rho_i[k+1] = \rho_i[k] &+ \mathbf{F}(\alpha_{i-1}[k])\Delta_i v_{i-1}\rho_{i-1}[k] + \mathbf{F}(\alpha_{i-1}[k])\Delta_i r_{i-1}[k] - \mathbf{F}(\alpha_{i-1}[k])\Delta_i s_{i-1}[k] \\
&+ \mathbf{C}(\alpha_{i-1}[k])\Delta_i w_i(\bar{\rho}_i - \rho_i[k]) + \mathbf{D_d}(\alpha_{i-1}[k])\Delta_i\bar{\Phi}_{i-1} + \mathbf{D_d}(\alpha_{i-1}[k])\Delta_i r_{i-1}[k] \\
&- \mathbf{D_d}(\alpha_{i-1}[k])\Delta_i s_{i-1}[k] + \mathbf{D_s}(\alpha_{i-1}[k])\Delta_i\bar{\Phi}_i - \mathbf{F}(\alpha_i[k])\Delta_i v_i\rho_i[k] \\
&- \mathbf{C}(\alpha_i[k])\Delta_i w_{i+1}(\bar{\rho}_{i+1} - \rho_{i+1}[k]) + \mathbf{C}(\alpha_i[k])\Delta_i r_i[k] - \mathbf{C}(\alpha_i[k])\Delta_i s_i[k] \\
&- \mathbf{D_d}(\alpha_i[k])\Delta_i\bar{\Phi}_i - \mathbf{D_s}(\alpha_i[k])\Delta_i\bar{\Phi}_{i+1} + \mathbf{D_s}(\alpha_i[k])\Delta_i r_i[k] \\
&- \mathbf{D_s}(\alpha_i[k])\Delta_i s_i[k]
\end{aligned}$$

Which can be rearranged in the vector formulation

$$\begin{aligned}
\rho_i[k+1] = & \\
& \Big[\mathbf{F}(\alpha_{i-1}[k])\Delta_i v_{i-1}\Big|1-\mathbf{C}(\alpha_{i-1}[k])\Delta_i w_i-\mathbf{F}(\alpha_i[k])\Delta_i v_i\Big|\mathbf{C}(\alpha_i[k])\Delta_i w_{i+1}\Big]\begin{bmatrix}\rho_{i-1}[k]\\ \rho_i[k]\\ \rho_{i+1}[k]\end{bmatrix} \\
& +\Big[\mathbf{F}(\alpha_{i-1}[k])\Delta_i+\mathbf{D_d}(\alpha_{i-1}[k])\Delta_i\Big|\mathbf{C}(\alpha_i[k])\Delta_i+\mathbf{D_s}(\alpha_i[k])\Delta_i\Big]\begin{bmatrix}r_{i-1}[k]\\ r_i[k]\end{bmatrix} \\
& +\Big[-\mathbf{F}(\alpha_{i-1}[k])\Delta_i-\mathbf{D_d}(\alpha_{i-1}[k])\Delta_i\Big|-\mathbf{C}(\alpha_i[k])\Delta_i-\mathbf{D_s}(\alpha_i[k])\Delta_i\Big]\begin{bmatrix}s_{i-1}[k]\\ s_i[k]\end{bmatrix} \\
& +\mathbf{C}(\alpha_{i-1}[k])\Delta_i w_i\bar{\rho}_i-\mathbf{C}(\alpha_i[k])\Delta_i w_{i+1}\bar{\rho}_{i+1}+\mathbf{D_d}(\alpha_{i-1}[k])\Delta_i\bar{\Phi}_{i-1} \\
& \qquad +\big(\mathbf{D_s}(\alpha_{i-1}[k])-\mathbf{D_d}(\alpha_i[k])\big)\Delta_i\bar{\Phi}_i-\mathbf{D_s}(\alpha_i[k])\Delta_i\bar{\Phi}_{i+1}
\end{aligned}$$

This formulation is slightly modified for the upstream boundary $i=1$ where we have

$$\begin{aligned}
\rho_1[k+1] = & \\
& \Big[1-\mathbf{C}(\alpha_0[k])\Delta_1 w_1-\mathbf{F}(\alpha_1[k])\Delta_1 v_1\Big|\mathbf{C}(\alpha_1[k])\Delta_1 w_2\Big]\begin{bmatrix}\rho_1[k]\\ \rho_2[k]\end{bmatrix} \\
& +\Big[\mathbf{C}(\alpha_1[k])\Delta_1+\mathbf{D_s}(\alpha_1[k])\Delta_1\Big]\Big[r_1[k]\Big] \\
& +\Big[-\mathbf{C}(\alpha_1[k])\Delta_1-\mathbf{D_s}(\alpha_1[k])\Delta_1\Big]\Big[s_1[k]\Big] \\
& +\Big[\mathbf{F}(\alpha_0[k])\Delta_1 v_1\Big]\Big[\rho_0[k]\Big] \\
& +\mathbf{C}(\alpha_0[k])\Delta_1 w_1\bar{\rho}_1-\mathbf{C}(\alpha_1[k])\Delta_1 w_2\bar{\rho}_2+\big(\mathbf{D_s}(\alpha_0[k])-\mathbf{D_d}(\alpha_1[k])\big)\Delta_1\bar{\Phi}_1-\mathbf{D_s}(\alpha_1[k])\Delta_1\bar{\Phi}_2
\end{aligned}$$

Similarly, for the downstream boundary $i=N$, we have

$$\begin{aligned}
\rho_N[k+1] = & \\
& \Big[\mathbf{F}(\alpha_{N-1}[k])\Delta_N v_{N-1}\Big|1-\mathbf{C}(\alpha_{N-1}[k])\Delta_N w_N-\mathbf{F}(\alpha_N[k])\Delta_N v_N\Big]\begin{bmatrix}\rho_{N-1}[k]\\ \rho_N[k]\end{bmatrix} \\
& +\Big[\mathbf{F}(\alpha_{N-1}[k])\Delta_N+\mathbf{D_d}(\alpha_{N-1}[k])\Delta_N\Big]\Big[r_{N-1}[k]\Big] \\
& +\Big[-\mathbf{F}(\alpha_{N-1}[k])\Delta_N-\mathbf{D_d}(\alpha_{N-1}[k])\Delta_N\Big]\Big[s_{N-1}[k]\Big] \\
& +\Big[\mathbf{C}(\alpha_N[k])\Delta_N w_N\Big]\Big[\rho_{N+1}[k]\Big] \\
& +\mathbf{C}(\alpha_{N-1}[k])\Delta_N w_N\bar{\rho}_N-\mathbf{C}(\alpha_N[k])\Delta_N w_N\bar{\rho}_N+\mathbf{D_d}(\alpha_{N-1}[k])\Delta_N\bar{\Phi}_{N-1} \\
& \qquad +\big(\mathbf{D_s}(\alpha_{N-1}[k])-\mathbf{D_d}(\alpha_N[k])\big)\Delta_N\bar{\Phi}_N
\end{aligned}$$

Using the above equations, the discretized LWR model can be written in the form of

the following piecewise affine system

$$\begin{cases} \rho_{k+1} &= A_{\alpha_k}\rho_k + B_{\alpha_k}u_k + W_{\alpha_k}w_k + a_{\alpha_k} \\ \alpha_k &= g(\rho_k, u_k, w_k) \end{cases} \tag{8.1.12}$$

where $\rho_k = (\rho_1[k], ..., \rho_N[k])$ is the density state, $u_k = (r_1[k], ..., r_m[k])$ is the control variables consisting of the metered onramp flows and $w_k = (\rho_0[k], s_1[k], ..., s_{N-1}[k], \rho_{N+1}[k])$ is a vector of measured exogenous signals composed of the boundary densities and the offramp flows. $\alpha_k = (\alpha_0[k], ..., \alpha_{N+1}[k])$ is the concatenated discrete state and is computed according to the switching rule $g(\rho_k, u_k, w_k)$ which basically select which entry should be selected in the minimum formulas (8.1.8) and (8.1.9). The matrices A_{α_k}, B_{α_k}, W_{α_k} and the vector a_{α_k} define the state space representation for the evolution of the continuous variable $\rho[k]$, which is valid for the time interval k to $k+1$. One interest of the PWA formulation is that an explicit formulation of the involved data A_{α_k}, B_{α_k}, W_{α_k} and a_{α_k} can be computed a priori as soon as the subset of α_k that may occur is known. In practice, the possible value taken by α_k depends on the waves allowed to propagate in the freeway section. As possible scenarios are often reduced for a specific section, the set of possible α_k can often be reduced to a reasonable number of discrete states. In this situation, the involved matrix data can be computed a priori and automatically thanks to the vector formulations presented above. Explicit formulations of these data will be given later in the case of the local ramp metering application. The PWA formulation (8.1.12) is extensively used in the next section to perform the controller design.

8.2 Feedback Controller Designs

As shown in the previous section, one-dimensional scalar conservation laws can be put, after discretization and piecewise linearization, in the form of the piecewise affine system given in Equation (8.1.12). It can be shown that the discrete system (8.1.12) is always open-loop stable for the LWR model as it has eigenvalues smaller or equal to 1. Moreover, some states are not controllable or observable due to the transport phenomenon and the partial actuation and measurement. Such phenomena was already mentioned in [Munoz et al., 2003] and [Munoz et al., 2006].

8.2.1 Background on PWA system stabilization

Let consider the PWA system with state-space equation

$$\begin{cases} \rho_{k+1} = A_{\alpha_k}\rho_k + B_{\alpha_k}u_k + W_{\alpha_k}w_k + a_{\alpha_k} \\ \alpha_k = g(\rho_k, u_k, w_k) \\ \rho_{k=0} = \rho_0 \quad \text{and} \quad \alpha_{k=0} = \alpha_0 \end{cases} \tag{8.2.1}$$

where $\alpha_k \in \mathcal{I} = \{1, ..., h\}$ is the piecewise constant discrete state relabeled for notational convenience, $\rho_k \in \mathbb{R}^n$ the continuous state, $u_k \in \mathbb{R}^m$ the control variable and $w_k \in \mathbb{R}^p$

an exogenous signal subject to perturbations. The discrete state α_k depends on the switching rule $g(\rho_k, u_k, w_k)$ that sets the active matrices

$$A_{\alpha_k} \in \{A_1, ..., A_h\},\ B_{\alpha_k} \in \{B_1, ..., B_h\},\ W_{\alpha_k} \in \{W_1, ..., W_h\},\ a_{\alpha_k} \in \{a_1, ..., a_h\}$$

Let consider a predefined reference $\bar{u}_k$ computed for instance by the optimal control strategies presented in a previous chapter. This control reference, along with the estimated disturbances $\bar{w}_k$, gives rise through the freeway dynamics (8.2.1) to the density reference $\bar{\rho}_k$ which we would like to track. This reference design leads to an a priori switching sequence denoted $\bar{\alpha}_k$. With $(\bar{u}_k, \bar{\rho}_k, \bar{w}_k)$ known in advance, we make the somewhat strong assumption that the reference and actual switching sequences are identical, i.e. $\alpha_k = \bar{\alpha}_k$, which leads to the continuous state error dynamics

$$\tilde{\rho}_{k+1} = A_{\alpha_k}\tilde{\rho}_k + B_{\alpha_k}\tilde{u}_k + W_{\alpha_k}\tilde{w}_k \tag{8.2.2}$$

with $\tilde{\rho}_k = \rho_k - \bar{\rho}_k$, $\tilde{u}_k = u_k - \bar{u}_k$ and $\tilde{w}_k = w_k - \bar{w}_k$. Let consider the problem of designing a switched piecewise linear full state controller of the form $\tilde{u}_k = K_{\alpha_k}\tilde{\rho}_k$. Plugging this expression into (8.2.2) gives, with $\Pi_{\alpha_k} = A_{\alpha_k} + B_{\alpha_k}K_{\alpha_k}$, the following closed loop equation

$$\begin{cases} \tilde{\rho}_{k+1} = \Pi_{\alpha_k}\tilde{\rho}_k + W_{\alpha_k}\tilde{w}_k \\ \alpha_k = g(\bar{\rho}_k + \tilde{\rho}_k, \bar{u}_k + \tilde{u}_k, \bar{w}_k + \tilde{w}_k) \end{cases} \tag{8.2.3}$$

So Equation (8.2.3) is composed of a switched linear system along with a discrete state α_k that is assumed to be measured in real time.

Before going further, let first come back to the identical sequence assumption $\alpha_k = \bar{\alpha}_k$ and see what would happen if $\alpha_k \neq \bar{\alpha}_k$. As $\bar{\alpha}_k$ is computed a priori, this situation may happen for instance if the control action does not manage to follow the reference quickly enough or if a strong disturbance enters in the system. As will be seen later, α_k being available in real time, the controller K_{α_k} that applies at time k is a stabilizing controller for subsystem $(A_{\alpha_k}, B_{\alpha_k}, W_{\alpha_k}, a_{\alpha_k})$. Moreover, the family of controllers K_i is designed such that the switched controller gain K_{α_k} ensure the stability of the closed loop system when $\alpha_{k+1} \neq \alpha_k$. Now, is $\alpha_k \neq \bar{\alpha}_k$ then we have

$$\begin{aligned} \bar{\rho}_{k+1} &= A_{\bar{\alpha}_k}\bar{\rho}_k + B_{\bar{\alpha}_k}\bar{u}_k + W_{\bar{\alpha}_k}\bar{w}_k + a_{\bar{\alpha}_k} \\ \rho_{k+1} &= A_{\alpha_k}\rho_k + B_{\alpha_k}u_k + W_{\alpha_k}w_k + a_{\alpha_k} \end{aligned}$$

which gives

$$\tilde{\rho}_{k+1} = A_{\alpha_k}\rho_k - A_{\bar{\alpha}_k}\bar{\rho}_k + B_{\alpha_k}u_k - B_{\bar{\alpha}_k}\bar{u}_k + W_{\alpha_k}w_k - W_{\bar{\alpha}_k}\bar{w}_k + a_{\alpha_k} - \bar{a}_{\alpha_k}$$

Adding $(A_{\alpha_k} - A_{\alpha_k})\bar{\rho}_k + (B_{\alpha_k} - B_{\alpha_k})\bar{u}_k + (W_{\alpha_k} - W_{\alpha_k})\bar{w}_k$ to the right hand side gives

$$\tilde{\rho}_{k+1} = A_{\alpha_k}\tilde{\rho}_k + B_{\alpha_k}\tilde{u}_k + W_{\alpha_k}\tilde{w}_k + (A_{\alpha_k}\bar{\rho}_k + B_{\alpha_k}\bar{u}_k + W_{\alpha_k}\bar{w}_k + a_{\alpha_k} - \bar{a}_{\alpha_k})$$

We thus obtain a formulation similar to Equation (8.2.3) with an additional perturbation term that depends on the current configuration α_k and the predefined reference signals

$(\bar{\rho}_k, \bar{u}_k, \bar{w}_k, \bar{a}_{\alpha_k})$. If we can design a set of controller gains K_i such that (8.2.3) is asymptotically stable, then the additional perturbation entering the above equation should not destabilize the system if it is nonzero on a finite time interval.

We now give some definition for passive systems. The discrete-time PWA system (8.2.3) is said to be strictly passive with supply rate $W : \mathbb{R}^q \times \mathbb{R}^p \to \mathbb{R}$ if there exists a non negative storage function $V : \mathcal{I} \times \mathbb{R}^n \to \mathbb{R}$ with $V(\cdot, 0) = 0$ such that the following dissipation inequality holds

$$\forall\ w,\ \forall\ k,\quad \Delta V_k = V_{k+1} - V_k < W(\tilde{\rho}_k, \tilde{w}_k) \tag{8.2.4}$$

where $V_k = V(\alpha_k, \tilde{\rho}_k)$, whose an equivalent useful formulation is

$$\forall\ w,\ \forall\ N,\ \forall\ x_0,\quad V_{N+1} - V_0 < \sum_{k=0}^{N} W(\tilde{\rho}_k, \tilde{w}_k)$$

The following supply rates are classical and define different control objectives

$$\begin{aligned} W_\infty &= \gamma^2 \tilde{w}_k^T \tilde{w}_k - \tilde{\rho}_k^T \tilde{\rho}_k \\ W_{G2} &= \tilde{w}_k^T \tilde{w}_k \\ W_{LQ} = W_2 &= -\tilde{\rho}_k^T Q \tilde{\rho}_k \end{aligned}$$

W_∞ defines the $\mathcal{H}_\infty$ perturbation attenuation criteria, W_{G2} the so-called generalized $\mathcal{H}_2$ performance criteria and W_{LQ} the LQ performance criteria, whose special case $Q = I$ corresponds to the $\mathcal{H}_2$ norm.

For PWA systems, a candidate storage function that depends only on the internal states α_k and $\tilde{\rho}_k$ is the piecewise quadratic (PWQ) Lyapunov function

$$V_k = V(\alpha_k, \tilde{\rho}_k) = \tilde{\rho}_k^T P_{\alpha_k} \tilde{\rho}_k \quad \text{with} \quad P_i > 0 \text{ and } P_i^T = P_i$$

where the matrices P_i are considered symmetric without loss of generality. The decrease $\Delta V_k = V_{k+1} - V_k$ in the storage function along the system trajectory then writes

$$\begin{aligned} \Delta V_k &= V(\alpha_{k+1}, \tilde{\rho}_{k+1}) - V(\alpha_k, \tilde{\rho}_k) \\ &= \tilde{\rho}_{k+1}^T P_{\alpha_{k+1}} \tilde{\rho}_{k+1} - \tilde{\rho}_k^T P_{\alpha_k} \tilde{\rho}_k \\ &= (\tilde{\rho}_k^T \Pi_{\alpha_k}^T + \tilde{w}_k^T W_{\alpha_k}^T) P_{\alpha_{k+1}} (\Pi_{\alpha_k} \tilde{\rho}_k + W_{\alpha_k} \tilde{w}_k) - \tilde{\rho}_k^T P_{\alpha_k} \tilde{\rho}_k \\ &= \begin{pmatrix} \tilde{\rho}_k \\ \tilde{w}_k \end{pmatrix}^T \begin{pmatrix} \Pi_{\alpha_k}^T P_{\alpha_{k+1}} \Pi_{\alpha_k} - P_{\alpha_k} & \Pi_{\alpha_k}^T P_{\alpha_{k+1}} W_{\alpha_k} \\ W_{\alpha_k}^T P_{\alpha_{k+1}} \Pi_{\alpha_k} & W_{\alpha_k}^T P_{\alpha_{k+1}} W_{\alpha_k} \end{pmatrix} \begin{pmatrix} \tilde{\rho}_k \\ \tilde{w}_k \end{pmatrix} \end{aligned} \tag{8.2.5}$$

which simplifies without uncertainties, i.e. $\tilde{w}_k = 0$ to

$$\Delta V_k = \tilde{\rho}_k^T (\Pi_{\alpha_k}^T P_{\alpha_{k+1}} \Pi_{\alpha_k} - P_{\alpha_k}) \tilde{\rho}_k$$

We can now proceed to the controller designs.

8.2.2 State Feedback Stabilization Without Uncertainties

A sufficient condition of global stability for the PWA system (8.2.3) without uncertainties, i.e. $\tilde{w}_k = 0$, is that $\Delta V(\alpha_k, \tilde{\rho}_k)$ is negative definite along the system trajectories. Considering all the possible discrete state trajectories in Equation (8.2.5), i.e. either $\alpha_{k+1} = \alpha_k$ or $\alpha_{k+1} \neq \alpha_k$ when a transition occurs, global stability is obtained if one can find a set of symmetric positive definite matrices P_i and constant vector gains K_i such that the following set of LMIs are satisfied

$$P_i - \Pi_i^T P_j \Pi_i > 0 \quad , \quad \forall\, i \to j \tag{8.2.6}$$

Such set of matrices can be found with the following theorem.

Theorem 8.2.1 *If there exists symmetric positive definite matrices $Q_i = Q_i^T > 0$ and matrices U_i of appropriate dimension satisfying the set of Linear Matrix Inequalities (LMI)*

$$\begin{pmatrix} Q_i & \star \\ A_i Q_i + B_i U_i & Q_j \end{pmatrix} > 0 \qquad \forall\, (i,j) \in \mathcal{T} \tag{8.2.7}$$

for all possible transitions $\mathcal{T}$ of the discrete state α_k then the state $\tilde{\rho}$ converges globally towards the origin with the piecewise linear static feedback gains $K_i = U_i Q_i^{-1}$.

Proof. We multiply by P_i^{-1} from the left and right in (8.2.6) to get by congruence

$$P_i^{-1} - P_i^{-1} \Pi_i^T P_j \Pi_i P_i^{-1} > 0$$

which develops as

$$P_i^{-1} - P_i^{-1}(A_i^T + K_i^T B_i^T) P_j (A_i + B_i K_i) P_i^{-1} > 0$$

Making the change of variables $Q_i = P_i^{-1}$ and $U_i = K_i P_i^{-1}$, we get with $(P_i^{-1})^T = P_i^{-1}$

$$Q_i - (Q_i A_i^T + U_i^T B_i^T) Q_j^{-1} (A_i Q_i + B_i U_i) > 0$$

The schur complement finally gives the theorem. □

The feasibility problem for the set of LMIs (8.2.7) requires all the pairs (A_i, B_i) to be stabilisable and can be solved efficiently with the Matlab LMI toolbox. Note that the size of the LMI constraint (8.2.7) depends directly on the number of transitions (i,j) considered in the set $\mathcal{T}$. If we may be tempted to choose $\mathcal{T} = \mathcal{I} \times \mathcal{I}$ for its exhaustibility, diminishing the cardinal of $\mathcal{T}$ reduces the size of the problem and thus its complexity along with its conservativeness. Such a reduction is possible when the PWA system comes from the discretization of a conservation law as we known that only some waves are allowed in these equations, and thus some transitions (i,j) in $\mathcal{T}$, due to the entropy condition. Equation (8.2.7) is a feasibility problem and may well have no solution, a problem shared by many LMI based design methodologies. Moreover, (8.2.7) does not ensure any performance for the closed loop system besides stability. This issues will be treated later with the $\mathcal{H}_\infty$ and the LQ designs.

8.2.3 Integral Action Without Uncertainties

Integral action for disturbance rejection is obtained setting

$$\tilde{u}_{k+1} = \tilde{u}_k + hv_k \quad \text{and} \quad v_k = K_{\alpha_k}\tilde{\rho}_k$$

with h a free design parameter. The extended system becomes

$$\begin{pmatrix}\tilde{\rho}\\ \tilde{u}\end{pmatrix}_{k+1} = \begin{pmatrix}A_{\alpha_k} & B_{\alpha_k}\\ 0 & I\end{pmatrix}\begin{pmatrix}\tilde{\rho}\\ \tilde{u}\end{pmatrix}_k + \begin{pmatrix}0\\ hI\end{pmatrix}v_k$$

Theorem 8.2.1 can be used directly, replacing

$$A_i \text{ by } \begin{pmatrix}A_i & B_i\\ 0 & I\end{pmatrix} \text{ and } B_i \text{ by } \begin{pmatrix}0\\ hI\end{pmatrix}$$

8.2.4 $\mathcal{H}_\infty$ synthesis for perturbation attenuation

In this section, some robustness requirements are added to the control problem. We consider here an $\mathcal{H}_\infty$ problem which consists in minimizing or bounding to a predefined value γ the system gain between $||\tilde{w}_k||_2$ and $||\tilde{\rho}_k||_2$ so that the influence of the exogenous signal w on the state ρ is controlled.

The supply rate W_∞ can be written in the matrix form

$$\begin{aligned}W_\infty(\tilde{\rho}_k, \tilde{w}_k) &= \gamma^2\tilde{w}_k^T\tilde{w}_k - \tilde{\rho}_k^T\tilde{\rho}_k\\ &= \begin{pmatrix}\tilde{\rho}_k\\ \tilde{w}_k\end{pmatrix}^T\begin{pmatrix}-I & 0\\ 0 & \gamma^2 I\end{pmatrix}\begin{pmatrix}\tilde{\rho}_k\\ \tilde{w}_k\end{pmatrix}\end{aligned}$$

Applying the S-procedure to the passivity inequality (8.2.4) with the Lyapunov function difference with uncertainties (8.2.5), we get the classical Bounded Real Lemma which states that $||\tilde{\rho}_k||_2 < \gamma||\tilde{w}_k||_2$ is equivalent to

$$\begin{pmatrix}\Pi_{\alpha_k}^T P_{\alpha_{k+1}}\Pi_{\alpha_k} - P_{\alpha_k} + I & \Pi_{\alpha_k}^T P_{\alpha_{k+1}} W_{\alpha_k}\\ W_{\alpha_k}^T P_{\alpha_{k+1}}\Pi_{\alpha_k} & W_{\alpha_k}^T P_{\alpha_{k+1}} W_{\alpha_k} - \gamma^2 I\end{pmatrix} < 0 \tag{8.2.8}$$

We have the following theorem for the $\mathcal{H}_\infty$ synthesis.

Theorem 8.2.2 *The attenuation $||\tilde{\rho}_k||_2 < \gamma||\tilde{w}_k||_2$ is realized by the family of static feedback gains K_i for all signal $\tilde{w}_k$ in l_2 if one can find matrices $Q_i = Q_i^T > 0$ and R_i of suitable dimension such that*

$$\begin{pmatrix}Q_i & \star & \star & \star\\ 0 & \gamma^2 I & \star & \star\\ A_iQ_i + B_iR_i & W_i & Q_j & \star\\ Q_i & 0 & 0 & I\end{pmatrix} > 0 \quad \forall\ (i,j) \in \mathcal{T}$$

with $\mathcal{T}$ the set of possible transitions. The feedback gains are given by $K_i = U_iQ_i^{-1}$.

Proof. By congruence of (8.2.8) with $diag(P_k^{-1}, I)$ and by setting $Q_k = P_k^{-1}$, we have

$$\begin{pmatrix} Q_k\Pi_k^T P_{k+1}\Pi_k Q_k - Q_k + Q_k^T Q_k & Q_k\Pi_k^T P_{k+1} W_k \\ W_k^T P_{k+1}\Pi_k Q_k & W_k^T P_{k+1} W_k - \gamma^2 I \end{pmatrix} < 0$$

which can be rewritten

$$-\begin{pmatrix} \Pi_k Q_k & W_k \\ Q_k & 0 \end{pmatrix}^T \begin{pmatrix} P_{k+1} & 0 \\ 0 & I \end{pmatrix} \begin{pmatrix} \Pi_k Q_k & W_k \\ Q_k & 0 \end{pmatrix} + \begin{pmatrix} Q_k & 0 \\ 0 & \gamma^2 I \end{pmatrix} > 0$$

The Schur complement Lemma then gives the equivalent LMI

$$\begin{pmatrix} Q_k & 0 & Q_k\Pi_k^T & Q_k \\ 0 & \gamma^2 I & W_k^T & 0 \\ \Pi_k Q_k & W_k & Q_{k+1} & 0 \\ Q_k & 0 & 0 & I \end{pmatrix} > 0$$

Setting $U_k = K_k Q_k$, the nonlinear term becomes $\Pi_k Q_k = A_k Q_k + B_k U_k$, giving the theorem. □

8.2.5 Generalized $\mathcal{H}_2$

The generalized $\mathcal{H}_2$ norm $\sup \frac{||z||_{l_\infty}}{||w||_{l_2}}$ can be bounded by γ if we can find a Lyapunov function such that

$$\begin{cases} \Delta V_k < \tilde{w}_k^T \tilde{w}_k \\ \tilde{\rho}_k^T \tilde{\rho}_k < \gamma V_k \end{cases} \tag{8.2.9}$$

which leads by summation on $k = 0, ..., N$ to the inequality $V_{N+1} - V_0 < ||\tilde{w}||_{l_2(0,N)}$. Assuming that $V_0 = 0$ and using $\tilde{\rho}_{N+1}^T \tilde{\rho}_{N+1} < \gamma V_{N+1}$, we get

$$\tilde{\rho}_{N+1}^T \tilde{\rho}_{N+1} < \gamma ||w||_{l_2(0,N)}$$

Equation (8.2.9) can be transformed to the set of LMIs

$$\begin{pmatrix} P & C^T \\ C & \gamma I \end{pmatrix} > 0 \qquad \begin{pmatrix} -Q_j & \star & \star \\ A_j Q_j + B_i Y_j & -Q_i & \star \\ 0 & B_j^T & -I \end{pmatrix} < 0 \qquad \text{for all } (i,j) \in \mathcal{T}$$

The controller gains are then given by $K_i = Y_i Q_i^{-1}$.

8.2.6 Guaranteed Cost LQ Control without Uncertainties

In this section, an LMI condition is provided to synthesize a static state feedback controller for the unperturbed system that guarantees a upper bound for the LQ cost functional

$$J = \sum_{k=0}^{\infty} \tilde{\rho}_k^T Q \tilde{\rho}_k + \tilde{u}_k^T R \tilde{u}_k \leq J_m$$

where Q and R are positive definite symmetric matrices, R weighting the control energy. If we can find a control Lyapunov function V_k that satisfies

$$\Delta V_k = V_{k+1} - V_k < -(\tilde{\rho}_k^T Q \tilde{\rho}_k + \tilde{u}_k^T R \tilde{u}_k)$$

then simple summation for $k = 0, ..., \infty$ gives with $V_\infty = 0$

$$J < V_0$$

Considering again a piecewise quadratic Lyapunov function $V_k = \tilde{\rho}_k^T P_{\alpha_k} \tilde{\rho}_k$, then ΔV_k writes for the discrete state transition $i \to j$

$$\Delta V_k = \tilde{\rho}_k^T (\Pi_i^T P_j \Pi_i - P_i) \rho_k < \rho_k^T (-Q - K_i^T R K_i) \tilde{\rho}_k$$

which is equivalent to the matrix inequality

$$\Pi_i^T P_j \Pi_i - P_i + Q + K_i^T R K_i < 0$$

Linearization is then done as following. Left and right multiplying by $P_i^{-1} = S_i$ gives

$$S_i \Pi_i^T P_j \Pi_i S_i - S_i + S_i Q S_i + S_i K_i^T R K_i S_i < 0$$

which rewrites

$$S_i - \begin{pmatrix} \Pi_i S_i \\ S_i \\ K_i S_i \end{pmatrix}^T \begin{pmatrix} P_j & \star & \star \\ 0 & Q & \star \\ 0 & 0 & R \end{pmatrix} \begin{pmatrix} \Pi_i S_i \\ S_i \\ K_i S_i \end{pmatrix} > 0$$

Using the Schur complement with the linearizing change of variables

$$\Pi_i S_i = A_i S_i + B_i K_i S_i = A_i S_i + B_i U_i$$

we get

$$\begin{pmatrix} S_i & \star & \star & \star \\ A_i S_i + B_i U_i & S_j & \star & \star \\ S_i & 0 & Q^{-1} & \star \\ U_i & 0 & 0 & R^{-1} \end{pmatrix} \quad \text{for all } (i,j) \in \mathcal{T}$$

Knowing the initial condition $\tilde{\rho}_I$, the upper bound J_m can be optimized by solving the problem $\min \tilde{\rho}_I^T P_{\alpha_0} \tilde{\rho}_I$, which is a linear cost function, subject to the above set of LMIs.

8.2.7 Strategies to reduce the discrete state space

One drawback of the proposed approach is that the set of possible transitions $\mathcal{T}^N$ for a problem with N cells is usually very large, even for n small. Indeed, there are $N+1$ interfaces for N cells, each of them being able to take the 3 possible values **F**, **C** and **D** if there is no situations where **D** should be decomposed in $\mathbf{D}_d$ and $\mathbf{D}_s$. We thus have a cardinal $\text{Card}(\mathcal{T}^N) = 3^{N+1}$ which grows exponentially with N, making the approach untractable even for reasonable values of N. The following table illustrates this unmanageable increase of complexity:

N	Card($\mathcal{T}^N$)
1	9
2	27
3	81
4	243
5	729
6	2187
7	6561

Nevertheless, this complexity can be largely decreased by using the following arguments:

- First triangular fundamental diagrams are often used for freeway models as in [Munoz et al., 2003; Munoz et al., 2006]. In doing so, all interfaces without a ramp have only 2 possible states called free for **F** and congested to **C**. Triangular fundamental diagrams thus reduce the size of Card($\mathcal{T}^N$) or allow for more cells in homogeneous links for the same level of complexity.

- Using the entropy condition for the LWR model, only some waves are allowed which restrains the set of possible transitions from Card($\mathcal{T}^N$) to Card($\mathcal{T}_R^N$) $<$ Card($\mathcal{T}^N$) with $\mathcal{T}_R^N$ the set of realizable transitions. If this method enable a sharp reduction of the number of possibilities, this set $\mathcal{T}_R^N$ is difficult to compute a priori when several onramps and offramps are present.

- To overcome the difficulty of getting an exhaustive description of $\mathcal{T}_R^N$, we can restrict to a specific scenario. Though quite restrictive, this approach is reasonable as the traffic evolution is often the same on a given freeway section, except in the case of unpredictable situtations like an accident. This approach leads to a set $\mathcal{T}_S^N$ with Card($\mathcal{T}_S^N$) $<$ Card($\mathcal{T}_R^N$).

- The last possibilities is to restrict the time horizon on which the feedback controller should stabilize the traffic, leading to a set of possible transitions $\mathcal{T}_M^N$ with M the time steps taken into account. Doing so reduces dramatically the size of the sets Card($\mathcal{T}_R^N$) and Card($\mathcal{T}_S^N$) but requires to solve some sets of LMI online before each new time horizon.

8.3 Application to ramp metering

Based on the theory presented in the previous sections, we propose a feedback ramp metering strategy which is potentially more effective than local version of [Papageorgiou et al., 1997] as more sensor data are used and no a-priori controller structure is given.

8.3.1 Traffic Model used for the experiment

We propose here to use a simple model where the fundamental diagram is assumed to be triangular. Moreover, the parameters of this flux functions are assumed to be constant along the considered stretch of freeway. By approximating the concave flux function by 2 affine branches as represented on Figure 8.5 the discretized LWR model can be put in the form of a PWA system like Equation (8.1.12) similar to the CTM model proposed in [Daganzo, 1994] and close to the switched model proposed in [Munoz et al., 2003; Munoz et al., 2006]. In the fundamental diagram of Figure 8.5, ρ_m is the maximal density, ϕ_m is the maximal flow, $v > 0$ is the slope for the free flow wave speed and $w < 0$ is the slope for the the congestion wave speed.

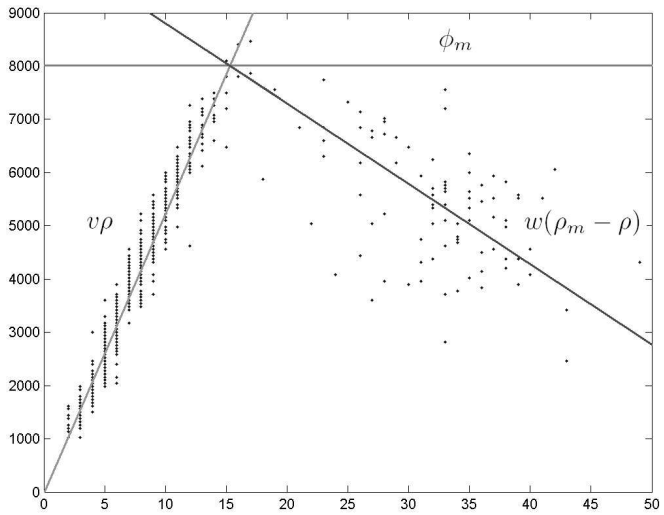

Figure 8.5: Concave fundamental diagram with traffic data from Lyon Est beltway.

8.3.2 Proposed controller structure and study case

The proposed controller structure is presented in Figure 8.6. $\bar{r}$ and $\bar{\rho}$ are respectively the on-ramp flow and density references which are provided by an other method such as the optimization routine proposed in [Jacquet, Canudas de Wit & Koenig, 2005]. The needed measurements in this architecture are the mainlane densities ρ in each cell, the boundary densities $(\rho_{\mathrm{Up}}, \rho_{\mathrm{Do}})$, the exit ratios β and the actual on-ramp flows r. Based on these measurement, the current discrete state α and the current tracking error $\tilde{\rho}$ can be computed and feed to the controller that generates in real time the correction term $\tilde{r}$ leading to the applied metering rates r.

The quantities ρ_{Up}, ρ_{Do} and β are partially known exogenous signals that can be subject to substantial errors. In addition, the freeway model is approximate and its parameters v, w and ρ_m are necessarily uncertain. The control objective is thus to ensure that the regulation $\tilde{\rho} \to 0$ follows some performance criteria and is robust to the various uncertainties present in the control loop. As discussed in the previous sections, a

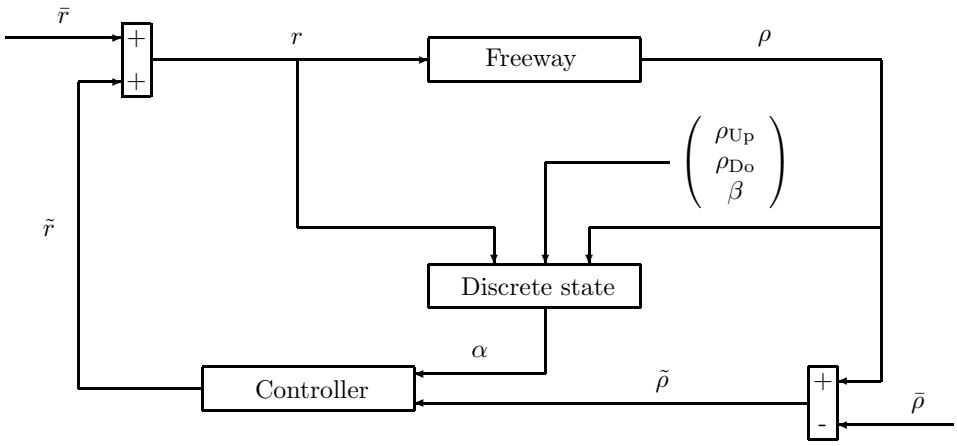

Figure 8.6: Block diagram for controlling a freeway section.

piecewise linear state feedback controller can be used to fulfill this objective. A potential drawback of such approach is the combinatorics implied by the interface discrete state that may lead to very large LMIs that may fail to have a solution or can be untractable.

Let consider as a study case the 2.83 km section of the South-Est beltway of Lyon, France, which is depicted in Figure 8.7. This section is composed of one on-ramp, one off-ramp along with three homogeneous links and is equipped with four inductive mainlane sensors and one sensor for each on and off ramps. As shown in this figure, the velocity time series plotted between 11am and 11pm for the upstream and downstream boundaries can be used to conclude that the only on-ramp present in the section is responsible of the congestion that propagates upstream. Moreover, this pattern appears repeatedly, motivating the use of a ramp metering algorithm in this situation, the goal being to modulate the on-ramp inflow to eliminate or at least reduce the congestion.

Having identified the bottleneck on Lyon's South-Est beltway, the freeway is modelled as a concatenation of 3 homogeneous links interconnected through an on-ramp and an off-ramp. The first link is divided into two cells so that the congestion wave propagation can be observed and the other two links are modelled by a single cell. We obtain a model with 4 cells as represented on 8.8, leading to a 5 state discrete variable $\alpha(k) = (\alpha_0(k), \alpha_1(k), \alpha_2(k), \alpha_3(k), \alpha_4(k))$. The boundary data and the off-ramp flow are provided by the measurements at the corresponding inductive loops. Moreover, all the cell densities are assumed available in the feedback controller design in our simulation.

As mentioned above, the possible discrete state transitions should be identified before the design. The on-ramp responsible of the congestion being on the third interface, the possible transitions are given by

$$(F, F, F, F, F) \rightleftarrows (F, F, D, F, F)$$
$$(F, F, D, F, F) \rightleftarrows (F, C, D, F, F)$$
$$(F, D, C, F, F) \rightleftarrows (D, D, C, F, F)$$

The freeway being initially in free flow, the considered transitions are the only one that

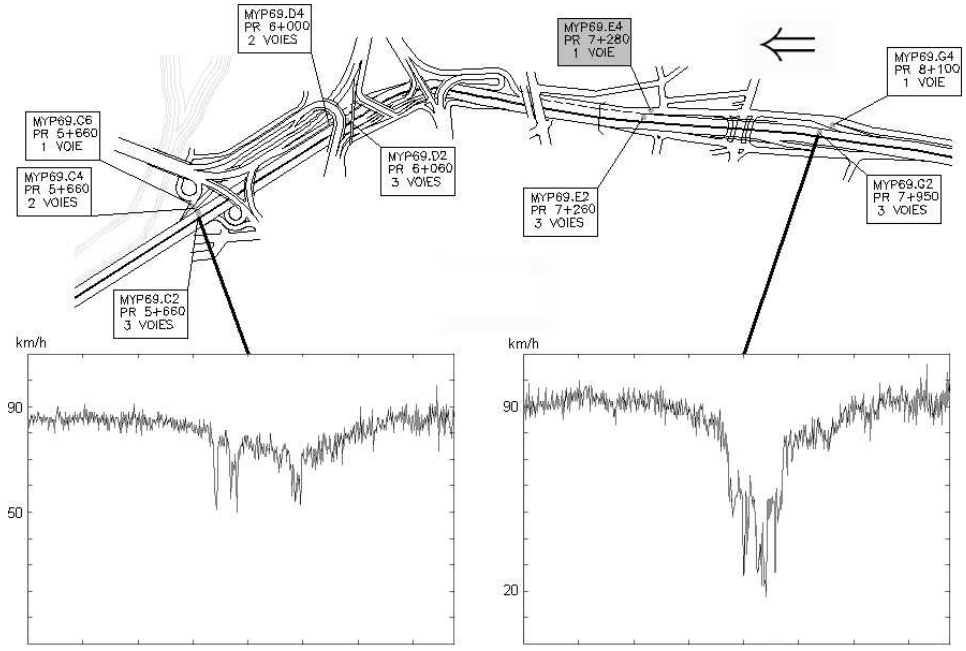

Figure 8.7: Freeway section treated in the example where the arrow indicates the traffic direction and the gray dots the locations of the labelled inductive loops. The plotted velocity time series on 18/10/2005 from 11am and 11pm show that the on-ramp with the shaded label is responsible of the congestion.

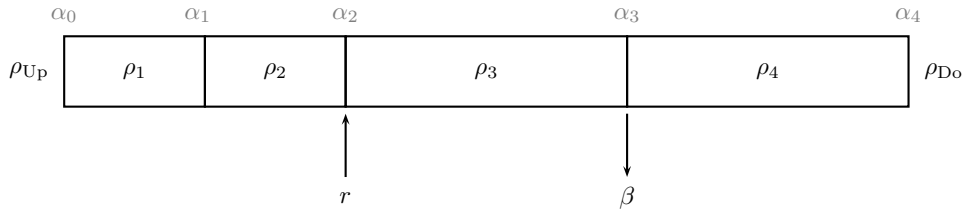

Figure 8.8: Abstracted network for the considered link.

are allowed in the LWR model. For instance, the state space matrices of $FFDFF$ are explicitly given by

$$A(CCDFF) = \begin{pmatrix} 1-w_1c_1 & w_2c_1 & 0 & 0 \\ 0 & 1-w_2c_2 & 0 & 0 \\ 0 & 0 & 1-v_3c_3 & 0 \\ 0 & 0 & v_3c_4 & 1-v_4c_4 \end{pmatrix}$$

$$B(CCDFF) = \begin{pmatrix} 0 \\ c_2 \\ 0 \\ 0 \end{pmatrix} \quad W(CCDFF) = \begin{pmatrix} 0 & 0 & 0 \\ 0 & 0 & 0 \\ 0 & 0 & 0 \\ -c_4 & 0 & 0 \end{pmatrix}$$

$$a(CCDFF) = \begin{pmatrix} c_1 w_1 \rho_{m1} - c_1 w_2 \rho_{m2} \\ c_2 w_2 \rho_{m2} - c_2 \Phi_{m3} \\ c_3 \Phi_{m3} \\ 0 \end{pmatrix}$$

and similar matrices are computed for all of the 4 considered discrete states.

The LMIs for the stabilizing controller have been coded in the Matlab LMI Control Toolbox. These LMIs being feasible for the Lyon beltway study case, we were able to compute the feedback gains that stabilize the freeway error dynamics. The choice of a suitable density reference is an important task that should not be underestimated. Though the critical density corresponds to the maximal flow, it should not be taken as the reference as it may lead to unrealistically large on-ramp queues. Instead, the freeway should be allowed to be partially congested due to the unavoidable excess demand. This objective is met by requiring a minimum on-ramp flow that keeps ramp queues at a reasonable level. The simulations shown below have a minimal on-ramp flow of 1100 veh/h which leads to a maximal queue of around 350 vehicles at the on-ramp.

Figure 8.9 shows the efficiency of the feedback method with a simulation from 3:30pm to 10pm with a congestion from 5:30pm to 8pm. Figure 8.10 shows the demand and the resulting on-ramp queue. As can be expected, reducing the minimum on-ramp flow in the reference increases the peak ramp queue. The computed feedback gains are provided in Figure 8.11 for all discrete states.

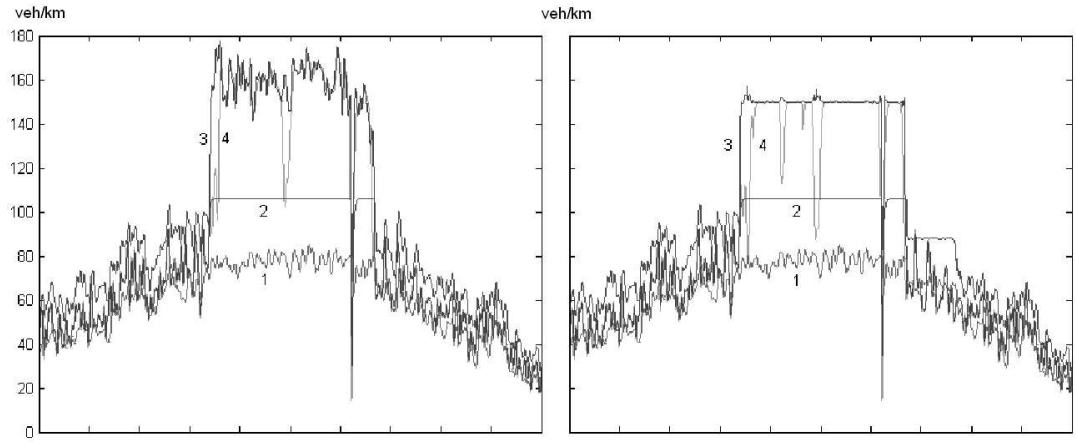

Figure 8.9: Comparison of the density time series at cells 1, 2, 3 and 4 without (left) and with (right) ramp metering when a minimum of 1100 veh/h is required at the on-ramp.

An interesting observation is that the obtained feedback gains are local, implying that local algorithm such as ALINEA [Papageorgiou et al., 1991] are sufficient when a single on-ramp is metered. Moreover, as the dominant coefficient moves from the cell downstream of the ramp to the one upstream of it depending on the discrete state, a switched version of ALINEA as the one proposed in [Sun & Horowitz, 2005] should be considered in local ramp metering strategies. It is a remarkable fact to arrive to this

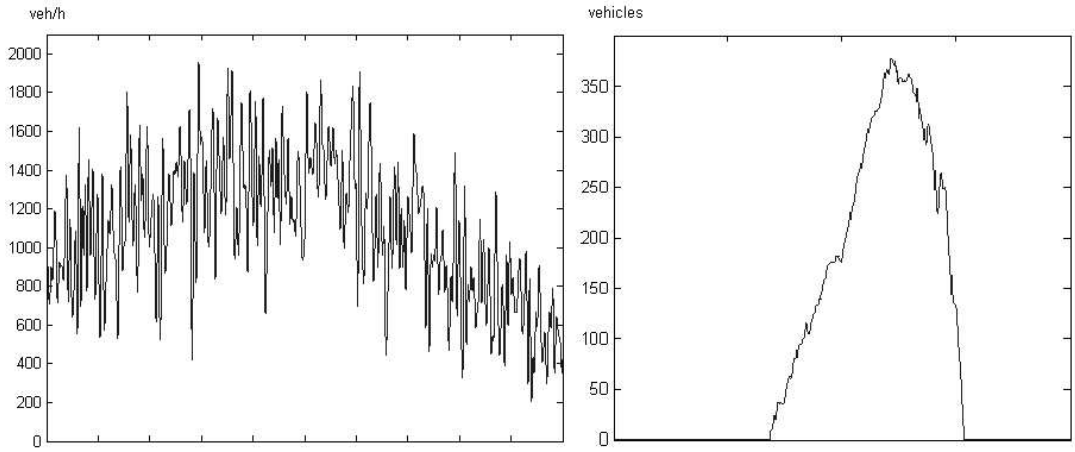

Figure 8.10: Demand (left) and queue length (right) with 1100 veh/h allowed.

conclusion, which is intuitive to some extend, as no local structure is set a priori in the LMI formulation.

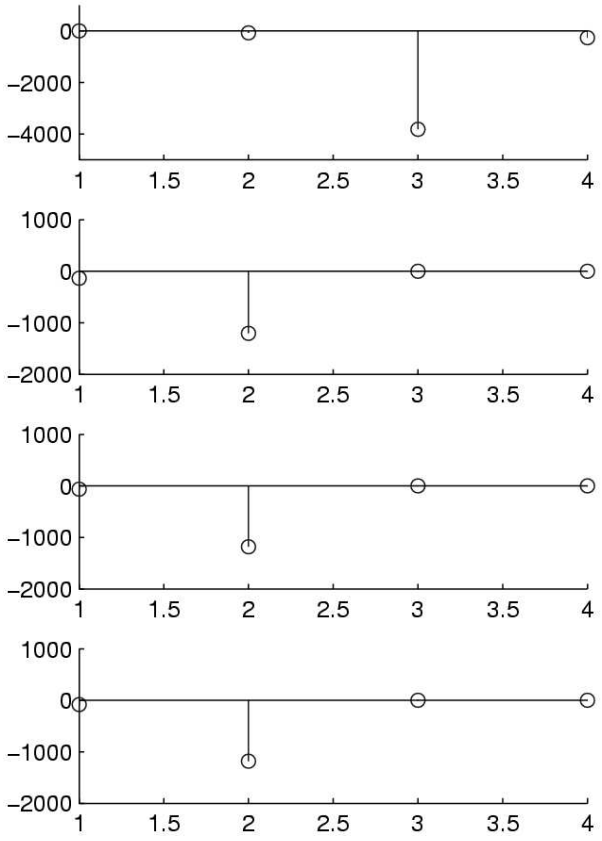

Figure 8.11: Feedback gains of the 4 cells for the discrete state $FFFFF$ (top), $FFDFF$, $FCDFF$ and $CCDFF$ (bottom).

A pupil from whom nothing is ever demanded that he cannot do, never does all he can.

John Stuart Mill (1806-1873),
English philosopher and political economist.

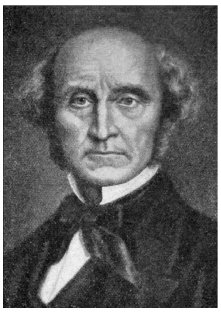

Conclusion and perspectives

The first contribution of this book is to provide a unified analytical and numerical treatment of 3 traffic model: the Lighthill-Whitham-Richards (LWR) model, the Aw-Rascle-Zhang (ARZ) model and the Multiclass Origin-Destination (MOD) model. These models do not have the same level of complexity and one of them should generally be preferred for a specific application. These three models have been studied in the mathematical community too as in [Garavello & Piccoli, 2006*b*] and we strongly believe that they will be the building blocks of forthcoming freeway control and monitoring algorithms.

The second contribution of this book is to propose two methodologies, respectively based on the optimal control theory and the dissipatedly theory, to control freeway systems. These methods have proven to be relatively easy to implement and the proposed simulation results are encouraging for further investigation and field tests.

The freeway management applications treated in the book rely heavily on the availability of trafic measurement along the freeway as provided in many places by inductive loop detectors. Nowadays, image processing provides an alternative technique to obtain these traffic data and several tests have been conducted around the world, with some datasets now available. For instance, on dataset maintained by the Federal HighWay Administration (FHWA) in USA consists of all vehicle trajectories along a 800 meters stretch of th Interstate 80 Eastbound. These trajectories, along with the vehicle class, the vehicle length, the space/time headway and much more are extracted from the recordings of 6 cameras mounted on top of a building neighboring the I80 in Emerville, California close to Berkeley. Figure 8.12 is a map of the monitored section and Figure 8.13 gives an example of the image processing required to extract the valuable information. The availability of the vehicle trajectories open new perspectives in freeway traffic modelling, both from the microscopic and the macroscopic viewpoints. For instance, they may be used to calibrate or validate existing traffic models base of this ground truth, to develop lane changing models, stop and go wave model, capacity drop models, instantaneous breakdown models as well as more realistic on/off-ramp models. For instance, the vehicle trajectories for lane 4 depicted on Figure 8.14 show how small perturbations can lead to the backward propagation of congestion waves. This phenomenon is not taken into account in purely macroscopic models and these data may help to improve existing models. Similarly, Figure 8.15-left shows smooth traffic perturbed by a lane-changing, which lead later to a stopped traffic upstream of the perturbation. Similarly, Figure 8.15-right shows the upstream propagation of stop and go waves that we all have experienced on

crowed freeways!

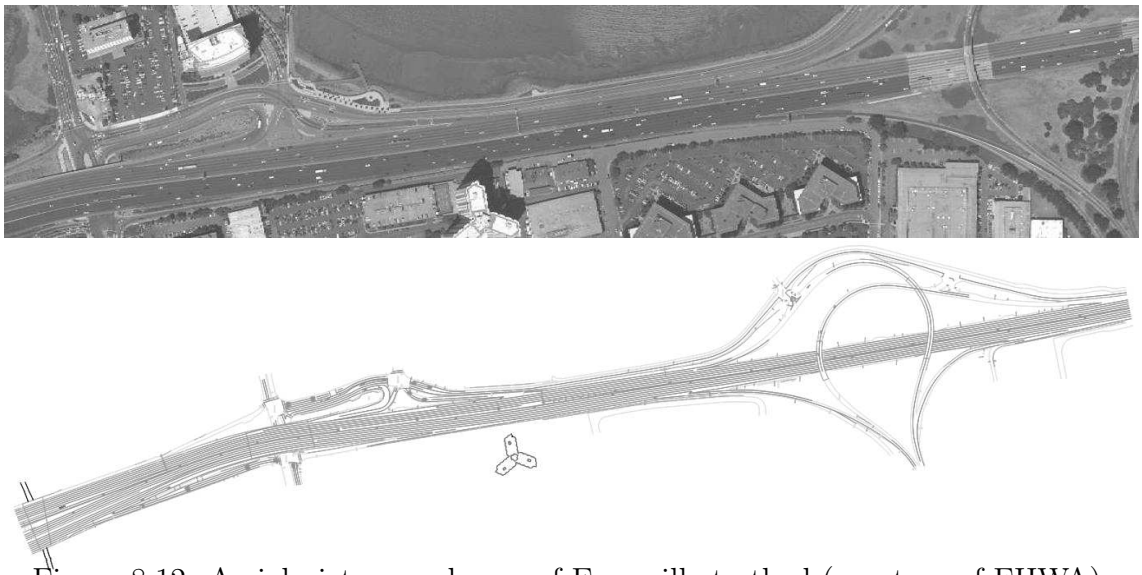

Figure 8.12: Aerial picture and map of Emerville testbed (courtesy of FHWA).

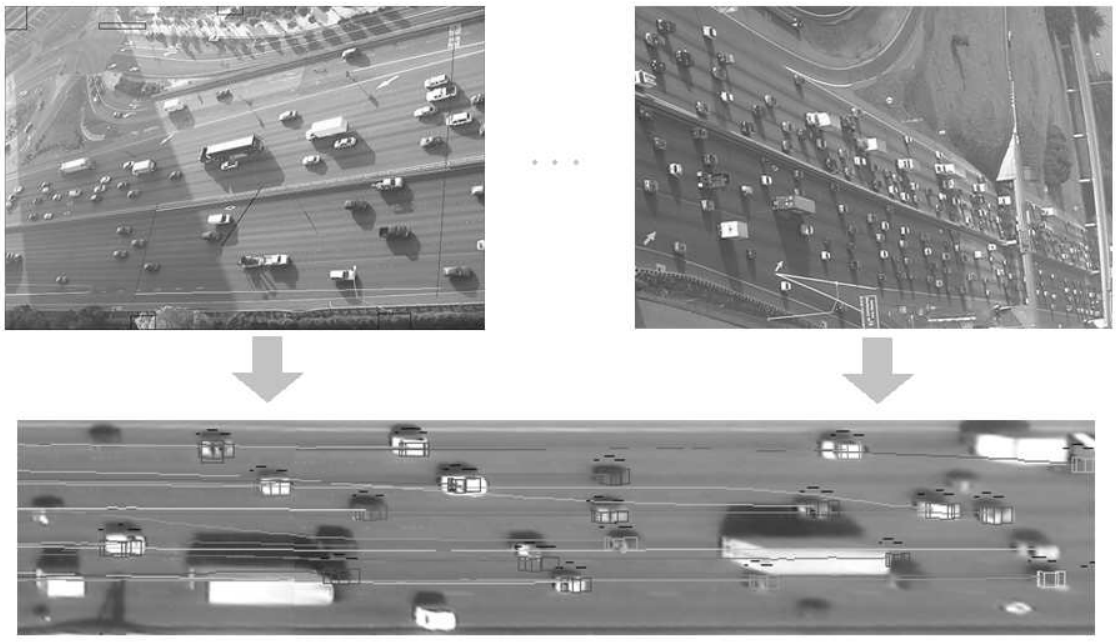

Figure 8.13: Two video frames and the reconstituted traffic picture (courtesy of FHWA).

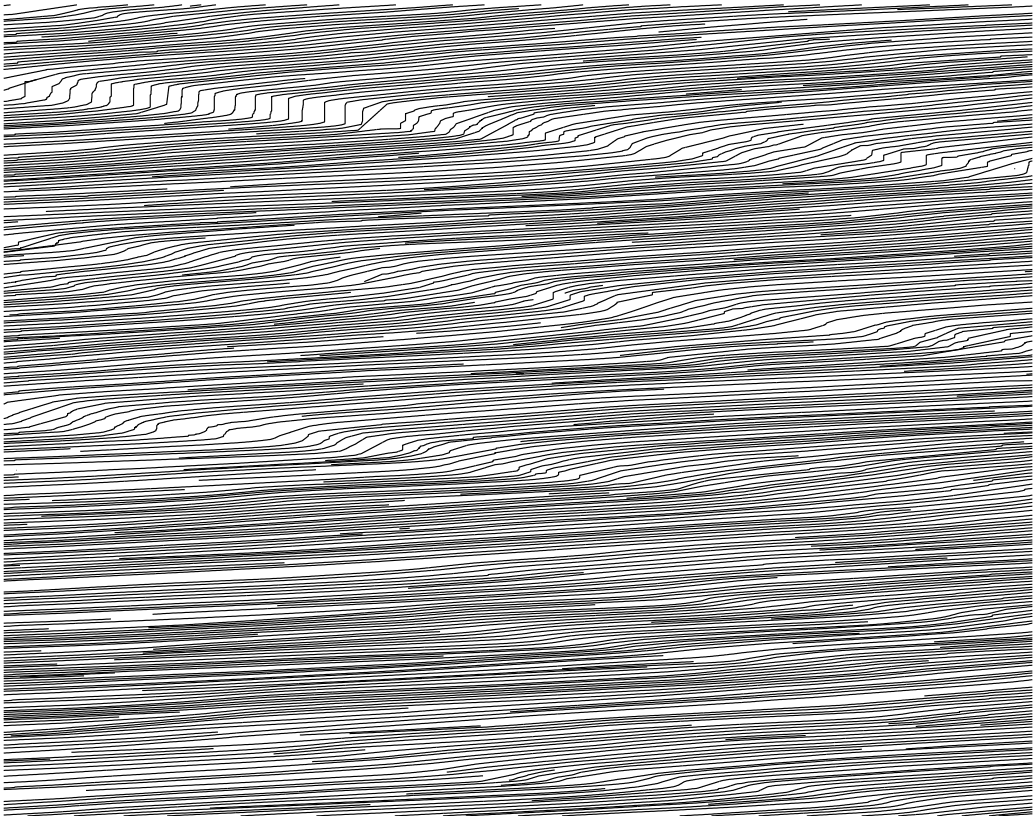

Figure 8.14: Example of vehicle trajectories on lane 4 (courtesy of FHWA).

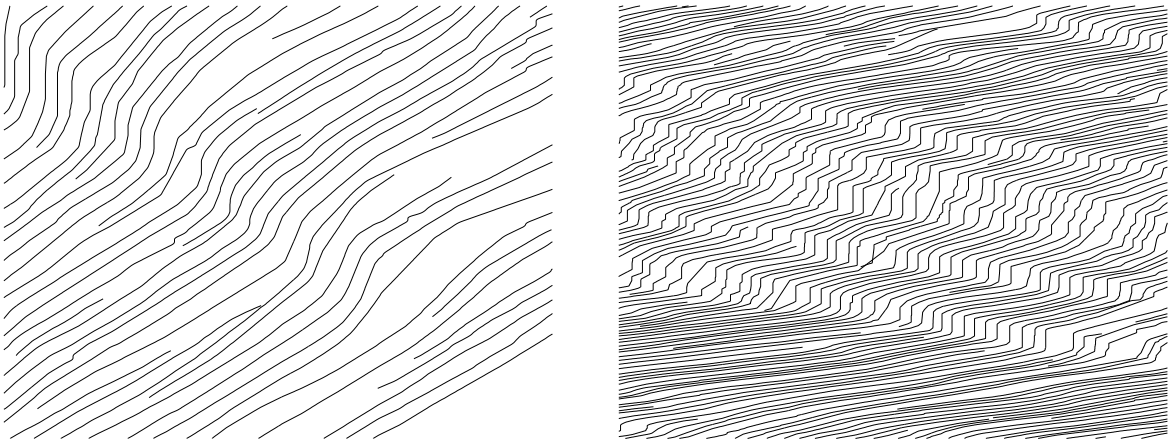

Figure 8.15: Example of stop and go waves (courtesy of FHWA).

Appendix A

Notations

A	a set
$\setminus$	set difference
$\bigcup$	set union
$\bigcap$	set intersection
Ω	a subset of $\mathbb{R}^n$
$\partial\Omega$	the boundary of Ω
$\mathcal{X}$	a functional space
$\mathcal{L}(\mathcal{X},\mathcal{Y})$	space of linear mappings from $\mathcal{X}$ to $\mathcal{Y}$
$\mathcal{L}(\mathcal{X})$	space of linear functionals $\mathcal{L}(\mathcal{X},\mathbb{R})$
$\mathcal{X}^*$	dual of $\mathcal{X}$, i.e. $\mathcal{X}^* = \mathcal{L}(\mathcal{X})$
$\langle \mathcal{A}, f\rangle_{\mathcal{X}^*,\mathcal{X}}$	duality pairing for $\mathcal{A} \in \mathcal{L}(\mathcal{X})$
$\langle f_1, f_2\rangle_{\mathcal{X}}$	scalar product

Appendix A. Notations

$\cdot$	scalar product in euclidian spaces
$\mathcal{A}^\star$	adjoint operator of operator $\mathcal{A}$
$D\mathcal{A}$	Fréchet derivative of $\mathcal{A}$
$D\mathcal{A}[\ \bar{f}\ ]$	Fréchet derivative of $\mathcal{A}$ at $\bar{f}$
$D\mathcal{A}[\ \bar{f}\ ](\ \tilde{f}\ )$	Fréchet differential of $\mathcal{A}$ at $\bar{f}$ in direction $\tilde{f}$
$V \subset\subset U$	V compactly contained in U
$\mathcal{L}^n$	$n-$dimensional Lebesgue measure
$\mathcal{H}^n$	$n-$dimensional Hausdorff measure
$\mu \llcorner f$	measure with density f with respect to measure μ
$\nu \ll \mu$	ν absolutely continuous with respect to μ
$\nu \perp \mu$	ν and μ are mutually singular
$C_0^k(\Omega, \mathbb{R}^n)$	space of $k-$times continuously differentiable functions $f : \Omega \to \mathbb{R}^n$ with compact support
$C_0^k(\Omega)$	space of functionals $C_0^k(\Omega, \mathbb{R})$
$BV(\Omega)$	space of functions with bounded variations on Ω
$[Df]$	vector measure for the gradient of $f \in BV(\Omega)$
$[Df]_{\text{ac}}$	absolutely continuous part of $[Df]$

Appendix A. Notations

$[Df]_{\mathrm{s}}$	singular part of $[Df]$
f^-	left limit of $f \in BV(\mathbb{R})$
f^+	right limit of $f \in BV(\mathbb{R})$
Tf	trace of $f \in BV(\Omega)$
δ_Γ	Dirac measure supported by the set Γ
$A > 0$	positive definiteness of matrix A
$\mathrm{Conv}(a, b)$	Convex set of $\mathbb{R}$ with extremities $a \in \mathbb{R}$ and $b \in \mathbb{R}$
$\begin{pmatrix} A & B \\ \star & D \end{pmatrix}$	symmetric matrix $\begin{pmatrix} A & B \\ B^T & D \end{pmatrix}$
ρ, v, ϕ	Density, velocity and flow of the traffic stream
I, y	Relative velocity and relative flow
u	State vector for scalar equations, e.g. $u = \rho$
$\mathbf{u}$	State vector for systems, e.g. $\mathbf{u} = (\rho, y)$
u^- and u^+	State value on the left and right of a single shock
$u^-_{\vert_{x=s_i(t)}} = u^-(s_i(t), t)$	State value at the left of the shock $x = s_i(t)$
$\Phi(\cdot)$	Concave flux function
ρ_c	Critical density such that $\Phi'(\rho_c) = 0$

Appendix A. Notations

ρ_m	Maximal density such that $\Phi(\rho_m) = 0$ and $\rho_m \neq 0$
$D(\cdot)$	Demand for the flux function $\Phi(\cdot)$
$S(\cdot)$	Supply for the flux function $\Phi(\cdot)$
$D^{\varphi}(\cdot)$	Demand for flux function $\Phi(\cdot)$ with exogenous flow φ
$\Phi_i, D_i, D_i^{\varphi_i}, S_i$	Flux, demand and supply functions for link i or cell i
$\Phi^I(\cdot)$	Modified flux function with relative velocity I
$D^I(\cdot), S^I(\cdot)$	Modified demand and supply functions
$D^{I,\varphi}(\cdot)$	Modified demand function with exogenous flow φ
$\Phi_i^I, D_i^I, D_i^{I,\varphi_i}, S_i^I$	Modified flux, demands and supply for link i or cell i
$\rho_L, \rho_R, \rho_-, \rho_+, \rho_0, \rho_M$	States involved in a Riemann problem
$\Phi_{num}(\cdot,\cdot)$	Numerical flux function
$\Phi_{num}^{\varphi}(\cdot,\cdot)$	Numerical flux function with exogenous flow φ
Δx_i	Length of cell i
Δ_t	Discretization time period
$u_i^n, \mathbf{u}_i^n$	State value in cell i at time $n\Delta_t$ in numerical schemes
$u_i[k]$	State value in cell i at discrete time k for control

Appendix B

Mathematical background

This appendix gives a brief review of some tools from functional analysis, conservation theory and linear algebra used throughout the book. The treatment of the material presented here is by no means complete and we refer the interested readers to the mentioned literature for further details.

B.1 Functional analysis

We refer the reader to [Lax, 2002] for all the functional analysis notions introduced in this section. The definitions and theorems presented here are mainly used in the optimal control chapter.

Definition B.1.1 (Dual of a Banach space) *Given a Banach space $\mathcal{X}$, the dual space $\mathcal{X}^* = \mathcal{L}(\mathcal{X})$ is the set of all bounded linear functionals defined on $\mathcal{X}$.*

Definition B.1.2 (Duality pairing) *Let $x \in \mathcal{X}$ with $\mathcal{X}$ being a Banach space and let $f \in \mathcal{X}^* = \mathcal{L}(\mathcal{X})$, then the duality pairing is defined by*

$$f(x) = \langle f, x \rangle_{\mathcal{X}^*,\mathcal{X}}$$

Definition B.1.3 (Adjoint operator) *Given an operator $\mathcal{A} \in \mathcal{L}(\mathcal{X}, \mathcal{Y})$ with $\mathcal{X}$ and $\mathcal{Y}$ two Banach spaces, the adjoint operator $\mathcal{A}^\star \in \mathcal{L}(\mathcal{Y}^*, \mathcal{X}^*)$ is given by the duality identity*

$$\langle y, \mathcal{A}(x) \rangle_{\mathcal{Y}^*,\mathcal{Y}} = \langle \mathcal{A}^\star(y), x \rangle_{\mathcal{X}^*,\mathcal{X}} \qquad \forall\ x \in \mathcal{X} \text{ and } y \in \mathcal{Y}^*$$

Definition B.1.4 (Inner product in Hilbert spaces) *If $\mathcal{X}$ is an Hilbert space (a Banach space with an inner product) then $\mathcal{X}^* = \mathcal{X}$ and the duality pairing is equivalent to the inner product, i.e. $\langle f, x \rangle_{\mathcal{X}^*,\mathcal{X}} = \langle f, x \rangle_{\mathcal{X}}$.*

Definition B.1.5 (Fréchet derivative) *Let $\mathcal{X}$ and $\mathcal{Y}$ be Banach spaces, $f : \mathcal{X} \to \mathcal{Y}$ be an operator and $x_0 \in \mathcal{X}$. If there exists $D_x f[x_0] \in \mathcal{L}(\mathcal{X}, \mathcal{Y})$, such that:*

$$\lim_{\|\delta x\|_{\mathcal{X}} \to 0} \frac{\|f(x_0 + \delta x) - f(x_0) - D_x f[x_0](\delta x)\|_{\mathcal{Y}}}{\|\delta x\|_{\mathcal{X}}} = 0$$

then f is Fréchet differentiable at x_0 and $D_x f[x_0]$ is called the Fréchet derivative of f at x_0. If f has a Fréchet derivative at x_0, it is unique and f is continuous at x_0.

For a real valued function $f : \mathcal{X} \to \mathbb{R}$, $D_x f[x_0] \in \mathcal{X}^* = \mathcal{L}(\mathcal{X})$ and verifies

$$\lim_{\|\delta x\|_{\mathcal{X}} \to 0} \frac{f(x_0 + \delta x) - f(x_0) - \langle D_x f[x_0], \delta x \rangle_{\mathcal{X}^*, \mathcal{X}}}{\|\delta x\|_{\mathcal{X}}} = 0$$

which is equivalent to the Taylor expansion

$$f(x_0 + \delta x) = f(x_0) + \langle D_x f[x_0], \delta x \rangle_{\mathcal{X}^*, \mathcal{X}} + R(\delta x) \quad \text{with} \quad \lim_{\|\delta x\|_{\mathcal{X}} \to 0} R(\delta x) = 0$$

Theorem B.1.1 (Implicit function theorem) *Let $\mathcal{Y}$, $\mathcal{U}$ be Banach spaces and let $\mathcal{C} : \mathcal{Y} \times \mathcal{U} \to \mathcal{W}$. Assume that there exists $\bar{y}$ and $\bar{u}$ belonging respectively to the open neighborhoods $\mathcal{O}_{\bar{y}} \in \mathcal{Y}$ and $\mathcal{O}_{\bar{u}} \in \mathcal{U}$ such that $\mathcal{C}(\bar{y}, \bar{u}) = 0$. If $\mathcal{C}$ is continuously Fréchet-differentiable on $\mathcal{O}_{\bar{y}} \times \mathcal{O}_{\bar{u}}$ and if the partial Fréchet-derivative $D_y \mathcal{C}[\bar{y}, \bar{u}]$ is bijective, then there exists a neighborhood $\tilde{\mathcal{O}}_{\bar{u}} \subset \mathcal{O}_{\bar{u}}$ and a continuously differentiable function defined by $y : \tilde{\mathcal{O}}_{\bar{u}} \to \mathcal{Y}$ such that $\mathcal{C}(y(u), u) = 0$ for all $u \in \tilde{\mathcal{O}}_{\bar{u}}$. The Fréchet derivative of $y(u)$ with respect to u exists and is given as the solution of*

$$D_y \mathcal{C}(y(u), u) \circ D_u y(u) + D_u \mathcal{C}(y(u), u) = 0$$

Theorem B.1.2 (Riesz representation theorem) *Let $\mathcal{X}$ be a Hilbert space with dual $\mathcal{X} = \mathcal{X}^*$. For each $f \in \mathcal{X}^*$, there is a unique $x_f \in \mathcal{X}$ such that $\langle f, x \rangle_{\mathcal{X}^*, \mathcal{X}} = \langle x_f, x \rangle_{\mathcal{X}}$ for all $x \in \mathcal{X}$. In addition $\|x_f\|_{\mathcal{X}} = \|f\|_{\mathcal{X}^*}$.*

B.2 Measure theory

A measure is a mathematical object that affects a size to sets and subsets, generalizing the concept of length. The main application of measure theory is the Lebesgue integration which is much more powerful than the Riemann integration. We tried in this section to keep the semantic complexity to its minimum and refer the interested reader to [Evans & Gariepy, 1991] for more information.

Definition B.2.1 (Measures) *Let X denote a set and 2^X the collection of subsets of X. A mapping $\mu : 2^X \to [0, \infty]$ is called a measure on X if*

- $\mu(\emptyset) = 0$

- $\mu(A) \leq \sum_{k=1}^{\infty} \mu(A_k)$ whenever $A \subset \bigcup_{k=1}^{\infty} A_k$

The set of measures in noted $\mathcal{M}$.

Definition B.2.2 (Measurable sets) *A set* $A \subset X$ *is* μ*-measurable if for each set* $B \subset X$*, we have*

$$\mu(A) = \mu(B \cap A) + \mu(B \backslash A)$$

Definition B.2.3 (Measurable functions) *A function* $f : X \to Y$ *is called* μ*-measurable if for each open set* $U \subset Y$*,* $f^{-1}(U)$ *is* μ*-measurable.*

Definition B.2.4 (Borel sets) *A Borel set is a set which may be obtained as the result of not more than a countable number of operations of union and intersection of closed and open sets in a topological space. In* $\mathbb{R}^n$*, the class* $\mathcal{B}$ *of Borel sets is the smallest collection of sets that includes the open and closed sets such that if* E_i *are in* $\mathcal{B}$*, then so are* $\bigcup_{i=1}^{\infty} E_i$*,* $\bigcap_{i=1}^{\infty} E_i$ *and* $\mathbb{R}^n \backslash E_i$*.*

Definition B.2.5 (Borel measures) *A Borel measure is a measure* $\mu : \mathcal{B} \to \mathbb{R}$ *where* $\mathcal{B}$ *is the class of Borel sets. For a Borel measure* μ*, all continuous functions are measurable. The set of Borel measures in noted* $\mathcal{M}_B$*.*

Definition B.2.6 (Measure properties) *A Borel measure* μ *is said to be:*

- *inner regular if*
$$\mu(A) = \sup_{K \subset\subset A} \mu(K)$$
- *outer regular if*
$$\mu(A) = \inf_{A \subset\subset K} \mu(K)$$
- *regular if it is inner regular and outer regular,*
- *locally finite if every point has a neighborhood of finite measure,*
- *finite if* $\mu(K) < \infty$ *for each compact* $K \subset \mathbb{R}^n$*.*

with $K \subset\subset A$ *meaning that* K *is compactly contained in* A*.*

Definition B.2.7 (Radon measures) *A Radon measure is a regular Borel measure that is finite on compact sets. The set of Radon measures is noted* $\mathcal{M}_R$*. On a locally compact Hausdorff space, Radon measures corresponds to positive linear functionals on the space of continuous functions with compact support, i.e.* $\mathcal{M}_R = C_0^* = \mathcal{L}(C_0)$*. As a consequence, for all* $L : C_0(\Omega) \to \mathbb{R}$*, there exist* $\mu \in \mathcal{M}_R$ *such that for all* $f \in C_0(\Omega)$

$$L(f) = \int_{\Omega} f \, \mathrm{d}\mu$$

Example B.2.1
Examples of Radon measure are the Dirac measure on any toplogical space as well as the Gaussian and Lebesgue measure on Euclidean space. The counting measure on Euclidean space is an example of a measure that is not a Radon measure, since it is not locally finite.

Definition B.2.8 (Absolutely continuous measures) *The measure ν is absolutely continuous with respect to μ, written $\nu \ll \mu$, provided $\mu(A) = 0$ implies $\nu(A) = 0$ for all $A \subset \mathbb{R}^n$.*

Definition B.2.9 (Mutually singular measures) *The measures ν and μ are mutually singular, written $\nu \perp \mu$, if there exists a Borel subset $B \subset \mathbb{R}^n$ such that*

$$\mu(\mathbb{R}^n - B) = \nu(B) = 0$$

B.3 BV functions

Practically speaking, BV functions are measure theoretically C^1 with jumps along measure theoretically C^1 surfaces. The space BV of functions with bounded variations can be defined in at least 2 different but equivalent ways. We restrict here to real valued functions of the form $u : \Omega \to \mathbb{R}$ where $\Omega \in \mathbb{R}^n$ is open and bounded. For more information on this topic, we recommend [Evans & Gariepy, 1991] an [Ziemer, 1989].

Definition B.3.1 (BV functions) *$u(x) \in BV(\Omega) \subset L^1(\Omega)$ if its first order partial distributional derivatives $[D_{x_i}u]$ are Radon measures, i.e. if there exists locally finite Borel measures $[D_{x_i}u]$ with $|[D_{x_i}](K)| < \infty$ for each compact subset $K \subset \Omega$, such that*

$$-\int_\Omega u(x)\frac{\partial\phi(x)}{\partial x_i}\,\mathrm{d}x = \int_\Omega \phi(x)\,\mathrm{d}[D_{x_i}u] \qquad \forall\phi \in C_0^1(\Omega)$$

An alternative definition is that

$$-\int_\Omega u(x)\mathrm{div}\phi(x)\,\mathrm{d}x = \int_\Omega \phi(x)\,\mathrm{d}[Du] \qquad \forall\phi \in C_0^1(\Omega)$$

with $[Du]$ the vector valued measure for the gradient of u.

Definition B.3.2 (Total variation of BV functions) *$u(x) \in BV(\Omega) \subset L^1(\Omega)$ if its total variation is bounded, i.e.*

$$TV(u) = \sup\left\{\int_\Omega u(x)\ \mathrm{div}\phi(x)\ \mathrm{d}x\ :\ \phi \in C_0^1(\Omega,\mathbb{R}^n),\ |\phi| \le 1\right\} < \infty$$

Theorem B.3.1 (Lebesgue decomposition theorem for BV fields) *The vector valued measure $[Du]$ for the gradient of $u \in BV(\Omega)$ may be decomposed as follow*

$$[Du] = [Du]_{\mathrm{ac}} + [Du]_{\mathrm{s}} = \mathcal{L}^n \llcorner Df + [Du]_{\mathrm{s}}$$

where $Df \in L^1(\Omega, \mathbb{R}^n)$ is the density of the absolutely continuous part $[Du]_{\mathrm{ac}}$ and $[Du]_{\mathrm{s}}$ is the singular part with respect to the Lebesgue measure.

Example B.3.1
$W^{1,p}_{\mathrm{loc}}(\Omega) \subsetneq BV_{\mathrm{loc}}(\Omega)$ for $1 \leq p \leq \infty$ and $u(x) \in BV_{\mathrm{loc}}(\Omega)$ belongs to the Sobolev space $W^{1,p}_{\mathrm{loc}}(\Omega)$ if and only if $u \in L^p_{\mathrm{loc}}(\Omega)$, $[Du]_{\mathrm{s}} = 0$ and $Du \in L^p_{\mathrm{loc}}(\Omega)$. Thus, one property of BV functions that are not Sobolev functions is to have a non vanishing singular part $[Du]_s$.

Theorem B.3.2 (Compactness of BV) *Let $\Omega \subset \mathbb{R}^n$ be open and bounded with Lipschitz boundary $\partial\Omega$ and let take $||u||_{BV} = ||u||_{L^1} + TV(u)$ as a norm for BV. Assume $\{u_k\}_{k=1}^{\infty}$ is a sequence of $BV(\Omega)$ satisfying*

$$\sup_k ||u_k||_{BV(\Omega)} < \infty$$

Then there exists a subsequence $\{u_{k_j}\}_{j=1}^{\infty}$ and $u \in BV(\Omega)$ such that

$$u_{k_j} \to u \ \text{ in } L^1(\Omega) \text{ as } j \to \infty$$

Theorem B.3.3 (Trace operator for BV fields) *Let Ω be open and bounded with Lipschitz boundary $\partial\Omega$. There exists a bounded linear mapping*

$$T : BV(\Omega) \to L^1(\partial\Omega, \mathcal{H}^{n-1})$$

such that

$$\int_\Omega u \ \mathrm{div}\phi \ \mathrm{d}x = -\int_\Omega \phi \cdot \mathrm{d}[Du] + \int_{\partial\Omega} (\phi \cdot \nu) \ Tu \ \mathrm{d}\mathcal{H}^{n-1}$$

for all $u \in BV(\Omega)$ and $\phi \in C^1(\mathbb{R}^n, \mathbb{R}^n)$. The function Tu, which is defined up to a set of $\mathcal{H}^{n-1}$-measure 0 is called the trace of u on $\partial\Omega$ and can be interpreted as the boundary value of u at $\partial\Omega$. Indeed, for $\mathcal{H}^{n-1}$ almost every $x \in \partial\Omega$, we have

$$Tu(x) = \lim_{r \to 0} \frac{1}{|B(x,r) \cap \Omega|} \int_{B(x,r)\cap\Omega} f \ \mathrm{d}y$$

B.4 Kružkov theory for scalar conservation laws

We give in this section a brief overview of the wellposedness theory for scalar conservation laws. In addition to the original papers [Kružkov, 1970] and [Bardos et al., 1979], we recommend [Serre, 1996], [LeFloch, 2002], [LeVeque, 1992] and [Bressan, 2000].

Definition B.4.1 (Scalar conservation law IBVP) *An initial boundary value problem (IBVP) on $\Omega = (0, L) \times (0, \infty)$ involving the scalar conservation law with flux function $f \in C^2$ and source term $g \in C^2$ writes*

$$\begin{cases} \partial_t y + \partial_x f(x, y) = g(x, y) \\ y(x, 0) = y_I(x) \\ y(0, t) \sim y_0(t) \text{ and } y(L, t) \sim y_L(t) \end{cases} \tag{B.4.1}$$

where the symbol $\sim$ means that the boundary conditions are only proposed and may not apply for some time intervals.

Theorem B.4.1 (Kružkov generalized solution) *Problem (B.4.1) admits a unique generalized solution $y \in BV(\Omega) \cap L^\infty(\Omega)$ characterized by the infinite set of inequalities*

$$\begin{aligned} &\int_0^\infty \int_0^L \Big(|y-k| \partial_t \phi + \operatorname{sg}(y-k)\big(f(x,y)-f(x,k)\big)\partial_x \phi - \operatorname{sg}(y-k)\big(g(x,y)-\partial_x f(x,k)\big)\phi \Big) \mathrm{d}x\mathrm{d}t \\ &+ \int_0^\infty \Big(\operatorname{sg}(y_0-k)\big(f(y(0,t)-f(k))\big)\phi(0,t) - \operatorname{sg}(y_L-k)\big(f(y(L,t)-f(k))\big)\phi(L,t) \Big) \mathrm{d}t \\ &+ \int_0^L |y_0-k|\phi(x,0)\ \mathrm{d}x \quad \geq \quad 0 \end{aligned} \tag{B.4.2}$$

for all $k \in \mathbb{R}$ and for all $\phi \in C^2(\Omega)$ with $\phi \geq 0$ and $\lim_{t\to\infty} \phi = 0$. The complete proof of this theorem can be found in [Kružkov, 1970] and [Bardos et al., 1979].

Lemma B.4.2 (Shock conditions) *Let $\Gamma = \{(x, t) : x = s(t),\ t \in [t^I, t^F]\}$ be a discontinuity of $y \in BV(\Omega) \cap L^\infty(\Omega)$ solution of (B.4.1) according to (B.4.2). Let define $y^- = \lim_{x \uparrow s(t)} y(x, t)$ and $y^+ = \lim_{x \downarrow s(t)} y(x, t)$ respectively the left and right traces of y along Γ. Then, we have*

- *The Rankine-Hugoniot condition:*

$$\dot{s}(t) = \frac{\mathrm{d}}{\mathrm{d}t} s(t) = \frac{f(y^+) - f(y^-)}{y^+ - y^-}$$

- *The Oleĭnik entropy condition:*

$$\frac{f(y^+) - f(y^-)}{y^+ - y^-} \leq \frac{f(k) - f(y^-)}{k - y^-}$$

  for all $k \in \mathbb{R}$.

- *The Lax entropy condition:*

$$f'(y^+) \leq \dot{s} \leq f'(y^-)$$

remark B.4.1 *A geometric interpretation of the Oleĭnik entropy condition is that a discontinuity between y^- and y^+ is allowed to propagate if the graph of f is below (respectively above) the line connecting y^- and y^+ when $y^+ \leq y^-$ (respectively $y^- \leq y^+$). A geometric interpretation of the Lax entropy condition is that the characteristic lines, which have slope $f'(y)$, should be oriented towards the shock curve on the immediate left and right of it.*

Proof. Let $\mathcal{O} \subset \Omega$ be a neighborhood of the curve Γ and let consider the decomposition $\mathcal{O} = \mathcal{O}_1 \cup \Gamma \cup \mathcal{O}_2$ where the solution y is assumed to be C^1 on $\mathcal{O}_1$ and $\mathcal{O}_2$. From the Kružkov characterization (B.4.2) with $\phi \in C_0^2(\mathcal{O})$, an integration by parts gives

$$\begin{aligned}
&\int_0^\infty\!\!\int_{\mathcal{O}_1}\Big(\partial_t|y-k| + \partial_x \mathrm{sg}(y-k)\big(f(x,y)-f(x,k)\big) - \mathrm{sg}(y-k)\big(g(x,y)-\partial_x f(x,k)\big)\Big)\phi \,\mathrm{d}x\mathrm{d}t \\
&+\int_0^\infty\!\!\int_{\mathcal{O}_2}\Big(\partial_t|y-k| + \partial_x \mathrm{sg}(y-k)\big(f(x,y)-f(x,k)\big) - \mathrm{sg}(y-k)\big(g(x,y)-\partial_x f(x,k)\big)\Big)\phi \,\mathrm{d}x\mathrm{d}t \\
&+\int_\Gamma \big(|y^- - k| - |y^+ - k|\big)\eta_t + \big(\mathrm{sg}(y^- - k)(f(u^-) - f(k)) - \mathrm{sg}(y^+ - k)(f(u^+) - f(k))\big)\eta_x\Big)\phi \,\mathrm{d}\Gamma \geq 0
\end{aligned}$$

where (η_x, η_t) is the outward normal to the open set $\mathcal{O}_1$. By taking the special test function $\phi^\epsilon(x,t) = \theta(t)\sigma_\Gamma^\epsilon(x)$ with $\theta(t) \in C^2$, $\sigma_\Gamma^\epsilon(x) \in C^2$ and $\sigma_\Gamma^\epsilon(x) = 1$ in the interval $(s(t) - \epsilon, s(t) + \epsilon)$ and 0 elsewhere, we get with $\epsilon \to 0$

$$-\big(|y^- - k| - |y^+ - k|\big)\dot{s} + \big(\mathrm{sg}(y^- - k)(f(u^-) - f(k)) - \mathrm{sg}(y^+ - k)(f(u^+) - f(k))\big) \quad \geq \quad 0$$

as $(1, -\dot{s})$ is collinear to and has the same orientation than (η_x, η_t). Taking successively $k > \max(y^-, y^+)$ and $k < \min(y^-, y^+)$, we get

$$f(y^+) - f(y^-) \leq \dot{s}(y^+ - y^-) \leq f(y^+) - f(y^-)$$

which is the Rankine-Hugoniot condition. Now, taking k between y^- and y^+, we get

$$\mathrm{sg}(y^+ - y^-)(y^+ + y^- - 2k)\dot{s} \geq \mathrm{sg}(y^+ - y^-)(f(y^+) + f(y^-) - 2f(k))$$

which rewrites using simple manipulations and the fact that $f(y^+) - f(y^-) = \dot{s}(y^+ - y^-)$

$$\begin{aligned}
&\mathrm{sg}(y^+ - y^-)(y^+ - y^- + 2y^- - 2k)f(y^+) - f(y^-) \\
&\qquad \geq \mathrm{sg}(y^+ - y^-)(y^+ - y^-)(f(y^+) - f(y^-) + 2f(y^-) - 2f(k))
\end{aligned}$$

Simple cancellations and dividing by 2 leads to

$$\big(f(y^+) - f(y^-)\big)(y^- - k) + \big(f(k) - f(y^-)\big)(y^+ - k) \geq 0$$

with gives the Oleĭnik entropy condition by dividing by $(y^+ - y^-)(k - u^-) \geq 0$. Half of the Lax entropy condition is immediate by taking $k \uparrow y^-$ in the Oleĭnik entropy condition. The other half follows using simple manipulations of the Oleĭnik entropy condition and then $k \downarrow y^+$. □

Definition B.4.2 (Riemann problem for scalar conservation laws) *A Riemann problem for the scalar conservation law*

$$\partial_t y + \partial_x f(y) = 0 \tag{B.4.3}$$

is a Cauchy problem with the piecewise constant initial condition

$$y(x,0) = \begin{cases} y^- & , \quad x < 0 \\ y^+ & , \quad x > 0 \end{cases} \tag{B.4.4}$$

Lemma B.4.3 (Solution of the Riemann problem with concave flux) *The Riemann problem (B.4.3) with a concave flux function f and initial data (B.4.4) has a self-similar (i.e. y(x,t)=y(x/t)) analytical solution given by*

- *if* $y^- \leq y^+$

$$y(x,t) = \begin{cases} y^- & , \quad x \leq \left(\frac{f(y^+)-f(y^-)}{y^+-y^-}\right) t \\ y^+ & , \quad x > \left(\frac{f(y^+)-f(y^-)}{y^+-y^-}\right) t \end{cases} \tag{B.4.5}$$

- *if* $y^- > y^+$

$$y(x,t) = \begin{cases} y^- & , \quad x \leq f'(y^-)\ t \\ f'^{-1}(x/t) & , \quad f'(y^-)\ t < x < f'(y^+)\ t \\ y^+ & , \quad x \geq f'(y^+)\ t \end{cases} \tag{B.4.6}$$

(B.4.5) and (B.4.6) are respectively called a shock and a rarefaction wave.

B.5 Linear algebra

Definition B.5.1 (Schur complement) *Consider the block matrice*

$$M = \begin{pmatrix} A & B \\ C & D \end{pmatrix}$$

with matrices A, B, C and D respectively of size $p \times p$, $p \times q$, $q \times p$ and $q \times q$. If D is invertible, the Schur complement with respect to D writes

$$A - BD^{-1}C$$

Similarly, if A is invertible, the Schur complement with respect to A writes

$$D - CA^{-1}B$$

Definition B.5.2 (Positive definiteness) *A square matrix A is said to be positive definite if $x^T Ax > 0$ for all x.*

Theorem B.5.1 (Positive definiteness and Schur complement) *The nonlinear matrix inequalities $A - BD^{-1}C > 0$ and $A - BD^{-1}C > 0$ and equivalent to*

$$\begin{pmatrix} A & B \\ C & D \end{pmatrix} > 0$$

Appendix C

Entropy inequalities for on-ramps

In this appendix, we prove 2 theorems related to the Cauchy problem that involves the pointwise on-ramp model

$$\partial_t \rho + \partial_x \hat{\Phi}(x,t,\rho) = 0 \tag{C.0.1}$$

where $\hat{\Phi}(x,t,\rho)$ is the discontinuous flux function

$$\hat{\Phi}(x,t,\rho) = \Phi(\rho) + H(-x)\hat{\phi}_i(t)$$

Kruzkov's theory [Kružkov, 1970] cannot be applied directly to Equation (C.0.1) as the flux function is not continuously differentiable. Nevertheless, inspired from [Seguin & Vovelle, 2003], which itself relies heavily on [Temple, 1982] and [Towers, 2000], we can prove the following theorems that extends quite transparently Kruzkov's theory. Moreover, the second theorem provides an entropy condition that should be verified at $x = 0$ and enables to select the unique physical solution is some Riemann problems.

Theorem C.0.1 *Given the initial condition $\rho_I \in BV(\mathbb{R}^+ \times \mathbb{R}) \cap L^\infty(\mathbb{R}^+ \times \mathbb{R})$ and a concave flux function $\Phi(\cdot)$, the Cauchy problem with (C.0.1) admits an entropy solution $\rho \in BV(\mathbb{R}^+ \times \mathbb{R}) \cap L^\infty(\mathbb{R}^+ \times \mathbb{R})$ satisfying the following entropy inequalities: $\forall k \in \mathbb{R}$, $\forall \phi \in C_0^2(\mathbb{R}^+ \times \mathbb{R})$ with $\phi \geq 0$,*

$$\int_{\mathbb{R}^+}\int_{\mathbb{R}} \Big(|\rho - k|\partial_t\phi + \operatorname{sign}(\rho - k)\big(\Phi(\rho) - \Phi(k)\big)\partial_x\phi \Big) \mathrm{d}x\mathrm{d}t + \int_{\mathbb{R}^+} \hat{\phi}_i(t)\phi(0,t)\ \mathrm{d}t + \int_{\mathbb{R}} |\rho_I - k|\phi(x,0)\ \mathrm{d}x \ \geq\ 0 \tag{C.0.2}$$

Proof. Let consider a regularization of Equation (C.0.1) with $H_\epsilon(\cdot)$ a smooth monotone non-increasing functions, as depicted on Figure C.1, verifying

$$H_\epsilon(x) = \begin{cases} 0 & , \quad x \leq -\epsilon \\ 1 & , \quad x \geq \epsilon \\ \in [0,1] & , \quad x \in [-\epsilon, \epsilon] \end{cases}$$

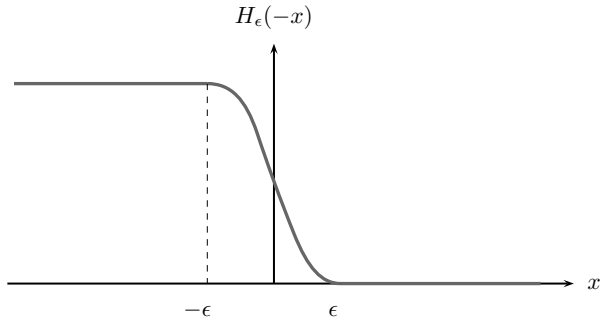

Figure C.1: Regularized Heaviside distribution.

In that setting, Kruzkov's theory [Kružkov, 1970] applies to the Cauchy problem

$$\begin{cases} \partial_t \rho + \partial_x \hat{\Phi}_\epsilon(x,t,\rho) = 0 \\ \rho_\epsilon(x,0) = \rho_I(x) \end{cases} \tag{C.0.3}$$

with the regularized flow function given by

$$\hat{\Phi}_\epsilon(x,t,\rho) = \Phi(\rho) + H_\epsilon(-x)\hat{\phi}_i(t)$$

Consequently, Problem (C.0.3) admits a unique entropy condition $\rho_\epsilon \in BV \cap L^\infty$ characterized (see appendix) by the entropy inequalities: $\forall k \in \mathbb{R}$, $\forall \phi \in C_0^2(\mathbb{R}^+ \times \mathbb{R})$, $\phi \geq 0$,

$$\int_{\mathbb{R}^+}\int_{\mathbb{R}} \Big(|\rho_\epsilon - k| \partial_t \phi + \operatorname{sign}(\rho_\epsilon - k)\big(\hat{\Phi}_\epsilon(t,x,\rho_\epsilon) - \hat{\Phi}_\epsilon(t,x,k)\big)\partial_x \phi \\ - \operatorname{sign}(\rho_\epsilon - k)\partial_x \hat{\Phi}_\epsilon(t,x,k)\phi \Big) \mathrm{d}x\mathrm{d}t + \int_{\mathbb{R}} |\rho_I - k| \phi(x,0)\ \mathrm{d}x \geq 0$$

which can be rewritten

$$\int_{\mathbb{R}^+}\int_{\mathbb{R}} \Big(|\rho_\epsilon - k| \partial_t \phi + \Psi(\rho_\epsilon, k)\partial_x \phi + \operatorname{sign}(\rho_\epsilon - k) H'_\epsilon(-x)\hat{\phi}_i(t)\phi \Big) \mathrm{d}x\mathrm{d}t \\ + \int_{\mathbb{R}} |\rho_I - k| \phi(x,0)\ \mathrm{d}x \geq 0 \tag{C.0.4}$$

with the so-called entropy flux given by

$$\begin{aligned} \Psi(\rho_\epsilon, k) &= \operatorname{sign}(\rho_\epsilon - k)\big(\hat{\Phi}_\epsilon(t,x,\rho_\epsilon) - \hat{\Phi}_\epsilon(t,x,k)\big) \\ &= \operatorname{sign}(\rho_\epsilon - k)\big(\Phi(\rho_\epsilon) - \Phi(k)\big) \end{aligned}$$

The inequalities given in (C.0.4) means that the measure

$$\partial_t |\rho_\epsilon - k| + \partial_x \Psi(\rho_\epsilon, k) - \operatorname{sign}(\rho_\epsilon - k) H'_\epsilon(-x)\hat{\phi}_i(t) \leq 0$$

is non positive and thus bounded for all $\epsilon > 0$. As $\rho_\epsilon \in BV \cap L^\infty$, $\partial_t \rho_\epsilon$ is a Radon measure, $\partial_t |\rho_\epsilon - k|$ is a bounded measure. Moreover, $TV\big(H_\epsilon(-x)\hat{\phi}_i(t)\big) \leq \hat{\phi}_i(t)$ ensures

that $\text{sign}(\rho_\epsilon - k)H'_\epsilon(-x)\hat{\phi}_i(t)$ is a bounded measure as well. We conclude that $\partial_x \Psi(\rho_\epsilon, k)$ is a bounded measure and then $\Psi(\rho_\epsilon, k)$ is a BV function with $||\Psi(\rho_\epsilon, k)||_{BV}$ uniformly bounded for all $\epsilon > 0$. Using Helly's theorem then ensures that a subsequence of $\Psi(\rho_\epsilon, k)$ converges strongly in L^1 thanks to the compactness property of BV.

We now use the fact that $\Phi(\cdot)$ is concave and so has a unique maximum, implying that the function $\Psi(\cdot, \rho_c)$ is monotonically decreasing as depicted on Figure C.2. The fact that $\Psi(\cdot, \rho_c)$ is invertible with continuous inverse then ensures that a subsequence of ρ_ϵ converges to $\rho \in BV$. The function $\Psi(\cdot, \rho_c)$ is called a Temple function and was first used in [Temple, 1982] to prove the wellposedness of a nonstrictly hyperbolic conservation law. It was used in [Towers, 2000] to prove the wellposedness of a conservation law with discontinuous flux function.

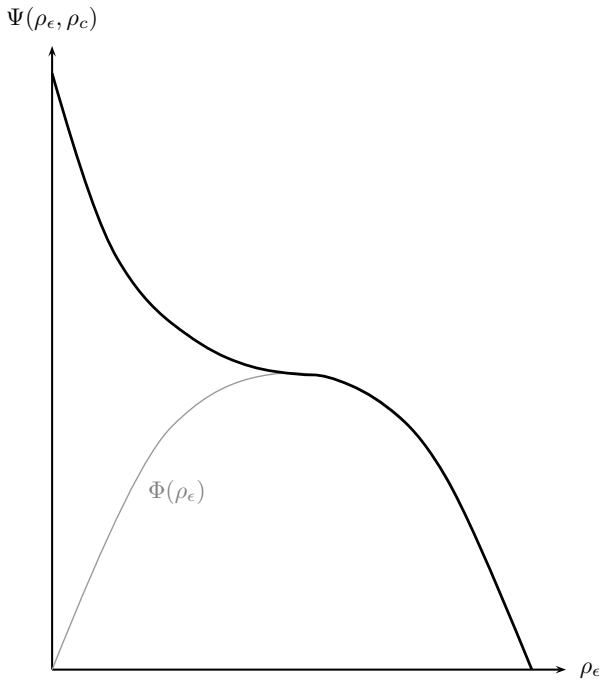

Figure C.2: Temple function used in the proof.

We now show that every limit ρ of a subsequence of ρ_ϵ verify the entropy inequalities (C.0.2). First, as a subsequence of ρ_ϵ converges in L^1 to ρ, we have $|\rho_\epsilon - k| \to |\rho - k|$ and $\Psi(\rho_\epsilon, k) \to \Psi(\rho, k)$ in L^1 in Equation (C.0.4). For the third term of Equation (C.0.4), we have

$$\int_{\mathbb{R}^+}\int_{\mathbb{R}} \text{sign}(\rho_\epsilon - k)H'_\epsilon(-x)\hat{\phi}_i(t)\phi \, \mathrm{d}x\mathrm{d}t \leq \int_{\mathbb{R}^+}\int_{\mathbb{R}} |H'_\epsilon(-x)|\hat{\phi}_i(t)\phi \, \mathrm{d}x\mathrm{d}t$$

As $|\text{sign}(\rho_\epsilon - k)| \leq 1$. Now, $H_\epsilon(-x)$ being monotonically decreasing, we conclude

$$\begin{aligned}
\int_{\mathbb{R}^+}\int_{\mathbb{R}} |H'_\epsilon(-x)|\hat{\phi}_i(t)\phi \ \mathrm{d}x\mathrm{d}t &= -\int_{\mathbb{R}^+}\int_{\mathbb{R}} H'_\epsilon(-x)\hat{\phi}_i(t)\phi \ \mathrm{d}x\mathrm{d}t \\
&= \int_{\mathbb{R}^+}\int_{\mathbb{R}} H_\epsilon(-x)\hat{\phi}_i(t)\partial_x\phi \ \mathrm{d}x\mathrm{d}t \\
&\xrightarrow[\epsilon\to 0]{} \int_{\mathbb{R}^+}\int_{\mathbb{R}} H(-x)\hat{\phi}_i(t)\partial_x\phi \ \mathrm{d}x\mathrm{d}t \\
&= \int_{\mathbb{R}^+}\int_{\mathbb{R}} \delta(x)\hat{\phi}_i(t)\phi \ \mathrm{d}x\mathrm{d}t \\
&= \int_{\mathbb{R}^+} \hat{\phi}_i(t)\phi(0,t) \ \mathrm{d}t
\end{aligned}$$

which gives the entropy inequalities (C.0.2) given in the theorem. As the solution ρ_ϵ of the regularized problem (C.0.3) is compact in L^1 and has at least one adherence value ρ which verifies (C.0.2), we conclude that there exists at least one solution to (C.0.1) with initial data in BV that verifies the entropy inequalities (C.0.2). Theorem C.0.1 do not provide the uniqueness of ρ but (C.0.2) turns out to be enough to compute the unique possible solution to the Riemann problems associated to (C.0.1). □

As for the homogeneous situation, choosing adequate test functions give the following Rankine-Hugoniot and entropy conditions.

Theorem C.0.2 *Let $\rho^- = \lim_{x\uparrow 0}\rho$ and $\rho^+ = \lim_{x\downarrow 0}\rho$ be the traces of $\rho \in BV$ at $x = 0$. A weak solution of (C.0.1) verifying the entropy inequalities (C.0.2) also verifies the following local characterizations:*

- *Rankine-Hugoniot condition:*

$$\Phi(\rho^+) = \Phi(\rho^-) + \hat{\phi}_i(t)$$

- *Entropy condition:*

$$\Phi'(\rho^-) > 0 \qquad \textit{or} \qquad \Phi'(\rho^+) \leq 0 \qquad \textit{or both}$$

Proof. A weak solution of (C.0.1) satisfies

$$\int_{\mathbb{R}^+}\int_{\mathbb{R}} \Big(\rho\partial_t\phi + \hat{\Phi}(x,t,\rho)\partial_x\phi\Big)\mathrm{d}x\mathrm{d}t - \int_{\mathbb{R}} \rho_I\phi(x,0) \ \mathrm{d}t = 0 \quad \text{ for all } \phi \in C_0^2(\mathbb{R}\times\mathbb{R}^+)$$

Let consider the small neighborhood $\mathcal{O}$ of $\mathbb{R}\times\mathbb{R}^+$ near the line $x = 0$, sufficiently small that ρ is smooth in $\mathcal{O}$, except on $\{x = 0\}$. Taking test functions $\phi \in C_0^2(\mathcal{O})$, the weak formulation gives

$$\int\int_{\mathcal{O}\setminus\{x=0\}} \Big(\partial_t\rho\phi + \partial_x\hat{\Phi}(x,t,\rho)\phi\Big)\mathrm{d}x\mathrm{d}t + \hat{\Phi}(x,t,\rho^+) - \hat{\Phi}(x,t,\rho^-) = 0$$

For sufficiently small $\mathcal{O}$, ρ solves (C.0.1) strongly in $\mathcal{O}\backslash\{x=0\}$ and the remaining term is $\hat{\Phi}(x,t,\rho^+) - \hat{\Phi}(x,t,\rho^-) = 0$, which writes explicitly

$$\Phi(\rho^+) = \Phi(\rho^-) + \hat{\phi}_i(t)$$

and thus gives the Rankine-Hugoniot condition of the theorem. Note that this condition is no more that the flow conservation principle at $x = 0$.

To prove the entropy condition, let consider, as depicted in Figure C.3, a smooth cut-off function $\sigma_\epsilon(x)$ which is monotonically increasing for $x \leq 0$ and monotonically decreasing for $x \geq 0$. Such a function $\sigma_\epsilon(x) \in C_0^2(\mathbb{R})$ can be defined by

$$\sigma_\epsilon(x) = \begin{cases} 0 & , \quad |x| \geq 2\epsilon \\ 1 & , \quad |x| \leq \epsilon \\ \in [0,1] & , \quad \epsilon < |x| < 2\epsilon \end{cases}$$

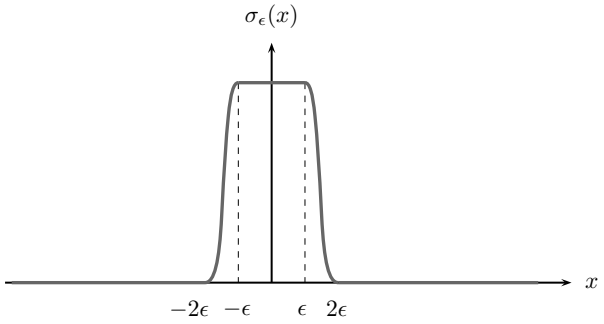

Figure C.3: Example of a cut-off function.

By choosing the test function ϕ in (C.0.2) to be $\phi_\epsilon = \theta(t)\sigma_\epsilon(x)$ with $\theta(t) \in C_0^2(\mathbb{R})$ and $\theta(t) \geq 0$, we get

$$\int_{\mathbb{R}^+}\int_{\mathbb{R}} \Big(|\rho - k|\partial_t\theta'(t)\sigma_\epsilon(x) + \Psi(\rho,k)\theta(t)\sigma_\epsilon'(x)\Big)\mathrm{d}x\mathrm{d}t \\ + \int_{\mathbb{R}^+} \hat{\phi}_i(t)\theta(t)\sigma_\epsilon(0)\ \mathrm{d}t + \int_{\mathbb{R}} |\rho_I - k|\theta(0)\sigma_\epsilon(x)\ \mathrm{d}x \ \geq\ 0$$

with $\Psi(\rho,k) = \mathrm{sign}(\rho - k)\big(\Phi(\rho) - \Phi(k)\big)$. Now, making $\epsilon \to 0$, we obtain

$$\int_{\mathbb{R}^+} \Big(\Psi(\rho^-,k) - \Psi(\rho^+,k) + \hat{\phi}_i(t)\Big)\theta(t)\ \mathrm{d}x\mathrm{d}t \geq 0$$

which is equivalent to

$$\Psi(\rho^-,k) - \Psi(\rho^+,k) + \hat{\phi}_i(t) \geq 0$$

Taking $k = \rho_c$ and using the Rankine-Hugoniot condition $\hat{\phi}_i(t) = \Phi(\rho^+) - \Phi(\rho^-)$, we get

$$\big(\Psi(\rho^-,\rho_c) - \Phi(\rho^-)\big) - \big(\Psi(\rho^+,\rho_c) - \Phi(\rho^+)\big) \geq 0$$

Let consider the new Temple-like function $\Upsilon(\rho)$ defined by $\Upsilon(\rho) = \Psi(\rho, \rho_c) - \Phi(\rho)$, as depicted on Figure C.4. The last inequality becomes

$$\Upsilon(\rho^-) \geq \Upsilon(\rho^+) \tag{C.0.5}$$

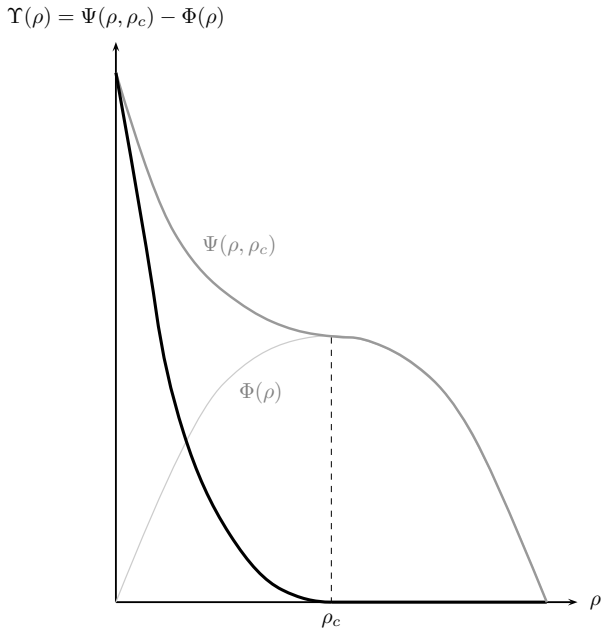

Figure C.4: Temple-like function $\Upsilon(\rho)$.

We now proceed by contradiction. Let assume that $\Phi'(\rho^-) \leq 0$ and $\Phi'(\rho^+) > 0$. Then, necessarily $\rho^- \geq \rho_c$ and $\rho^+ < \rho_c$ so $\Upsilon(\rho^-) < \Upsilon(\rho^+)$, which contradict (C.0.5). The theorem follows. □

Appendix D

Switched formulation for onramps

We propose in this section to completely solve the Riemann problem with initial data ρ^- for $x < 0$ and ρ^+ for $x \geq 0$ when an on-ramp with inflow $\hat{\phi}$ is present at $x = 0$. To do so, we do not have an other choice than considering all the possible situations for the different values of ρ^-, ρ^+ and $\hat{\phi}$.

D.1 Admissible boundary values

First, we determine all the admissible boundary values for the cases $\rho^- < \rho_c$, $\rho^- > \rho_c$, $\rho^+ < \rho_c$ and $\rho^+ > \rho_c$. Figure D.1 gives a compact representation of these admissible

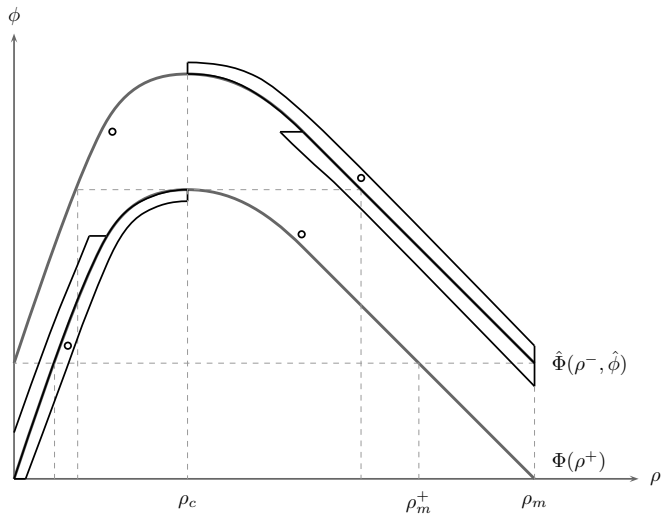

Figure D.1: Sets of admissible boundary values for all configurations.

sets for these 4 cases, the 2 fundamental diagrams being $\Phi(\rho)$ for the downstream link and $\hat{\Phi}(\rho) = \Phi(\rho) + \hat{\phi}$ for the upstream link. In Figure D.1, the dots are the proposed boundary conditions for the upstream link (on $\hat{\Phi}(\rho^-, \hat{\phi})$) and the downstream link (on $\Phi(\rho^+)$) and the stripes as well as the isolated dots are the sets of admissible boundary values according to the BLN formulation [Bardos et al., 1979]. The proposed boundary

values and admissible sets are drawn below the fundamental diagrams for densities below ρ_c and above them for densities above ρ_c.

D.2 Analytical solution of the Riemann problem

We adopt the following methodology to compute the solution to the Riemann problem. First, ρ^- is swept in the interval $(0, \rho_m)$ with $\hat{\phi}$ a positive constant. then, ρ^+ is swept in $(0, \rho_m)$ and we deduce all the possible wave interactions. Each case is then labelled with a letter in a box and a circled number, the letter being related to the value of ρ^- and the number to the value of ρ^+. To simplify the exposition, all the possible wave patterns are given in the graphical form.

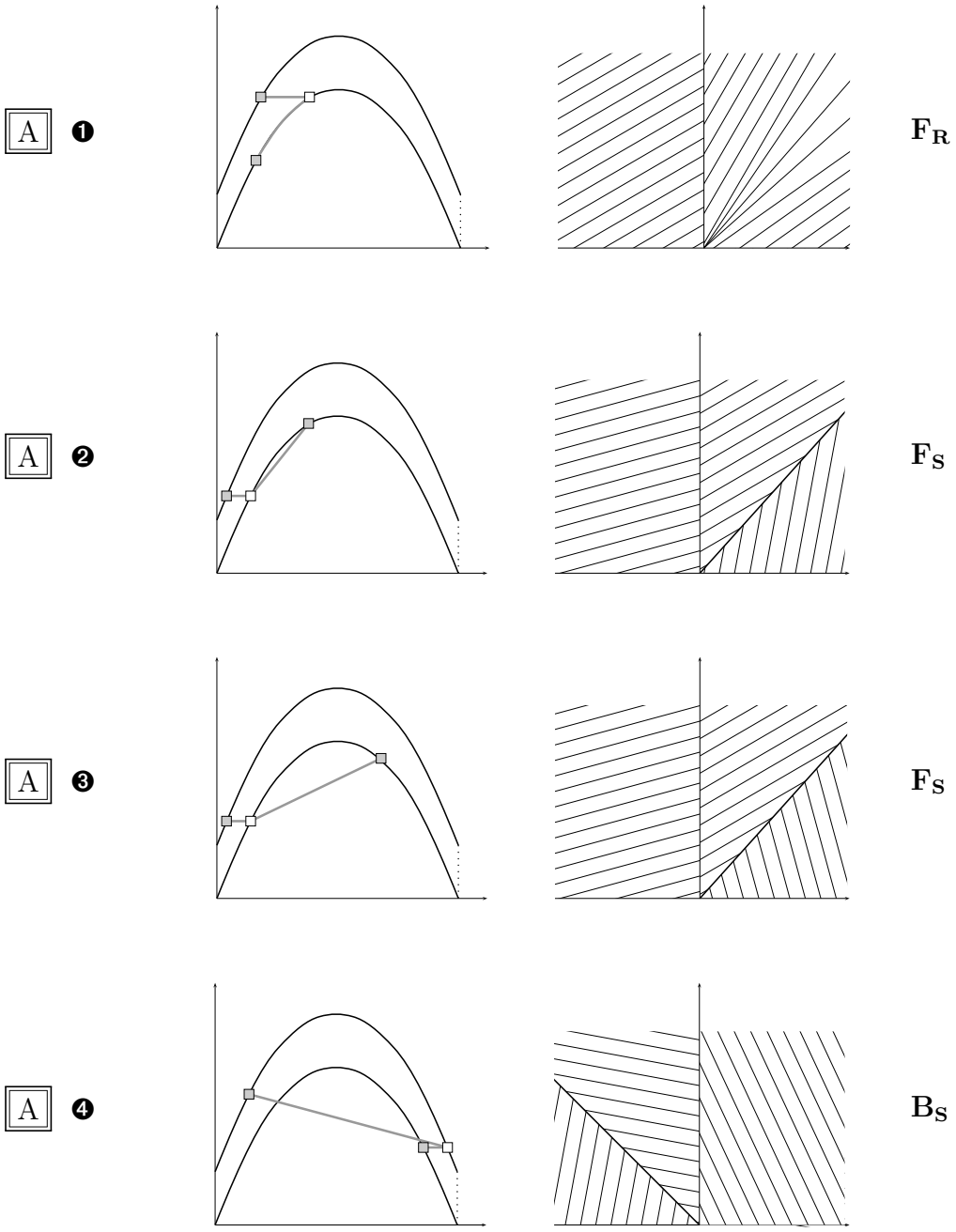

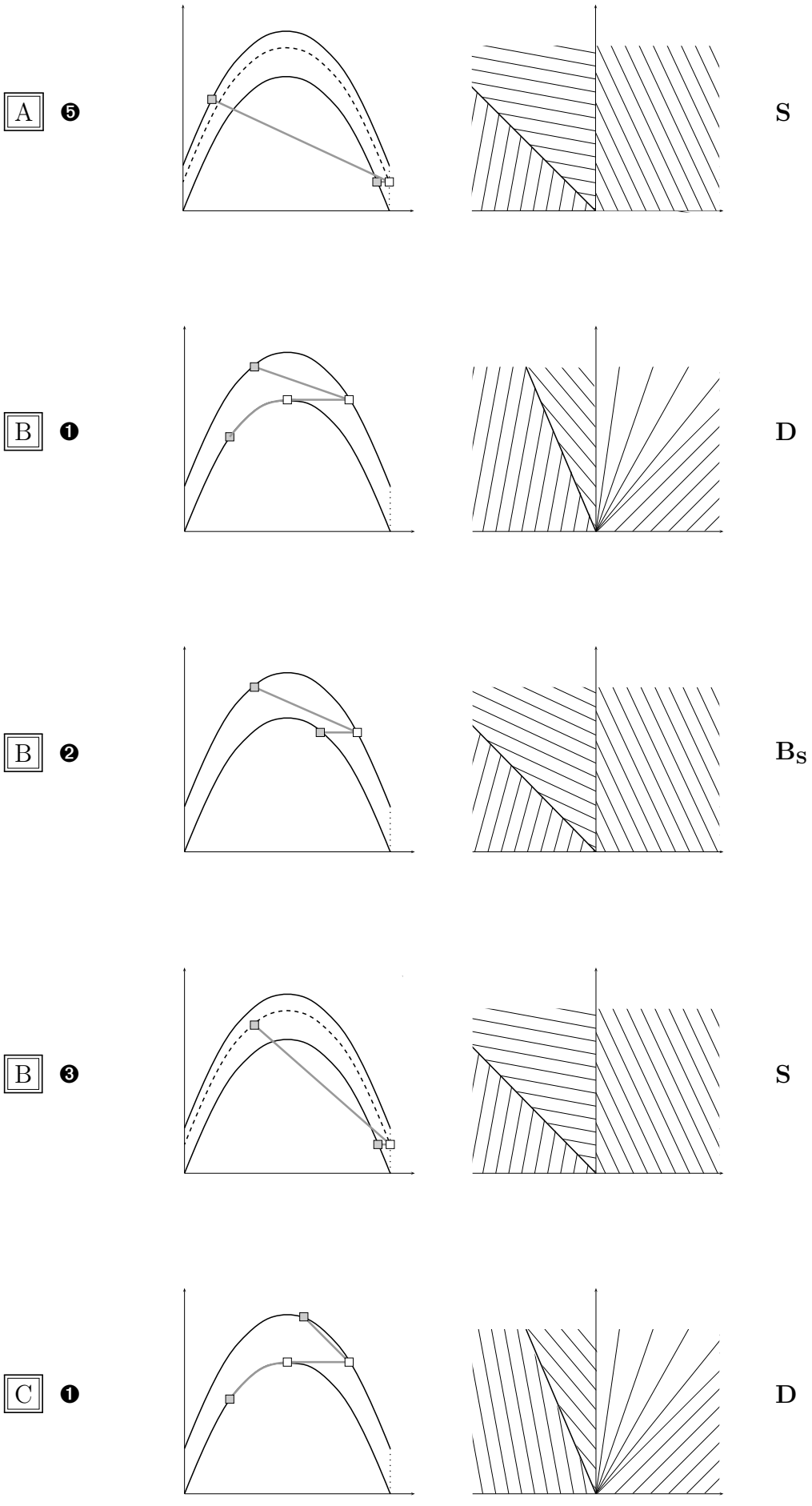

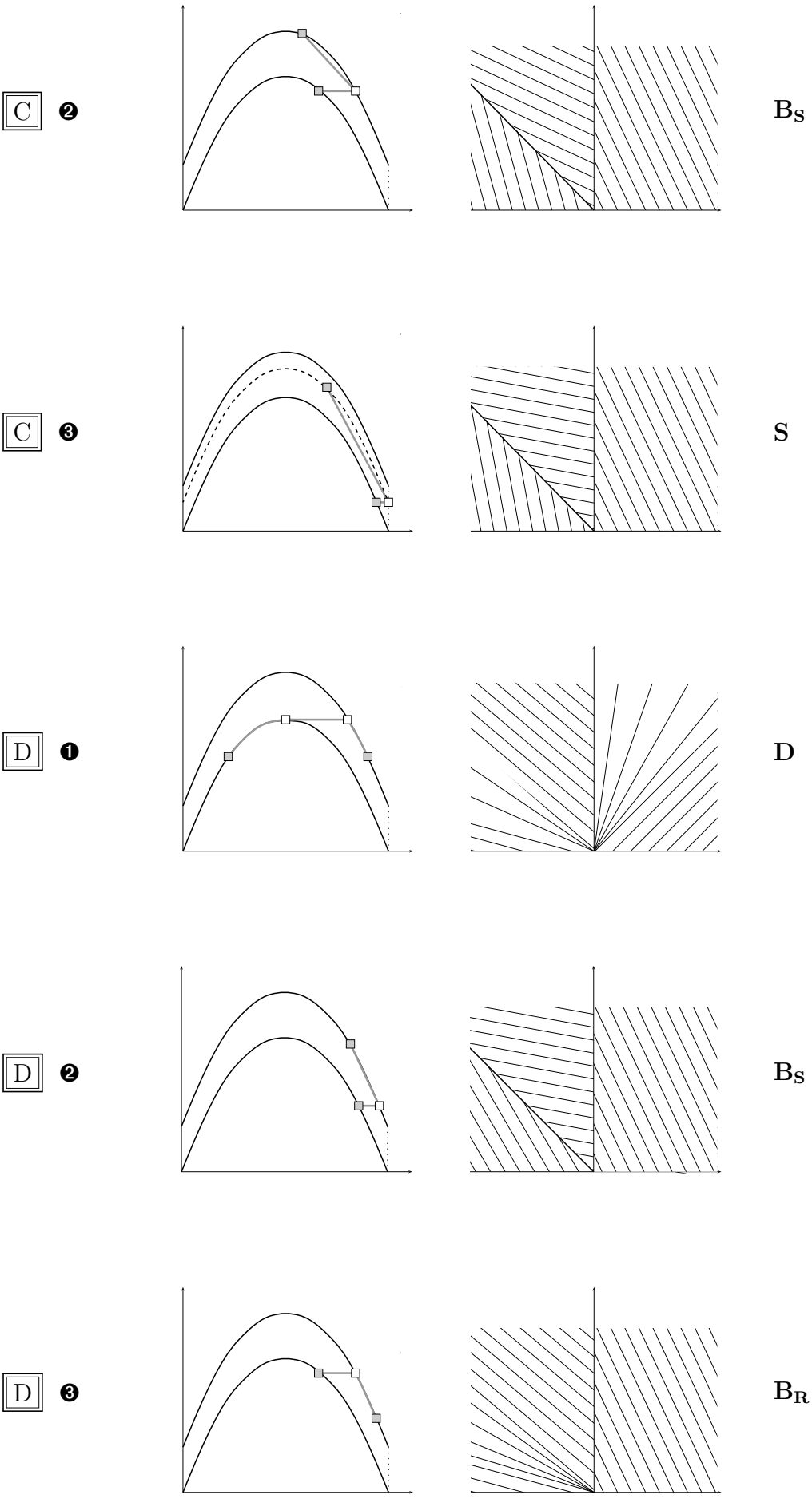

Appendix D. Switched formulation for onramps

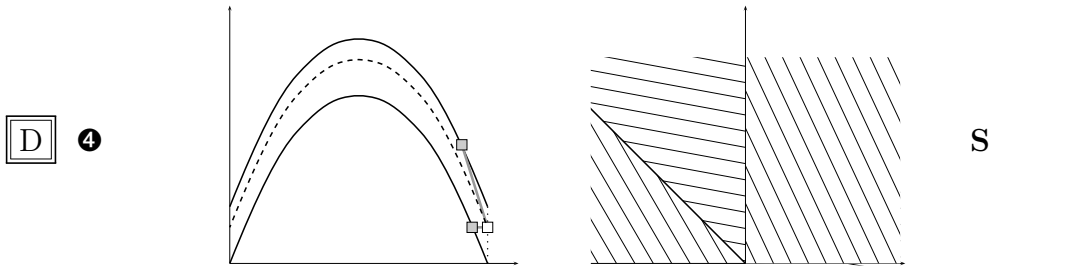

We conclude that there is 15 possibilities in total when solving an on-ramp interface problem. All these wave patterns are summarized in Figure D.2 and Table D.1, which are more convenient for the remaining analysis.

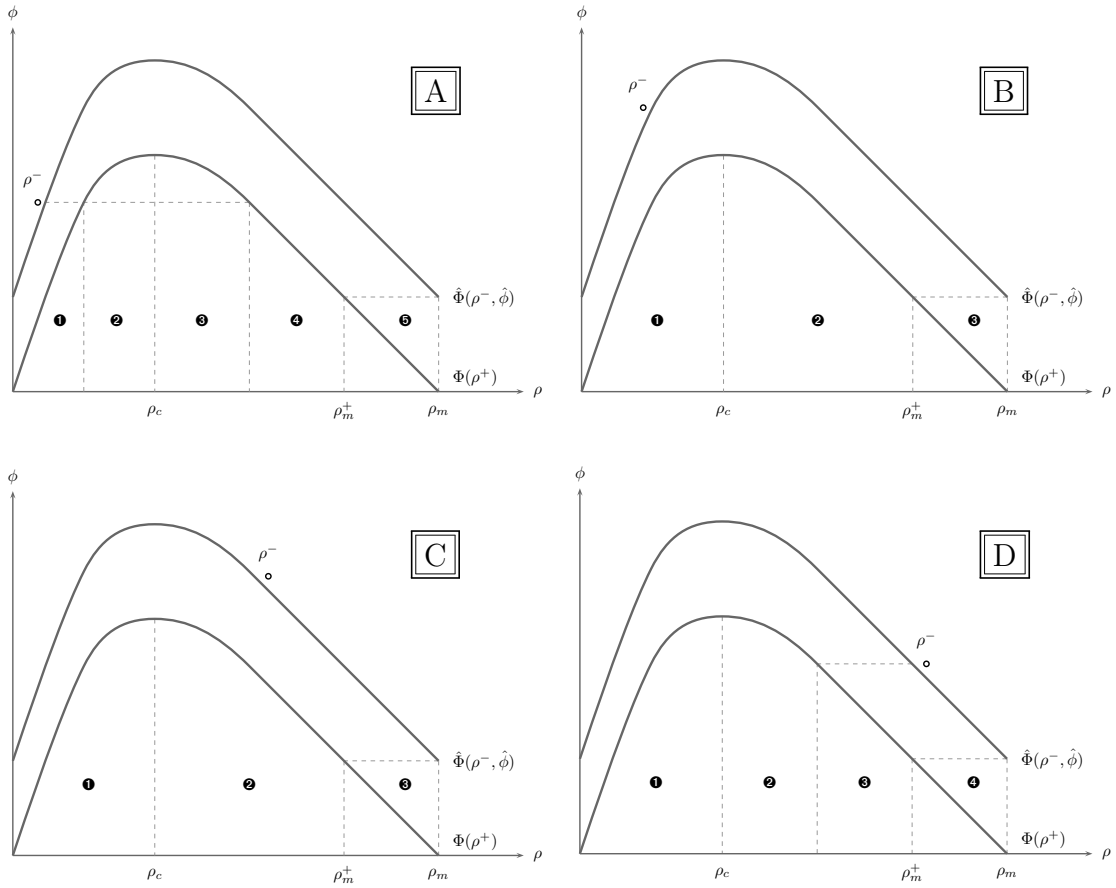

Figure D.2: Possible situations when solving the Riemann problem at interfaces with an on-ramp. Each plot corresponds to a representative value of ρ^- and each number represents a region where the value of ρ^+ gives a specific solution.

The situations $\left[\boxed{\text{C}}, ❶ \right]$ and $\left[\boxed{\text{D}}, ❶ \right]$ cannot occur in normal conditions as they correspond to a congested state upstream of the ramp and a free state downstream of it. Such situations can only be obtained if the vehicles are not allowed to enter freely in the next freeway section, which is not realistic.

The remaining states can be classified in the following 4 groups:

- **Free**: $\left[\boxed{\text{A}}, ❶ \right]$, $\left[\boxed{\text{A}}, ❷ \right]$ and $\left[\boxed{\text{A}}, ❸ \right]$ correspond to a situation where

A $\rho^- < \rho_c$ $\hat{\Phi}(\rho^-, \hat{\phi}) < \Phi_m$	❶	$\rho^+ < \rho_c$ $\Phi(\rho^+) < \hat{\Phi}(\rho^-, \hat{\phi})$	$\mathbf{F_R}$
	❷	$\rho^+ < \rho_c$ $\Phi(\rho^+) > \hat{\Phi}(\rho^-, \hat{\phi})$	$\mathbf{F_S}$
	❸	$\rho_m^+ > \rho^+ > \rho_c$ $\Phi(\rho^+) > \hat{\Phi}(\rho^-, \hat{\phi})$	$\mathbf{F_S}$
	❹	$\rho_m^+ > \rho^+ > \rho_c$ $\Phi(\rho^+) < \hat{\Phi}(\rho^-, \hat{\phi})$	$\mathbf{B_S}$
	❺	$\rho^+ > \rho_m^+$	$\mathbf{S}$
B $\rho^- < \rho_c$ $\hat{\Phi}(\rho^-, \hat{\phi}) > \Phi_m$	❶	$\rho^+ < \rho_c$	$\mathbf{D}$
	❷	$\rho_m^+ > \rho^+ > \rho_c$	$\mathbf{B_S}$
	❸	$\rho^+ > \rho_m^+$	$\mathbf{S}$
C $\rho^- > \rho_c$ $\hat{\Phi}(\rho^-, \hat{\phi}) > \Phi_m$	❶	$\rho^+ < \rho_c$	$\mathbf{D}$
	❷	$\rho_m^+ > \rho^+ > \rho_c$	$\mathbf{B_S}$
	❸	$\rho^+ > \rho_m^+$	$\mathbf{S}$
D $\rho^- > \rho_c$ $\hat{\Phi}(\rho^-, \hat{\phi}) < \Phi_m$	❶	$\rho^+ < \rho_c$	$\mathbf{D}$
	❷	$\rho_m^+ > \rho^+ > \rho_c$ $\Phi(\rho^+) < \hat{\Phi}(\rho^-, \hat{\phi})$	$\mathbf{B_S}$
	❸	$\rho_m^+ > \rho^+ > \rho_c$ $\Phi(\rho^+) > \hat{\Phi}(\rho^-, \hat{\phi})$	$\mathbf{B_R}$
	❹	$\rho^+ > \rho_m^+$	$\mathbf{S}$

Table D.1: Possible wave patterns for the Riemann problem of an onramp interface.

the upstream boundary condition is transferred downstream according to the relationship $\rho^+ = \Phi^{-l}\left(\Phi(\rho^-) + \hat{\phi}\right)$ with $\Phi^{-l}(\cdot)$ the left inverse of $\Phi(\cdot)$.

- **Congested**: $\left[\boxed{\boxed{\text{A}}}, ❹\right]$, $\left[\boxed{\boxed{\text{B}}}, ❷\right]$, $\left[\boxed{\boxed{\text{C}}}, ❷\right]$, $\left[\boxed{\boxed{\text{D}}}, ❷\right]$ and $\left[\boxed{\boxed{\text{D}}}, ❸\right]$ correspond to a situation where the downstream boundary condition is transferred upstream according to $\rho^- = \Phi^{-r}\left(\Phi(\rho^+) - \hat{\phi}\right)$ with $\Phi^{-r}(\cdot)$ the right inverse of $\Phi(\cdot)$.

- **Decoupled**: $\left[\boxed{\boxed{\text{B}}}, ❶\right]$ corresponds to a ramp flow that is large enough to create a congestion wave. This situation typically occurs when the on-ramp becomes a bottleneck. In this situation, the maximal flow crosses the interface with $\rho^+ = \rho_c$ and $\rho^- = \Phi^{-r}\left(\Phi_m - \hat{\phi}\right)$. The term decoupled is proposed here as there is no transmission (causality) of the boundary values in this case. As a consequence, the 2 links can be virtually disconnected without modifying the solution.

- **Saturated**: $\left[\boxed{\boxed{\text{A}}}, ❺\right]$, $\left[\boxed{\boxed{\text{B}}}, ❸\right]$, $\left[\boxed{\boxed{\text{C}}}, ❸\right]$ and $\left[\boxed{\boxed{\text{D}}}, ❹\right]$ correspond to a situation where the prescribed on-ramp flow $\hat{\phi}$ is not realizable as $\Phi(\rho^+) < \hat{\phi}$. In this case, $\hat{\phi}$ is decreased to $\Phi(\rho^+)$ by storing vehicles on the ramp, leading to $\rho^- = \rho_m$. It can be noted that this modification is the only one that preserves the conservation of vehicles. However, the onramp flows are usually assumed to be feasible, which removes the **Saturated** state.

Going further, the on-ramp interface behavior can be put in the form of a Finite State Machine (FSM) revealing the hybrid nature of the LWR model. In this FSM, the states are **F**, **C**, **D** and **S** respectively for Free, Congested, Decoupled and Saturated and transitions occur when the boundary values ρ^- and ρ^+ cross some prescribed values, possibly depending on the ramp flow. The Riemann problem solutions given in Table D.1 provide the following possible transitions:

- **F** → **F**: $\left[\boxed{\boxed{\text{A}}}, ❶\right]$, $\left[\boxed{\boxed{\text{A}}}, ❷\right]$ and $\left[\boxed{\boxed{\text{A}}}, ❸\right]$.
- **F** → **C**: $\left[\boxed{\boxed{\text{A}}}, ❹\right]$ and $\left[\boxed{\boxed{\text{B}}}, ❷\right]$.
- **F** → **D**: $\left[\boxed{\boxed{\text{B}}}, ❶\right]$.
- **D** → **D**: $\left[\boxed{\boxed{\text{B}}}, ❶\right]$.
- **D** → **F**: $\left[\boxed{\boxed{\text{A}}}, ❷\right]$.
- **D** → **C**: $\left[\boxed{\boxed{\text{D}}}, ❷\right]$.
- **D** → **S**: $\left[\boxed{\boxed{\text{D}}}, ❹\right]$.
- **S** → **C**: $\left[\boxed{\boxed{\text{D}}}, ❸\right]$.

- **F** → **S**: $\left[\boxed{\text{A}}, ❺ \right]$ and $\left[\boxed{\text{B}}, ❸ \right]$.
- **C** → **C**: $\left[\boxed{\text{A}}, ❹ \right]$, $\left[\boxed{\text{C}}, ❷ \right]$, $\left[\boxed{\text{D}}, ❷ \right]$ and $\left[\boxed{\text{D}}, ❸ \right]$.
- **C** → **F**: $\left[\boxed{\text{A}}, ❸ \right]$.
- **C** → **S**: $\left[\boxed{\text{C}}, ❸ \right]$, $\left[\boxed{\text{D}}, ❹ \right]$.

Note that some Riemann problem solution can be affected to several transition. For instance, if $\left[\boxed{\text{A}}, ❸ \right]$ occurs when in the **F** state, it means that the congestion wave that came from downstream was not strong enough the put the upstream link in a congested state. On the other side, if $\left[\boxed{\text{A}}, ❸ \right]$ occurs when in the **C** state, it means that a free flow wave came from upstream and is strong enough to free the traffic downstream. Moreover, note that **S** is an intermediate state where a queue builds up at the on-ramp and leads to **C**. This queue can be taken into account by adding its length as a continuous state in **S**, its evolution being modelled by a simple integrator. Nevertheless, we generally assume that the state **S** never occurs.

For this reason, the state **S** is often not mentioned explicitly in the book.

The switched interface model presented above can then be put in the form of the Finite State Machine given in Figure D.3. The off-ramp case can be treated in a similar way, leading to a FSM which is very similar to the one given in Figure D.3.

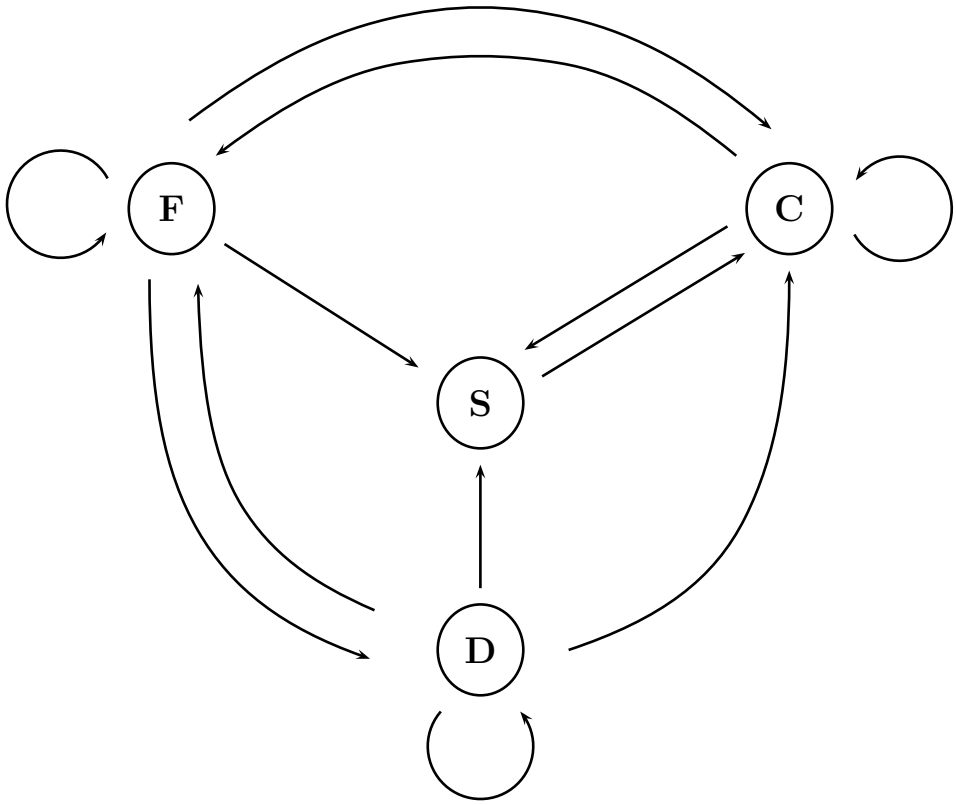

Figure D.3: Finite State Machine modelling the on-ramp interface behavior.

Appendix E

Analysis of the LWR model with a singular source term

E.1 The method of generalized characteristics

We recall that the LWR model with a singular source term is

$$\partial_t \rho(t,x) + \partial_x \Phi(\rho(t,x)) = \sum_{i=1}^{N_{\text{on}}} \delta(x - \hat{x}_i)\hat{\phi}_i(t) + \sum_{j=1}^{N_{\text{off}}} \delta(x - \check{x}_j)\check{\phi}_j(t) \tag{E.1.1}$$

Let analyse this model using the method of generalized characteristics introduced in [Dafermos, 1977*b*]. The homogeneous LWR model on $x \in (0, L)$ writes in quasi-linear form

$$\partial_t \rho(t,x) + \Phi'(\rho(t,x))\partial_x \rho(t,x) = 0 \tag{E.1.2}$$

It can be partially solved by the method of characteristics [Evans, 1998] which states that $\rho(\xi(t,x_0),t) = \sigma(t,x_0)$ where (ξ,σ) solves the ordinary differential equation

$$\begin{cases} \dot{\xi}(t,x_0) = \Phi'\big(\sigma(t,x_0)\big) \\ \dot{\sigma}(t,x_0) = 0 \\ \xi(0,x_0) = x_0 \\ \sigma(0,x_0) = y_I(x_0) \end{cases} \tag{E.1.3}$$

with t the independent variable and $x_0 \in (0, L)$ parameterizing the initial condition. Assuming that the solution ρ is piecewise-C^1, then the product $\Phi'(\rho(t,x))\partial_x\rho(t,x)$ in (E.1.2) is not well-defined in general as it may involves a Dirac measure and a discontinuous function at the jump locations. To overcome this difficulty and allow the use of the characteristic method, the author of [Dafermos, 1977*b*] introduced the concept of generalized characteristics and showed that (E.1.3) is still valid if interpreted in the sense of Filippov [Filippov, 1988] when the right side of (E.1.3) is irregular. For the homogeneous LWR model (E.1.2), it is shown in [Dafermos, 1977*b*] that the characteristics

$\xi(t, x_0)$ are Lipschitz curves with corners when reaching a shock wave. Outside shocks, they are straight lines as mentioned in [Ansorge, 1990].

Let now consider the Charatheodory ordinary differential equation [Filippov, 1988]

$$\begin{cases} \dot{\xi}(t, x_0) \doteq \Phi'\big(\rho_I(x_0)\big) \\ \dot{\sigma}(t, x_0) \doteq \sum_{i=1}^{N_{\text{on}}} \delta(\xi(t, x_0) - \hat{x}_i)\hat{\phi}_i(t) + \sum_{j=1}^{N_{\text{off}}} \delta(\xi(t, x_0) - \check{x}_j)\check{\phi}_j(t) \\ \xi(0, x_0) = x_0 \\ \sigma(0, x_0) = \rho_I(x_0) \end{cases} \tag{E.1.4}$$

where the symbol $\doteq$ means that the left and right hand sides are equals almost everywhere due to the possible presence of discontinuous terms or singular measures. Setting $\sigma(t, x_0) = \rho(\xi(t, x_0), t)$, we get

$$\begin{aligned} \dot{\sigma}(t, x_0) = \frac{\mathrm{d}}{\mathrm{d}t}\rho(\xi(t, x_0), t) &= \partial_t \rho(\xi(t, x_0), t) + \dot{\xi}(t, x_0)\partial_x \rho(\xi(t, x_0), t) \\ &= \partial_t \rho(\xi(t, x_0), t) + \Phi'\big(\sigma(t, x_0)\big)\partial_x \rho(\xi(t, x_0), t) \\ &= \sum_{i=1}^{N_{\text{on}}} \delta(\xi(t, x_0) - \hat{x}_i)\hat{\phi}_i(t) + \sum_{j=1}^{N_{\text{off}}} \delta(\xi(t, x_0) - \check{x}_j)\check{\phi}_j(t) \end{aligned}$$

Following the method developed in [Filippov, 1988] and [Dafermos, 1977*b*], the ordinary differential equation (E.1.4) has a unique *continuous* solution for all x_0 even if it is defined almost everywhere and has an irregular right hand side. The local characteristic behavior is analysed in a subset $(x, t) \in (x_L, x_R) \times (t^-, t^+)$ where $\xi(t, x_0)$ is assumed to be a piecewise straight line with a corner at the on-ramp location, as represented on Figure E.1. In particular, this local analysis enables to consider one on-ramp only and analyse its local behavior. Two cases are considered in the analysis, the case of monotonic wave

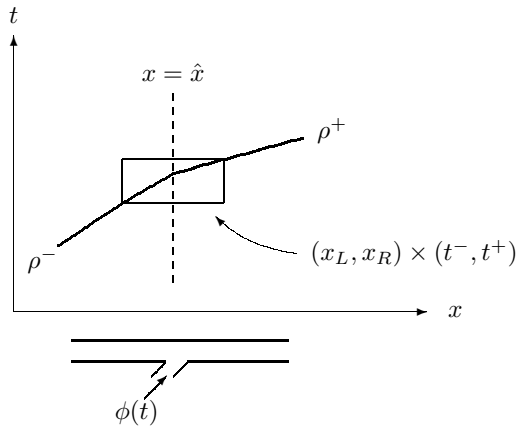

Figure E.1: Restricted region with a ramp.

propagation when the characteristic crosses the on-ramp and the case of reflexive wave propagation then the characteristic is reflected at the on-ramp.

E.2 Case of monotonic wave propagation

We consider in this section the special case (represented on Figure E.1) where $\xi(t, x_0)$ is monotonic and invertible.To solve (E.1.4), a regularization of the problem is considered. Let set $\delta_\epsilon(x) = \frac{1}{\epsilon} g\left(\frac{x}{\epsilon}\right)$ with $\epsilon > 0$ and $g(x) \in C^\infty(\mathbb{R})$ satisfying

1. $g(x) = 0 \quad \text{for } |x| \geq 1$
2. $g(x) \geq 0$
3. $\int_{-1}^{1} g(x)dx = 1$

Then $\delta_\epsilon(x)$ approximates the Dirac distribution, i.e. $\lim_{\epsilon \downarrow 0} \delta_\epsilon(x) = \delta(x)$, and we have the regularized Heaviside distribution

$$H_\epsilon(x) = \int_{-\infty}^{\infty} \delta_\epsilon(s)ds$$

with the inherited properties

1. $H_\epsilon(x) = 0 \quad \text{for } x \leq \epsilon$
2. $H_\epsilon(x) = 1 \quad \text{for } x \geq \epsilon$
3. $\sup_{\mathbb{R}} |H_\epsilon(x)| = 1$

Regularizing the problem consist in replacing $\delta(\cdot)$ by $\delta_\epsilon(\cdot)$ in Equation (E.1.4) to get

$$\begin{cases} \dot{\xi}(t, x_0) = \Phi'\big(\sigma(t, x_0)\big) \\ \dot{\sigma}(t, x_0) = \delta_\epsilon(\xi(t, x_0) - \hat{x})\phi(t) \end{cases} \tag{E.2.1}$$

In that case, we choose $x_L < \xi(t^-) < \hat{x} - \epsilon$ and $x_R > \xi(t^+) > \hat{x} - \epsilon$ for the local analysis. For ϵ small enough, we consider that no shock occurs in $(x_L, x_R) \times (t^-, t^+)$, leading to a solution as represented in figure E.2. Multiplying the first and the second equations in

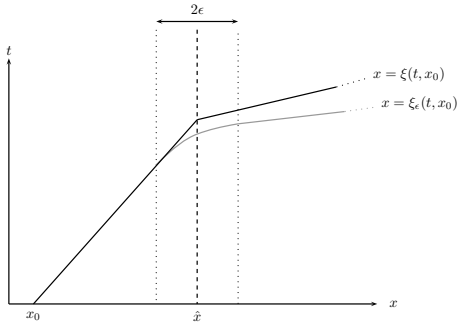

Figure E.2: Regularized problem close to the interface.

(E.2.1) and integrating between t^- and t^+, we get

$$I = \int_{t^-}^{t^+} \Phi'\big(\sigma(t,x_0)\big)\dot{\sigma}(t,x_0)dt = \int_{t^-}^{t^+} \delta_\epsilon(\xi(t,x_0)-\hat{x})\dot{\xi}(t,x_0)\phi(t)dt$$

The left side gives

$$I = \Phi\big(\sigma(t^+,x_0)\big) - \Phi\big(\sigma(t^-,x_0)\big)$$

and the right side gives

$$\begin{aligned}
I &= \int_{\xi(t^-,x_0)}^{\xi(t^+,x_0)} \delta_\epsilon(s-\hat{x})\phi(\xi^{-1}(s,x_0))ds \\
&= \big[H_\epsilon(s-\hat{x})\phi(\xi^{-1}(s,x_0))\big]_{\xi(t^-,x_0)}^{\xi(t^+,x_0)} - \int_{\xi(t^-,x_0)}^{\xi(t^+,x_0)} H_\epsilon(s-\hat{x})\frac{d\phi(\xi^{-1}(s,x_0))}{ds}ds \\
&= \phi(t^+) - \int_{\hat{x}-\epsilon}^{\hat{x}+\epsilon} H_\epsilon(s-\hat{x})\frac{d\phi(\xi^{-1}(s,x_0))}{ds}ds - \int_{\hat{x}+\epsilon}^{\xi(t^+,x_0)} d\big(\phi(\xi^{-1}(s,x_0))\big) \\
&= \phi(\xi^{-1}(\hat{x}+\epsilon,x_0)) + \int_{\hat{x}-\epsilon}^{\hat{x}+\epsilon} H_\epsilon(s-\hat{x})\dot{\phi}(\xi^{-1}(s,x_0))ds
\end{aligned}$$

with the last term verifying

$$\int_{\hat{x}-\epsilon}^{\hat{x}+\epsilon} |H_\epsilon(s-\hat{x})\dot{\phi}(\xi^{-1}(s,x_0))|ds \leq 2\epsilon \sup_{s\in(-\epsilon,\epsilon)} |\dot{\phi}(\xi^{-1}(\hat{x}+s,x_0))|$$

Making $\epsilon \to 0$, $(x_L,x_R)\times(t^-,t^+)$ becomes an infinitely small neighborhood around the interface and with $\phi(t)$ Lipschitz, we get

$$\Phi\big(\sigma(t^+,x_0)\big) = \Phi\big(\sigma(t^-,x_0)\big) + \phi(\xi^{-1}(\hat{x},x_0))$$

which is exactly the flow balance at the on-ramp interface. A closer look shows that the map $\Phi(\cdot)$ is locally invertible in the special case of monotonic wave propagation, which explains the result. As in the strong formulation, the characteristics may intersect after crossing the interface, leading to a classical shock.

Note that distributional calculus cannot be used here as $\dot{\sigma}\Phi'(\sigma)$ is the product of a measure with a discontinuous function, which is ill-defined in distribution theory. Moreover, we could be tempted to use the identity

$$\delta(\xi(t,x_0)-\hat{x}) = \frac{\delta(t-\xi^{-1}(\hat{x},x_0))}{|\dot{\xi}(\xi^{-1}(\hat{x},x_0))|}$$

but again, it is the same kind of product and $\dot{\xi}(\xi^{-1}(\hat{x}))$ is not defined.

E.3 Case of reflexive wave propagation

Let consider a freeway which is in free flow upstream to an on-ramp at the initial condition. Such a case is illustrated in Figure E.3. As time evolves, a characteristic may be

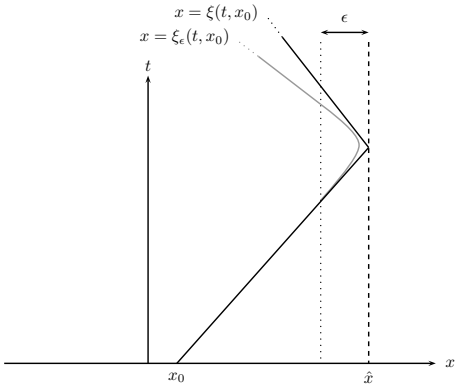

Figure E.3: Regularized problem close to the interface.

reflected if the on-ramp flow exceeds the flow that can be transmitted downstream, i.e. the capacity. Note that we do not consider the interaction between characteristics and consider each characteristic as if it was isolated.

We consider again a regularized problem as represented in Figure E.3. If a characteristic is reflected then there must be a time $\tilde{t}(\epsilon)$ when

$$\dot{\xi}(\tilde{t}(\epsilon), x_0) = 0 \quad \Leftrightarrow \quad \Phi'(\sigma(\tilde{t}(\epsilon), x_0)) = 0 \quad \Leftrightarrow \quad \Phi(\sigma(\tilde{t}(\epsilon), x_0)) = \Phi_{\mathrm{m}}$$

So, formally, as $\epsilon \to 0$, we have $\tilde{t}(\epsilon) \to \tilde{t}$ and $\xi(\tilde{t}(\epsilon), x_0) \to \hat{x}$. We can thus assume reasonably that $\Phi(\rho(\hat{x}, t)) = \Phi_{\mathrm{m}}$ constitute the boundary condition for the downstream domain.

The flow conservation principle then tells that $\Phi(\rho^+) = \max \Phi(\cdot) - \hat{\phi}(t)$ with ρ^+ the downstream state when the characteristic goes forward at the initial condition.

For illustration, we provide below some simulation of the aforementioned situations. Figure E.4 shows the characteristics ξ and the density values σ for different values of the regularizing parameter ϵ in the monotonic wave propagation case. We can see the numerical convergence towards the physical solution. Figure E.5 shows the same variables in a reflexive wave propagation case where we can observe again the numerical convergence towards the physical solution. Figure E.6 shows the birth and propagation of a shock wave at an on-ramp and its dissipation through a rarefaction wave when the in flow vanishes. This figure illustrates how a shock generates upstream as characteristics intersect.

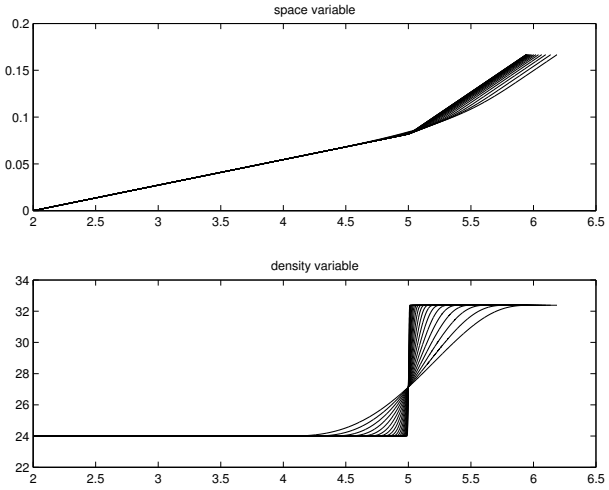

Figure E.4: Regularized problem for the forward monotonic propagation case.

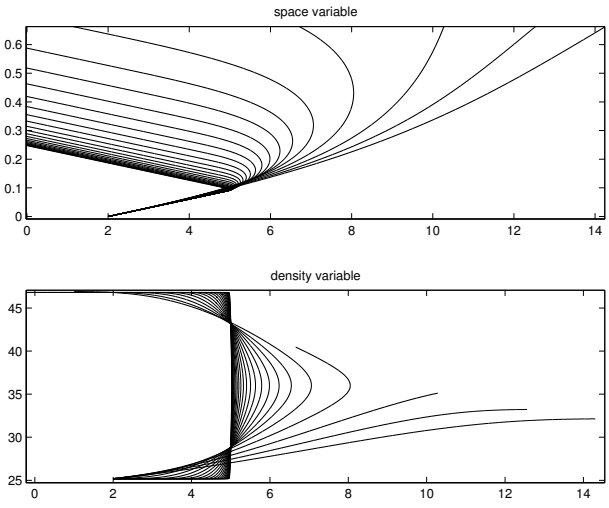

Figure E.5: Regularized problem convergence for the forward reflective propagation case.

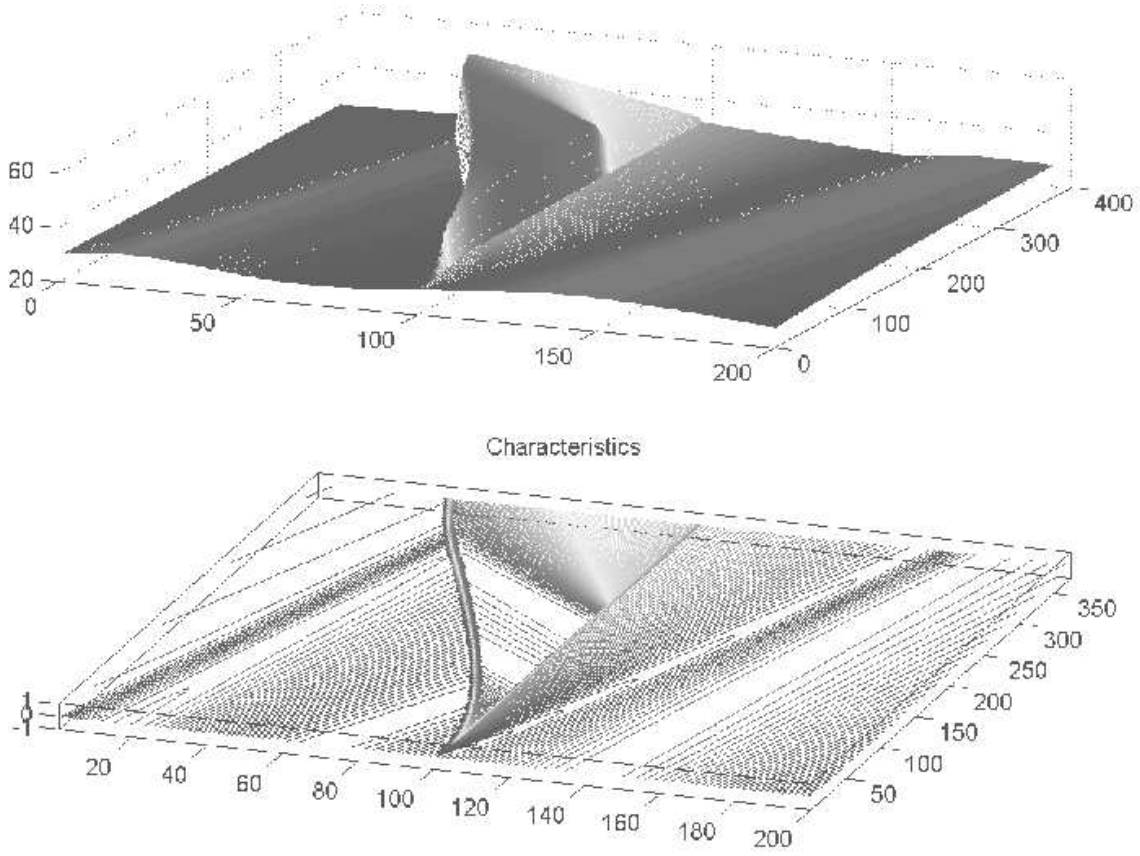

Figure E.6: Example of the birth of a shock and its dissipation when the inflow stops.

Appendix E. Analysis of the LWR model with a singular source term

Bibliography

Alessandri, A., Febbaro, A. D., Ferrara, A. & Punta, E. [1998], 'Optimal control of freeways via speed signalling and ramp metering', *Control Engineering Practice* **6**.

Ancona, F. & Coclite, G. [2005], 'On the attainable set for temple class systems with boundary controls', *SIAM Journal on Control and Optimization* **43**(6).

Ansorge, R. [1990], 'What does the entropy condition mean in traffic flow theory?', *Transportation Research Part B: Methodological* .

Aw, A., Klar, A., Materne, T. & Rascle, M. [2002], 'Derivation of continuum traffic flow models from microscopic follow-the-leader models', *SIAM Journal of Applied Mathematics* **63**(1).

Aw, A. & Rascle, M. [2000], 'Resurrection of 'second order' models of traffic flow', *SIAM Journal on Applied Mathematics* .

Balogh, A. & Krstic, M. [2004], 'Stability of partial difference equations governing control gains in infnite-dimensional backstepping', *Systems and Control Letters* **51**.

Bardos, C., LeRoux, A. & Nedelec, J. [1979], 'First order qusilinear equations with bounday conditions', *Communications in Partial Differential Equations* .

Bardos, C. & Pironneau, O. [2003], 'Derivatives and control in the presence of shocks', *Computational Fluid Dynamics Journal* **11**(4), 383–392.

Bayen, A. M., Raffard, R. & Tomlin, C. J. [2004], Adjoint-based constrained control of eulerian transportation networks: Application to air traffic control, *in* 'IEEE Proceeding of the American Control Conference'.

Bermudez, A. & Vazquez, M. [1994], 'Upwind methods for hyperbolic conservation laws with source terms', *Computers Fluids* **23**.

Bewley, T., Temam, R. & Ziane, M. [2000], 'A general framework for robust control in fluid mechanics', *Physica D* **138**.

Bouchut, F. & James, F. [1998], 'One-dimensional transport equations with discontinuous coefficients', *Nonlinear Analysis: Theory, Methods and Applications* **32**.

Bouchut, F. & James, F. [1999], *Hyperbolic Problems: Theory, Numerics, Applications*, Vol. 129 of *International Series of Numerical Mathematics*, Birkh"auser, chapter Differentiability with respect to initial data for a scalar conservation law.

Boyd, S. & Vandenberghe, L. [2004], *Convex Optimization*, Cambridge University Press.

Bressan, A. [2000], *Hyperbolic Systems of Conservation Laws - The One-dimensional Cauchy Problem*, Oxford University Press.

Bressan, A., Crasta, G. & Piccoli, B. [2000], *Well posedness of the Cauchy problem for nxn systems of conservation laws*, Vol. 694, AMS Memoirs.

Bui, D., Nelson, P. & Narasimhan, S. [1992], Computational realizations of the entropy condition in modelling congested traffic flow, Technical Report 1232-7, Texas Transportation Institute.

Buisson, C., Lebacque, J. & Lesort, J. [1996], Strada, a discretized macroscopic model of vehicular flow in complex networks based on the godunov scheme, *in* 'Proceedings of the CESA'96 IEEE Conference'.

Castillo, J. D. & Benitez, F. [1995], 'On the functional form of the speed-density relationship. I: General theory. II: Empirical investigation.', *Transportation Research Part B: Methodological* **29**.

Chen, M.-L. & Georges, D. [1999], Nonlinear optimal control of an open-channel hydraulic system based on an infinite-dimensional model, *in* 'Proceedings of the 1999 Conference on Decision and Control'.

Coclite, G., Garavello, M. & Piccoli, B. [2005], 'Traffic flow on a road network', *SIAM Journal on Mathematical Analysis* **36**.

Collis, S. S., Ghayour, K., Heinkenschloss, M., Ulbrichf, M. & Ulbrich, S. [2002], 'Optimal control of unsteady compressible viscous flows', *International Journal for Numerical Methods in Fluids* **40**.

Colombo, R. M. & Groli, A. [2004], 'On the optimization of a conservation law', *Calc. Var. Partial Differential Equations* **19**.

Coron, J.-M., d'Andréa Novel, B. & Bastin, G. [2004], A strict lyapunov function for boundary control of hyperbolic systems of conservation laws, *in* 'Proceedings of the 43rd IEEE Conference on Decision and Control'.

Cuzzola, F. & Morari, M. [2002], 'An lmi approach for h_∞ analysis and control of discrete-time piecewise affine systems', *International Journal of Control* **75**(16-17).

Dafermos, C. [1977*a*], Characteristics in hyperbolic conservation laws. a study of the structure and the asymptotic behaviour of solutions, *in* R. Knops, ed., 'Nonlinear analysis and mechanics: Heriot-Watt Symposium', Vol. 1 of *Research Notes in Mathematics*, Pitman.

Dafermos, C. [1977*b*], 'Generalized characteristics and the structure of solutions of hyperbolic conservation laws', *Indiana University Mathematics Journal* .

Dafermos, C. [2000], *Hyperbolic conservation laws in continuum physics*, Springer.

Daganzo, C. [1995*a*], 'The cell transmission model part II: Network traffic', *Transportation Research Part B: Methodological* **29**(2).

Daganzo, C. [1995*b*], 'Requiem for second-order fluid approximations of traffic flow', *Transportation Research Part B: Methodological* **29**.

Daganzo, C. [2005], 'A variational formulation of kinematic waves. I: Basic theory and complex boundary conditions. II: Solution methods.', *Transportation Research Part B: Methodological* **39**.

Daganzo, C. F. [1994], 'The cell transmission model: A dynamic representation of highway traffic consistent with the hydrodynamic theory', *Transportation Research Part B: Methodological* **28**(4).

de Halleux, J., Prieur, C., Coron, J.-M., d'Andréa Novel, B. & Bastin, G. [2003], 'Boundary feedback control in networks of open channels', *Automatica* .

DiPerna, R. [1979], The structure of solutions to hyperbolic conservation laws, *in* R. Knops, ed., 'Nonlinear analysis and mechanics: Heriot-Watt Symposium', Vol. 4 of *Research Notes in Mathematics*, Pitman.

Diperna, R. [1985], 'Measure-valued solutions to conservation laws', *Archive for Rational Mechanics and Analysis* **88**.

DiPerna, R. J. [1975], 'Singularities of solutions of nonlinear hyperbolic systems of conservation laws', *Archive for Rational Mechanics and Analysis* **60**.

Dubois, F. & LeFloch, P. [1988], 'Boundary conditions for nonlinear hyperbolic systems of conservation laws', *Journal of Differential Equations* .

Evans, L. [1998], *Partial Differential Equations*, American Mathematical Society.

Evans, L. & Gariepy, R. F. [1991], *Measure Theory and Fine Properties of Functions*, CRC-Press.

Federer, H. [1969], *Geometric measure theory*, Springer.

Ferrari-Trecate, G., Cuzzola, F., Mignone, D. & Morari, M. [2002], 'Analysis of discrete-time piecewise affine and hybrid systems', *Automatica* **38**(12).

Filippov, A. [1988], *Differential Equations with Discontinuous Right-hand Side*, Kluwer Academic Publisher.

Garavello, M. & Piccoli, B. [2005], 'Source-destination flow on a road networks', *Communications in Mathematical Sciences* **3**.

Garavello, M. & Piccoli, B. [2006*a*], 'Traffic flow on a road network using the aw-rascle model', *Communications in Partial Differential Equations* **31**.

Garavello, M. & Piccoli, B. [2006*b*], *Traffic flow on network*, number 1 *in* 'Applied Mathematics Series', American Institute of Mathematical Sciences.

Gavage, S. B. & Colombo, R. [2003], 'An n-populations model for traffic flow', *European Journal of Applied Mathematics* **14**.

George, D. L. & LeVeque, R. J. [2006], 'Finite volume methods and adaptive refinement for global tsunami propagation and local inundation', *Science of Tsunami Hazards* **24**.

Ghattas, O. & Bark, J. [1997], 'Optimal control of two- and three- dimensional incompressible navier-stokes flows', *Journal of Computational Physics* **136**.

Giles, M. & Pierce, N. [2001], 'Analytic adjoint solutions for the quasi-one-dimensional euler equations', *Journal of Fluid Mechanics* **426**.

Godlewski, E. & Raviart, P. [1996], *Numerical Approximation of Hyperbolic Systems of Conservation Laws*, Applied Mathematical Sciences, Springer.

Godlewski, E. & Raviart, P. [1999], 'The linearized stability of solutions of nonlinear hyperbolic systems of conservation laws. a general numerical approach.', *Mathematics and Computers in Simulation* **50**.

Godunov, S. [1959], 'A difference method for the numerical calculation of discontinuous solutions of hydrodynamic equations', *Matematicheskii Sbornik* **47**.

Gomes, G. & Horowitz, R. [2003], A study of two onramp metering schemes for congested freeways, *in* 'Proceedings of the American Control Conference'. Control-like analysis of ALINEA and an other controller.

Gomes, G. & Horowitz, R. [2004], Globally optimal solutions to the onramp metering problem - part i and ii., *in* 'IEEE Proceedings of the Intelligent Transportation Systems Conference'.

Gomes, G. & Horowitz, R. [2006], 'Optimal freeway ramp metering using the asymmetric cell transmission model', *Transportation Research Part C: Emerging Technologies* **Under review**.

Greenberg, H. [1959], 'An analysis of traffic flow', *Operation Research* **7**.

Greenberg, J. M. [2001], 'Extensions and amplifications of a traffic model of aw and rascle', *SIAM Journal on Applied Mathematics* **62**.

Greenshields, B. D. [1935], 'A study of traffic capacity', *Highway Research Board Proceedings* **14**.

Haut, B. & Bastin, G. [2005], A second order model for road traffic networks, *in* 'Proceedings of the 2005 Conference on Decision and Control'.

Hegyi, A., Schutter, B. D., Hellendoorn, H. & van den Boom, T. [2002], Optimal coordination of ramp metering and variable speed control - an MPC approach, *in* 'Proceedings of the 2002 American Control Conference'.

Herty, M., Kirchner, C. & Moutari, S. [2006], 'Multi-class traffic models on road networks', *Communications in Mathematical Sciences* **4**.

Herty, M., Moutari, S. & Rascle, M. [2006], 'Optimization criteria for modelling intersections of vehicular traffic flow', *Networks and Heterogeneous Media* **1**.

Herty, M. & Rascle, M. [2006], 'Coupling conditions for a class of second order models for traffic flow', *SIAM Journal on mathematical analysis* **38**.

Hinze, M. & Kunisch, K. [2001], 'Second order methods for optimal control of time-dependent fluid flow', *SIAM Journal on Control and Optimization* **40**(3).

Hiriart-Urruty, J. & Lemaréchal, C. [1993], *Convex analysis and minimization algorithms. I: Fundamentals. II: Advance theory and bundle methods.*, Springer-Verlag.

Holden, H., Holden, L. & Hoegh-Krohn, R. [1988], 'A numerical method for first order nonlinear scalar conservation laws in one-dimension', *Comput. Math. Applic* **15**(6-8).

Holden, H. & Risebro, N. [1995], 'A mathematical model of traffic flow on a network of unidirectional roads', *SIAM Journal on Mathematical Analysis* **26**.

Hopf, E. [1950], 'The partial differential equation $u_t + uu_x = \mu u_{xx}$', *Communications on Pure and Applied Mathematics* **3**.

Jacquet, D., Canudas de Wit, C. & Koenig, D. [2005], Traffic control and monitoring with a macroscopic model in the presence of strong congestion waves, *in* 'Proceedings of the 2005 Conference on Decision and Control'.

James, F., Peng, Y. & Perthame, B. [1995], 'Kinetic formulation for chromatography and some other hyperbolic systems', *Journal de Mathématiques Pures et Appliquées* **74**(4).

Jameson, A. [1995], Optimum aerodynamic design using CFD and control theory, *in* '12th AIAA Computational Fluid Dynamics Conference'.

Jameson, A. [2003], 'Aerodynamic shape optimization using the adjoint method', Lecture Series at the Von Karman Institute, Brussels, Belgium.

Jameson, A., Martinelli, L. & Pierce, N. [1998], 'Optimum aerodynamic design using the navier-stokes equations', *Theoretical Computational Fluid Dynamics* **10**.

Jin, W. L. & Zhang, H. M. [2003], 'The inhomogeneous kinematic wave traffic flow model as a resonant nonlinear system', *Transportation Science* **37**(3).

Jin, W. & Zhang, H. [2004], A multicommodity kinematic wave simulation model of network traffic flow, *in* 'TRB 2004 Annual Meeting'.

Johansson, M. & Rantzer, A. [1998], 'Computation of piecewise quadratic lyapunov functions for hybrid systems', *IEEE Transactions on Automatic Control* **43**(4).

Joseph, K. & LeFloch, P. [1999], 'Boundary layers in weak solution of hyperbolic conservation laws', *Archive for Rational Mechanics and Analysis* **147**.

Kotsialos, A. & Papageorgiou, M. [2004], 'Nonlinear optimal control applied to coordinated ramp metering', *IEEE Transactions on Control Systems Technology* **12**(6).

Kröner [1997], *Numerical schemes for conservation laws*, Wiley-Teubner. Boundary conditions, equivalence of the BLN and DL conditions in the scalar case.

Krstic, M. [1999], 'On global stabilization of burgers equation by boundary control', *Systems and Control Letters* **37**.

Kružkov, S. [1970], 'First order quasilinear equations in several independent variables', *Mathematics of the USSR Sbornik* **10**. Mat. Sb. 81 (1970).

Lax, P. [1957], 'Hyperbolic systems of conservation laws II', *Communications on Pure and Applied Mathematics* **10**.

Lax, P. [1973], Hyperbolic systems of conservation laws and the mathematical theory of shock waves, *in* 'SIAM Regional conference series in applied mathematics', Vol. 11.

Lax, P. [2002], *Functional Analysis*, Wiley.

Lebacque, J. [1984], Semimacroscopic simulation of urban traffic., *in* 'AMSE International Minneapolis Summer Conference'.

Lebacque, J. [1996], The godunov scheme and what it means for first order traffic flow models, *in* 'Proceedings of the ISTTT Conference'.

Lebacque, J. [1997], A finite acceleration scheme for first order macroscopic traffic flow models, *in* M. Papageorgiou & A. Pouliezos, eds, 'Proceedings of the 8th IFAC symposium on transportation systems'.

Lebacque, J. [2003*a*], Intersection modeling, application to macroscopic network traffic flow modeling and traffic management, *in* 'Proceedings of the Traffic Granular Flow Conference'. equivalence of supply/demand and the BLN formulations.

Lebacque, J. [2003*b*], Two-phase bounded acceleration traffic flow model: analytical solutions and applications, *in* T. R. Board, ed., '82nd annual meeting of the Transportation Research Board'.

Lebacque, J., Haj-Salem, H. & Mammar, S. [2005], Second order traffic flow modeling: supply-demand analysis of the inhomogeneous riemann problem and of boundary conditions, *in* 'Proceedings of the 10th Euro Working Group on Transportation (EWGT)'.

Lebacque, J. & Khoshyaran, M. [2002], Macroscopic flow models, *in* M. Patriksson & M. Labbé, eds, 'Transportation planning: the state of the art - Proceedings of the 6th Meeting of the EURO Working Group on Transportation', Kluwer Academic Press.

Lebacque, J. & Khoshyaran, M. [2005], First order macroscopic traffic flow models: intersection modeling, network modeling, *in* 'Proceedings of the 16th ISTTT'.

LeFloch, P. [1988], 'Explicit formula for scalar conservation laws with boundary condition', *Mathematical Methods in the Applied Sciences* **10**.

LeFloch, P. [2002], *Hyperbolic Systems of Conservation Laws : The Theory of Classical and Nonclassical Shock Waves*, Birkh"auser.

Leo, C. & Pretty, R. [1992], 'Numerical simulation of macroscopic continuum traffic models', *Transportation Research Part B: Methodological* **26**.

LeVeque, R. J. [1992], *Numerical Methods for Conservation Laws*, Birkhäuser.

Lighthill, M. & Whitham, G. [1955], On kinematic waves II: a theory of traffic flow on long crowded roads, *in* 'Proceedings Royal Society, London Series A'.

Lions, J. [1971], *Optimal control of systems governed by partial differential equations*, Springer.

Lions, P.-L. [1982], *Generalized solutions of Hamilton-Jacobi equations*, Research Notes in Mathematics 69, Pitman.

Mammar, S., Lebacque, J. & Haj-Salem, H. [2005], Resolution of aw, rascle & zhang macroscopic second order traffic flow, *in* 'Proceedings of the 4th IMA conference on Mathematics in Transportation'.

Melikyan, A. [1998], *Generalized Characteristics of First Order PDEs: Applications in Optimal Control and Differential Games*, Birkh"auser.

M.Herty & Klar, A. [2003], 'Modeling, simulation, and optimization of traffic flow networks', *SIAM Journal on Scientific Computing* **25**.

Michalopoulos, P. G., Beskos, D. E. & Lin, J. K. [1984], 'Analysis of interrupted traffic flow by finite difference methods', *Transportation Research Part B: Methodological* **18**.

Michalopoulos, P. G., Stephanopoulos, G. & Stephanopoulos, G. [1981], 'An application of shockwave theory to traffic signal control', *Transportation Research Part B: Methodological* **15**.

Munoz, L., Sun, X., Horowitz, R. & Alvarez, L. [2003], Traffic density estimation with the cell transmission model, *in* 'Proceedings of the 2003 American Control Conference'.

Munoz, L., Sun, X., Horowitz, R. & Alvarez, L. [2006], A piecewise-linearized cell transmission model and parameter calibration methodology, *in* 'Proceedings of the Transportation Research Board 85th Annual Meeting'.

Newell, G. [1961], 'Nonlinear effects in the dynamics of car following', *Operations Research* **9**.

Newell, G. [1993], 'A simplified theory of kinematic waves in highway traffic. I: General theory. II: Queuing at freeway bottlenecks. III: Multi-destination flows.', *Transportation Research Part B: Methodological* **27**.

Oleĭnik, O. [1964], 'Uniqueness and stability of the generalized solution of the cauchy problem for a quasi-linear equation', *AMS Translations Series 2* **33**. Uspekhi Mat. Nauk 14 (1959).

Osher, S. [1984], 'Riemann solvers, the entropy condition and difference approximations', *SIAM Journal of Numerical Analysis* **21**.

P. Biswas, P. Grieder, J. L. & Morari, M. [2005], A survey on stability analysis of discrete-time piecewise affine systems, *in* 'Proceeding of the 16th IFAC World Congress'.

Papageorgiou, M. [1983], *Application of Automatic Control Concepts in Traffic Flow Modeling and Control*, Springer-Verlag.

Papageorgiou, M. [1984], 'Multilayer control system design applied to freeway traffic', *IEEE Transactions on Automatic Control* **29**.

Papageorgiou, M. [1990], 'Dynamic modelling, assignment and route guidance in traffic networks', *Transportation Research Part B: Methodological* .

Papageorgiou, M., Blosseville, J. & Haj-Salem, H. [1990], 'Modelling and real-time control of traffic flow on the southern part of boulevard périphérique in Paris. part II: Coordinated on-ramp metering', *Transportation Research Part A: Policy and Practice* **24**.

Papageorgiou, M., Blosseville, J. & Haj-Salem, H. [1991], 'Alinea: A local feedback control law for on-ramp metering', *Transportation Research Record* **1320**.

Papageorgiou, M., Haj-Salem, H. & Middelham, F. [1997], 'Alinea local ramp metering: Summary of field results', *Transportation Research Record* (1603).

Payne, H. [1971], Models of freeway traffic and control, *in* G. Bekey, ed., 'Mathematical Models of Public Systems', Vol. 1 of *Simulation Council Proceedings*.

Pipes, L. [1967], 'Car following models and the fundamental diagram of road traffic', *Transportation Research* .

Poupaud, F. & Rascle, M. [1997], 'Measure solutions to the linear multi-dimensional transport equation with non-smooth coefficients', *Communications in Partial Differential Equations* **22**.

Richards, P. I. [1956], 'Shock waves on the highway', *Operations Research* **4**(1).

Sanders, B. & Katopodes, N. [2000], 'Sensitivity analysis of shallow water flow by adjoint method', *Journal of Engineering Mechanics* **126**(9), 909–919.

Schrank, D. & Lomax, T. [2004], The 2004 urban mobility report, Available: http://mobility.tamu.edu, Texas Transportation Institute.

Seguin, N. & Vovelle, J. [2003], 'Analysis and approximation of a scalar law with a flux function with discontinuous coefficients', *Mathematical Models and Methods in Applied Sciences* **13**(2).

Serre, D. [1996], *Systèmes de Lois de Conservation (I-II)*, Diderot.

Sun, X. & Horowitz, R. [2005], Localized switching ramp-metering controller with queue length regulator for congested freeways, *in* 'Proceedings of the IEEE 2005 American Control Conference'.

Szepessy, A. [1989], 'Measure-valued solutions of scalar conservation laws with boundary conditions', *Archive for Rational Mechanics and Analysis* **107**.

Temple, B. [1982], 'Global solution of the cauchy problem for a class of 2x2 nonstrictly hyperbolic conservation laws.', *Advances in Applied Mathematics* **3**(3).

Temple, B. [1983], 'Systems of conservation laws with invariant submanifolds', *AMS Transactions* **280**.

Towers, J. [2000], 'Convergence of a difference scheme for conservation laws with a discontinuous flux', *SIAM Journal on Numerical Analysis* **38**.

Twin Cities Ramp Meter Evaluation Report [2001], Prepared by Cambridge Systematics Inc. for the Minnesota Department of Transportation.

Underwood, R. [1961], Speed, volume and density relationships, quality and theory of traffic flow, Technical report, Yale Bureau of Highway Traffic.

Whitham, G. [1974], *Linear and Nonlinear Waves*, Pure and applied mathematics, John Wiley & Sons.

Wong, G. C. K. & Wong, S. C. [2002], 'A multi-class traffic flow model - an extension of LWR model with heterogeneous drivers', *Transportation Research Part A: Policy and Practice* **36**.

Zhang, H. M. [1998], 'A theory of nonequilibrium traffic flow', *Transportation Research Part B: Methodological* **32**.

Zhang, H. M. [2002], 'A non-equilibrium traffic model devoid of gas-like behavior', *Transportation Research Part B: Methodological* **36**.

Zhang, H. M. & Jin, W. L. [2002], 'A kinematic wave traffic flow model for mixed traffic', *Transportation Research Record* **1802**.

Zhang, L. & Levinson, D. [2004], 'Optimal freeway ramp control without origin-destination information', *Transportation Research Part B: Methodological* **38**(10).

Zhang, M., Ritchie, W. & Jayakrishnan, R. [2001], 'Coordinated traffic-responsive ramp control via nonlinear state feedback', *Transportation Research Part C: Emerging Technologies* **9**.

Ziemer, W. [1989], *Weakly differentiable functions. Sobolev spaces and functions of bounded variation.*, Springer.

Résumé : Cette thèse traite de la modélisation des infrastructures autoroutières et de leur gestion par des méthodes de régulation telles que le contrôle d'accès. L'approche retenue est macroscopique et conduit à des modèles distribués sous forme d'équations aux dérivées partielles non linéaires. Nous apportons plusieurs éclairages sur l'analyse et la résolution de ces modèles (condition d'entropie pour les rampes d'accès, discrétisation simplifiée) et proposons une interprétation hybride des inhomogénéités (conditions aux limites, rampes d'accès et de sorties, variations brutales des paramètres) adaptée aux problèmes de contrôle. Deux nouvelles méthodologies calculatoires sont ensuite introduites pour concevoir des contrôleurs dynamiques s'appliquant à la gestion du trafic. La première est formulée comme un problème de commande optimale en boucle ouverte et nécessite l'adaptation de la méthode adjointe traditionnelle en raison de l'irrégularité des solutions. La seconde repose sur une discrétisation sous la forme d'un système affine commuté et une synthèse boucle fermée utilisant la dissipativité et les inégalités matricielles linéaires.

Mots clefs : modèles macroscopiques de trafic, contrôle d'accès coordonné, systèmes de lois de conservation, contrôle optimal des systèmes distribués, systèmes affines par morceaux, dissipativité des systèmes commutés, inégalités matricielles linéaires.

Macroscopic Freeway Modelling and Control.

Abstract: This PhD thesis deals with the issue of modelling and controlling freeway systems. The macroscopic approach is adopted and gives rise to distributed models represented by nonlinear partial differential equations. We provide several improvements in the analysis of these models (entropy inequality, simplified numerical schemes) and propose an hybrid formulation for the inhomogeneities (boundary conditions, on and off ramps and abrupt parameter changes) that suits controller design tasks. Based on these models, two computational control methodologies are introduced to conceive new dynamic ramp metering strategies. The first one follows an optimal control formulation and requires some extensions of the classical adjoint method due to the solution irregularity. The second one relies on a discretization scheme that leads to a piecewise affine system and uses dissipativity theory along with linear matrix inequalities to compute feedback controllers.

Keywords : macroscopic freeway models, coordinated ramp metering, nonlinear systems of conservation laws, optimal control of distributed systems, piecewise affine systems, dissipativity of switched systems, linear matrix inequalities.

Discipline : Automatique-Productique

Laboratoire d'Automatique de Grenoble - ENSIEG - BP 46, 38402 Saint-Martin d'Hères, FRANCE.